NICOLAUS COPERNICUS UNIVERSITY

IN TORUŃ

FACULTY OF BIOLOGICAL AND VETERINARY SCIENCES

ARASH MATINAHMADI

DOCTORAL DISSERTATION

Post-Transcriptional Regulation of mRNA Mediated by Decapping and Degradation Proteins in the Cytoplasm and Processing Bodies of *Larix Decidua*

Doctoral dissertation completed at the
Department of Cellular and Molecular Biology

Main supervisor: Dr. hab Dariusz Jan Smoliński, prof. Nicolaus Copernicus University

Co-supervisor: Prof. Mehrdad Hashemi, Tehran Medical Sciences University

TORUŃ 2025

ACKNOWLEDGEMENTS

I would like to express my deepest gratitude to all those who have supported me during my doctoral studies.

I am especially grateful to my supervisor, Prof. Dariusz Jan Smoliński, for his invaluable guidance, encouragement, patience, and constant support throughout this work.

I am also thankful to my co-supervisor, Prof. Mehrdad Hashemi, for his valuable assistance and helpful advice during my work.

I would like to extend my thanks to all the members of our research group for their collaboration, insightful discussions, and encouragement. In particular, I would like to thank the lab members, whose technical support, dedication, and teamwork made this work possible. I am also grateful to the administrative and technical staff of the department for their assistance and for providing a supportive working environment.

Finally, I would like to express my deepest and most heartfelt gratitude to my parents for their unwavering love, endless patience, and constant encouragement, which have shaped who I am today. I am especially thankful to my spouse, Zoofa, whose steadfast support, understanding, and boundless inspiration have been my anchor throughout this journey. I would also like to thank my friends for their encouragement, for sharing in both my challenges and triumphs, and for always being there when I needed them.

FINANCING

This work was developed with the financial support of:

1. NCN grant 2016/21/D/NZ3/00369 (2018–2023) — The role of Cajal bodies in nuclear retention and post-transcriptional modifications of mRNA in plants. Principal Investigator: Dr Agnieszka Kołowerzo-Lubnau.

2. Grant by the 4th edition of "Grants4NCUStudents" at Nicolaus Copernicus University, Torun, Poland (May 2022) (File number: 90-SIDUB.6102.3.2021.G4NCUS).

3. Grant by the 6th edition of "Grants4NCUStudents" at Nicolaus Copernicus University, Torun, Poland (May 2023) (File number:90-SIDUB.6102.4.2023.G4NCUS6).

4. Mini-grant from AC-IDS (Academia Copernicana Interdisciplinary Doctoral School) at Nicolaus Copernicus University, Torun, Poland (June 2023).

5. NCN grant 2022/45/N/NZ3/02015 (2023–2026) — Regulation of mRNA export during global nuclear retention of poly(A) RNA in plant cells. Scientific supervisor: Dr hab. Dariusz J. Smoliński, Prof. NCU.

6. Mini-grant from AC-IDS (Academia Copernicana Interdisciplinary Doctoral School) at Nicolaus Copernicus University, Torun, Poland (Sep 2024).

7. Erasmus+ grant for an Internship in Spain (Sep 2024).

8. A part of the research, which was done in Spain, was supported by grants (CIBEROBN, CB06/03/1012) from CIBER Fisiopatología de la Obesidad y Nutrición as an initiative of FEDER-ISCIII, Ministerio de Ciencia e Innovación-Fondo Europeo de Desarrollo Regional (Grant PID2022-1364140B-I00) and Fondo Social Europeo-Gobierno de Aragón (Grant B16_23R).

9. Ministry of Science and Higher Education (MNiSW) funds for a research-related investment in 2024, Agreement No. 7472/IA/SP/2024 — Consortium Leader: Dr hab. Dariusz Jan Smoliński, Prof. NCU. Equipment: Abberior Facility Line STED super-resolution laser microscope.

10. NCN grant 2023/50/O/NZ3/00010 (2025–2029) — Nuclear mRNA retention and delayed translation as a novel mechanism of post-transcriptional regulation of mRNA in plants. Principal Investigator: Dr hab. Dariusz J. Smoliński, Prof. NCU.

Publications

I. Publications directly resulting from this dissertation:

1. **Matinahmadi, A**., Zayani, Z., Majewska, K., Smoliński, D. J. (2025). Plant P-Bodies in Post-Transcriptional Control: Composition, Dynamics, and Context-Dependent Roles. Plant Communications (Manuscript under revision, Ref: PLANT-COMMUNICATIONS-D-25-01114).

2. **Matinahmadi, A.**, Majewska, K., Kołowerzo-Lubnau, A., Szcześniak, M.W., Bidooki, S.H., Osada, J., Hashemi, M. Smoliński, D. J. (2025). Cytoplasmic Decapping Proteins and P-bodies Assembly Operate in a Developmentally Programmed poly(A) RNA Turnover Cycle in *Larix decidua* (Manuscript under submission).

II. Other publications during the doctoral study period:

1. Zayani Z, **Matinahmadi A**, Tavakolpournegari A, SS Moosavi, Bidooki SH. The Crosstalk Between Non-Coding RNAs and Lipid Metabolism in Chronic Disease Progression. Lipidology, 2025 Oct 2(4), 19.

2. Zayani Z, **Matinahmadi A**, Tavakolpournegari A, Bidooki SH. Exploring Stressors: Impact on Cellular Organelles and Implications for Cellular Functions. Stresses, 2025 Apr 4;5(2):26.

3. Hashemi M, Hosseini AS, Monjezi S, Hasany S, Binaei S, Nejat M, Melyani H, Bashandeh N, **Matinahmadi A**, Zayani Z, Orouei S, Bidooki SH, Raesi R, Farahani N & Entezari M. Prostate Cancer, Apoptosis, Autophagy and Ferroptosis: Cell Death Mechanisms and Their Cross-talk. Book title: Prostate Cancer: Molecular Events and Therapeutic Modalities. Springer, Singapore. 2024 Nov; pp 71–107.

4. Hashemi M, Khosroshahi EM, Tanha M, Khoushab S, Bizhanpour A, Azizi F, Mohammadzadeh M, **Matinahmadi A**, Koohpar ZK, Asadi S, Taheri H. Targeting autophagy can synergize the efficacy of immune checkpoint inhibitors against therapeutic resistance: New promising strategy to reinvigorate cancer therapy. Heliyon. 2024 Sep 30;10(18).

5. Hashemi M, Daneii P, Asadalizadeh M, Tabari K, **Matinahmadi A**, Bidoki SS, Motlagh YS, Jafari AM, Ghorbani A, Dehghanpour A, Nabavi N. Epigenetic regulation of hepatocellular carcinoma progression: MicroRNAs as therapeutic, diagnostic and prognostic factors. The International Journal of Biochemistry & Cell Biology. 2024 May 1;170:106566.

6. Gholamzad A, Khakpour N, Khosroshahi EM, Asadi S, Koohpar ZK, **Matinahmadi A**, Jebali A, Rashidi M, Hashemi M, Sadi FH, Gholamzad M. Cancer stem cells: The important role of CD markers, signaling pathways, and microRNAs. Pathology-Research and Practice. 2024 Feb 28:155227.

7. Hashemi M, Khosroshahi EM, Chegini MK, Abedi M, **Matinahmadi A**, Hosnarody YS, Rezaei M, Saghari Y, Fattah E, Abdi S, Entezari M. miRNAs and exosomal miRNAs in lung cancer: New emerging players in tumor progression and therapy response. Pathology-Research and Practice. 2023 Oct 26:154906.

8. Hashemi M, Ghadyani F, Hasani S, Olyaee Y, Raei B, Khodadadi M, Ziyarani MF, Basti FA, Tavakolpournegari A, **Matinahmadi A**, Salimimoghadam S. Nanoliposomes for doxorubicin delivery: Reversing drug resistance, stimuli-responsive carriers and clinical translation. Journal of Drug Delivery Science and Technology. 2023 Feb 1;80:104112.

9. Tavakolpournegari A, Hashemi M, Karizi SZ, **Ahmadi AM**, Bidooki SH, Banaei G. Expression Patterns of miR181a and miR30d in Patients with Breast Cancer. Iranian Journal of Public Health. 2022 Jul;51(7):1594.

Table of Contents Page

List of Figures

Abstract

Importance: Post-transcriptional mRNA turnover is a central regulator of gene expression during development, determining which transcripts are available for translation and when. Yet the cellular sites and mechanistic timing of decay pathways as modes of post-transcriptional regulation (most notably decapping-dependent 5′→3′ decay) remain insufficiently defined in a developmental context. *Larix decidua* microsporocytes provide a natural model; during a prolonged diplotene (several months), they execute reproducible, cyclical bursts of transcription and a clear five-stage poly(A) RNA cycle, thereby creating a temporal window to link mRNA fate to developmentally programmed events.

Research gap: Many studies have characterized P-bodies and decapping machinery in non-plant systems or outside defined developmental programmes; far less is known about whether visible P-bodies assemble and actively mediate decapping-dependent decay during plant development, and how quantitative changes in P-body architecture relate to substrate load. In *Larix decidua* microsporocytes, the poly(A) cycle continues with a conspicuous late-stage (stage 5) reduction of cytoplasmic polyadenylated RNA, but the mechanistic contribution of P-body–centered decapping (DCP2, DCP5, EDC4/VCS, and LSM4) and downstream 5′→3′ exonucleolysis (XRN4) has not been tested. This gap prevents confident linkage of spatial RNP dynamics and transcriptome-level outcomes during meiosis.

Objectives: The thesis therefore pursued three coordinated aims: (1) to determine whether P-bodies form and act as sites of decapping/decay during the five-stage poly(A) cycle and specifically whether decapping contributes to the late-stage poly(A) decline, (2) to quantify how P-body metrics (number per cell, mean volume and volume-class distribution) and protein composition (DCP5, DCP2, EDC4, LSM4, XRN4) change across stages, and (3) to identify sets of transcript associated with individual decapping components by RNA-immunoprecipitation sequencing (RIP-seq), thereby generating candidate substrates for functional tests. These objectives were formulated to move beyond descriptive imaging toward mechanistic inference and target discovery.

Methodology: To connect space, time, and molecules, stage-resolved confocal microscopy was used to measure cytoplasmic poly(A) RNA and distributions of DCP5, DCP2, EDC4/VCS,

LSM4, and XRN4, alongside P-body counts, and size classes across stages 1-5 were combined. Biochemical P-body enrichment and co-immunoprecipitation validated protein interactions, while RIP-seq captured RNAs associated with DCP2, DCP5, EDC4, and LSM4.

Key findings: Visible P-bodies assemble during the diplotene and are dynamically regulated across the poly(A) cycle: mid-sized P-bodies (0.3-1.2 μm^3) constitute the dominant functional class throughout, whereas larger P-bodies (1.2-6 μm^3) become more prominent as catalytic factors engage. Protein recruitment follows a reproducible temporal order, organizational/pre-decapping factors DCP5 and LSM4 peak earlier (stage 3), the catalytic decapping module (DCP2 and EDC4/VCS) engages at stage 4, and XRN4 colocalization rises at stages 4-5, identifying stage 4 as the control/peak activity point and stage 5 as the resolution/cleanup phase. Co-immunoprecipitation supports a candidate DCP5/DCP2/EDC4 core module, whereas LSM4 and XRN4 exhibit more dynamic or downstream behaviour. Finally, RIP-seq recovered 413 mRNA sequences (216 annotated mRNAs), comprising shared and protein-specific sets enriched for mitochondrial, chloroplast, and membrane-associated functions, thereby delivering concrete candidate substrates for follow-up tests.

Implications: Taken together, these results define a supply-responsive, staged programme of cytoplasmic mRNA turnover in *Larix decidua* microsporocytes, in which P-bodies serve as principal reaction hubs coordinating decapping-dependent 5′→3′ decay during meiosis. The work fills a key gap by demonstrating P-body activity within a defined developmental programme, presenting a quantitative imaging/molecular pipeline and a validated RIP-seq resource. While spatiotemporal overlap implicates decapping-mediated 5′→3′ decay in the late-stage poly(A) RNA decline in the deplotene phase of *Larix decidua* microsporocytes, alternative pathways (deadenylation/exosome, transcriptional downregulation) are also likely to contribute; accordingly, the thesis establishes the experimental roadmap and molecular entries needed to distinguish these routes.

Streszczenie

Znaczenie. Potranskrypcyjna kontrola stabilności i degradacji mRNA jest centralnym regulatorem ekspresji genów w trakcie rozwoju, decydując o tym, które transkrypty są dostępne do translacji i kiedy. W kontekście rozwoju wciąż słabo wiemy, gdzie w komórce i kiedy działają szlaki degradacji mRNA. Dotyczy to szczególnie dekapingu inicjującego degradację 5′→3′. Mikrosporocyty Larix decidua stanowią naturalny model: podczas długiego okresu diplotenu (trwającego kilka miesięcy) wykazano powtarzalne, cykliczne fale transkrypcji oraz wyraźny, pięcioetapowy cykl poli(A) RNA, tworzy to doskonały model pozwalający powiązać losy mRNA z zaprogramowanymi zdarzeniami rozwojowymi.

Luka badawcza. Liczne prace opisywały ciałka P oraz aparat dekapingu głównie w modelach komórki zwierzęcej oraz poza ściśle zdefiniowanymi programami rozwojowymi. Znacznie mniej wiadomo o tym, czy ciałka P formują się i aktywnie pośredniczą w dekapingu zależnym od degradacji 5′→3′ w trakcie rozwoju roślin. W mikrosporocytach *Larix decidua* cykl poli(A) RNA kończy się wyraźnym, spadkiem (etap 5) poziomu mRNA w cytoplazmie. Nie zweryfikowano dotąd, w jakim stopniu dekaping zachodzący w ciałkach P (DCP2, DCP5, EDC4/VCS, LSM4) oraz następująca po nim degradacja egzonukleolityczna 5′→3′ z udziałem XRN4 przyczyniają się do tego procesu. W konsekwencji brakuje jednoznacznych danych łączących zmiany liczby i objętości ciałek P oraz etapową rekrutację tych białek z efektami transkryptomowymi — w szczególności ze spadkiem poziomu cytoplazmatycznego poli(A) RNA w etapie 5 i innymi wskaźnikami losów transkryptów podczas mejozy.

Cele. W rozprawie zrealizowałem trzy skoordynowane cele.

(1) Sprawdzić, czy ciałka P formują się i pełnią funkcję miejsc dekapingu/degradacji w pięcioetapowym cyklu poli(A) RNA oraz czy dekaping przyczynia się do późnego spadku poziomu poli(A).

(2) Ilościowo opisać, jak między etapami zmieniają się parametry ciałek P (liczba na komórkę, średnia objętość, rozkład klas objętościowych) oraz ich skład białkowy (DCP5, DCP2, EDC4, LSM4, XRN4).

(3) Zidentyfikować zestawy transkryptów powiązanych z poszczególnymi komponentami dekapingu metodą RIP-seq (RNA-immunoprecypitacja z sekwencjonowaniem), aby wytypować kandydatów do dalszej weryfikacji funkcjonalnej.

Cele sformułowano tak, by przejść od opisu morfologicznego do wnioskowania mechanistycznego oraz identyfikacji celów eksperymentalnych.

Metodyka. Aby precyzyjnie powiązać lokalizację sygnałów z ich zmianami w czasie rozwoju, zastosowano mikroskopię konfokalną i analizę w pięciu kolejnych etapach (1–5). Oznaczano: (i) poziom cytoplazmatycznego RNA poli(A), (ii) liczbę ciałek P, ich objętość i rozkład klas objętości, oraz (iii) rozmieszczenie i kolokalizację białek DCP5, DCP2, EDC4/VCS, LSM4 i XRN4. Interakcje białko–białko weryfikowano za pomocą biochemicznego wzbogacania frakcji ciałek P oraz koimmunoprecypitacji. Z kolei metoda RIP-seq (immunoprecypitacja RNA z sekwencjonowaniem) posłużyła do identyfikacji transkryptów związanych z DCP2, DCP5, EDC4 i LSM4.

Najważniejsze wyniki. Ciałka P powstają w diplotenie i ulegają dynamicznym zmianom w całym cyklu poli(A) RNA. Ciałka średnie (0,3-1,2 μm^3) stanowią klasę dominującą, natomiast większe (1,2-6 μm^3) pojawiają się liczniej wraz z rekrutacją składników katalitycznych. Kolejność rekrutacji białek jest stała: DCP5 i LSM4 (białka organizujące i przygotowujące kompleks do dekapingu) osiągają wczesne maksimum (etap 3), następnie na etapie 4 uaktywnia się moduł katalityczny dekapingu (DCP2, EDC4/VCS), a kolokalizacja XRN4 wyraźnie rośnie w etapach 4-5. Wskazuje to na etap 4 jako punkt kontrolny i szczyt aktywności, a na etap 5 jako fazę wygaszania i końcowego porządkowania. Koimmunoprecypitacja potwierdza istnienie rdzeniowego modułu DCP5–DCP2–EDC4, natomiast LSM4 i XRN4 wykazują bardziej dynamiczne, późniejsze włączanie się w szlak. Analiza RIP-seq zidentyfikowała 413 sekwencji (w tym 216 adnotowanych transkryptów mRNA), obejmujących zarówno zbiór wspólny, jak i zestawy specyficzne dla poszczególnych białek. Analiza funkcjonalna tych transkryptów wskazała nadreprezentację procesów i komponentów związanych z mitochondriami, chloroplastami i błonami, co wskazuje konkretne transkrypty będące kandydatami do dalszej weryfikacji funkcjonalnej.

Wnioski. Wyniki łącznie opisują etapowy, zależny od dostępności substratu program kontroli stabilności i degradacji cytoplazmatycznego mRNA w mikrosporocytach Larix decidua. W tym układzie ciałka P są głównymi miejscami reakcji, koordynując dekaping i następującą po nim degradację 5′→3′ w trakcie mejozy. Praca wypełnia istotną lukę, pokazując aktywność ciałek P w ramach jasno zdefiniowanego programu rozwojowego, oraz przedstawia zestaw metod: ilościowe obrazowanie, analizy molekularne oraz zweryfikowany zbiór danych RIP-seq. Zbieżność czasowo-przestrzenna wskazuje, że dekaping przyczynia się do późnego spadku poziomu poli(A) RNA w diplotenie mikrosporocytów L. decidua, choć najpewniej biorą w nim udział również inne ścieżki (deadenylacja/egzosom, obniżenie transkrypcji). Dlatego praca przedstawia konkretny plan doświadczeń i precyzuje cele molekularne, które umożliwią jednoznaczne rozróżnienie tych ścieżek.

1. Introduction

1.1 Gene processing in eukaryotic cells

Transcription and translation are two fundamental cellular processes involved in protein synthesis that can be maintained throughout the development of an organism. Transcription happens in four main steps: the assembly of the pre-initiation complex (PIC), initiation, elongation, and termination (1,2). Initiation refers to the step that involves the formation of a complex between RNA polymerase II (Pol II) and transcription factors (activators/repressors) with a mediator to stabilize the assembly (3). With the help of proteins known as activators and repressors, elongation begins immediately after this complex formation. During elongation, an RNA copy of the DNA sequence is produced, and the process terminates with a mechanism called polyadenylation that is still not fully understood. (4). Transcription is followed by post-transcriptional events, where RNA-binding proteins play versatile roles in the regulation and processing of the RNA (5).

After transcription in the nucleus, transcription produces an intermediate product, precursor messenger RNA (pre-mRNA), which must undergo a set of conserved processing steps to generate mature mRNA, capable of translation in the cytoplasm. Nuclear processing, such as 5'-end capping (7-methylguanosine cap), splicing (gene splicing), and 3'-end cleavage/polyadenylation, results in the formation of a mature polyadenylated mRNA (Figure 1-1). The myriad of RNA-binding proteins (RBP) that interact with the nascent mRNA directly influence the nuclear processing events from the moment the 5′-end of the mRNA is captured by RNA polymerase II. These RNA-binding proteins help to package the RNA into an mRNP complex that is competent for export to the cytoplasm (6). Export is facilitated by specific mRNA export receptors that mediate interactions with the nuclear pore complex. The remodeling of the mRNP complex at the cytoplasmic side of the nuclear pore ensures the proper directionality of this transport (7). Once in the cytoplasm, the mRNA can either be translated into protein, stored in cytoplasmic bodies for later use, localized to particular areas of the cell, or directed for degradation (8). All these steps are fundamental to achieving gene expression and supporting diverse cellular functions.

Translation is the synthesis of proteins from an mRNA template. It is a tightly regulated process not only with mRNA, but also with tRNA, ribosomes, and translation initiation and elongation factors (9). Like transcription, the translation process is divided into four steps: initiation, elongation, termination, and ribosome recycling. In particular, translation needs to be properly regulated for accurate protein synthesis and the normal progress of the cell cycle (10).

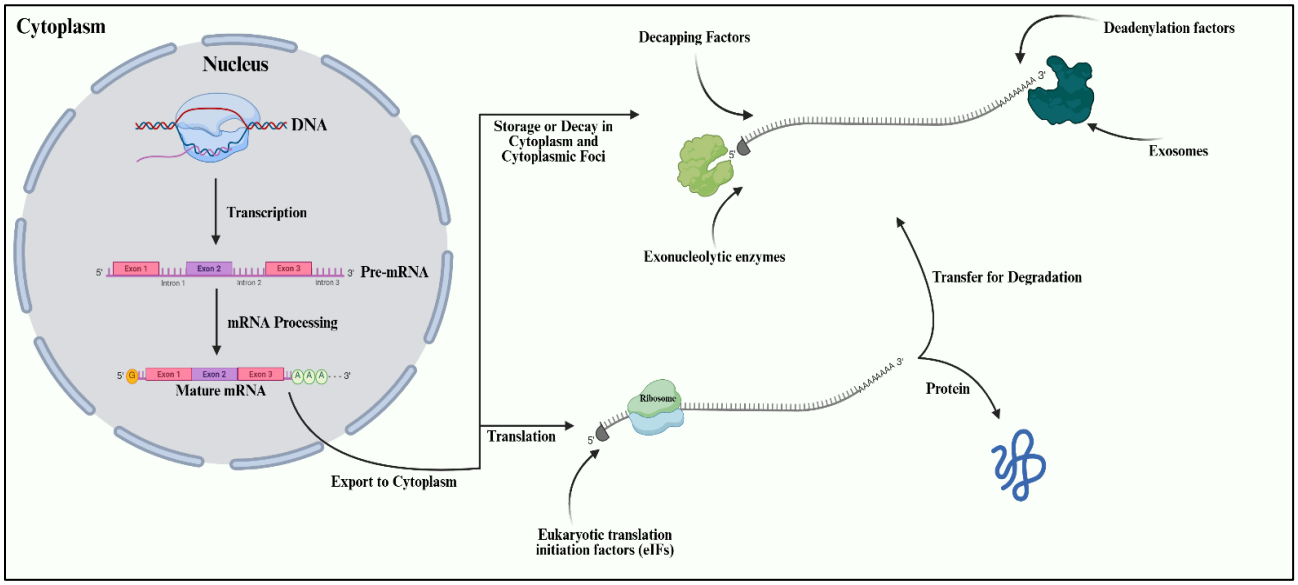

Figure 1-1. The picture shows the gene processing in eukaryotic cells. The pre-mRNA is transcribed by the transcription process inside the nucleus, and then, after mRNA processing, the mature mRNAs are exported to the cytoplasm for further regulation, like translation, storage, or decay. The mentioned enzymes and factors are required to

1.2 Post-transcriptional regulation of gene expression in eukaryotes

Post-transcriptional regulation is essential and is well known not only for controlling diverse essential traits but also for the value of genetic modification in organisms. Post-transcriptional regulation includes RNA processing and transport (notably nuclear export, where RBPs often play key roles) and post-transcriptional mechanisms such as alternative splicing and transcript degradation. Proteins that may be involved in the regulation of RNA processing are the protein-containing RNP (ribonucleoprotein) domains. RNPs have an important function in post-transcriptional regulation of gene expression. During RNA processing, nearly 60% of all genes may be alternatively processed to generate a much greater diversity of proteins to compensate for the relatively small number of genes in the genome (11,12). Several mechanisms are implicated in post-transcriptional regulation:

1.2.1 Pre-mRNA Processing

The pre-mRNA maturation process in eukaryotic cells involves several steps that convert the pre-mRNA to mature mRNA for translation into a protein. This process occurs in the nucleus before the mature mRNA is exported to the cytoplasm. The key stages of mRNA maturation are 5'-end capping, intron splicing, and 3'-end polyadenylation (13).

1.2.1.1 5'-end Capping

5'-end capping is a post-transcriptional modification that occurs at the 5'-end of the pre-mRNA that is transcribed from the DNA. Eukaryotic mRNA universally possesses a cap structure, consisting of an N7-methylated guanosine connected to the first nucleotide of the RNA through a reverse 5′ to 5′ triphosphate bond. Beyond its critical role in cap-dependent initiation of protein synthesis, the mRNA cap serves as a protective element against 5′→3′ exonuclease cleavage and acts as a distinct marker for recruiting protein factors involved in pre-mRNA splicing, polyadenylation, and nuclear export. It also remains the anchor for recruiting initiation factors that promote protein synthesis and the 5′→3′ mRNA loop during translation (14). Capping is a co-transcriptional modification carried out by RNA polymerase II, beginning as soon as the first 25–30 nucleotides are incorporated into a newly growing transcript in the nucleus (Figure 1-2). The cap 0 structure is assembled with 3 types of enzymatic activities, including RNA triphosphatase (TPase), RNA guanylyltransferase (GTase), and guanine-N7 methyltransferase (guanine-N7 MTase) (15).

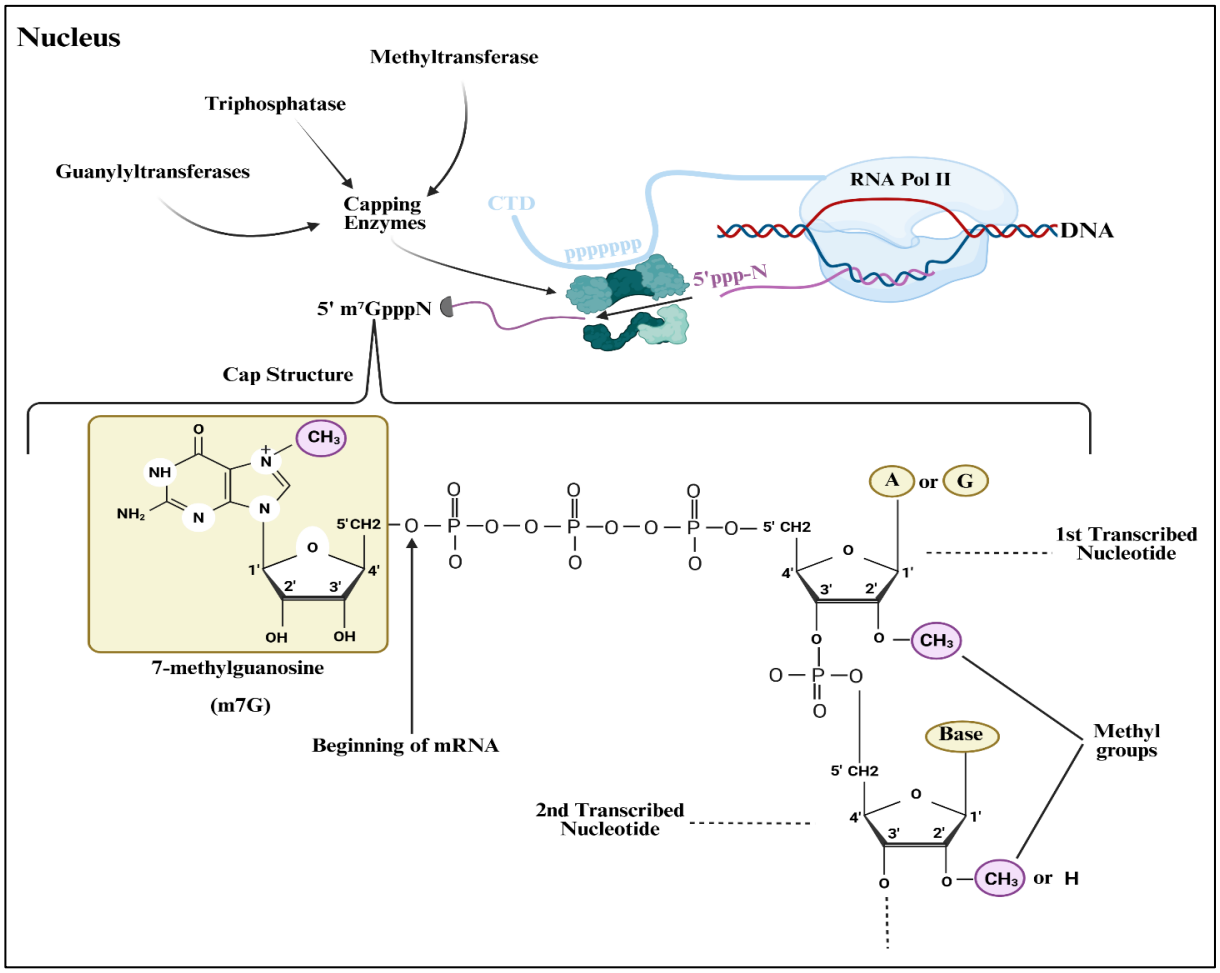

Figure 1-2. The picture shows the 5'-end capping process of mRNA. The CTD (C-terminal domain) is the tail of RNA polymerase II and plays a central role in coordinating mRNA capping. It is like a landing pad for capping enzymes, and its phosphorylation state controls when and how the 5′ cap is added during transcription. The cap structure is known as 7-methylguanosine triphosphate-nucleotide (m^7GpppN).

1.2.1.2 mRNA splicing

The splicing of pre-mRNA is an essential process in the post-transcriptional regulation of gene expression, significantly enhancing the functional proteome in eukaryotic organisms with a limited number of genes (16). Genes in eukaryotes, unlike prokaryotes, contain non-coding sequences that are excised from pre-mRNAs shortly after transcription. These regions are called introns. Introns are considered non-coding DNA, which has been traditionally viewed as "junk" DNA without any apparent functional relevance (17). The removal of introns, resulting in mature mRNA transcripts, is executed by a multi-megadalton RNP complex called a spliceosome, along with a host of other factors that contribute to alternative splicing and regulation (18). Spliceosomal introns can be categorized into two groups based on the

spliceosome involved in their excision from pre-mRNA. Most introns are removed by the U2 spliceosome, while the remaining introns are excised by the U12 spliceosome. The U2-dependent spliceosome catalyzes the removal of U2-type introns, and the less abundant U12-dependent spliceosome is present in only a subset of eukaryotes and splices the rare U12-type class of introns (19). Consensus sequences at the exon-intron boundaries are crucial for the proper recognition and removal of introns. U2 introns, which are the most common, feature the GU dinucleotide at the donor 5′-splice site and the AG dinucleotide at the acceptor 3′-splice site (17,20).

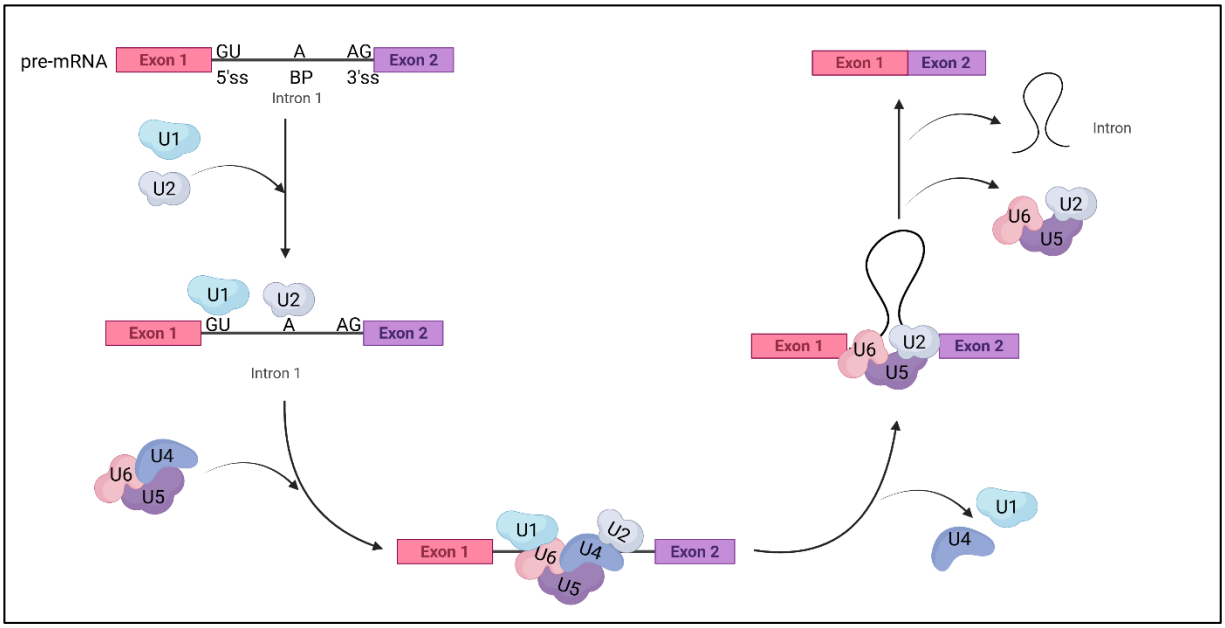

Figure 1-3. Schematic representation of pre-mRNA splicing by the U2-dependent major spliceosomes. modified from Krummel, D. A. P. (2010) (232). pre-mRNA splicing begins co-transcriptionally with the U1 and U2 snRNPs binding to the 5' SS and BP of the U2-type intronic sequences, respectively. Subsequently, the U4/U6-U5 tri-snRNP is recruited for the first splicing step. With the release of U1 and U4 snRNPs, the second splicing step ensues, releasing the ligated exons (mRNA) and the intron.

1.2.1.3 3'-end polyadenylation

The final essential step in mRNA maturation is polyadenylation, which is the cleavage of the 3'-end pre-mRNA and the subsequent addition of a poly(A) tail (21,22). The first step is endonucleolytic cleavage of the pre-mRNA to yield a free 3' hydroxyl that serves as the substrate for the second step, the non-templated addition of adenosines (polyadenylation). Cis-

acting elements and the specific RNA-binding proteins that are recognizable by these elements are utilized during polyadenylation, whereas cleavage is dependent on the formation of multi-subunit complexes containing the cleavage and polyadenylation machinery (23). The site of 3'-end cleavage is specified by the binding of other sequence elements in the pre-mRNA to a multiprotein complex referred to as the 3'-end processing complex. The essential unit of the 3' end processing complex is CPSF. CPSF, which binds specifically to the core-sequence element AAUAAA in the polyadenylation site and catalyzes cleavage (24). This polyadenosine poly(A) "tail" is a defining feature of mRNA with critical roles during several stages in the mRNA life cycle, with an average length of 250 nucleotides. 3'-end cleavage and polyadenylation of mRNA are necessary for transcription termination, release of mRNA from the site of transcription, and export to the cytoplasm. In the cytoplasm, the poly(A) tail protects mRNA from degradation and boosts mRNA translation in the cytoplasm (25).

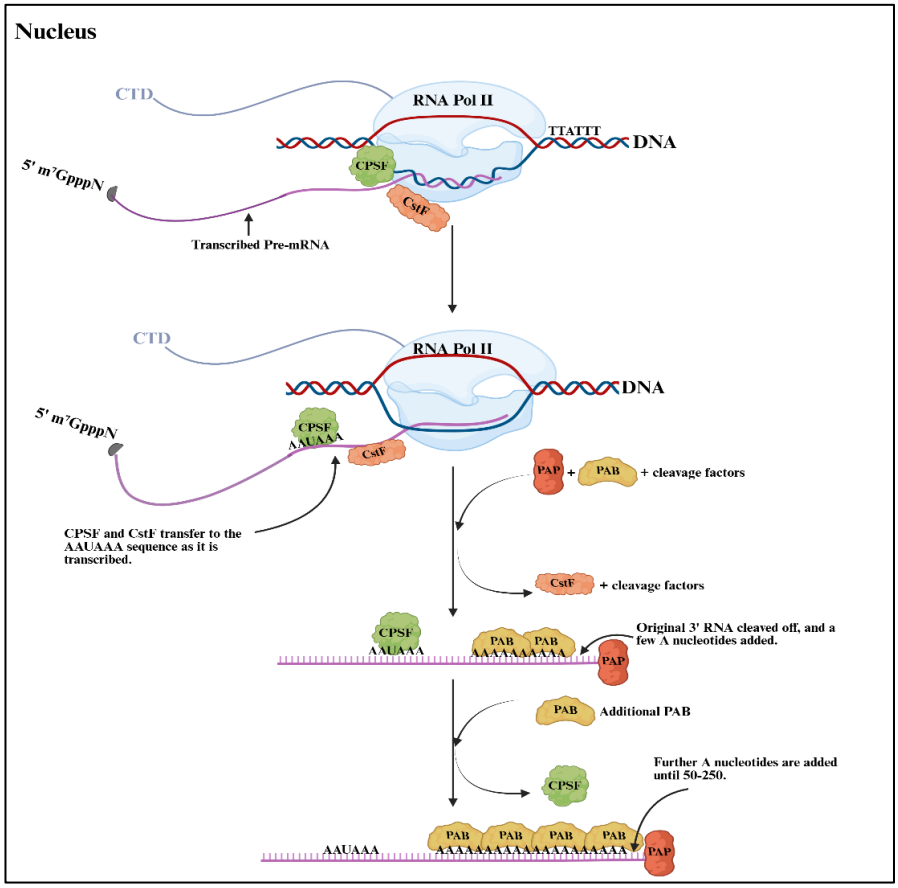

Figure 1-4. The picture shows the 3'-end polyadenylation process of mRNA. The AAUAAA sequence is detected by the CPSF and CstF and then the 3' end of the mRNA is cleaved by the cleavage factors and following cleavage, the enzyme poly(A) polymerase (PAP) adds a poly(A) tail to the newly exposed 3' hydroxyl group of the mRNA and next the PAB proteins add to the poly A tail.

1.2.2 Nuclear export of mRNA

Only fully processed mRNAs are competent for export as they are recognized by export factors. Nucleocytoplasmic transport events occur through the nuclear pore complex (NPC), a large transport channel that mediates the passage of proteins and diverse RNA classes such as mRNA, rRNA, tRNA, miRNA, and snRNA (26,27). The central channel of the NPC is filled with thousands of phenylalanine-glycine (FG) peptide repeats (28). mRNA transport through the NPC is unidirectional: as mRNA is synthesized and processed in the nucleus, it is packaged with RNA-binding proteins (RBPs) to form ribonucleoprotein particles (mRNPs) (29). Important export factors include the Nuclear Cap-Binding Complex (CBC), consisting of CBP20 and CBP80 (30), THO/TREX (transcription-export) (31), and NXF1/NXT1 (TAP/p15) Complex (32). Unlike other RNAs, mRNA export is generally Ran-independent because it relies on export receptor NXF1/NXT1 heterodimer (TAP/p15 in mammals) or Mex67-Mtr2 in yeast. These receptors directly interact with nucleoporins and facilitate bulk mRNA export without Ran-GTP involvement. The mRNP is actively translocated through the NPC in a process requiring ATP-dependent remodeling of the mRNP structure (33,34).

The TREX complex plays a crucial role in the formation, maturation, and export of mRNPs. In metazoans, this complex comprises a hexameric THO core along with additional proteins such as the RNA helicase UAP56, the CIP29/SARNP protein, and several export adaptors like ALY and UIF. TREX associates with newly synthesized transcripts during transcription elongation, a process that is closely linked to transcription and mRNA processing. This interaction promotes the recruitment of export adaptors that bind to mRNA. Ultimately, these adaptors interplay with THO components and facilitate the attachment of the NXF1/NXT1 export receptor to the mRNA. NXF1/NXT1 then enables the transport of the mRNA through the NPC by interacting with the TREX-2 complex at the nuclear side of the NPC and with FG-repeat nucleoporins lining the nuclear pore (35,36). The adaptor proteins stay within the nucleus, while the export receptor directs the mRNA through the NPC. Upon reaching the cytosolic side, the receptor detaches from the mRNA following mRNP remodeling mediated by DBP5 and GLE1. DBP5 helicase at the NPC removes nuclear export factors to prevent re-entry in the nucleus (37,38).

In plants, the mechanisms and regulatory proteins involved in mRNA export remain largely unknown. Notably, plant genomes lack genes encoding homologs of human TAP/NXF1 or yeast Mex67p, raising two possibilities: either plants possess structurally distinct proteins that perform similar functions, or they rely on an entirely different set of components for mRNA export. However, a potential *Arabidopsis* homolog of vertebrate p15 has been identified (32). Additionally, a 2006 study, characterized NTF2a and NTF2b as *Arabidopsis* homologs of the nuclear import receptor for RanGDP (39). In the nucleus of plant cells, export factors, including the THO/TREX complex, are recruited co-transcriptionally to the newly synthesized mRNA as it is being transcribed by the elongating RNA polymerase II (RNAPII). The RNA helicase UAP56 facilitates interactions with MOS11 and export adaptors (ALY1–4, UIEF1/2). Export factors are bound to the completely processed mRNA. CBC, which consists of CBP20 and CBP80, bound at the 5´-end, spliced, and 3´-polyadenylated. ALY or UIEF recruits an export receptor (ExR), whose identity in plants remains unknown. The export-competent mRNA is then translocated via NPC, potentially involving the TREX-2 complex. At the cytosolic side of the NPC, the RNA helicase LOS4 and GLE1 are believed to mediate mRNP remodeling, leading to the removal of the export receptor, ensuring that the mRNP does not re-enter the nucleus (40).

1.2.3 Eukaryotic mRNA Translation

Translation is the process by which eukaryotic cells decode mRNA to synthesize proteins. This highly regulated process occurs in the cytoplasm and consists of three main stages: initiation, elongation, and termination. Various regulatory mechanisms ensure efficient and accurate protein synthesis, allowing cells to respond dynamically to environmental and developmental cues (41,42).

1.2.3.1 Translation Initiation

During the initiation stage, 80S ribosomes are assembled with the initiator tRNA (Met-tRNAi Met), and the start codon is properly aligned in the P site. This process necessitates the involvement of at least ten eukaryotic initiation factors (eIFs). eIFs facilitate the recruitment of the 40S ribosomal subunit to the 5' end of the mRNA, where it scans for the start codon. The 5'

cap (m^7G) is recognized by eIF4F, a complex consisting of eIF4E (cap-binding protein), eIF4G (scaffold protein), and eIF4A (RNA helicase). The poly(A) tail, bound by poly(A)-binding protein (PABP), interacts with eIF4G, forming a circular mRNA structure that enhances translation efficiency. The Met-tRNAi^Met, bound to eIF2-GTP, associates with the 40S ribosomal subunit to form the 43S pre-initiation complex. Upon AUG recognition, eIF2-GTP is hydrolyzed to eIF2-GDP, leading to the release of initiation factors and the joining of the 60S ribosomal subunit, forming the 80S ribosome ready for elongation (43–45).

1.2.3.2 Translation Elongation

The elongation stage consists of three primary steps: decoding of mRNA codons by the corresponding aminoacyl-tRNAs, formation of peptide bonds, and translocation of the tRNA–mRNA complex. This movement shifts the peptidyl-tRNA from the A site to the P site, exposing the next codon in the A site. In eukaryotes, the elongation factor eEF1A binds aminoacyl-tRNA in a GTP-dependent manner and facilitates its delivery to the ribosomal A site. When the aa-tRNA successfully recognizes the codon, GTP hydrolysis by eEF1A occurs, releasing the factor and allowing the aa-tRNA to properly position itself in the A site. Once accommodated, peptidyl transferase, an enzymatic activity of the ribosome's 28S rRNA within the 60S subunit, catalyzes peptide bond formation. The ribosome then advances to the next codon with the assistance of eEF2-GTP, moving the peptidyl-tRNA to the P site and transferring the deacylated tRNA to the E site, from where it is ultimately released (45,46).

1.2.3.3 Translation Termination

Termination takes place when the ribosome encounters a stop codon (UAA, UGA, or UAG). This process is mediated by two protein factors: eRF1, which identifies all three stop codons, and the GTPase eRF3, which promotes termination through GTP hydrolysis. The hydrolysis of GTP by eRF3 aids in the disassembly of the ribosome and the release of both mRNA and tRNA, enabling the translation process to initiate anew with a different mRNA molecule (42,47).

1.2.4 Role of cytoplasmic bodies in Post-transcriptional regulation

To ensure the cell operates efficiently, its interior is organized into multiple compartments known as organelles. These specialized structures house various biomolecules, such as proteins and nucleic acids, and play essential roles in cellular function. Recent studies have focused on a specific category of organelles known as membrane-less organelles (MLOs), also referred to as biomolecular condensates, droplets, granules, foci, or bodies. These dynamic structures can be found in both the nucleus, such as nucleoli and Cajal bodies, and the cytoplasm, including stress granules (SGs) and processing bodies (PBs) (48,49).

MLOs form through a spontaneous process triggered by physicochemical changes in the cellular environment. This phenomenon, known as liquid-liquid phase separation (LLPS), has long been recognized in polymer chemistry, but recent research has demonstrated its relevance in biological systems as well (50). LLPS is primarily driven by weak, multivalent interactions (51). Over time, several defining characteristics of MLOs have been identified. Key features include their spherical shape, ability to merge, dynamic nature, and specific mode of assembly, independent of variations in composition, location, or function (50,52). Many MLOs exhibit liquid-like characteristics, making them highly dynamic structures that continuously exchange components with their environment. Moreover, the formation of these biomolecular condensates is reversible, allowing them to assemble and disassemble as needed. However, their properties and organization may undergo changes over time (53).

Precise post-transcriptional regulation of mRNA processing, transport, translation, storage, and degradation is essential for controlling gene expression. These processes are mediated by specific RNA-binding proteins (RBPs), which associate with mRNA to form larger complexes known as messenger ribonucleoprotein particles (mRNPs) (54). In eukaryotic cells, mRNPs are often localized to distinct cellular compartments, both as part of normal mRNA biogenesis under optimal conditions and as a response to environmental changes. Recent findings suggest that the self-organization of mRNPs into membrane-less subcellular structures, known as RNA granules, plays a crucial role in mRNA metabolism (55).

SGs and PBs are among the most well-characterized RNA granules. These membrane-less cytoplasmic structures arise through the condensation of translationally inactive mRNPs.

Although the specific mRNAs and RNA-binding proteins (RBPs) contained within SGs and PBs vary, both types of granules play critical roles in translational regulation, impacting proteome composition and cell survival. The accumulation and clustering of untranslated mRNPs into these distinct cytoplasmic granules are driven by similar molecular mechanisms, which are closely linked to various aspects of translational control (56). While P-bodies are constitutively present in the cell, SG formation is a stress-induced event (57).

1.2.4.1 Stress Granules (SGs)

SGs are well-known examples of membrane-less organelles that form in the cytoplasm in response to cellular stress. Their assembly involves the accumulation of various proteins, including Poly(A)-binding protein (PABP), eukaryotic initiation translation factors (eIFs), and GTPase-activating protein-binding protein (G3BP) (58). SGs function as temporary storage sites for translationally inactive mRNAs, which can either be directed to PBs for degradation or returned to polysomes for translation (59). Their dynamics are regulated by ATP-dependent remodeling, allowing them to rapidly adapt to cellular changes. SG formation is primarily driven by weak electrostatic, hydrophobic, and protein-protein interactions among RNA-binding proteins (RBPs) that contain intrinsically disordered regions. Additionally, RNA molecules play a crucial role in SG assembly, highlighting the importance of RNA-RNA interactions in their structural organization and behavior (60,61).

1.2.4.2 P-bodies (Processing bodies - PBs)

P-bodies are conserved structures across all eukaryotes and play essential roles in mRNA degradation, translational repression, mRNA storage, and RNA silencing, helping to regulate protein production. P-bodies are described as "mRNA purgatory" and specialized compartments that contain a common set of enzymes and proteins involved in mRNA metabolism, ensuring efficient post-transcriptional regulation in eukaryotic cells (62). The regulation of mRNA is essential for cell function and survival. In various species, P-bodies play a key role in enabling cells to regulate protein production effectively, which is vital for responding to stress, growth signals, cell development, and environmental alterations. The formation and structure of P-bodies highlight the significance of compartmentalization in eukaryotic cells, aiding in the

maintenance of cellular balance and adaptability to changing conditions. For instance, during cellular stress, such as nutrient scarcity or heat shock, P-bodies may proliferate, assisting the cell in conserving resources by selectively repressing or degrading unnecessary mRNAs (63). P-bodies are present in a wide range of organisms, from simple yeast to more complex mammals, emphasizing their essential function in cellular biology (64).

Early studies revealed cytoplasmic granules such as "P granules" in the germline cells of the nematode *Caenorhabditis elegans* (65), and "naugs" in animals (66). The discovery of P-bodies dates back to initial research on mRNA metabolism, where they were first identified in yeast as sites for mRNA storage and degradation (67,68). Later studies found similar granules in mammalian cells, showing that they contain essential mRNA decay factors, including decapping enzymes and exonucleases, reinforcing their role in post-transcriptional gene regulation (69). P-bodies were subsequently identified in plants, including the model organism *Arabidopsis thaliana*, further demonstrating their presence across various plant species (70). This widespread occurrence of P-bodies across eukaryotes highlights their evolutionary significance and conserved function (71). In plants, P-bodies have evolved to play specialized roles in responding to environmental stresses such as drought and pathogen attacks, which are vital for survival and post-transcriptional gene regulation (72). For example, in *Arabidopsis thaliana*, P-bodies help regulate the expression of stress-responsive genes, enabling the plant to adapt to challenging conditions like drought and high temperatures. This adaptation highlights the evolutionary pressure to maintain effective mRNA regulation mechanisms (70,73,74). In mammals, including humans, P-bodies are involved in various biological processes, including development, immune responses, and potentially even the regulation of neuronal plasticity, influencing functions like learning and memory (75,76).

Although P-bodies are conserved across different organisms, their composition and function vary slightly between plants and mammals, reflecting the distinct physiological and environmental challenges each faces. In plants, P-bodies contain specific proteins (Table 1-1), such as Decapping Protein 5 (DCP5), which are absent in mammals. Instead, mammalian P-bodies rely on an alternative decapping system (72,77). Additionally, plant P-bodies regulate mRNAs that encode proteins essential for plant metabolism, including those involved in photosynthesis and energy production, which are absent in mammals due to their different

lifestyles and energy requirements (78). Plant P-bodies frequently interact with stress granules to regulate stress-related mRNA, a crucial adaptation for responding to abiotic stress (79). While similar interactions occur in mammals, they are more associated with immune responses and pathological conditions such as cancer and neurodegenerative diseases (59). Furthermore, plant P-bodies are influenced by hormonal signaling pathways, such as abscisic acid (ABA), during drought stress (80), whereas mammalian P-bodies are not regulated by plant-like hormonal control. Instead, they are often linked to complex regulatory networks involving miRNAs and other non-coding RNAs (72). While yeast P-bodies prioritize mRNA decay (81,82), mammalian ones emphasize silencing and immune responses (59,83), plant P-bodies integrate both developmental regulation, supporting rapid mRNA turnover during different conditions. This evolutionary divergence underscores their functional significance as adaptive hubs in eukaryotic cells.

1.3 The significance of investigating P-bodies in Cells

Studying P-bodies can provide insights into the evolution of post-transcriptional regulation across species, deepening our understanding of cellular biology and the genetic factors that contribute to the resilience and adaptability of eukaryotic cells. Gaining knowledge of these mechanisms offers a broader perspective on how different species have evolved to sustain cellular homeostasis under diverse conditions (84). Investigating P-bodies in plant cells is essential for unraveling the complex mechanisms of mRNA regulation and gene expression. By studying these structures, researchers can gain insights into how plants regulate gene expression and post-transcriptional processes during development and in response to environmental challenges like drought, salinity, and pathogen attacks, allowing them to allocate resources efficiently for survival. This understanding not only advances molecular biology research in plants but also contributes to the development of crop varieties with improved stress tolerance, which is vital for enhancing agricultural productivity and sustainability amid climate change (85). Furthermore, studying P-bodies has important implications for disease research and therapeutic development. Dysregulation of P-body function has been associated with various human diseases, such as cancer and neurodegenerative disorders. Investigating their composition and dynamics can help identify molecular targets for drug discovery and therapeutic interventions. Additionally, this research enhances our understanding of RNA

interference and the role of non-coding RNAs in gene silencing, paving the way for novel treatment strategies and advancements in genetic engineering (86).

1.4 Composition and Architecture of P-Bodies in Plants

The composition of P-bodies is intricate, dynamically shifting based on the tissue type, organism, and cellular conditions. Early studies on P-bodies primarily focused on identifying their components and understanding their role in mRNA processing. In eukaryotic cells, P-bodies contain a conserved set of proteins, including decapping enzymes (DCP), enhancers of decapping enzymes (EDC), exonuclease enzymes (XRN), LSM proteins, and GW182, which interact with microRNAs (miRNAs) and RNA-induced silencing complexes (RISC). These structures play a key role in miRNA-mediated gene silencing, mRNA degradation, and translational repression. Additionally, P-body regulation is closely tied to cellular stress responses and has been linked to various human diseases, such as cancer and neurodegenerative disorders, emphasizing their importance in maintaining cellular homeostasis (87). In plants, P-bodies consist of a diverse array of proteins (Table 1-1) and RNA molecules that play essential roles in mRNA metabolism. The functional and physical interactions of P-body proteins in *Arabidopsis thaliana* are clearly illustrated in (Figure 1-5) Key components include decapping enzymes, exonucleases, and various RNA-binding proteins, which work together to mediate mRNA decapping, degradation, and storage within P-bodies. This suggests a conserved mechanism for mRNA turnover across different organisms (73).

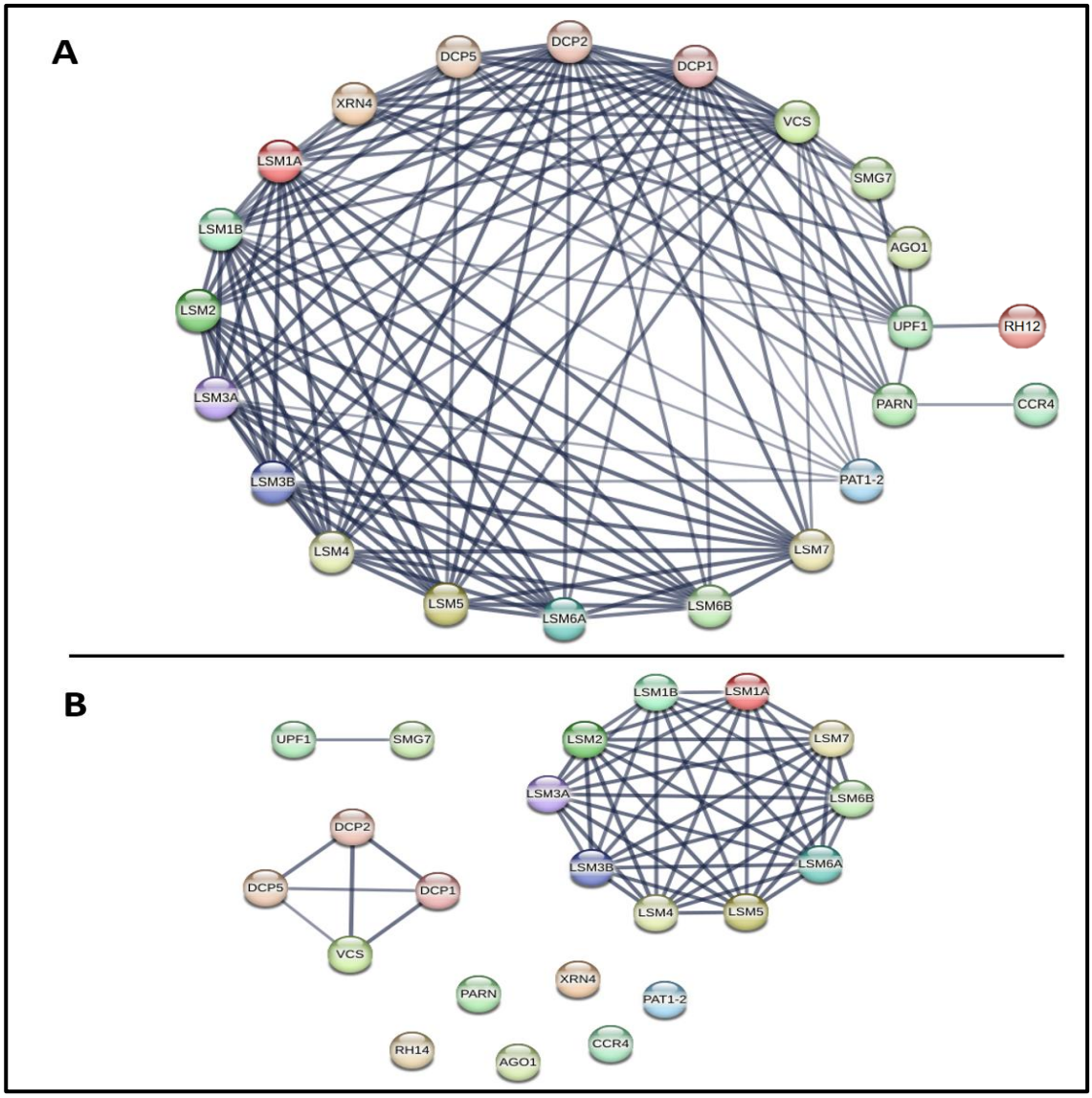

Figure 1-5. Functional protein associations and physical complex of P-Bodies Protein in *Arabidopsis Thaliana.* This visualized network comes from the (**https://string-db.org/**), multiple proteins identifier. A) The edges indicate functional associations with a confidence of 0.60. B) The edges indicate that the proteins are part of a physical complex with a confidence of 0.60. Each protein named by their main names or aliases (Table 1.1)

The structure of plant P-bodies is highly organized, ensuring efficient mRNA processing. They form through the assembly of cytosolic proteins (already identified as P-body components (Figure 1-6) along with non-translating mRNAs. Electron microscopy studies have shown that P-bodies appear as spherical or irregularly shaped structures of variable sizes. Their core houses the primary enzymatic machinery responsible for mRNA degradation, while a surrounding layer of RNA-binding proteins aids in the recruitment and processing of mRNAs. This well-structured organization is crucial for the effective role of P-bodies in mRNA regulation (84).

Plant P-bodies contain unique components not found in other eukaryotes, highlighting the specific requirements of plant cells. Certain plant-specific RNA-binding proteins play key roles in stress responses and development, which are vital for plant survival and adaptation. The presence of these distinctive components suggests that plant P-bodies have evolved specialized functions to support plant physiology and development, including processes such as photosynthesis and energy production. For example, research has shown that DCP1 and DCP2 are essential for post-embryonic development in *Arabidopsis thaliana*, as mutants lacking these proteins exhibit seedling lethality and vascular development defects. This strongly indicates that DCP1 and DCP2, as components of P-bodies, contribute significantly to plant development (72,88). The formation of P-bodies mediated by DCP5 is crucial for efficient mRNA decapping (73). Additionally, DCP5 has been shown to interact with the RNA chaperone cold shock domain protein 3 (AtCSP3), suggesting that RNA secondary structure unwinding may be required to facilitate decapping or suppress translation (89). In mutants with defects in P-body components, capped mRNAs accumulate due to the inability to degrade them through alternative RNA decay pathways. These mRNAs remain translatable by ribosomes, resulting in severe seedling lethality. Consequently, both mRNAs and their corresponding proteins become excessively abundant, leading to a dosage effect similar to that observed in gene overexpression (71)

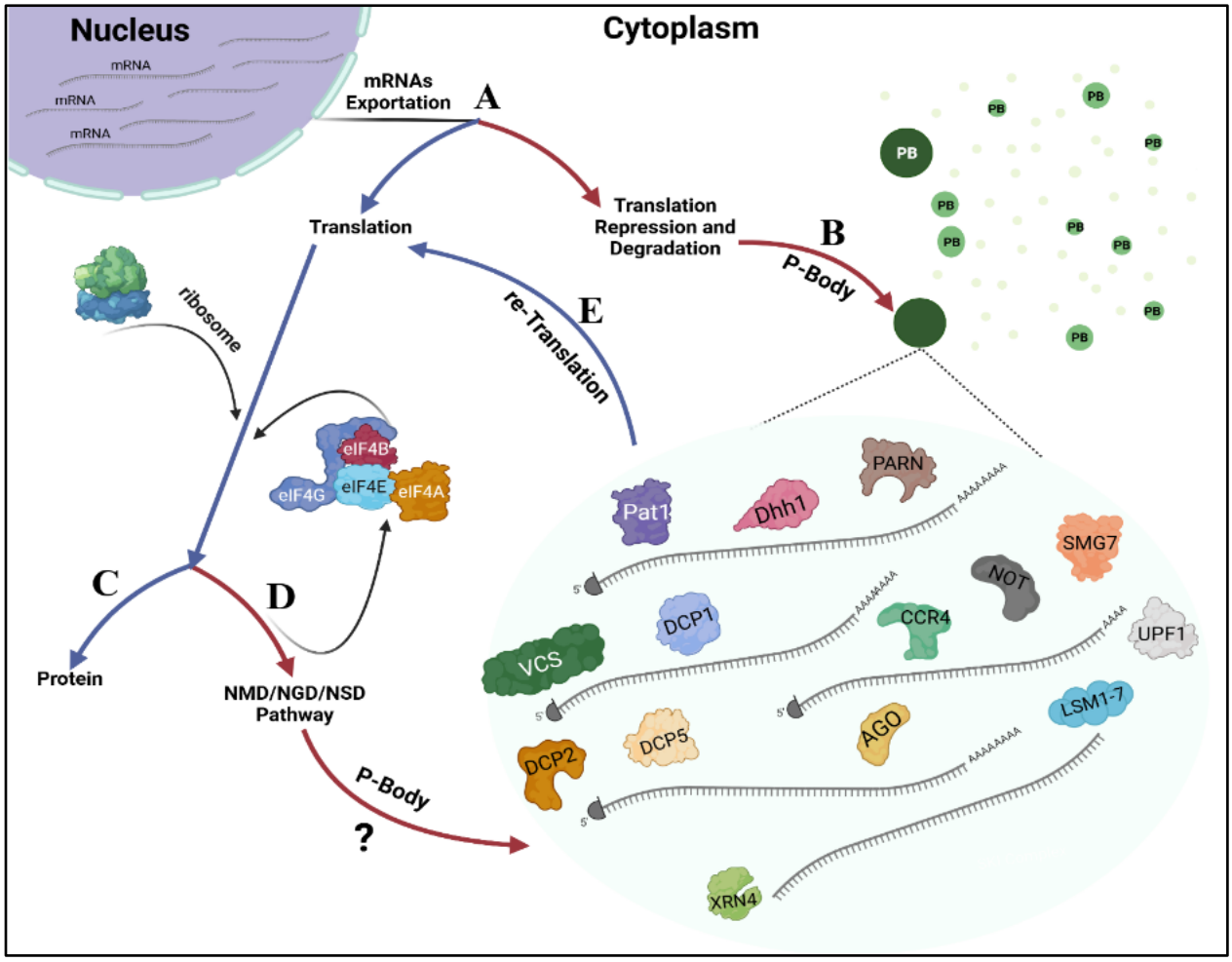

Figure 1-6. Overview of the mRNAs fate in the cytoplasm and the aggregation of P-bodies components. Blue arrows indicate the translation process, while **Red Arrows** denote the translational repression and decay process. **PB (P-Bodies)**: light green spots in the top-right cytoplasm represent cytosolic proteins known as PB components, which have not yet assembled in PBs. Medium green foci in the top-right cytoplasm show the accumulation of these proteins, forming PBs of various sizes. Dark green foci in the top-right cytoplasm indicate larger PBs. **A)** Exported mRNAs can undergo either translation or a repressed state and subsequently be decapped and degraded. **B)** Cytosolic proteins that facilitate PBs assembly, together with mRNAs targeted for translation repression, form PBs of different sizes throughout the cytoplasm (magnified PB). **C)** mRNAs intended for translation, along with Eukaryotic translation initiation factors (eIFs) and Ribosomes, form polysomes and proceed with translation. **D)** mRNAs with translation defects are degraded via multiple pathways. Transcripts containing a PTC are directed to nonsense-mediated decay (NMD). Meanwhile, mRNAs with stalled ribosomes in the coding region or those lacking a termination codon are targeted by no-go decay (NGD) and non-stop decay (NSD) pathways, respectively. These partially translated mRNAs may be transported to the PBs for degradation, although their transfer into plant P-bodies is still unclear. **E)** The re-translation of mRNAs from PBs allows the cell to rapidly adapt to changing conditions without transcribing new mRNAs, effectively "recycling" existing mRNAs in response to cellular needs.

Table 1-1. Recently Identified P-Body Proteins in Plants. The aliases and functions have been adapted by the Tair (www.arabidopsis.org/), Uniport (https://www.uniprot.org/) and NCBI (https://www.ncbi.nlm.nih.gov/).

Protein	Aliases	Function	References
DCP2 (mRNA-decapping enzyme subunit 2)	TRIDENT TDT	The catalytic component of the decapping complex, Removes the 7-methyl guanine cap structure from mRNA molecules.	(90,91)
DCP5 (Protein Decapping 5)	-	As a component of the decapping complex, it is involved in the degradation of mRNAs.	(73,92,93)
DCP1 (mRNA-decapping enzyme subunit 1)	-	The component of the decapping complex, Removes the 7-methyl guanine cap structure from mRNA molecules.	(94)
EDC4 (Enhancer of mRNA-decapping protein 4)	VARICOSE VCS	As a component of the decapping complex, promotes efficient removal of the monomethyl guanosine (m7G) cap from mRNAs.	(79,95)
XRN4 (5'-3' exoribonuclease 4)	AIN1 EIN5	Major 5'-3' exoribonuclease involved in mRNA decay, Degrades transcripts that lack a 5'-cap structure.	(72,96,97)
Lsm1-7 (U6 snRNA-associated Sm-like protein)	LSM1A LSM1B LSM3A LSM3B LSM5:SAD1 LSM7: EMB2816	Heptameric complex which is involved in mRNA degradation by promoting decapping and leading to accurate 5'-3' mRNA decay.	(79,98,99)
Pat1 (Protein-associated with topoisomerase1, 3'-5'-exoribonuclease)	PAT1H	Activator of decapping that acts as a general and active mechanism of translational repression and is required for P-body formation. Known as Deadenylation-dependent mRNA-decapping factor PAT1.	(100,101)
Dhh1 / DDX6 (DEAD/DExH box ATP-dependent RNA helicase)	RH6 RH8 RH12	ATP-dependent RNA helicase is involved in mRNA turnover, and more specifically in mRNA decapping by activating the decapping enzyme DCP1.	(102,103)
CCR4 (CCR4-Not complex 3'-5'-exoribonuclease)	ATCAF1 CAF1	A member of the CCR4-NOT complex, and acts for mRNA deadenylation and is	(104,105)

		linked to various cellular processes including bulk mRNA degradation.	
NOT (CCR4-Not complex 3'-5'-exoribonuclease)	-	A member of the CCR4-NOT complex, it acts for mRNA deadenylation and is linked to various cellular processes including bulk mRNA degradation.	(72,106)
PARN (Poly(A)-specific ribonuclease, 3'-5'-exoribonuclease)	AHG2	Interacts with the 3'-end poly(A) tail to remove the Poly(A) tail.	(107,108)
AGO1 (Protein argonaute)	-	The main component of the RNA-induced silencing complex (RISC) that binds to a short guide RNA such as miRNA or siRNA	(109)
UPF1 (UP-FRAMESHIFT1)	ATUPF1 LBA1 RENT1	RNA-dependent helicase is required for the nonsense-mediated decay (NMD) of aberrant mRNAs containing premature stop codons.	(110,111)
SMG7 (Nonsense-mediated mRNA decay factor SMG7)	F7K24	Involved in nonsense-mediated mRNA decay (NMD). It may provide a link to the mRNA degradation machinery to initiate NMD and serve as an adapter for the UPF protein function.	(79,112)

In this study, we focus on a subset of P-body proteins that play crucial roles in mRNA decapping and degradation, specifically DCP5, DCP2, LSM4 (a member of the LSM1-7 heptameric complex), EDC4 (VCS), and XRN4. These proteins were selected based on their functional significance and unique roles in plant mRNA metabolism.

1.4.1 Key mRNA-Decapping Enzymes in Plants: DCP1, DCP2, and DCP5

DCP1, DCP2, and DCP5 are key components of the mRNA decapping complex in plants, playing a crucial role in regulating gene expression in response to environmental stresses, developmental signals, and hormonal signals (73). This complex plays a significant role in controlling mRNA stability and degradation, making decapping a crucial step in post-transcriptional gene regulation (Figure 1-7). The efficient regulation of mRNA decay ensures

that transcripts are promptly eliminated once their function is complete or when the plant needs to adapt rapidly to changing conditions.

a. DCP2 (Decapping Protein 2) serves as the catalytic core of the decapping complex, responsible for removing the 5' cap from mRNA molecules. This cap removal signals the transcript for degradation by exonucleases like XRN4. DCP2 is also localized in P-bodies, where it interacts with DCP1, DCP5, and other decapping enhancers. Since uncontrolled decapping can result in unintended mRNA degradation and disrupt gene expression, DCP2 activity is highly regulated (92,94). The amino acid length of plant DCP2 is around 370 aa, and the molecular weight of the protein is 42 kDa (Uniport.org).

b. DCP1 (Decapping Protein 1) is a regulatory protein that acts as a scaffold, facilitating the recruitment of DCP2 and other decapping factors to assemble the decapping complex. While DCP1 lacks catalytic activity, it plays a crucial role in enhancing DCP2 function, ensuring efficient and selective mRNA decapping. It is predominantly localized in P-bodies (92,113). The amino acid length of plant DCP1 is around 367 aa, and the molecular weight of the protein is 40 kDa (Uniport.org).

c. DCP5 (Decapping Protein 5) functions as a cofactor that enhances the activity of the DCP1-DCP2 complex. It facilitates the recruitment of mRNAs to the decapping machinery, assisting in the assembly of the complex on target mRNA substrates. DCP5 plays a crucial role in regulating mRNA stability, particularly in response to stress, development, and growth regulation. Like DCP1 and DCP2, DCP5 is localized in P-bodies, where it contributes to the selective degradation of mRNAs (92). It is hypothesized that DCP5 initially binds to mRNA, keeping it in a translationally repressed state. It then facilitates the recruitment of DCP1 and DCP2 to assemble the active decapping complex, where DCP2 removes the 5' cap (71,73). DCP5 promotes the LLPS of Sister of FCA (SSF), enhancing SSF's ability to regulate Flowering Locus C (FLC) transcription. While PB components are typically associated with post-transcriptional regulation, DCP5's nuclear role in modulating RNA Polymerase II enrichment at the FLC locus highlights its involvement in transcriptional control (114). DCP5 has also been identified as a multifunctional osmosensor that participates in both osmosensing and osmotic stress adaptation, and suggests a stress sensory function for hyperosmotically induced stress granules. DCP5 undergoes phase separation in response to molecular crowding

via its intrinsically disordered region (IDR), which contains a land plant–specific intramolecular crowding sensor (ICS). This sensor detects crowding through conformational changes and promotes phase separation via hydrophobic interactions. DCP5 condensates represent a unique class of plant stress granules, termed DCP5-enriched osmotic stress granules (DOSGs), which recruit mRNAs through interactions with poly(A)-binding proteins (PABs). By sequestering mRNAs and translation regulators, DOSGs shift gene expression from growth to stress adaptation (115). In addition, the amino acid length of DCP5 is around 611 aa, and the molecular weight of the protein is 64 kDa (Uniport.org).

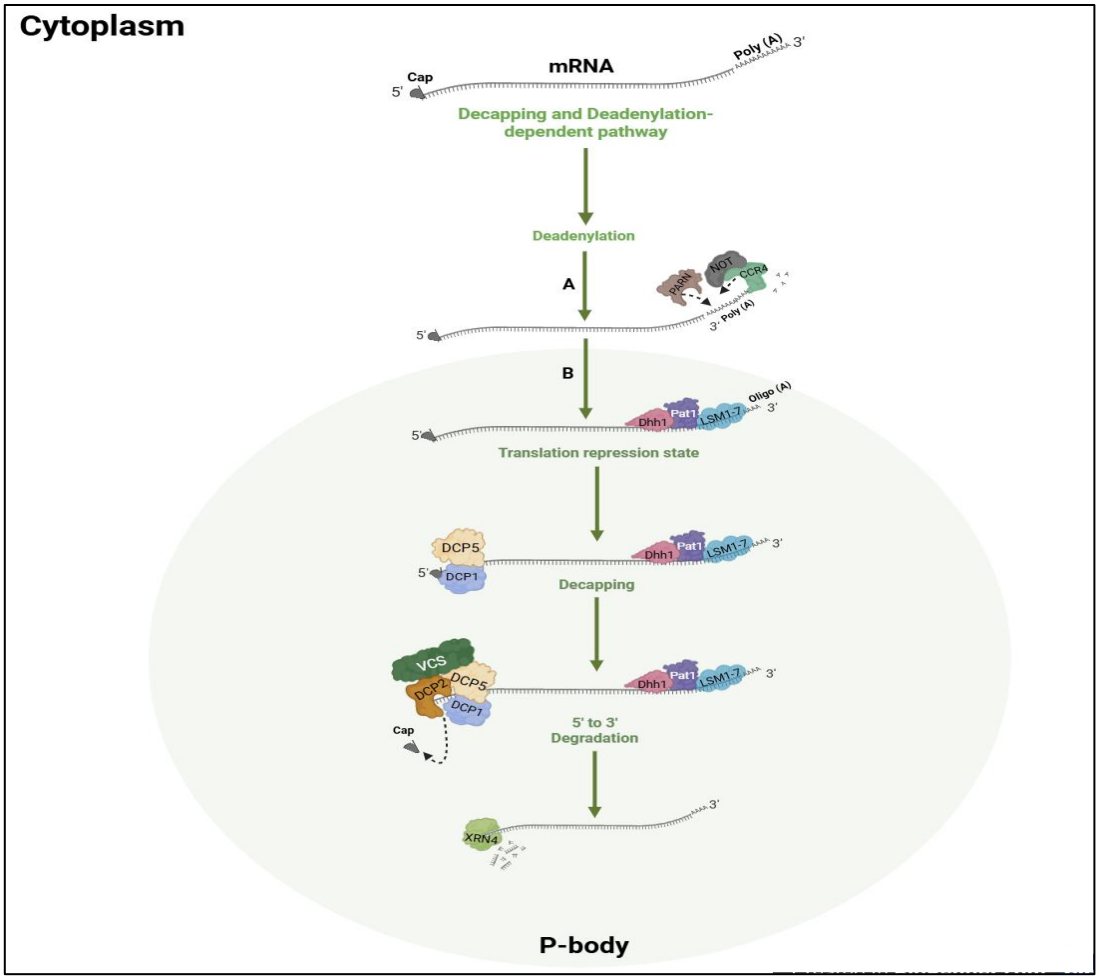

Figure 1-7. Schematic illustration of the mRNA degradation pathway associated with PBs in Plants. In the decapping and deadenylation-dependent pathway, mRNA degradation occurs involving sequential deadenylation, translation repression, decapping, and degradation. The polyadenylated tail is shortened by the PARN and CCR4-NOT complex, or they can act independently, which destabilizes the mRNA and makes the oligoadenylated tail or shortened polyA tail in the cytoplasm (A). The active deadenylation within PBs has not been confirmed yet in plants. LSM1-7-Pat1-Dhh1 complex recognizes the oligoadenylated tail of mRNAs to recruit the decapping proteins within PBs (B). The mRNA transitions into a translational repression form within PBs, where DCP5 and DCP1 are recruited (Translation repression state). The mRNA's 5′ cap is removed by the DCP2 enzyme, assisted by cofactors DCP1, DCP5, and VCS (Decapping). After decapping, the exonuclease XRN4 degrades the mRNA from the 5′ end (5′ to 3′ degradation).

1.4.2 EDC4 (VCS, Enhancer of Decapping 4)

The EDC4 protein, also known as VARICOSE (VCS) in plants, is a key regulator of mRNA decapping and plays a vital role in mRNA turnover. Acting as a scaffold, EDC4 coordinates the interactions of DCP1, DCP2, and DCP5, facilitating efficient mRNA decapping (Figure 1-7). The amino acid length of plant VCS is around 1,344 aa, and the molecular weight of the protein is 145 kD (Uniport.org). By directly binding to DCP1, it stabilizes DCP1 within the complex and aids in recruiting mRNA substrates. Additionally, EDC4 enhances the catalytic activity of DCP2. It also promotes the recruitment of DCP5, assisting in the assembly of the decapping machinery for specific mRNAs. Primarily localized in P-bodies, EDC4 is essential for maintaining proper gene expression during environmental stress and developmental processes, enabling plants to adapt effectively to changing conditions (94,95). The requirement of additional components for growth indicates that DCP2 activity may be a rate-limiting factor in vivo. The decapping process could depend on the formation of a complex involving DCP2, DCP1, DCP5, and VCS, or alternatively, DCP1, DCP5, and VCS may participate in upstream regulatory steps. One potential mechanism suggests that the assembly of translationally repressed RNPs is necessary before decapping can occur. This idea is reinforced by the fact that DCP5 alone has been shown to inhibit mRNA translation in vitro (73,94).

1.4.3 LSM Proteins (Like-Sm Proteins)

LSM (Like-Sm) proteins are a group of RNA-binding proteins that are crucial in various aspects of mRNA metabolism, such as splicing, stabilization, and degradation. They feature a Sm-like domain, enabling interactions with RNA and various protein partners. In plants, LSM proteins are vital for regulating mRNA decay, thereby ensuring proper gene expression under different developmental and environmental conditions (116). In addition, the LSM complex that functions in mRNA decay appears to be distinct from the U6-associated LSM complex, indicating that LSM proteins form specific complexes that affect different aspects of mRNA metabolism (117). The LSM protein family is categorized into two subfamilies: Sm and LSM. The Sm subfamily consists of seven core proteins (SmB/B′, SmD1, SmD2, SmD3, SmE, SmF, and SmG), which assemble into heteroheptameric complexes. These complexes associate with snRNAs from both the major spliceosome (U1, U2, U4, and U5 snRNAs) and the minor

spliceosome (U11, U12, and U4atac snRNAs). Conversely, the LSM subfamily consists of eight proteins (LSM1–LSM8), which also assemble into heteroheptameric complexes. Among them, six (LSM2, LSM3, LSM4, LSM5, LSM6, and LSM7) share homology with Sm proteins, while LSM8 exhibits a weak resemblance to SmB/B′, and LSM1 lacks notable similarity to any Sm protein (118). Two key heptameric complexes formed by LSM proteins, LSM1-7, localized in the cytoplasm, and LSM2-8, localized in the nucleus, each perform distinct yet interrelated functions in RNA processing and regulation (98). Both LSM complexes share a preference for the 3′ ends of RNAs, the LSM1-7 ring for 3′ oligoadenylated tracts, and the LSM2-8 for 3′ oligouridinylated (oligo-U) tracts (119,120).

1.4.3.1. LSM1-7 Complex

The LSM1-7 heptameric complex mainly functions in the cytoplasm, where it aids in mRNA degradation. It is responsible for recognizing the deadenylated mRNAs and binding to the 3' ends of oligoadenylated mRNAs that are targeted for decay. By recognizing and binding oligoadenylated 3′ ends of mRNAs targeted for decay, LSM1–7 plays a pivotal role in decapping (98,121):

Marking mRNA for Decay: The complex attaches to the 3′ ends of the mRNA, signaling that the transcript is ready for degradation.

Promoting Decapping: This binding event recruits decapping factors such as DCP1, DCP2, and DCP5, thus enhancing the low intrinsic enzymatic activity of the decapping complex (122). Once the 5′ cap is removed, exonucleases rapidly degrade the transcript.

Localization in P-bodies: LSM1-7 is mainly found in P-bodies (Figure 1-7), where it works with other RNA decay factors to control mRNA stability and turnover. It may also play a role in the selective degradation of specific mRNAs during environmental stresses, helping to regulate adaptive gene expression responses (98,123).

1.4.3.2. LSM2-8 Complex

In contrast, the LSM2–8 complex mainly operates in the nucleus, where it plays a role in pre-mRNA splicing. This heptameric structure is a component of spliceosomal complexes that

remove introns from pre-mRNA, ensuring that only mature mRNAs are transported for translation (123).

Splicing Facilitation: LSM2-8 binds to the 3' ends of pre-mRNAs, stabilizing them during processing and facilitating their proper export to the cytoplasm.

mRNA Stability: Although its main focus is splicing, LSM2–8 also helps shield newly spliced transcripts from premature degradation, thereby supporting overall mRNA integrity (123).

1.4.3.3 LSM4 (Like-Sm protein 4)

LSM4 is a member of the LSm protein family, which comprises RNA-binding proteins involved in various aspects of RNA metabolism, including mRNA processing, splicing, and degradation. Among the LSM proteins that form the LSM1-7 and LSM2-8 complexes, LSM1 promotes the constitution of an LSM1-7 complex in the cytoplasm that plays a crucial role in the decapping complex. In contrast, LSM8 directs the formation of the LSM2-8 complex that localizes in the nucleus and forms, together with the U6 snRNA, the U6 snRNP (small nuclear ribonucleoprotein) (118). Therefore, LSM1 is absent from the nuclear LSM2-8 complex, which is involved in snRNP biogenesis and splicing. Since LSM1 is exclusive to the LSM1-7 complex, it is often used among the other LSM proteins as the primary marker for P-body investigation in plants and other organisms. Although many studies reported the significance of LSM1 in P-body assembly, LSM4 is another essential protein inside the LSM1-7 complex for P-body function (98,123). In *Saccharomyces cerevisiae*, the C-terminal Q/N-rich domain of the LSM4 subunit within the LSM1-7 complex is crucial for P-body formation. However, in most eukaryotes, this C-terminal region consists of RGG domains instead of Q/N-rich sequences. The RGG domain of LSM4 enhances P-body accumulation in human cells, and the symmetric dimethylation of arginine residues within this domain further promotes this process. A mutant form of LSM4 lacking the RGG domain was unable to restore PB formation in cells where endogenous LSM4 was depleted. This deficiency persisted despite the mutant maintaining its capacity to assemble with the LSM1-7 complex, interact with decapping factors, and support mRNA decay and translational repression (124). In yeast, LSM1 and/or LSM4 subunits of the LSM1–7–Pat1 complex directly contact the RNA (121). In yeast and animal LSM complexes, LSM1 and LSM8 are flanked by LSM2 and LSM4, indicating that *Arabidopsis* LSM1A,

LSM1B, and LSM8 are capable of interacting in vivo with LSM2 and LSM4. Consistent with the typical cytoplasmic localization of LSM1 proteins in *Arabidopsis*, LSM1(A or B)–LSM2 and LSM1(A or B)– LSM4 interactions were mainly reported in the cytoplasm of the *Nicotiana benthamiana* cells. Conversely, interactions between LSM8 and LSM2 and LSM4 were essentially detected in the nucleus, which is consistent with the dual function of LSM4. Interactions between LSM2 and LSM4 proteins were not found. However, interactions between LSM2 and LSM3 (A and B), LSM3 (A and B) and LSM6 (A and B), LSM6 (A or B) and LSM5, LSM5 and LSM7, and LSM7 and LSM4 were identified in the plant (98).

1.4.4. XRN4 (5'-3' exoribonuclease 4)

In plants, XRN4 serves as the functional equivalent of XRN1 in yeast and plays a pivotal role in mRNA decay. As a 5' to 3' exonuclease, it degrades RNA by sequentially removing nucleotides from the 5' end toward the 3' end. By regulating mRNA turnover, XRN4 helps control gene expression in response to developmental signals and environmental stresses. Its activity becomes essential after mRNA has undergone decapping, once the protective 5' cap is removed, XRN4 recognizes the exposed 5' monophosphate end and initiates degradation. Functioning in coordination with DCP2, DCP5, DCP1, and EDC4, XRN4 operates as a key component of the mRNA decay pathway (Figure 1-7) (71). The amino acid length of plant XRN4 is around 947 aa, and the molecular weight of the protein is 107 kDa (Uniport.org). XRN4 acts downstream of the decapping process initiated by these proteins. After decapping is completed, XRN4 takes over and degrades the mRNA, ensuring the efficient removal of unwanted transcripts (125). XRN4 plays a crucial role in plants' responses to environmental stresses like heat, drought, and pathogen attacks. It controls the degradation of stress-related mRNAs, enabling plants to quickly modify their gene expression patterns and adapt to challenging conditions (126). XRN4 regulates the levels of unneeded proteins by degrading specific mRNAs, which plays a key role in fine-tuning gene expression in plant cells, highlighting its function in post-transcriptional regulation (127). XRN4 is predominantly localized in the cytoplasm, and in some cases in P-bodies to provide a compartmentalized environment that enhances the efficiency and regulation of mRNA degradation compared with the cytoplasm (128). Some studies indicate that XRN4 can degrade certain transcripts targeted for decay through mechanisms distinct from classical decapping. In this scenario, XRN4

selectively degrades specific transcripts in *Arabidopsis* based on their RNA sequence. This process may involve alternative exonucleolytic pathways that bypass the need for DCP1 and DCP2 activity, though this remains unclear in plants and other organisms (125,129).

1.5 Dynamic Formation and Dissolution of P-Bodies

A defining characteristic of P-bodies is their dynamic nature. Their formation, stability, and function are carefully controlled through various mechanisms, including post-translational modifications (PTMs) of associated proteins, signaling pathways that regulate their dynamics, and interactions with other cytoplasmic granules. P-body assembly occurs through the aggregation of proteins and mRNAs, often triggered by stress conditions such as nutrient deprivation, oxidative stress, or viral infection. Their disassembly, on the other hand, involves the breakdown of these components, typically facilitated by ATP-dependent processes (62,130,131). By regulating these factors, cells can adjust their mRNA processing strategies according to shifting environmental and cellular demands. P-bodies assemble and disassemble swiftly in response to cellular conditions, a dynamic property essential for their role in mRNA regulation. This adaptability enables cells to respond rapidly to environmental or metabolic changes. The formation of P-bodies allows the sequestration and potential degradation of mRNAs that are unnecessary under specific conditions, helping to conserve resources and safeguard the cell from potential damage (132). Phase-separating RBPs often contain intrinsically disordered regions (IDRs), protein sequences that do not fold into a fixed three-dimensional structure, and do not expose defined secondary structures until they contribute to molecular interactions (133). Decapping factors are often modular and feature folded domains flanked or connected by low-complexity disordered regions. These disordered regions contribute to the assembly of decapping complexes and promote phase transitions that drive RNP granule formation (134), for instance, DCP5 (115), DCP2 (135) and EDC4 (134). Some of these IDRs contain binding sites that promote multivalent interactions or a large number of low hydrophobic sequences that have the ability to drive proteins to undergo liquid–liquid phase separation and thus aggregate into MLOs (136). The involvement of IDRs in phase transitions provides a biophysical angle to the characterization of proteins that harbor disordered regions (137). The connection between water and LLPS is especially pronounced in intrinsically disordered proteins (IDPs) and proteins with IDRs, which are particularly prone to undergo

LLPS. The extended and flexible structures of IDPs/IDRs enable them to engage in multiple transient interactions (138). Many studies with deletion constructs have shown that the IDRs are sufficient and perhaps necessary for LLPS (139–145).

The disassembly of P-bodies is just as crucial for cellular function as it enables the release and reuse of mRNA molecules when conditions become favorable. This process is typically driven by ATP-dependent mechanisms, such as helicases and chaperones, which break down the protein and RNA aggregates within P-bodies (146). As already mentioned, P-body formation is largely driven by protein-protein interactions among its components, which associate with non-translating mRNPs. Disrupting these interactions leads to P-body disassembly and eventual loss. For example, the depletion of LSm1, RCK/p54, eIF4E-T, and key proteins involved in miRNA processing, such as Drosha and its binding partner DGCR8, results in the disappearance of P-bodies in mammalian cells (77). The controlled disassembly of P-bodies allows mRNAs to be swiftly released for translation when required, facilitating rapid cellular adaptation to fluctuating environmental conditions (147).

1.6 The Significance of P-Bodies in Post-Transcriptional mRNA Regulation:

Essential or Dispensable?

As previously noted, P-bodies serve as hubs for the accumulation of decapping proteins and exonucleolytic enzymes, sequestering non-translating mRNPs to promote their decapping and degradation. However, the key question remains: Are these distinct cytoplasmic granules (P-bodies) truly essential for effective mRNA decay?

- Improved Storage and Degradation

While not all mRNAs undergo degradation within P-bodies (148), evidence indicates that their presence enhances and supports cytoplasmic mRNA storage, decapping, and degradation (149). Since mRNA decapping factors are found throughout the cytoplasm, decapping and degradation could also take place outside of large P-bodies, potentially within smaller aggregates of similar biochemical composition that are too small to be detected by a light microscope (150). Studies indicate that while P-bodies concentrate decapping enzymes, they do not limit their activity solely to these locations (151,152). Thus, while P-bodies may promote mRNA decay, several

independent pieces of evidence demonstrate that they are neither essential nor the exclusive site for mRNA decapping and degradation. On the other hand, a simpler view proposes that the accumulation of deadenylation, decapping, and decay factors within P-bodies helps coordinate deadenylation and decay processes, enhancing their efficiency and ensuring proper mRNA turnover (57). For example, by employing Rapid Inducible Decay of RNA (RIDR), researchers tracked RNA decay dynamics in cells and discovered that mRNAs degrade more quickly in P-bodies than in the cytoplasm. Upon induction, target mRNAs rapidly localized to P-bodies, where they underwent faster degradation compared to the slower decay seen in the cytoplasm. Additionally, knocking down key P-body proteins and RNA degradation enzymes confirmed that P-bodies play an active role in RNA decay. This was the first study to measure RNA degradation kinetics across different cellular compartments, emphasizing the role of P-bodies as specialized sites for rapid RNA degradation (81). Therefore, they serve as locations where mRNAs are temporarily sequestered, either stored for later translation or targeted for decay, depending on the cellular conditions. This dual function enables cells to regulate gene expression dynamically in response to various stimuli, while also providing a unique form of compartmentalization (153).

- Selective mRNA Regulation

Instead, P-bodies could act as an "isolator," segregating specific groups of mRNAs from the cytoplasm and marking them for degradation according to cellular requirements (153). For instance, as components of the 3′ to 5′ decay pathway are absent from P-bodies, their localization may help direct specific mRNAs toward distinct decay pathways (154,155). The mechanisms by which specific mRNAs are selected for distinct degradation pathways and how their fate is determined within P-bodies are being discovered in eukaryotes. For instance, RNA modifications in selecting specific mRNAs for PB-mediated degradation uncovered that m6A in the coding sequence (CDS) triggers translation-dependent mRNA decay via CDS-m6A decay, and refers to the potential P-body involvement, and recruitment of YTHDF2 for accelerated degradation (156,157). In *Arabidopsis thaliana*, evolutionarily conserved C-terminal region 8 (ECT8) was identified as an m6A reader protein and showed that its m6A-binding capability is required for salt stress responses. ECT8 accelerates the degradation of its target transcripts through direct interaction with the DCP5 within P-bodies (158). Moreover, in

Arabidopsis, the reduction of P-bodies in light-grown rh6, rh8, and rh12 mutant seedlings results in elevated accumulation and translation of stress-related mRNAs under non-stress conditions, indicating that P-bodies may help suppress these transcripts under normal conditions (159).

On the other hand, sequestering mRNAs and decapping machinery within P-bodies offers three key benefits to the cell. First, it separates the decapping machinery from functional mRNAs, preventing premature decapping of mRNAs that are not intended for degradation. This segregation enables the cell to regulate access to the machinery, adding an additional layer of control beyond the enzymatic degradation steps. Similar to other degradative processes in compartments like lysosomes or proteasomes, this compartmentalization within P-bodies likely provides functional advantages (160).

Secondly, sequestering mRNAs in P-bodies may act as a cellular buffering mechanism to maintain a balance between translation capacity and the pool of mRNAs being translated. When too many mRNAs compete for limited translation factors, none may acquire the necessary proteins for proper initiation, reducing the overall translation rates of all mRNAs. By isolating non-translating mRNAs, the cell ensures that the remaining mRNAs are efficiently translated. This fundamental buffering system may have also evolved to regulate mRNA degradation and storage (160).

The third possibility indicates that translational repression and/or mRNA decay targeting happen in two separate stages. Initially, translation is reduced, either passively due to the removal of the poly(A) tail or actively by the binding of a repressor protein. As mRNP complexes are dynamic, mRNAs in this state could potentially resume translation at low levels to avoid unintended expression. The second phase may follow, where repression is fully established and maintained (160).

While numerous studies have examined P-bodies in mammals and yeast under conditions of stress or infection (161–163), as well as in human P-bodies during cancer or neurodegenerative diseases (164,165), the understanding of P-body assembly in normal cellular conditions and during development remains unclear. Moreover, limited data is available on the presence of P-bodies not only in response to stress, infections, or disorders but also in normal conditions, where they exist independently of stress and are further induced under stress, unlike stress

granules (84). For example, during plant seed development, the formation of P-bodies results in the translational repression and degradation of mRNAs. Plants lacking key P-body components show marked developmental defects, highlighting the essential role of these cytoplasmic structures in controlling gene expression throughout plant development (71). In mammals, multiple studies discuss the role and formation of P-bodies during cell development. In a mouse fibroblast cell line, the XRN1 protein was found to localize in small granules and was particularly concentrated in distinct, prominent foci (166). Subcellular localization analysis in human HeLa cells revealed that LSM1 is mainly located in the cytoplasm. However, it is not uniformly distributed, as it is concentrated in small, distinct foci (167). In yeast, a few observations also indicate the presence of P-bodies in wild-type cells (168) oocyte Maturation, and Innate Immunity (169). These indicate that the P-bodies are also formed in cells under normal conditions, not exactly during some specific conditions.

1.7 Role of Plant P-bodies in mRNA Degradation and Turnover

Cytoplasmic mRNA degradation serves as a form of post-transcriptional regulation, and it is not solely initiated by specific cellular conditions or environmental factors. It plays a crucial role in maintaining proper gene expression, cellular balance, and quality control. Even in the absence of stress, mRNA turnover ensures that only correctly formed transcripts—those with the proper 5′ cap, start codon, stop codon, and poly(A) tail—are preserved. In stable environments, cells must also regulate mRNA levels to maintain a balance between synthesis and decay, optimizing resource utilization. Understanding how cells distinguish these processes is key to unraveling the regulation of mRNA turnover. Evidence shows that eukaryotes often produce defective mRNAs, such as those resulting from splicing errors, which are swiftly degraded to maintain the integrity of the global mRNA pool (77,170–172). Recent studies in plants have also shown that mRNAs with structural or functional defects are recognized and rapidly degraded by translation-dependent RNA quality control mechanisms, ensuring the maintenance of translational accuracy (173). In plants, P-bodies contain essential components of the mRNA degradation machinery and facilitate the removal of the 5' cap from mRNA, signaling the transcript for degradation and halting further translation (79). The decapping complex, mainly made up of DCP1, DCP2, and DCP5, plays a crucial role in this process. DCP5 initially binds to target mRNAs, keeping them in a translationally repressed state and aiding in

the recruitment of the decapping complex and VCS (EDC4). DCP1 functions as a regulatory protein, bringing in DCP2, the catalytic enzyme responsible for removing the 5′ cap, a tightly controlled and irreversible step in mRNA degradation (73). Once the cap is removed, the 5′ to 3′ exonuclease XRN4 degrades the uncapped mRNA, effectively lowering the pool of available transcripts (71). Additionally, the LSM1–7 complex binds to the 3′ end of oligoadenylated mRNAs and helps recruit decapping enzymes (98,174). Proteins like Pat1 and DDX6 (Dhh1) play a role in translational repression before decapping, collaborating with the LSM1–7 complex to promote decapping by interacting with the decapping machinery (Figure 1-7) (100,175). Importantly, mRNA degradation in P-bodies is a selective process, where certain mRNAs are marked for swift degradation in response to factors like nutrient scarcity, oxidative stress, or pathogen invasion (176).

1.8 Developmental Roles of P-Bodies Across Plant Life Stages

P-bodies exert profound effects on plant development, from seed germination to leaf and root growth, modulated by environmental cues.

- Role in Seed Germination

During seed germination, P-bodies are crucial for managing mRNA related to seed storage proteins (SSPs), such as oleosins and 12S/2S seed storage proteins. Research indicates that in wild-type *Arabidopsis*, these mRNAs are translationally repressed and degraded to prevent unnecessary protein synthesis post-germination. An experiment highlights that DCP5, a plant P-body constituent, is required for this repression. In the dcp5-1 knockdown mutant, SSP mRNAs are translated, leading to significant accumulation of their products in 6-day-old germinated seedlings. This abnormal translation disrupts normal seedling development, underscoring P-bodies' role in ensuring proper germination by clearing unnecessary mRNAs. Additionally, DCP5 and DCP1 accumulate during seed maturation, peaking in dry seeds, but decrease upon germination, while DCP2 is induced post-germination, suggesting a dynamic assembly oef P-bodies for mRNA storage and decapping during this transition (73). In *Arabidopsis*, reduced P-bodies in light-grown RH6, RH8 and RH12 mutants seedlings lead to increased levels and translation of stress-related mRNAs under non-stress conditions,

suggesting a role for PBs in repressing such transcripts (159). This dynamic change ensures that mRNAs are appropriately managed to support germination and early growth.

- Role in Leaf and Root Growth

P-bodies are essential for postembryonic development, particularly in leaf and root growth. An experiment noted that mutants deficient in P-body components exhibit severe developmental perturbations. For instance, DCP5 and VCS mutants show abnormal leaves and vascular defects, indicating that P-bodies regulate mRNAs critical for leaf morphology and vascular system development. Similarly, XRN4/EIN5 mutants, which are ethylene-insensitive, suggest P-bodies involvement in growth regulation influenced by ethylene, a hormone affecting leaf and root development (72). Further support shows that dcp5-1 mutants share developmental abnormalities with other decapping-deficient mutants (dcp1-1, dcp2-1, vcs-6), including pale and weak cotyledons at 6 days, which are the first leaves. This indicates P-bodies' role in early leaf development. For root growth, the same study notes decreased P-body size in root tip cells of dcp5-1 mutants, visualized by DCP1-CFP, suggesting P-bodies are present and functional in roots, likely regulating mRNAs necessary for root elongation and development. This aligns with the broader understanding that P-bodies facilitate efficient mRNA decapping, which is crucial for postembryonic growth processes (73). Moreover, in *Arabidopsis*, VCS interacts with the decapping factor DCP5 and co-localizes in P-bodies, and overexpression of VCS enhances resistance to *Pseudomonas syringae* and boosts basal immunity. The vcs mutant shows altered ABA responses and reduced sensitivity to ABA-inhibited root growth, indicating a role in seed germination and development. VCS also promotes early flowering, seedling growth, and reduces transpiration. Overall, VCS contributes to stress tolerance and has potential for improving crop resilience (95).

1.9 Investigation of Cajal Bodies as nuclear biomolecular condensate in post-transcriptional regulation in *Larix decidua*

Eukaryotic cell nuclei contain distinct structures known as nuclear bodies, many of which play a role in RNA metabolism. The nuclear bodies identified in mammalian nerve tissue by the Spanish scientist Ramón y Cajal are recognized as part of this category. One hundred years after their discovery, they were renamed Cajal bodies (177). Cajal Bodies (CBs) are membraneless

subnuclear structures that play a crucial role in RNA metabolism and ribonucleoprotein (RNP) assembly. As biomolecular condensates, CBs form through LLPS, allowing the dynamic compartmentalization of molecules without physical barriers. CBs are primarily involved in the biogenesis and maturation of small nuclear RNAs (snRNAs), small nucleolar RNAs (snoRNAs), and other RNP complexes. These processes are essential for pre-mRNA splicing, ribosomal RNA modification, and the assembly of functional ribonucleoproteins. The formation of these bodies in both plant and animal cells relies heavily on the coilin protein. Besides coilin, the synthesis, processing, recruitment, and maturation of different RNAs play a vital role in the assembly of CBs across both plants and animals (178). These structures house various types of U RNAs associated with splicing, including U1–U5, which exist in their mature form and possess a trimethylguanosine (m3G) cap at the 5′ end, U6, and immature forms of these small nuclear RNAs. These structures have been shown to contain Sm proteins, which, in combination with U snRNA, form the spliceosome (179).

Genes in conifer *Larix Decidua* (European Larch) microsporocytes are transcribed in bursts. In European larch microsporocytes (male germline precursors), the diplotene stage takes approximately five months and can be subdivided into multiple substages, allowing for detailed observation of each phase. During diplotene, five distinct bursts were observed. This stage is characterized by significant microsporocyte growth, during which various RNAs and proteins are synthesized and accumulated. Over this extended period, microsporocytes expand in volume by more than three times. In larch, microsporocytes undergo chromatin morphology transitions, cycling between condensed, transcriptionally inactive states (contraction) and more relaxed, transcriptionally permissive phases (diffusion) (180). Previous findings revealed that a substantial amount of poly(A) RNA accumulates in the nucleus of larch microsporocytes at the onset of transcription. These transcripts remain in the nucleus for an extended duration, primarily stored within the nucleoplasm and CBs. The transcript pool within CBs progressively expands, peaking just before the large-scale release of poly(A) RNA into the cytoplasm. CBs serve as long-term storage sites for poly(A) transcripts, retaining them for several days. Notably, during the final stages of the poly(A) RNA cycle, most of these nuclear transcripts are sequestered within CBs (181). During the first three transcriptional bursts, mRNA is intensively synthesized. In the nuclei, large amounts of RNA polymerase II and high levels of snRNPs were

observed. During the late diffusion stages, including the fourth transcriptional burst and the poly(A) RNA cycle, newly synthesized mRNA is not immediately translated. Instead, it remains stored in the nucleus before being transported to the cytoplasm for translation at a later stage. In the fifth and final diffusion phase, poly(A) RNA levels experience a slight increase, even as splicing factors remain abundant. mRNA generated during the early phases is utilized throughout diplotene but does not persist into the dyad or tetrad stages. Conversely, mRNA synthesized in the later stages of diplotene, particularly those encoding splicing factors, essential enzymes, proteins, snRNAs, and ribosomal ribonucleoproteins, accumulate and are likely carried over to the dyad and tetrads, where they become active following the resumption of intensive transcription (180). CBs seem to play a crucial role in retaining mRNAs within the nucleus and regulating their eventual export to the cytoplasm.

1.10 Investigation of Sm bodies as cytoplasmic biomolecular condensate in post-transcriptional regulation in *Larix decidua*

Sm proteins are an evolutionarily conserved family of small RNA-binding proteins. In eukaryotic cells, the primary role of the spliceosome is in pre-mRNA splicing. However, limited research suggests that beyond this well-established function, Sm proteins may also influence mRNA processing at later stages of their lifecycle. Studies reported that canonical Sm proteins are integral components of the cytoplasmic mRNP complex, playing a role in the post-transcriptional regulation of gene expression in plants. Utilizing European larch microsporocytes as a model, a substantial pool of Sm proteins accumulating within distinct cytoplasmic structures were identified that also harbor polyadenylated poly(A) RNA. A link was established between the cyclic emergence of these cytoplasmic bodies and the cell's metabolic activity. Their formation was observed following transcriptional bursts, suggesting that these microdomains arise in response to episodic, large-scale mRNA synthesis. Based on the results obtained from studies on other model eukaryotic cells, it was proposed that Sm protein–mRNA bodies constitute newly described cytoplasmic domains involved in the post-transcriptional regulation of highly expressed transcripts, particularly in cells in which mRNA synthesis occurs in transcriptional bursts (182,183).

According to the information mentioned in the whole story, the study of P-bodies in plants has significantly advanced our understanding of post-transcriptional gene regulation, yet substantial gaps remain, particularly regarding their composition and function in *Larix decidua*. Despite extensive research on nuclear and cytoplasmic biomolecular condensates in this species, the intricate molecular architecture and specific roles of P-body components remain unexplored. This study seeks to bridge that knowledge gap by identifying and characterizing the essential proteins involved in mRNA decapping and degradation within *Larix decidua* P-bodies.

Understanding the contributions of these proteins—DCP5, DCP2, VCS (EDC4), LSM4, and XRN4 is crucial to unveiling the mechanisms underpinning post-transcriptional regulation in eukaryotes. These proteins are known to play indispensable roles in the decapping and subsequent degradation of mRNA, processes vital for maintaining cellular homeostasis, regulating gene expression, and enabling plants to respond to environmental stresses. Investigating their function within *Larix decidua* P-bodies extends beyond basic molecular biology, offering insights into the evolutionary conservation and species-specific adaptations of these regulatory networks.

Remarkably, no prior studies have simultaneously examined this unique combination of proteins in plant P-bodies during cell development. By elucidating their interactions and collective roles, this research aims to provide a more comprehensive picture of P-body functionality in plants. The simultaneous analysis of DCP5, DCP2, VCS, LSM4, and XRN4 represents a novel approach that could uncover new aspects of mRNA metabolism and degradation pathways. Such insights may further illuminate how plants fine-tune post-transcriptional regulation under the developmental phase, contributing to broader applications in plant biology.

Ultimately, this investigation addresses a critical void in the current understanding of cytoplasmic biomolecular condensates, emphasizing the importance of P-body components in *Larix decidua*. By shedding light on these unexplored mechanisms, the study paves the way for future research into plant post-transcriptional regulation, enhancing our knowledge of RNA dynamics and cellular adaptation strategies during homeostasis and developmental conditions.

2. Hypothesis and Objectives

P-bodies are widely implicated in post-transcriptional control, yet their developmental roles in plants, outside stress responses, remain poorly defined. Despite extensive work in yeast and metazoans, important gaps remain in our understanding of P-bodies' heterogeneous composition, dynamics, and transient functions across plant species, and the relative contributions of visible P-bodies versus smaller or transient RNP assemblies to mRNA fate are incompletely resolved. Moreover, there is little literature data on plants related to the simultaneous accumulation of isolated P-body components and mRNA; indeed, never in *Larix decidua*. In *Larix decidua* microsporocytes, diplotene spans ~5 months and features five cyclical waves of poly(A) RNA accumulation, followed by a marked cytoplasmic decline at the end of each cycle (Figure 2.1) (181,184,185). These observations have opened the crucial window onto cytoplasmic post-transcriptional regulation, stage-dependent RNA regulation in the *Larix decidua*, and led to a more detailed evaluation of the transcript degradation system in *Larix decidua* during diplotene of plant cell development. But it is unknown (i) whether P-bodies assemble developmentally (not only under stress), (ii) whether they act as sites of decapping/decay, and (iii) how P-body dynamics (number, size classes) relate to the poly(A) cycle.

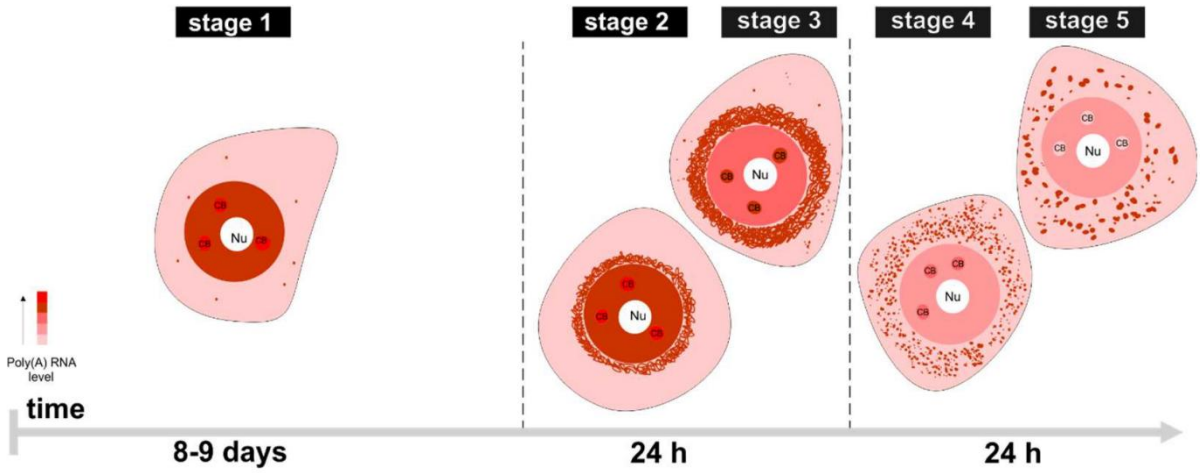

Figure 2.1 The stages of poly(A) RNA cycle (184)**.** During Stage 1, poly(A) RNA is predominantly confined to the nucleus, specifically within the nucleoplasm and Cajal bodies (CBs), where active transcription takes place. In Stages 2 and 3, poly(A) RNA begins its export to the cytoplasm. In Stage 2, substantial amounts still remain in the nucleus, whereas by Stage 3, the majority of poly(A) RNA has already been transported to the cytoplasm. Stages 4 and 5 are marked by reduced nuclear poly(A) RNA, with minimal levels in the nucleoplasm and none detected in CBs during Stage 5. Conversely, cytoplasmic concentrations remain high in both stages. CB – Cajal body; Nu – nucleolus.

Central hypothesis

During diplotene in *Larix decidua* microsporocytes, the late-cycle decline in cytoplasmic poly(A) RNA is contributed to by P-body-centered, decapping-dependent 5′→3′ decay. We further posit that DCP5–DCP2–EDC4 functions as a candidate core decapping module, while LSM4 (deadenylation cofactor) and XRN4 (5′→3′ exonuclease) act as stage-dependent partners. This suggests that the cytoplasmic degradation machinery plays a targeted role, warranting further investigation to uncover the mechanisms involved. Therefore, this doctoral thesis aims to reveal:

1- Determine whether the late-cycle poly(A) decline is driven by the decapping and degradation system.

2- Assess multiple components of the mRNA degradation machinery to determine the spatial distribution of decapping factors (DCP5 and DCP2), decapping cofactors (EDC4 and LSM4), the degradation enzyme XRN4, and the cytoplasmic poly(A) RNA cycle throughout the developmental stages of Larix decidua microsporocytes.

3- Examine whether these proteins play a key role in promoting P-body assembly during the developmental stages of *Larix decidua* microsporocytes, and verify that P-bodies are assembled under normal cellular developmental conditions, rather than exclusively in response to environmental stimuli previously reported in the literature.

4- Quantify P-body dynamics across the poly(A) cycle in the cell development of Larix decidua microsporocytes. Measure number/cell, mean volume, and volume-class distribution relate these metrics to poly(A) load and protein recruitment.

5- Verify whether P-bodies serve as the accumulation sites for mRNA transcripts during the poly(A) RNA cycle, thereby initiating the degradation process in *Larix decidua* microsporocytes.

6. Explore the enriched mRNA targets associated with decapping proteins (DCP2, DCP5, EDC4, and LSM4) to identify specific subsets of transcripts undergoing decapping and degradation during the poly(A) RNA cycle in *Larix decidua* microsporocytes.

3. Materials and Methods

3.1 Research Sample

The research material consists of microsporocytes of European larch (*Larix decidua Mill*.) during diplotene prophase I of the meiotic division. Microsporocytes are characterized by an extremely long period of meiosis, in which prophase I alone lasts about six months. Studies conducted in several growing seasons have shown that regardless of the temperatures in a given season, both the duration and the distribution pattern are similar. Microsporocytes initiate the leptotene stage in October, and the diplotene stage ends at the turn of March and April. In natural conditions, these cells demonstrate relatively high developmental synchronicity. Thanks to this, a relatively large and homogeneous population of microsporocytes can be obtained from larch anthers in individual phases of meiosis, which significantly facilitates studies of the processes occurring in these cells. Additionally, larch microsporocytes are characterized by a relatively thin pectocellulosic cell wall, which significantly facilitates the protoplasts for in situ studies. The selected cells are also characterized by their large size (approx. 70 μm in diameter), which allows for precise microscopic observation of individual cellular sub-compartments, as well as the nucleus and cytoplasm.

Earlier research from the Department of Cell Biology at Nicolaus Copernicus University demonstrated that larch microsporocytes undergo natural metabolic fluctuations across different developmental stages. These changes include variations in chromatin condensation, transcriptional activity (181), rRNA synthesis levels (186), and the spatial distribution of splicing machinery components (182). Moreover, in these cells, successive cycles of formation and disappearance of structures involved in RNA metabolism, such as nuclear Cajal bodies and cytoplasmic bodies rich in snRNP or mRNA, naturally occur (182,183). The features described above make *Larix decidua* microsporocytes a natural research model in which it is possible to observe individual stages of ribonucleoprotein metabolism under physiological and developmental conditions not induced by the experimenter.

3.2 Research Material

3.2.1 Oligonucleotides

The oligonucleotide that was used in this experiment was synthesized by the Genomed Company (ul. Ponczowa 12, 02-971 Warsaw, Poland).

In situ Hybridization		
Name	**Sequence (5' to 3')**	**Conjugated**
Poly(A) RNA	T(T) 42	Cy3

3.2.2 Antibodies

Primary Antibodies					
Name	**Clone**	**Origin**	**Antigen**	**Company**	**Labeled**
Anti-LSM4	polyclonal	Rabbit	LSM4	Sigma-aldrich HPA040932	unconjugated
Anti-LSM4	monoclonal	Mouse	LSM4	Sigma-aldrich SAB1412822	unconjugated
Anti-DCP5	polyclonal	Rabbit	DCP5	gift[1]	unconjugated
Anti-DCP5	polyclonal	Rabbit	DCP5	Davids Biotechnology 2601030019/2023/0146	unconjugated
Anti-DCP2	polyclonal	Rat	DCP2	Davids Biotechnology 2601030019/2023/0099	unconjugated
Anti-EDC4	polyclonal	Rabbit	EDC4	Davids Biotechnology 2601030019/2023/0146	unconjugated
Anti-XRN4	polyclonal	Rabbit	XRN4	Davids Biotechnology 2601030019/2024/0066	unconjugated
Anti-H3	polyclonal	Rabbit	Histone H3	Sigma-aldrich	unconjugated
Anti-ACTIN	polyclonal	Rabbit	Anti-α-Actin-1	Sigma-aldrich A2066	unconjugated
Secondary Antibodies					

[1] Gift from Prof. Shu-Hsing Wu, Academia Sinica, Taipei, Taiwan

Anti-Rabbit	polyclonal	Goat	Rabbit IgG	Thermo Fisher Scientific A32731	Alexa 488
Anti-Rabbit	polyclonal	Goat	Rabbit IgG	Thermo Fisher Scientific A21070	Alexa 633
Anti-Mouse	polyclonal	Goat	Mouse IgG	Thermo Fisher Scientific A11001	Alexa 488
Anti-Mouse	polyclonal	Goat	Mouse IgG	Thermo Fisher Scientific A21235	Alexa 647
Anti-Rat	polyclonal	Goat	Rat IgG	Thermo Fisher Scientific A11006	Alexa 488
Anti-Rat	polyclonal	Goat	Rat IgG	Thermo Fisher Scientific A21094	Alexa 633
Fab fragment Anti-Rabbit	polyclonal	Goat	Rabbit IgG	Jackson ImmunoResearch 111-007-003	unconjugated

3.2.3 Reagents

Name	Company
Formaldehyde 16%	Polysciences
Phosphate-buffered saline (PBS)	Sigma-Aldrich
Trisodium citrate ($C_6H_5Na_3O_7$)	POCH S.A.
Citric acid ($C_6H_8O_7$)	POCH S.A.
Cellulase Onozuka R-10	Duchefa Biochemie
Pectinase	Sigma-Aldrich
Triton X-100	Sigma-Aldrich
Formamid	Sigma-Aldrich
Saline-sodium citrate 20X (SSC)	Syngen
Ficoll 400	Sigma-Aldrich
Polyvinylpyrrolidone (PVP)	Sigma-Aldrich

Phosphate Buffer	Sigma-Aldrich
EDTA	Sigma-Aldrich
Bovine serum albumin (BSA)	Sigma-Aldrich
Acetylated BSA	Aurion
Hoechst 33342	Thermo Fisher Scientific
Prolong Gold antifade reagent	Thermo Fisher Scientific
Tris-HCL	Sigma-Aldrich
Sodium dodecyl sulfate (SDS)	Sigma-Aldrich
Sucrose	Sigma-Aldrich
Quick Start™ Bradford 1x Dye Reagent	Bio-Rad
Tris Base	Sigma-Aldrich
Acrylamide 30%	Sigma-Aldrich
Tetramethyl ethylene diamine (TEMED)	Sigma-Aldrich
Ammonium Persulfate (APS)	Sigma-Aldrich
Mini Format, 0.2 um PVDF	Bio-Rad
Midi Format, 0.2 um PVDF	Bio-Rad
Tween 20	Sigma-Aldrich
Dynabeads™ Protein G	Thermo Fisher Scientific
Dynabeads Protein A	Bio-Rad
Glycerol	Sigma-Aldrich
β-mercaptoethanol	Sigma-Aldrich
Bromophenol blue	Sigma-Aldrich
Potassium acetate	Sigma-Aldrich
Ditiotetriol (DTT)	Thermo Fisher Scientific
Magnesium chloride ($MgCl_2$)	POCH S.A.
Miracloth (Ø 22–25 um)	Sigma-Aldrich
Diethyl pyrocarbonate (DEPC)	Sigma-Aldrich
100 um Cell Strainer	Biologix
TriReagent	Sigma-Aldrich
Chloroform	POCH S.A.

Ethanol	POCH S.A.
	Stanlab
Isopropanol	Stanlab
PIPES	Sigma-Aldrich
Phasemarker™ Tubes	Thermo Fisher Scientific
Inhibitor Enzymes	
Protease Inhibitor Cocktail Tablets	Roche
ProClock Gold Plant Protease Inhibitor Cocktail	GoldBio
Phosphatase Inhibitor Cocktail Tablets	Roche
RNase Inhibitor 40U/ul	A&A Biotechnology
Reagents Kits	
Agilent RNA 6000 Pico Kit	Agilent
Qubit™ Protein Assay Kit, 100 assays	Thermo Fisher Scientific
Qubit™ RNA High Sensitivity (HS) Assay Kit	Thermo Fisher Scientific
Qubit™ 1X dsDNA High Sensitivity (HS) Assay Kits	Thermo Fisher Scientific
Agilent High Sensitivity DNA Kit	Agilent
Dynabeads® mRNA DIRECT™ Micro Kit	Thermo Fisher Scientific
RiboMinus™ Plant Kit for RNA-Seq	Invitrogen
NEBNext® Ultra™ II Directional RNA Library Prep Kit for Illumina®	New England Biolabs

3.2.4 Solutions, Buffers, and Mixtures

Buffer PBS 1x (200 ml)	
Phosphate-buffered saline (PBS)	1 Tablet
Double Distilled Water	200 ml

Paraformaldehyde 4% (Fixative Buffer) (40 ml)	
Formaldehyde 16%	10 ml
PBS 1x	20 ml
Double Distilled Water	Up to 40 ml

Citrate Buffer 10x (500 ml)	
Citric acid	4,2 g/200 ml H2O
Trisodium citrate	8,5 g/300 ml H2O
Adjust to pH 4.8	

Cell wall digestion buffer (2 ml)	
Cellulase Onozuka R-10	4%
Pectinase	27 U/ml
Citrate Buffer 10x	200 ul
Double Distilled Water	Up to 2 ml

Denhardt Solution 100x (100ml)	
Ficoll 400	1%
PVP	1%
BSA	1%
Double Distilled Water	Up to 100 ml

Antibody Buffer for Immunofluorescence (10 ml)	
acBSA	0.01%

PBS 1x	Up to 10 ml

Hybridization Buffer (5 ml)	
SSC 20x	1 ml
Denhardt Solution 100x	0.25 ml
EDTA 0.5 M	0.01 ml
Phosphate Buffer 0.5 M	0.5 ml
Formamid	1.5 ml
Double Distilled Water	Up to 5 ml

Protein Isolation Buffer (10 ml)	
Tris-HCL 1M PH 8	1 ml
Protease Inhibitor Cocktail (Roch)	1 Tablet
Phosphatase Inhibitor Cocktail	1 Tablet
Triton 100x	0.5% (v/v)
SDS 10%	100 ul
Double Distilled Water	Up to 10 ml

Lysis Buffer for CP-CoIP (10 ml)	
Tris-HCL 1M PH 8	500 ul
Protease Inhibitor Cocktail (Roch)	1 Tablet
Phosphatase Inhibitor Cocktail	1 Tablet
Potassium acetate 1M	1 ml
Magnesium acetate 1M	20 ul
Sodium fluoride 1M	10 ul
NP-40 10%	500 ul
DTT 1M	5 ul
Double Distilled Water	Up to 10 ml

Lower Buffer for Polyacrylamide Gel (1000 ml)	
Tris Base	168 gr
EDTA 0.5 M	16 ml
SDS 10%	40 ml
Double Distilled Water	700 ml
Adjust to pH 8.8 (Add HCL up to 1000 ml)	

Upper Buffer for Polyacrylamide Gel (500 ml)	
Tris Base	27.2 gr
EDTA 0.5 M	8 ml
SDS 10%	20 ml
Double Distilled Water	350 ml
Adjust to pH 8.8 (Add HCL up to 500 ml)	

Lower Part of Polyacrylamide Gel			
Glycin Gel for Western	**8%**	**10%**	**14%**
Acrylamide 30%	1.3 ml	1.625 ml	2.275 ml
Double Distilled Water	2.5 ml	2.125 ml	1.525 ml
Lower Buffer	1.25 ml	1.25 ml	1.25 ml
TEMED	4 ul	4 ul	4 ul
APS 10%	34 ul	34 ul	34 ul

Upper Part of Polyacrylamide Gel	
Glycin Gel for Western	**All Percentages of the Gel**
Acrylamide 30%	333 ul
Double Distilled Water	1.2 ml
Upper Buffer	500 ul
TEMED	7 ul
APS 10%	20 ul

Laemmli Buffer 4x (50 ml)	
Tris base	1.514 gr
SDS	4 gr
Glycerol	20 ml
β-mercaptoethanol	10 ml
Bromophenol blue	200 mg
Double Distilled Water	Up to 50 ml

Blocking Buffer for Western Blot (250 ml)	
BSA	5% 2.5% (w/v)
PBS 1x	Up to 250 ml

Antibody Buffer for Western Blot and Immunoprecipitation (250 ml)	
BSA	2.5% (w/v)
Tween 20	1% (v/v)
PBS 1x	Up to 250 ml

Washing Buffer for Western Blot and Immunoprecipitation (PBST) (250 ml)	
Tween 20	0.1% (v/v)
PBS 1x	Up to 250 ml

Elution Buffer for Immunoprecipitation (1 ml)	
Laemmli Buffer 1x	0.5 ml
Double Distilled Water	Up to 1 ml

DEPC-PBS (500 ml)	
DEPC	0.1% (v/v)
PBS 1x	Up to 500 ml

Buffer for RNA Immunoprecipitation (RIP) (10 ml)	
Tris-HCl 1M PH 8	2 ml
Triton 100x	0.5% (v/v)
Tween 20	0.1% (v/v)
DTT 1M	25 ul
Potassium acetate 1M	1.1 ml
Magnesium chloride (MgCl2) 1M	100 ul
ProClock Gold Plant Protease Inhibitor Cocktail	1% (v/v)
RNase Inhibitor 40U/ul	12.5 ul (50U/ml)
Double Distilled Water	Up to 10 ml

Washing Buffer for RNA Immunoprecipitation (RIP) (50 ml)	
Tris-HCl 1M PH 8	10 ml
Triton 100x	0.5% (v/v)
Tween 20	0.1% (v/v)
DTT 1M	125 ul
Potassium acetate 1M	5.5 ml
Double Distilled Water	Up to 50 ml

Elution Buffer for RNA Immunoprecipitation (RIP) (50 ml)	
Tris-HCl 1M PH 8	5 ml
EDTA 0.5 M	1 ml
SDS 10%	5 ml
Double Distilled Water	Up to 50 ml

3.3 Methods

3.3.1. Preparation of material for microscopic observation

Protoplast isolation for confocal microscopy

Male inflorescences of *Larix decidua* Mill. were collected at weekly intervals from October to March in five consecutive growing seasons (2020–2025). This period corresponds to successive stages of prophase I of meiosis.

After removing the covering scales, freshly collected inflorescences were fixed in 1.5 ml of 4% paraformaldehyde (PFA or Fixative Buffer) buffer at pH 7.2 for 12h. To eliminate air contained in the plant material, the fixation was carried out on ice in a vacuum pump (0.1 MPa) for the first hour, and then for 11h at 4°C. The fixed material was washed with 1xPBS pH 7.2 (3x 10 min) and three times in 1x citrate buffer pH 4.8 (3x 5 min). Then, microsporocytes were isolated by mechanical crushing of anthers with a glass rod on a watch glass (100 mm) in citrate buffer 1x pH 4.8. To remove the cell wall, the obtained cell suspension was subjected to enzymatic digestion in a mixture of 4% Onozuka R10 cellulase and 27 U/ml pectinase in citrate buffer 10x pH 4.8. Incubation was done for 12.5 min at 37°C, on the shaker (100 rpm). After digestion, the material was washed in 1x citrate buffer, pH 4.8 (3 x 3 min) and then in PBS 1x (3 x 3 min). Then, protoplasts were suspended in PBS and placed on previously frozen (-80°C) gelatinized glass slides and left to dry at RT for O/N.

3.3.2. Localization of Proteins and RNAs

Before starting the reaction, protoplasts were hydrated and permeabilized in 0.1% Triton X-100 in 1x PBS pH 7.2 for 15 min and then washed in 1x PBS pH 7.2 (3x 3 min). The controls of all reactions were performed according to the protocols given below, removing the incubation step with the primary antibody (only incubation in acBSA in 1x PBS pH 7.2) and the oligonucleotide probe (only incubation with hybridization buffer).

- Monolabeling of poly(A) RNA (In situ Hybridization)

Reactions were performed according to the protocol below:

1. Incubation with Cy3-conjugated oligo(dT) probe (poly(A) RNA), 1:200 in hybridization buffer, in a moist chamber (filled with 30% formamide) O/N at 26°C.

2- Washing in aqueous SSC solutions:

- 4 x SSC (4 x 1 min),
- 2 x SSC (4 x 1 min),
- 1 x SSC (1 x 10 min),
- PBS (1 x 3 min).

3. Sealing the preparations in ProLong Gold fluorescence-extending medium with ProLong Gold-Hoechst solution (Include 1:1000 of Hoechst in 27 µL of ProLong Gold/slide).

- Double labeling of poly(A) RNA and proteins (In situ Hybridization-Immunostaining)

Reactions were performed according to the protocol below:

1. Incubation with Cy3-conjugated oligo(dT) probe (poly(A) RNA), 1:200 in hybridization buffer, in a moist chamber (filled with 30% formamide) O/N at 26°C.

2- Washing in aqueous SSC solutions:

- 4 x SSC (4 x 1 min),
- 2 x SSC (4 x 1 min),
- 1 x SSC (1 x 10 min),
- PBS (1 x 3 min).

3- Incubation with 2% acBSA in 1xPBS pH 7.2 for 15 min at room temperature.

4- Incubation with Primary Antibody-Unconjugated (Anti-DCP5 1:800, Anti-DCP2 1:23, Anti-EDC4 1:96, Anti-LSM4 1:100, Anti-XRN4 1:78) in Antibody Buffer for Immunofluorescence, in a moist chamber (filled with water) O/N at 11°C.

5- Washing in 1x PBS pH 7.2 (4 x 3min).

6- Incubation with Secondary Antibody conjugated-Alexa488 (DCP5: Anti-rabbit, DCP2: Anti-rat, EDC4: Anti-rabbit, LSM4: Anti-rabbit, XRN4: Anti-rabbit) in a ratio of 1:200 in 0.01% acBSA in 1x PBS pH 7.2, in a moist chamber for 1.5 h at 37°C.

7- Washing in 1xPBS pH 7.2 (4 x 3min).

8- Sealing the preparations in ProLong Gold fluorescence-extending medium with ProLong Gold-Hoechst solution (Include 1:1000 of Hoechst in 27 µL of ProLong Gold/slide).

- Triple labeling of poly(A) RNA and proteins (In situ Hybridization-Immunostaining)

Reactions were performed like the above protocol in Double labeling up to the 7th step, and continued with the protocol below:

8- Incubation with Second Primary Antibody-Unconjugated (Anti-DCP5 1:100, Anti-DCP2 1:23, Anti-EDC4 1:96, Anti-LSM4 1:100, Anti-XRN4 1:78) in Antibody Buffer for Immunofluorescence, in a moist chamber (filled with water) O/N at 11°C.

9- Washing in 1xPBS pH 7.2 (4 x 3min).

10- Incubation with Second Secondary Antibody conjugated-Alexa633 (DCP5: Anti-rabbit, LSM4: Anti-rabbit, DCP2: Anti-rat, EDC4: Anti-rabbit, XRN4: Anti-rabbit) in a ratio of 1:200 in 0.01% acBSA in 1xPBS pH 7.2, in a moist chamber for 1.5 h at 37°C.

11- Washing in 1xPBS pH 7.2 (4 x 3min).

12- Sealing the preparations in ProLong Gold fluorescence-extending medium with ProLong Gold-Hoechst solution (Include 1:1000 of Hoechst in 27 µL of ProLong Gold/slide).

- Triple labeling of poly(A) RNA and proteins with primary antibodies from the same host species

Reactions were performed like the protocol in Double labeling up to the 7th step, and continued with the protocol below (Based on the mentioned protocol by (187):

8- Incubate in 10% normal serum from the same host as the primary antibodies (rabbit serum) for 3 hr RT to saturate open paratopes on the first secondary antibody.

9- Washing in 1xPBS pH 7.2 (3 x 3min).

10. Incubate with 50 μg/ml unconjugated monovalent anti-rabbit-Fab fragments (directed against the host of the primary antibodies in 0.01% acBSA in 1xPBS pH 7.2, to cover epitopes that could be recognized by the second secondary antibody, O/N at 4 °C.

11- Washing in 1xPBS pH 7.2 (3 x 3min).

12- Incubation with Second Primary Antibody-Unconjugated (Anti-DCP5 1:100, Anti-LSM4 1:100, Anti-XRN4 1:78) in Antibody Buffer for Immunofluorescence, in a moist chamber (filled with water) O/N at 11°C.

13- Washing in 1xPBS pH 7.2 (3 x 3min).

14- Incubation with Second Secondary Antibody conjugated-Alexa633 (Anti-rabbit) in a ratio of 1:200 in 0.01% acBSA in 1xPBS pH 7.2, in a moist chamber for 1.5 h at 37°C.

15- Washing in 1xPBS pH 7.2 (3 x 3min).

16- Sealing the preparations in ProLong Gold fluorescence-extending medium with ProLong Gold-Hoechst solution (Include 1:1000 of Hoechst in 27 μL of ProLong Gold/slide).

The controls of same host antibodies reactions were performed according to the protocols given below, while in one reaction removing the incubation step with the second primary antibody (only incubation in acBSA in PBS pH 7.2) to confirm the Fab-fragment function and in other one removing the incubation step with the first primary antibody (only incubation in acBSA in PBS pH 7.2) and second secondary antibody (only incubation in acBSA in PBS pH 7.2) to confirm the host-serum function.

3.3.3 Confocal Microscopy

Observations were performed using a Leica TCS SP8 confocal laser scanning microscope equipped with 7 laser lines exciting fluorescence from UV (405 nm) to far red (633 nm). In order to ensure the separation of recorded signals between channels, scanning of the slides was performed in sequential mode (separately for each channel). Optical sections were performed at 0.7 μm intervals. Results were recorded using LAS AF software.

3.3.4 Image Analysis

ImageJ software was used for image processing and analysis (188).

- Quantitative measurements

Images intended for quantitative measurements were recorded under identical acquisition conditions (laser power, range of light collected by the detector, amplification on the photomultiplier, and resolution). To eliminate non-specific background (mainly resulting from autofluorescence of plant cell cytoplasm), a threshold level was established based on the control reactions performed and then considered before starting the measurements. For each variant (stage), measurements were performed for 10–20 cells, depending on the experiment. Fluorescence levels were expressed in relative units, as mean intensity per μm3. Before the analyses, the images were appropriately processed (excluding the cell nucleus from the analyses, setting the background cut-off threshold).

- Intensity measurements

The cytoplasmic intensity of each picture was calculated using the measure option in ImageJ software. Additionally, to evaluate the statistical significance of the obtained intensity values in order to compare intensities in two groups and several groups, the Mann-Whitney U Test and Kruskal-Wallis one-way ANOVA test were performed, respectively.

- Colocalization measurements

The calculations of the ratio of colocalization of poly(A) RNA and each protein (DCP5, LSM4, DCP2, EDC4 and XRN4) in the cytoplasm of microsporocytes were performed in ImageJ, using the Colocalization analysis (Coloc-2) (https://imagej.net/imagej-wiki-static/Coloc2). Then the statistical analysis was performed as below:

- Pearson's colocalization coefficient (PC), taking values from -1 to 1, where the value -1 means inverse correlation (the presence of one factor excludes the co-presence of the other), 0 means no colocalization, and 1 means full colocalization.
- Manders co-localization coefficient (M1 and M2), taking values from 0 to 1, where 0 means no co-localization and 1 means full co-localization. In this work, the obtained

Manders coefficients were converted to percentage values, where the value 1 was converted to 100% co-localization.

M1: Represents the fraction of the intensity in Channel 1 that overlaps with Channel 2.

M2: Represents the fraction of the intensity in Channel 2 that overlaps with Channel 1.

$$M1 = \frac{\sum \mathrm{IC1} \cap \mathrm{C2}}{\sum \mathrm{IC1}}$$

$\sum \mathrm{IC1} \cap \mathrm{C2}$: The intensity of pixels in Channel 1 that have a non-zero intensity in Channel 2.

$\sum \mathrm{IC1}$: The total intensity in Channel 1.

M1 quantifies how much of the signal in Channel 1 is co-localized with Channel 2.

$$M2 = \frac{\sum \mathrm{IC2} \cap \mathrm{C1}}{\sum \mathrm{IC2}}$$

$\sum \mathrm{IC2} \cap \mathrm{C1}$: The intensity of pixels in Channel 2 that have a non-zero intensity in Channel 1.

$\sum \mathrm{IC2}$: The total intensity in Channel 2.

M2 quantifies how much of the signal in Channel 2 is co-localized with Channel 1.

To evaluate the statistical significance of the obtained colocalization coefficients (Pearson or Manders) values to compare colocalization of different stages, the Mann-Whitney U Test was performed.

- Measurement of volume and number of P-bodies

Measurements were performed by ImageJ, using the 3D Suite, 3D Manager, and Counter plugin (https://imagej.net/imagej-wiki-static/3D_ImageJ_Suite). Results are presented as the mean number of P-bodies per cell in each stage ± standard error of the mean (SEM), mean number of P-bodies per cell that classified by their volume (um3), mean volume of each P-body (μm3) in each stage ± standard error of the mean (SEM). Portion of P-body classified volume per cell in comparison with the sum volume in each stage. Differences between groups were statistically analysed using GraphPad Prism 9.0.0 software. One-way ANOVA with multiple comparisons was used to compare the numbers and volume of P-bodies in different stages.

3.3.5 Protein Analysis

Protein analyses were performed by the group of Biochemistry, Molecular and Cellular Biology, Veterinary School at Zaragoza University in Spain.

3.3.5.1 Total Protein Isolation (TP)

To isolate the total protein, the plant material was ground in liquid nitrogen, and then the protein isolation buffer was added in a proportion of 2 ml per 0.5 gr of material. The material was centrifuged at 16,000 g for 20 min, 4°C, and then the supernatant containing the total protein was stored in -20°C.

3.3.5.2 Cytoplasmic Fractionation (P-body enrichment) for Co-Immunoprecipitation (CP-CoIP)

Freshly collected anthers of *Larix decidua* Mill. were immediately frozen in liquid nitrogen and stored at -80°C. The protocol below was performed based on the modified protocol of (189,190):

1. 1.5- 2 gr of sample.

2- Samples were ground by dried ice in a microtube and homogenized (Homogenizer produced by Biospec Products) with 1.5 ml of sucrose (0.25M) for 1 min (4 microtubes were prepared to get more concentrated protein in the last step).

3- Centrifuge the microtubes (Eppendorf 5415R Refrigerated Centrifuge) for 5 min at 300 rcf, 4°C.

4- Transfer the supernatant of all microtubes to a new falcon (50 ml).

5- Centrifuge the falcon for 10 min at 1500 rcf, 4°C.

6- Transfer supernatants to a new falcon (50 ml).

7- Centrifuge the falcon for 15 min at 18000 rcf, 4°C.

8- Transfer supernatant to a new falcon.

9- Centrifuge the Falcon for 60 min at 100,000 rcf (60,000 rpm) (Optima ultracentrifuge beckman coulter), 4°C.

10. Add 500 µl Lysis Buffer for CP-CoIP to the pellet and pipette gently several times.

11- Transfer pellet to a filter falcon for protein purification (Amicon® Ultra Centrifugal Filter, 10 kDa MWCO).

12- Centrifuge the filter falcon for 5 min at 5000 rcf, 4°C to remove the sucrose and concentrate the isolated protein. Repeat this step up to get 300 µl of concentrated protein in the filter falcon.

13- Transfer the concentrated protein solution to a new microtube.

14- Put the microtube on the sonicator (Produced by Sonics Vibra Cell) (1min, Pulse on 10", Pulse off 15", amplitude 50%).

15- Store the protein in -20°C.

The obtained solution constituted the P-body fraction of anther cells, used for Western blot and Immunoprecipitation.

- Microscopic analysis to ensure the presence of P-bodies in the cytoplasmic fractionation solution

Reactions were performed according to the protocol below:

1- Isolated P-bodies from section 3.3.5.2 were suspended in fixative buffer and placed on previously frozen (-80°C) gelatinized glass slides and left to dry at RT for 24 h.

2- Incubation with Primary Antibody-Unconjugated (Anti-DCP5 1:800, Anti-DCP2 1:23, Anti-XRN4 1:78) in Antibody Buffer for Immunofluorescence, in a moist chamber (with few drops of water) O/N at 11°C.

3- Washing in 1xPBS pH 7.2 (3 x 3min).

4- Incubation with Secondary Antibody conjugated-Alexa488 (DCP5: Anti-rabbit, DCP2: Anti-rat, XRN4: Anti-rabbit) in a ratio of 1:200 in 0.01% acBSA in 1xPBS pH 7.2, in a moist chamber for 1.5 h at 370C.

5- Washing in 1xPBS pH 7.2 (3 x 3min).

6- Incubation with Second Primary Antibody-Unconjugated (Anti-DCP5 1:100, Anti-DCP2 1:23, Anti-EDC4 1:96, Anti-LSM4 1:100, Anti-XRN4 1:78) in Antibody Buffer for Immunofluorescence, in a moist chamber (filled with water) O/N at 11°C.

7- Washing in 1xPBS pH 7.2 (3 x 3min).

8- Incubation with Second Secondary Antibody conjugated-Alexa633 (DCP5: Anti-rabbit, DCP2: Anti-rat, XRN4: Anti-rabbit) in a ratio of 1:200 in 0.01% acBSA in 1xPBS pH 7.2, in a moist chamber for 1.5 h at 37°C.

9- Washing in 1xPBS pH 7.2 (3 x 3min).

10- Check the slide under the microscope.

To perform the control for this reaction, the above protocol was followed, except that the incubation steps with the first and second primary antibodies were omitted. Instead, incubation was carried out only in acBSA in PBS pH 7.2.

3.3.5.3 Bradford for measuring the protein concentration

The Bradford measurement was done by SPECTROstar Nano | BMG LABTECH, as protocol below:

1- Make the dilution from the samples

Dilution	
1:1	1 µl sample
1:2	1 µl sample:1 µl water
1:5	1 µl:4 µl
1:10	1 µl:9 µl
1:20	1 µl:19 µl
1:50	1 µl:49 µl
1:100	1 µl:99 µl
1:200	1 µl:199 µl

2- Add 2 µl from each dilution to each well of the plate (special plate for Bradford), 4 wells for each dilution needed for replication.

3- Make the dilution from the BSA

Dilution	
0	0
1:100	1 µg BSA:100 µl water
1:200	1 µg BSA:200 µl water
1:400	1 µg:400 µl
1:600	1 µg:600 µl
1:800	1 µg:800 µl
1:1000	1 µg1000 µl

4- Add 2 µl from each dilution of BSA to adjacent wells of the sample, 4 wells for each dilution needed.

5- Add 100 µl of Bradford control to each well.

6- When we add the Bradford, depending on the concentration of protein, the color of the wells should change.

7- Put the plate into the device for Bradford and measure the protein concentration.

3.3.5.4 Western blot (WB)

<u>- Gel preparation</u>

1- Gel concentration was prepared based on the size of each protein, as the size range in the picture below: (DCP5: 10%, LSM4: 14%, DCP2: 10%, EDC4: 8%, XRN4: 8%)

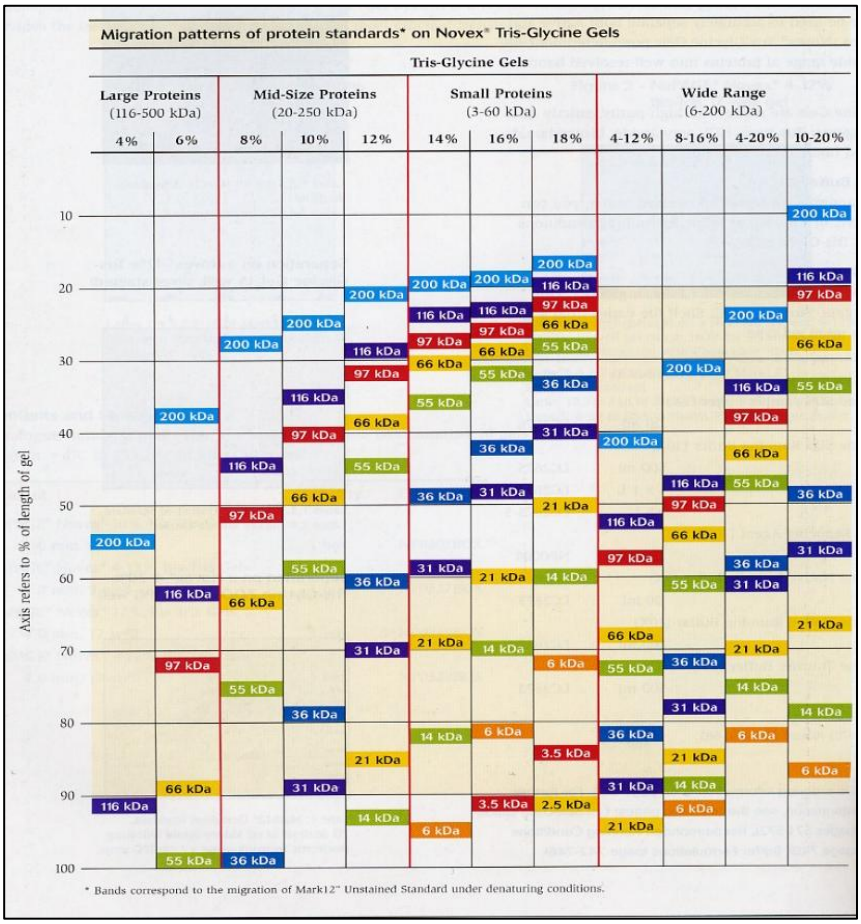

2- The glass size used for gel preparation was 0.75 mm.

3- Prepare the lower part of the gel: add Lower Buffer for Polyacrylamide Gel inside the glasses, then add the isopropanol (up to leaking from the upper part of the glasses) to make the gel heavy to remove the bubbles. Wait 20 min for gel polymerization.

4- Remove the isopropanol and dry the residue of the isopropanol with filter paper.

5- Prepare the upper part of the gel: add Upper Buffer for Polyacrylamide Gel on top of the lower part up to leaking from the glasses, and then put the comb immediately. Wait for 10 minutes for the upper part polymerization.

- Electrophoresis

6- Prepare 10 µg of protein (Obtained last solution from the Cytoplasmic Fractionation protocol-(CP-CoIP) in section 3.3.5.2, and solution from total protein (TP) isolation in section 3.3.5.1) for each well and add Laemmli buffer (3.33 µL:10 µl) and add water up to a final volume of 15 µl.

7- Put the microtube for 10 min in the hot block at 95°C and then put it on ice for 2 min.

8- Add 15 µl of prepared protein solution to each well.

9- Add 5 µl ladder to the well related to the ladder.

10- Electrophoresis for 2:20 hr, 30 mA, 90 V.

- Semi-Dry Transfer

11- Transfer of gel to membrane was done by the Bio-Rad Trans-Blot® Turbo™ Transfer System.

12- Put the membrane of Bio-Rad (Trans-Blot Turbo Mini 0.2 µm PVDF Transfer Packs #1704156 and Trans-Blot Turbo Midi 0.2 µm PVDF Transfer Packs #1704157) on the tray related to the Trans-Blot Turbo Bio-Rad device.

13- Put the gel on the membrane, and then cover the surface of the gel with filter paper (PVDF Transfer Packs include the filter paper)

14- Close the lid of the tray and put the tray on the Bio-Rad Trans-Blot® Turbo™ Transfer System for 10 min.

- Blocking the membrane

15- After transferring the gel to the membrane, mark the face of the membrane where had been touched by the gel. Then cut out the part of the membrane that is not the region of interest.

16- Block the membrane for 1hr with Blocking Buffer for Western Blot at RT.

17- Wash the membrane (2 x 10 min) with PBST.

- Add Primary antibody

18- Prepare 10 μg/ml of Primary antibody (DCP5 1:91, LSM4 1:100, DCP2 1:23, EDC4 1:96, XRN4 1:78) in Antibody Buffer for Western Blot and Immunoprecipitation.

19- Add the antibody to the membrane and incubate at RT for 1 hr on the shaker (70 rpm).

20- Then incubate at 4°C O/N on the shaker (70 rpm).

- Add Secondary antibody

21- Incubate the membrane for 1 hr at RT on the shaker (70 rpm).

22- Wash the membrane (3 x 10 min) with PBST.

23- Add conjugated-secondary antibody 1:60000 with Antibody Buffer for Western Blot and Immunoprecipitation. (DCP5: Anti-rabbit, LSM4: Anti-mouse, DCP2: Anti-rat, EDC4: Anti-rabbit, XRN4: Anti-rabbit).

24- Add the secondary antibody to the membrane and incubate the membrane at RT for 1h on the shaker (70 rpm).

25- Wash the membrane with PBST (3 x 10 min)

26- Wash the membrane with DDW (Double Distilled Water) for 10 min.

27- Check the membrane with the Odyssey CLx Imager.

- Control

The Control used for Western blot was the Anti-ACTIN antibody with uniport ID: P0CJ46.

3.3.5.5 Immunoprecipitation (IP)

The Immunoprecipitation was performed by the modified protocol of the SureBeads™ Magnetic Beads Standard Immunoprecipitation Protocol:

(https://www.bio-rad.com/webroot/web/pdf/lsr/literature/10043651.pdf)

1. Add 200 µl protein G/A magnetic beads into a 1.5 ml microtube and vortex.

2- Magnetize beads and remove the solution, then wash the beads (3 x 1 min) with PBST. For each time washing, the beads should be magnetized to remove the buffer, and a new washing buffer should be added.

3- Add 10 µg/ml of Antibody (DCP5 1:91), up to 200 µl Antibody Buffer for Western Blot and Immunoprecipitation, and rotate 10 min at RT.

4- Add 300 µg of protein (Obtained last solution from the Cytoplasmic Fractionation protocol, CP-CoIP in section 3.3.5.2) up to 500 µl volume.

5- Incubate the microtube in RT for 1h with a rotator.

6- Incubate microtube 4°C O/N with the rotator.

7- Incubate the microtube at RT for 1h with a rotator.

8- Magnetize the beads and remove the solution. Be careful not to lose the beads.
9- Wash the beads (3 x 1 min) with PBST. (To avoid contamination, when adding the second washing buffer, transfer the solution, including magnetic beads, to a new 1.5 ml microtube, magnetize the beads, remove the second washing buffer, and add the last washing buffer.)

10- Magnetize the beads and remove the PBST.

- Sample Elution

The Second Elution Strategy of the SureBeads™ Magnetic Beads Standard Immunoprecipitation Protocol was used for the experiments:

11- Add 40 µl of Elution Buffer (1x Laemmli buffer) for Immunoprecipitation and incubate for 10 min at 70°C (Hot block)

12- Magnetize beads and move eluent to a new microtube.

13- Store the microtube at -20°C for Western blot analysis.

- Microscopic analysis to ensure the presence of P-bodies enrichment and beads in the immunoprecipitation

Reactions were performed like the above protocol in the immunoprecipitation section 3.3.5.5 up to the 9th step, and continued with the protocol below:

10- Resuspend the beads with Cy3-conjugated oligo (dT) probe (poly(A) RNA), 1:200 in hybridization buffer, and rotate it at 26°C O/N.

11- Resuspend 20 µl of the solution (including the beads and oligo (dT) probe) with fixative buffer and add the solution to the gelatinized glass slides.

12- Check the slide under the microscope.

To perform the control for this reaction, the non-immunoprecipitated magnetic beads and Washing buffer were incubated with Cy3-conjugated oligo (dT) probe (poly(A) RNA), 1:200 in hybridization buffer, and rotated at 26°C O/N.

3.3.5.6 Co-Immunoprecipitation

To investigate the co-immunoprecipitated proteins, the obtained solution from the 13th step in the given Immunoprecipitation protocol in section 3.3.5.5 (Immunoprecipitated DCP5 protein) was subjected for Western blot analysis as given in the explained Western blot protocol in section 3.3.5.4 with the following modification:

Instead of using the protein solution described in step 6 of the Western blot protocol, the solution obtained from step 13th of the Immunoprecipitation protocol was used.

3.3.6 RNA-transcripts Analysis

3.3.6.1 Cytoplasmic fractionation for RNA analysis (CP-RNA)

Freshly collected anthers of *Larix decidua* Mill. were immediately frozen in liquid nitrogen and stored at -80°C. To obtain the cytoplasmic fraction for RNA-Immunoprecipitation (RIP), the plant material was ground in liquid nitrogen, and then the Buffer for RNA Immunoprecipitation was added in a proportion of 10 ml per 1.5 gr of material. After thawing on ice (~5 min), the material was filtered through a single layer of Miracloth (ø 22-25 μm; Merck Millipore) and centrifuged at 1,500 g for 2 min, 4°C. The obtained supernatant constituted the cytoplasmic fraction of anther cells, used for RNA-RNA-Immunoprecipitation (RIP), control samples, and reference samples (input – total cytoplasmic fraction).

3.3.6.2 Total RNA isolation

Supernatant obtained from part 3.3.6.1 was subjected to RNA isolation according to the protocol below:

1- Squeeze gently the material on a watch glass (100 mm) in cold DEPC-PBS. Then, collect microsporocytes into a 50 ml tube capped with a filter size of 100 nm.

2- Transfer the collected material to 2 ml microtubes and centrifuge for 1.5 min. 8,000 rpm at 4°C.

3- Discard the supernatant and transfer the sediments to 2 or 3 microtubes in 1.5 ml and centrifuge for 1.5 min. 8,000 rpm, 4°C.

4- Discard all supernatant thoroughly and add 750 μl of cold TRI Reagent, freeze microtubes with Trisol for 10 minutes at -80°C.

5- Take the microtubes from -80 and wait for refreezing at room temperature for 10 min. Then centrifuge for 5 minutes at 10,000 g, 4°C.

6- Transfer the supernatant to Phasemaker Tubes (Invitrogen™ Phasemaker™ Tubes). Incubate for 5 min at RT.

7- Add 150 µl of chloroform to the sample and incubate for 2-3 minutes at RT.

8- Centrifuge the microtubes for 5 min at 12,000 - 16,000 g, 4°C.

8- The sample will be separated into 3 phases. The top phase should be transferred to the new microtube.

9- Add 375 µl of Isopropanol to the RNA solution. Then incubate for 10 min at RT.

10- Centrifuge for 10 min at 12,000 g, 4°C. Total RNA will be visible as a white precipitate. Discard the supernatant.

11- Add 750 µl of 75% ethanol to the sediment and centrifuge for 5 min at 7,500 g, 4°C.

12- Discard the supernatant and wait for 10 min to air dry the pellet.

13- Dissolve the pellet in 20-50 µl of RNase-free water. Then incubate in a thermoblock at 60°C for 10 min.

14- Measure the RNA quantity and quality.

- Quantitative and qualitative analysis of isolated RNAs

The RNA quantity measurement was done based on the protocol by Qubit™ RNA High Sensitivity (HS) Assay Kit and Invitrogen™ Qubit™ 4 Fluorometer, and using a NanoDrop 2000 spectrophotometer (Thermo Fisher Scientific). While the quality of RNA was determined by the Agilent RNA 6000 Pico Kit and the 2100 Bioanalyzer Instrument, based on its instructions.

3.3.6.3 mRNA isolation and RNA depletion from isolated total RNA

To isolate mRNA from total RNA samples, the Dynabeads® mRNA DIRECT™ Micro Kit (Thermo Fisher Scientific) was used. The procedure was performed according to the manufacturer's protocol. The main stages of isolation included:

- preparation of Dynabeads® oligo(dT)$_{25}$ magnetic beads (washing)

- preparation of total RNA samples

- performing two rounds of mRNA isolation, each consisting of the steps: binding of mRNA to magnetic beads, washing, and elution of mRNA.

mRNA isolated in this manner was used for subsequent cDNA library synthesis.

For the next step, total RNA was also subjected to ribosomal RNA depletion using the RiboMinus™ Plant Kit for RNA-Seq (Invitrogen), according to the protocol provided by the manufacturer. The resulting RNA was evaluated for quality and quantity, and then used as a template for the synthesis of cDNA libraries intended for sequencing.

3.3.6.4 RNA-Immunoprecipitation (RIP)

Supernatant obtained from part 3.3.6.1 was subjected to RNA-Immunoprecipitation by the protocol below:

1. Add 100 µl protein G magnetic beads into a 1.5 ml microtube and vortex.

2- Magnetize beads and remove the solution, then wash the beads (3 x 1 min) with Washing Buffer for RNA Immunoprecipitation. For each time washing, the beads should be magnetized to remove the buffer, and a new washing buffer should be added.

3- Add 10 µg/ml of Antibody (DCP5 1:91, LSM4 1:100, DCP2 1:23, EDC4 1:96), up to 200 µl Antibody Buffer for Western Blot and Immunoprecipitation.

4- Add 300 µg of protein (Obtained from the last solution in the Cytoplasmic Fractionation for RNA-Immunoprecipitation in section 3.3.6.1) up to a 500 µl volume.

5- Incubate microtube 4°C O/N with the rotator.

6- Magnetize the beads and remove the solution. Be careful not to lose the beads.
7- Wash the beads (3 x 1 min) with the Washing Buffer for RNA Immunoprecipitation. (To avoid contamination, when adding the second washing buffer, transfer the solution including

magnetic beads to a new 1.5 ml microtube and then magnetize the beads, remove the second washing buffer, and add the last washing buffer).

10- Magnetize the beads and remove the last Washing buffer.

11- The beads were directly subjected to RNA isolation.

For each Antibody, 3 repetitions were considered. To perform the control for RIP, the magnetic beads were incubated with the Washing Buffer for RNA Immunoprecipitation without any antibodies in 3 repetitions as well.

3.3.6.5 RNA Isolation from beads-RIP

The RNA isolation from the beads was done immediately after RNA-Immunoprecipitation according to the mentioned total RNA isolation protocol in section 3.3.6.2; 750 µl of TRI reagent was added to the beads, and then the other steps of the mentioned protocol were continued (From the 4^{th} step to the end). The RNA quantity and quality measurements were also done based on the explained protocol in section 3.3.6.2.

3.3.6.6 Preparation of cDNA Library for Sequencing

The final solutions from mRNA isolation and RNA depletion in section 3.3.6.3, the solution from isolated RNA by beads RIP in section 3.3.6.5, and also the solution from the control (without Antibody), were subjected to cDNA library preparation. It was performed using a commercial kit of NEBNext® Ultra™ II Directional RNA Library Prep Kit for Illumina® according to the protocol for use with purified mRNA or rRNA-depleted RNA, provided by the manufacturer. The procedure sequentially comprised: RNA fragmentation and primer annealing, first-strand then second-strand cDNA synthesis, purification of double-stranded cDNA using magnetic beads, library end preparation, adapter ligation, purification of ligation products using NEBNext® beads, enrichment of adapter-ligated DNA by PCR, and final purification of PCR reaction products.

3.3.7 Sequencing and Bioinformatics Analysis

cDNA libraries were sequenced by the Genomed Company in Warsaw, and preliminary data analysis was performed by Dr. habil. Michał Szcześniak from the Institute of Human Biology and Evolution, Faculty of Biology, Adam Mickiewicz University in Poznań. High-throughput sequencing of libraries was performed on the Aviti platform from Element Biosciences in 2x150 cycle mode using Cloudbreak FS High Output reagents, with the aim of obtaining an average of 6 billion bases per sample. The data were already trimmed by the company, but for assurance, the resulting reads were trimmed using the BBDuk2 (191). With the following settings: qtrim=w, trimq=20, maq=10, k=23, mink=11, hdist=1, tbo, tpe, minlength=100, removeifeitherbad=t. Additionally, Bowtie 2 was applied to discard rRNA-mapped reads by mapping (192), against larch ribosomal RNAs (own sequences as well as larch rRNAs sourced from Ensembl Plants v. 49).

3.3.7.1 Transcriptome assembly

In total, twelve RNA-seq samples were generated, corresponding to DCP2, DCP5, EDC4, and LSM4 proteins, each represented by three biological replicates. During data quality assessment and clustering analysis (Figure 4-24A), two samples were identified as outliers (related to the DCP5 and DCP2) and excluded from transcriptome assembly, resulting in ten high-quality samples. The reads corresponding to each of the ten samples were subject to *de novo* transcriptome assembly using Trinity (193), with a --SS_lib_type RF parameter. Then, the ten transcriptomes were merged into a single dataset of unique and high-quality transcripts.

First, only transcripts showing an expression level higher than 1 TPM (Transcript Per Million) in at least one condition were retained. This filtering step removed lowly expressed or spurious transcripts, which otherwise would lead to excessively large, merged assemblies (>2–3 million unique transcripts).

Then, the preliminary merged dataset, containing 1,790,640 transcripts, was further filtered by retaining only transcripts detected in at least two different independent transcriptomes. Pairwise similarity searches were performed using BLAST, requiring a minimum of 95% sequence

identity over at least 200 nucleotides. This step reduced the dataset to 788,152 transcripts by removing potential assembly artifacts and redundant low-confidence sequences.

Finally, to consolidate similar sequences into representative clusters, the remaining transcripts were clustered using VSEARCH. Sequences sharing ≥95% identity were grouped together, and the centroid sequence from each cluster was retained as the representative transcript.

The final non-redundant reference transcriptome comprised 264,851 unique transcripts and was used for further analyses.

3.3.7.2 Assessment of transcriptome completeness

The completeness of the merged *de novo* transcriptome assembly was evaluated using BUSCO (Benchmarking Universal Single-Copy Orthologs) with the embryophyta_odb10 lineage dataset as the reference. Out of 1614 expected single-copy orthologs, 1443 were identified as complete (89.4%), including 758 single-copy (47.0%) and 685 duplicated (42.4%) BUSCOs. An additional 48 orthologs were found as fragmented (3.0%), and 123 were missing (7.6%). These results indicate a high level of completeness of the merged transcriptome, consistent with a comprehensive and representative assembly.

3.3.7.3 Annotation of RIP-Seq results

The transcripts of genes highlighted in the RIP-Seq analysis were subject to annotation using Trinotate (194), which included blastp and blastx searches against SwissProt (195), Viridiplantae proteins, as well as scanning protein structural and functional domains from Pfam with hmmscan (hmmer.org).

3.3.7.4 Expression quantification

Gene and transcript expression levels were estimated using RSEM v1.2.28 (RNA-Seq by Expectation Maximization) (196), with the merged *de novo* transcriptome as reference using the following settings: --forward-prob 0, --no-bam-output, --bowtie2. Read alignment was performed internally by RSEM using Bowtie2, and expression estimates were generated for each sample under paired-end mode using 16 computational threads.

3.3.7.5 Differential expression analysis of RIP-Seq data

Differential expression analysis was performed using the DESeq2 package in R/Bioconductor. Four immunoprecipitated (IP) conditions (DCP2, DCP5, EDC4, and LSM4) were analysed, each with three biological replicates, and compared against three control replicates. Raw count data obtained from RSEM were imported into DESeq2, and normalization was performed using the regularized log (rlog) transformation, which stabilizes variance across samples. Hierarchical clustering and visualization of expression variability were performed by generating heatmaps of the top 500 most variable genes (Figure 4-24A). Significantly enriched transcripts were identified based on adjusted p-values < 0.05.

4. Results

4.1 During diplotene prophase I, the DCP5 protein colocalizes with cytoplasmic poly(A) RNA in *Larix decidua* microsporocytes

The DCP5 protein, as a specific decapping factor in plants, was selected to be analyzed in the case of the presence of the decapping process in *Larix decidua* microsporocytes. Microscopic observations using immunofluorescence methods, fluorescence in situ hybridization (FISH), and confocal microscopy revealed the occurrence of P-bodies rich in poly(A) RNA and DCP5-decapping factor. Interestingly, our finding reveals the cytoplasmic co-localization of the poly(A) RNA and DCP5 proteins (Figure 4-1).

4.1.1 Distribution pattern of poly (A) and DCP5 in the Cytoplasm and P-bodies

Stage 1: Nuclear poly(A) RNA levels are significantly higher than in the cytoplasm, where poly(A) RNA reaches its lowest concentration compared to all other stages (Figures 4-1A and 4-2A). Only a small portion of cytoplasmic poly(A) RNA localizes to P-bodies (Figure 4-2A), with the majority found in mid-sized P-bodies (0.3-1.2 μm^3) (Figure 4-2C). This implies that only a small fraction of poly (A) was localized to P-bodies, consistent with limited mRNA sequestration or decapping at this stage. DCP5 is predominantly localized to P-bodies rather than being diffusely distributed in the cytoplasm (Figures 4-1B and 4-2B). The majority of cytoplasmic DCP5 fluorescence is concentrated in P-bodies (Figure 4-2B), while DCP5 proteins were present in P-bodies of various volumes; the majority were detected within a volume range of large P-bodies (1.2-6 μm^3) (Figure 4-2D). Reflecting a baseline presence of the decapping protein in these structures.

Stage 2: Nuclear poly(A) RNA accumulation is gradually decreased, though it is still retained in Cajal bodies (CBs), while cytoplasmic levels increase (Figures 4-1D and 4-2A). The presence of poly(A) RNA in P-bodies remains low relative to the cytoplasm but is higher than in stage 1. Like the first stage, the vast amount of poly (A) in P-bodies is localized in the mid-sized volume (Figure 4-2C). Indicating a rise in polyadenylated RNA levels, possibly due to enhanced transcription related to the previous stage or mRNA stabilization as the cycle progresses into an active phase, leads to a gradual increase in the poly (A) level not only in the cytoplasm, but also

in P-bodies. DCP5 becomes partially distributed throughout the cytoplasm (Figures 4-1E and 4-2B), reflecting heightened recruitment of DCP5 to the cytoplasm to facilitate decapping activities. The highest accumulation was observed in mid-sized volume of P-bodies (Figure 4-2D).

Stage 3: Cytoplasmic poly(A) RNA levels rise markedly (Figures 4-1G, 4-2A), accompanied by a notable increase in localization within P-bodies, particularly in the small (0.1-0.3 μm^3) and mid-sized (0.3-1.2 μm^3) volume ranges, respectively (Figure 4-2C). DCP5 protein levels surge in the cytoplasm (Figures 4-1H and 4-2B), with a significant proportion concentrated in P-bodies (Figure 4-2B), reflecting heightened cytoplasmic activity of DCP5 compared to the previous stages. Notably, unlike prior stages, the largest volume of P-bodies (6-2 μm^3) is absent, and most P-bodies appear in the 0.1-0.3 μm^3 and 0.3-1.2 μm^3 size ranges, respectively (Figure 4-2D).

Stage 4: Cytoplasmic poly(A) RNA levels show a marginal increase compared to stage 3 (Figures 4-1J and 4-2A), while the localization within P-bodies remains similar in total amount, but the poly(A) distribution in P-bodies shifts: enrichment is greater in 0.3-1.2 μm^3 and 0.1-0.3 μm^3 P-bodies, respectively. poly(A) levels in large P-bodies (1.2-6 μm^3) surpass those in the smallest ones (0.05-0.1 μm^3), reversing the trend observed in the third stage (Figure 4-2C). This suggests a shift toward poly(A) accumulation in larger P-bodies during this stage compared with stage 3. DCP5 levels in the cytoplasm moderately decline compared to stage 3 but remain elevated (Figures 4-1K and 4-2B). Over half of DCP5 is localized to P-bodies (Figure 4-2B). Largest-volume P-bodies are still absent, and most structures fall within the 0.3-1.2 μm^3 and 0.1-0.3 μm^3 size ranges, respectively (Figure 4-2D).

Stage 5: Cytoplasmic poly(A) RNA levels are reduced compared to stages 3 and 4 (Figures 4-1M and 4-2A); likewise, localization within P-bodies diminishes. These RNAs are absent in the smallest P-bodies and are often concentrated in 0.3-1.2 μm^3 and 0.1-0.3 μm^3, respectively, albeit at significantly lower levels than in stages 3 and 4. Notably, a small fraction of poly(A) RNA localizes to the largest P-bodies, a feature absent in stages 3 and 4 (Figure 4-2C). Cytoplasmic DCP5 levels decline sharply compared to stages 3 and 4, falling slightly below stage 2 levels (Figures 4-1N and 4-2B). Over half of DCP5 remains localized to P-bodies (Figure 4-2B), the

largest-volume P-bodies appear, resembling distributions observed in stage 1, and DCP5 predominantly occupies the 1.2-6 μm³ and 0.3-1.2 μm³ size ranges, respectively (Figure 4-2D).

4.1.2 Alteration in Number and Volume of P-bodies (DCP5)

Stage 1: The total number of P-bodies is low compared to the other stages, indicating that few P-bodies were formed (Figures 4-2E and F), possibly due to reduced need for mRNA regulation. Individual P-bodies are relatively large (Figure 4-2G). The ratio of the sum volume of each P-body classification in the total volume of P-bodies shows a greater proportion of P-bodies belong to the 1.2-6 μm³ volume (Figure 4-2H).

Stage 2: The number of P-bodies increases, indicating that cells formed more P-bodies to manage the increased mRNA load (Figure 4-2E), driven by a rise in smaller P-bodies (0.05-0.1 μm³ and 0.1-0.3 μm³) (Figure 4-2F). This is the reason that the mean volume of each P-body is slightly decreasing compared with the first stage (Figures 4-2G and H).

Stage 3: The total number of P-bodies escalates significantly (Figure 4-2E), primarily due to an increase in 0.1-0.3 μm³, 0.3-1.2 μm³, and 0.05-0.1 μm³, respectively (Figure 4-2F), leading to a reduction in average P-body volume compared to the previous stages (Figures 4-2G and H).

Stage 4: The total number of P-bodies remains nearly identical to stage 3 (Figure 4-2E), with a slight decrease in the smallest P-bodies (0.05-0.1 μm³) and marginal increases in the 0.1-0.3 μm³ and 0.3-1.2 μm³ volumes, respectively (Figure 4-2F). This results in a modest rise in average P-body volume compared to stage 3 (Figures 4-2G, H).

Stage 5: The total number of P-bodies approximates stage 2 levels, lower than in stages 3 and 4 (Figure 4-2E). While the abundance of the largest and smallest P-bodies remains like stage 2, mid-sized P-bodies (0.3-1.2 μm³) increase in number compared with stage 2, still less than stages 3 and 4 (Figure 4-2F). The mean P-body volume aligns with stage 2, exceeding that of stages 3 and 4 (Figures 4-2G and H).

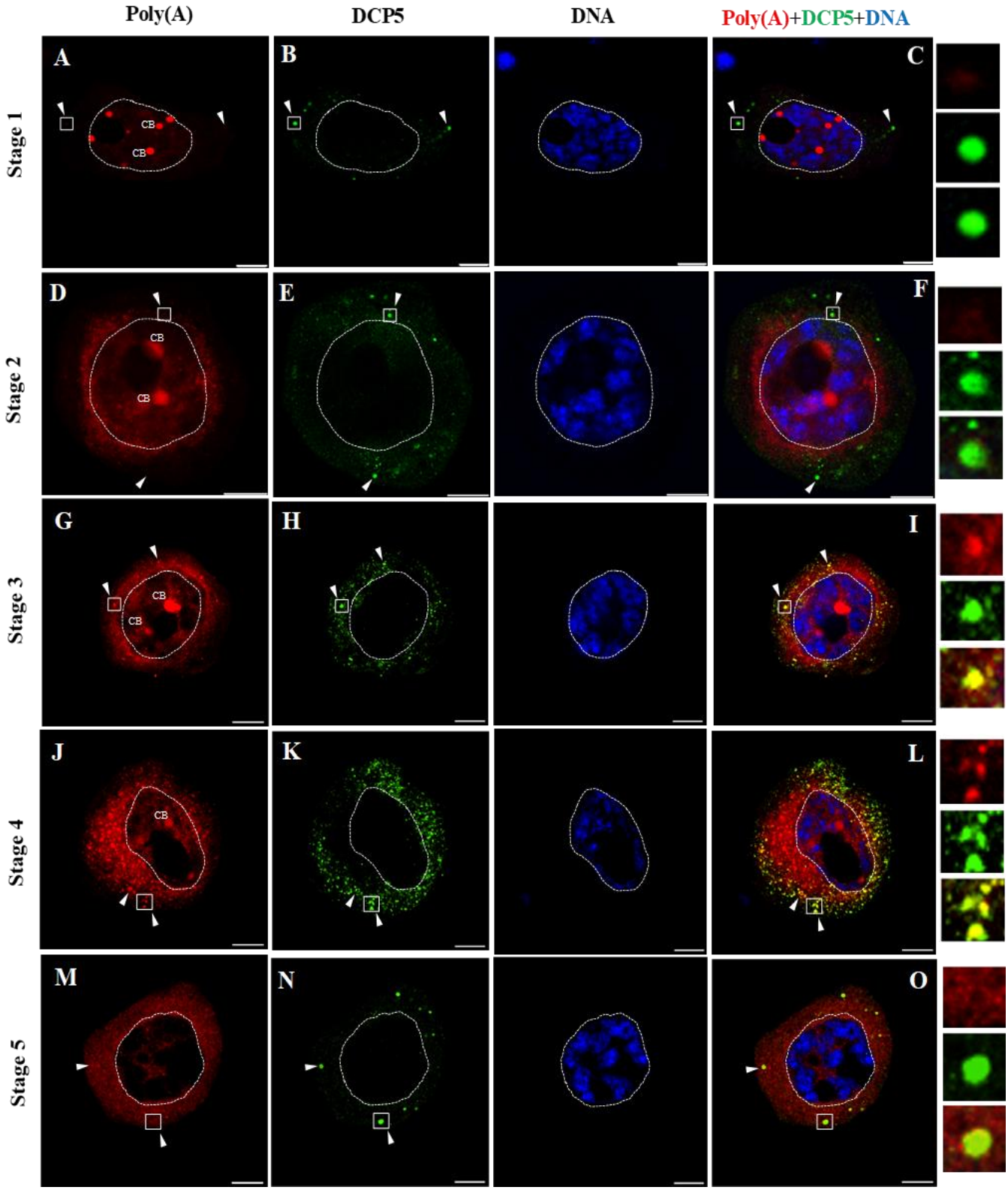

Figure 4-1. Localization of DCP5 proteins and poly(A) RNA in microsporocytes during diplotene. A detailed description is provided in the text. Multiple accumulations of DCP5 proteins colocalized with poly(A) RNA are visible (arrowheads). The right-hand panel represents the magnification of the fragments of the cytoplasm, which are marked with a square, arrowheads pointing to the P-bodies. CB – Cajal body. Scale bar 10 μm.

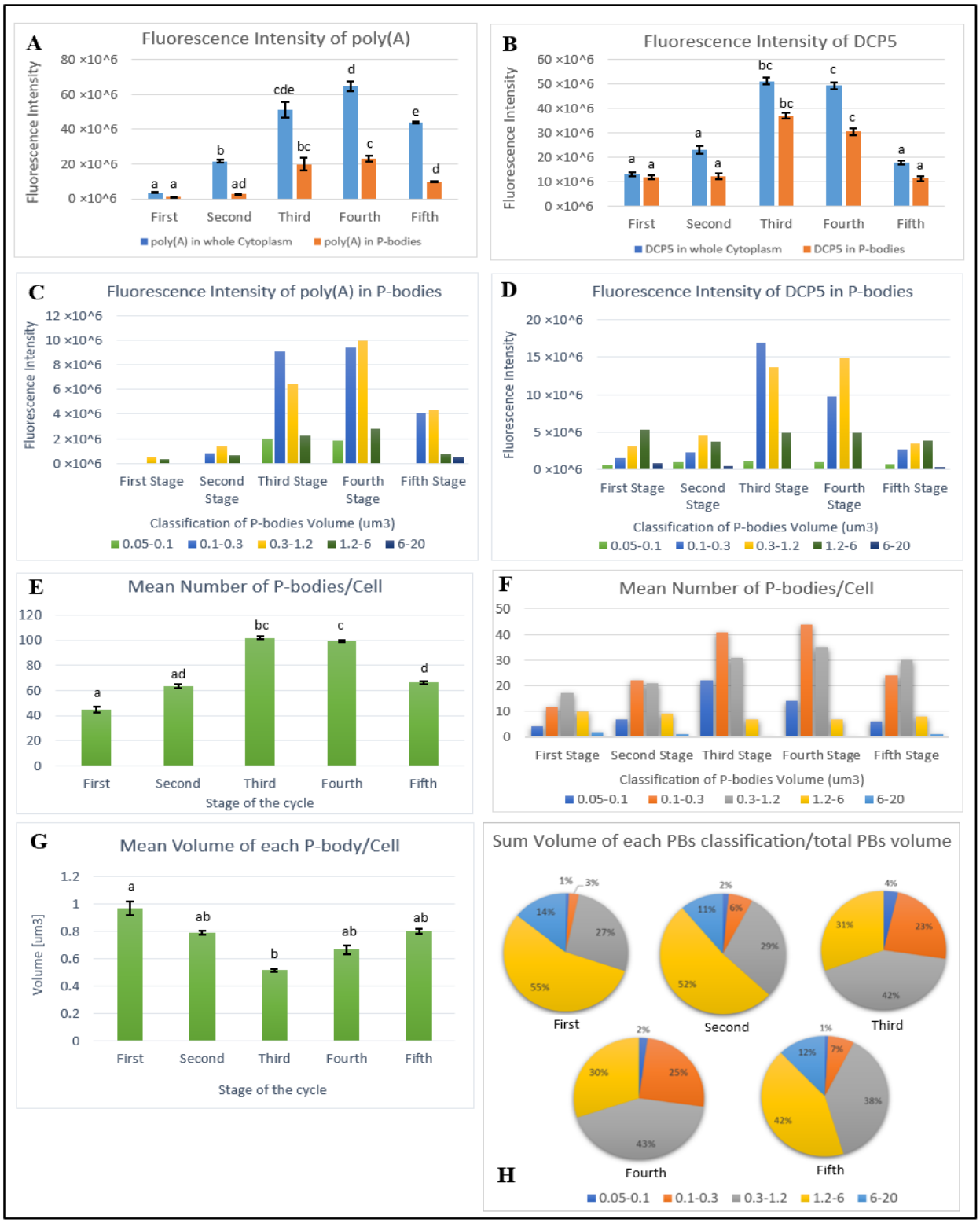

Figure 4-2. Statistical outcomes of the distribution pattern of DCP5 along with poly(A) RNA transcripts in the cytoplasm and P-bodies. A detailed description is provided in the text. (**A and B**) Fluorescence intensity of poly(A) RNA and DCP5 proteins during the five stages, respectively. (**C and D**) Fluorescence intensity of poly(A) RNA and DCP5 proteins in different types of P-bodies volumes, during the five stages, respectively. (**E**) The mean number of P-bodies per cell in the five stages. (**F**) The mean number of P-bodies per cell based on the P-bodies volume classification. (**G**) The mean volume of each P-body per cell. (**H**) The ratio of the sum volume of each P-body classification to the sum volume of total P-bodies in the five stages. The values are shown as means ± standard errors of the mean (SEMs). Based on Tukey's HSD test, the same letters indicate no significant difference ($p > 0.05$), while different letters indicate significant differences ($p \leq 0.05$).

4.1.3 Colocalization of poly(A) RNA and DCP5

Stage 1: The accumulation of poly(A) RNA in the nucleoplasm and Cajal bodies (CBs), coupled with their minimal cytoplasmic fluorescence intensity, results in limited co-localization between cytoplasmic poly(A) RNA and DCP5 (Figure 4-1C). The overall colocalization between poly(A) RNA and DCP5 across the entire cytoplasm (including P-bodies) is low, with values below 20% (Figure 4-3A). Similarly, Pearson colocalization analysis restricted to P-bodies also shows a modest correlation of approximately 30% (Figure 4-3B) and reveals the strongest association in mid-sized P-bodies (0.3-1.2 μm^3), while the largest P-bodies exhibit the lowest level of colocalization (Figure 4-3C). Suggesting a weak spatial association between the two components, both globally in the cytoplasm and specifically within the P-bodies. This minimal overlap implies that P-bodies may not yet be actively engaged in processing poly(A)-associated mRNA in conjunction with DCP5. Mander's colocalization, which is directly related to the fluorescence intensities, was also evaluated. Colocalization of poly(A) RNA with DCP5 is approximately 40%, while DCP5 with poly(A) RNA is about 20% (Figures 4-3D and E). Most colocalization occurs within P-bodies rather than the cytoplasm (Figures 4-3F and G), suggesting negligible interaction outside P-bodies. This stage likely represents an initial or resting phase with minimal functional association between poly (A) and DCP5.

Stage 2: Colocalization remains below 20%, consistent with stage 1 (Figures 4-1F and 4-3A). However, unlike the first stage, colocalization analysis focused solely on P-bodies reveals a decline in overlap to less than 20% (Figures 4-3B and C). This suggests that the elevated cytoplasmic poly(A) RNA levels have not yet concentrated within P-bodies, remaining diffusely distributed in the cytoplasm. The persistently low overlap indicates that, similar to the first stage, P-bodies likely still remain inactive in processing poly(A)-tagged mRNA in coordination with DCP5. Mander's Colocalization of poly(A) RNA with DCP5 is lower than in stage 1 (Figures 4-3D and F), while colocalization of DCP5 with poly(A) RNA remains approximately like stage 1 (Figure 4-3E). In addition, there is a slight increase in colocalization within the cytoplasm compared to stage 1 (Figure 4-3F), which is related to the increased cytoplasmic poly (A) RNA and distribution of DCP5 around the cytoplasm.

Stage 3: Colocalization between poly(A) RNA and DCP5 increases substantially both cytoplasm-wide and within P-bodies (Figure 4-1I), exceeding 50% (Figures 4-3A and B), with

the strongest overlap in mid-sized P-bodies (0.3-1.2 μm³) (Figure 4-3C). This suggests poly(A) RNA is now actively concentrated in P-bodies, where it likely undergoes coordinated processing with DCP5, a shift from earlier inactivity. Manders' analysis confirms Pearson's colocalization data, showing more than 55% overlap between poly(A) and DCP5 (Figures 4-3D and F). Intriguingly, almost 80% of cytoplasmic DCP5 colocalizes with poly(A) RNA (Figure 4-3E), though not all co-occur within P-bodies (Figure 4-3G). Collectively, these findings indicate that this stage marks the onset of cytoplasmic mRNA processing, potentially preparing transcripts for decapping.

Stage 4: Colocalization declines slightly to approximately 50% (Figures 4-1L and 4-3A). Colocalization within P-bodies decreases to approximately 42% (Figure 4-3B). Mid-sized P-bodies (0.3-1.2 μm³) still show the strongest overlap, though it is weaker than in stage 3 (Figure 4-3C). Manders' analysis revealed reduced overlap between poly(A) and DCP5 (Figures 4-3D and F). It is worth noting that, although the level of Mander's for poly (A) with DCP5 colocalization in the stage 4 and stage 1 appears similar, analytically, both are totally different, as both have different intensities of poly (A). DCP5 colocalization with poly(A) RNA also decreases slightly but remains high (Figure 4-3E), though not all colocalized signals reside within P-bodies (Figure 4-3G). Together, these findings position stage 4 as a continuation of mRNA decapping processes initiated in the third stage, with DCP5 playing a sustained, albeit slightly diminished, role in coordinating poly(A)-tagged mRNA processing within P-bodies.

Stage 5: poly(A) RNA and DCP5 colocalization declines cytoplasm-wide < 30% (Figures 4-1O and 4-3A), with a modest reduction (~35%) within P-bodies compared to stages 3 and 4 (Figure 4-3B). Mid-sized P-bodies (0.3-1.2 μm³) retain the highest colocalization, albeit reduced from the stages 3 and 4. Intriguingly, colocalization emerges in the largest P-bodies (6-2 μm³) during stage 5, while it is absent in stages 3 and 4, and exceeds levels seen in stages 1 and 2 (Figure 4-3C). Manders' analysis confirms reduced overlap between poly(A) RNA and DCP5 (Figures 4-3D and F). While DCP5 colocalization with poly(A) RNA remains higher than in stages 1 and 2, it declines relative to stages 3 and 4 (Figure 4-3E), and not all colocalized signals reside within P-bodies (Figure 4-3G).

Figure 4-3. Statistical outcomes of the poly(A) RNA and DCP5 colocalization in the cytoplasm and P-bodies. A detailed description is provided in the text. (**A**) Pearson's colocalization coefficient of poly (A) RNA and DCP5 in the whole cytoplasm. (B) Pearson's colocalization coefficient of poly (A) RNA and DCP5 in P-bodies. (**C**) Pearson's colocalization coefficient of poly (A) RNA and DCP5 in different types of P-bodies volume sizes. (**D**) Mander's colocalization coefficient of poly (A) RNA with DCP5 in the cytoplasm. (**E**) Mander's colocalization coefficient of DCP5 with poly (A) RNA in the cytoplasm. (**F and G**) Distribution of colocalization between DCP5 and poly (A) RNA in cytoplasm and P-bodies, based on Mander's colocalization coefficient. The values are shown as means ± standard errors of the mean (SEMs). Based on Tukey's HSD test, the same letters indicate no significant difference ($p > 0.05$), while different letters indicate significant differences ($p \leq 0.05$).

4.2 During diplotene prophase I, the LSM4 protein colocalizes with cytoplasmic poly(A) RNA in *Larix decidua* microsporocytes

The LSM4 protein, another protein factor that is recruited during the decapping process, was selected to be analyzed in the case of its presence during cell development in *Larix decidua* microsporocytes. Observations revealed the occurrence of P-bodies rich in poly(A) RNA and LSM4 protein. Notably, our finding reveals the cytoplasmic co-localization of the poly(A) RNA and LSM4 proteins (Figure 4-4).

4.2.1 Distribution pattern of poly (A) and LSM4 in the Cytoplasm and P-bodies

Stage 1: The fluorescence intensity of poly (A) almost shows a similar distribution to that mentioned in 4.1.2 (Figures 4-4A and 4-5A). Only a small portion of cytoplasmic poly(A) RNA localizes to P-bodies (Figure 4-5A), with the majority found in 0.1-0.3 μm^3 P-bodies (Figure 4-5C). Although the LSM4 protein is distributed in the cytoplasm, around half of them are concentrated in P-bodies (Figures 4-4B and 4-5B). The majority were detected within a volume range of 0.3-1.2 μm^3 (Figure 4-5D). Reflecting a baseline presence of the deadenylation protein in these structures.

Stage 2: Nuclear poly(A) RNA is gradually decreased along with an increase in cytoplasmic levels (Figures 4-4D and 4-5A). The presence of poly(A) RNA in P-bodies is still low, although it is a bit higher than in stage 1. Like stage 1, the vast amount of poly (A) in P-bodies is localized in 0.1-0.3 μm^3 volume (Figure 4-5C). The cytoplasmic level of LSM4 protein is increasing, while the half amount is detected within the P-bodies (Figures 4-4E and 4-5B), indicating that with a rise in cytoplasmic poly (A) RNA, the need for LSM4 protein is increased to facilitate decapping activities. Moreover, the highest aggregation of LSM4 was observed in small P-bodies (0.1–0.3 μm^3) (Figure 4-5D).

Stage 3: Significant increase in cytoplasmic poly(A) RNA levels observed (Figures 4-4G, 4-5A), along with a notable increase in P-bodies, particularly in the 0.3-1.2 μm^3 and 0.1-0.3 μm^3 volume ranges, respectively (Figure 4-5C). Considerable increase of LSM4 protein levels was observed in the cytoplasm and P-bodies compared with the previous stages (Figures 4-4H and 4-5B). This likely reflects the high cytoplasmic activity of LSM4 caused by a high amount of

cytoplasmic poly (A) RNA, compared to the previous stages. Interestingly, unlike prior and next stages, the largest-volume P-bodies (6-2 μm^3) appear, although with a low concentration of LSM4. Most LSM4 concentration moves to the 0.1-0.3 μm^3 and 0.3-1.2 μm^3 size ranges of P-bodies, respectively (Figure 4-5D).

Stage 4: Cytoplasmic poly(A) RNA levels are slightly higher than in stage 3 (Figures 4-4J and 4-5A). Localization within P-bodies is marginally decreasing, but with the same distribution as observed in stage 3: localization in 0.3-1.2 μm^3 P-bodies is still higher than the localization in 0.1-0.3 μm^3 (Figure 4-5C). LSM4 levels in the cytoplasm are slightly reduced compared to stage 3 but still remain higher than the other stages (Figures 4-4K and 4-5B). Almost half of the cytoplasmic LSM4 protein is localized to P-bodies (Figure 4-5B). Largest-volume P-bodies disappear, and like the previous stage, most LSM4 localization falls within the 0.1-0.3 μm^3 and 0.3-1.2 μm^3 volume, respectively (Figure 4-5D).

Stage 5: poly(A) RNA levels are being reduced in cytoplasm and P-bodies compared to stages 3 and 4 (Figures 4-4M and 4-5A). The poly (A) RNA is often concentrated in 0.1-0.3 μm^3 and 0.3-1.2 μm^3, respectively, albeit at lower levels than in stages 3 and 4. Notably, a small observed fraction of poly(A) RNA that localized in 1.2-6 μm^3 of P-bodies in stages 3 and 4, disappears in stage 5 (Figure 4-5C). Cytoplasmic LSM4 levels are declining compared to stages 3 and 4, and almost reach the same level as stage 2 (Figures 4-4N and 4-5B), and around half of them remain localized to P-bodies (Figure 4-5B). While the largest-volume P-bodies (6–20 μm^3) disappeared from stage 4, the large volume (1.2-6 μm^3) of P-bodies is also disappearing in stage 5, and LSM4 predominantly occupies the 0.1-0.3 μm^3 and 0.3-1.2 μm^3 volumes, respectively (Figure 4-5D).

4.2.2 Alteration in Number and Volume of P-bodies (LSM4)

Stage 1: The total number of P-bodies is lower than in the other stages, indicating that few P-bodies were formed (Figure 4-5E), while a high amount are classified into smaller P-bodies (0.05-0.1 μm^3 and 0.1-0.3 μm^3, respectively) (Figure 4-5F), leads to reduction of each P-body volume size (Figure 4-5G). Although the highest number of P-bodies is classified within 0.05-0.1 μm^3, the greater portion of P-bodies volume in total volume is related to the 0.1-0.3 μm^3 (Figure 4-5H).

Stage 2: The number of P-bodies increases compared with stage 1 (Figure 4-5E), driven by a rise in 0.1-0.3 μm^3 and 0.3-1.2 μm^3, respectively (Figure 4-5F). The small number of large P-bodies (1.2-6 μm^3) also appears. This is the reason that the mean volume of each P-body is slightly increasing compared with stage 1 (Figures 4-5G and H).

Stage 3: The total number of P-bodies considerably increases (Figure 4-5E), and the highest number is related to the 0.1-0.3 μm^3 (Figure 4-5F). Increasing the number of large P-body volumes compared to the previous stages leads to the rise of the mean volume of each P-body (Figures 4-5G and H) and shows the highest mean volume of each P-body compared with other stages.

Stage 4: The total number of P-bodies decreases compared with stage 3 (Figure 4-5E), with the elimination of 6-20 μm^3 and reduction in other volume sizes (Figure 4-5F). This results in a reduction in average P-body volume compared to stage 3 (Figures 4-5G and H).

Stage 5: The total number of P-bodies is slightly decreasing, and almost reaches stage 2 levels, lower than in stages 3 and 4 (Figure 4-5E). While the abundance of the 1.2-6 μm^3 P-bodies volume disappears, 0.3-1.2 μm^3, and 0.1-0.3 μm^3 show relatively the same amount as in stage 2 (Figure 4-5F). The mean P-body volume aligns with stage 2, less than that of stages 3 and 4 (Figures 4-5G and H).

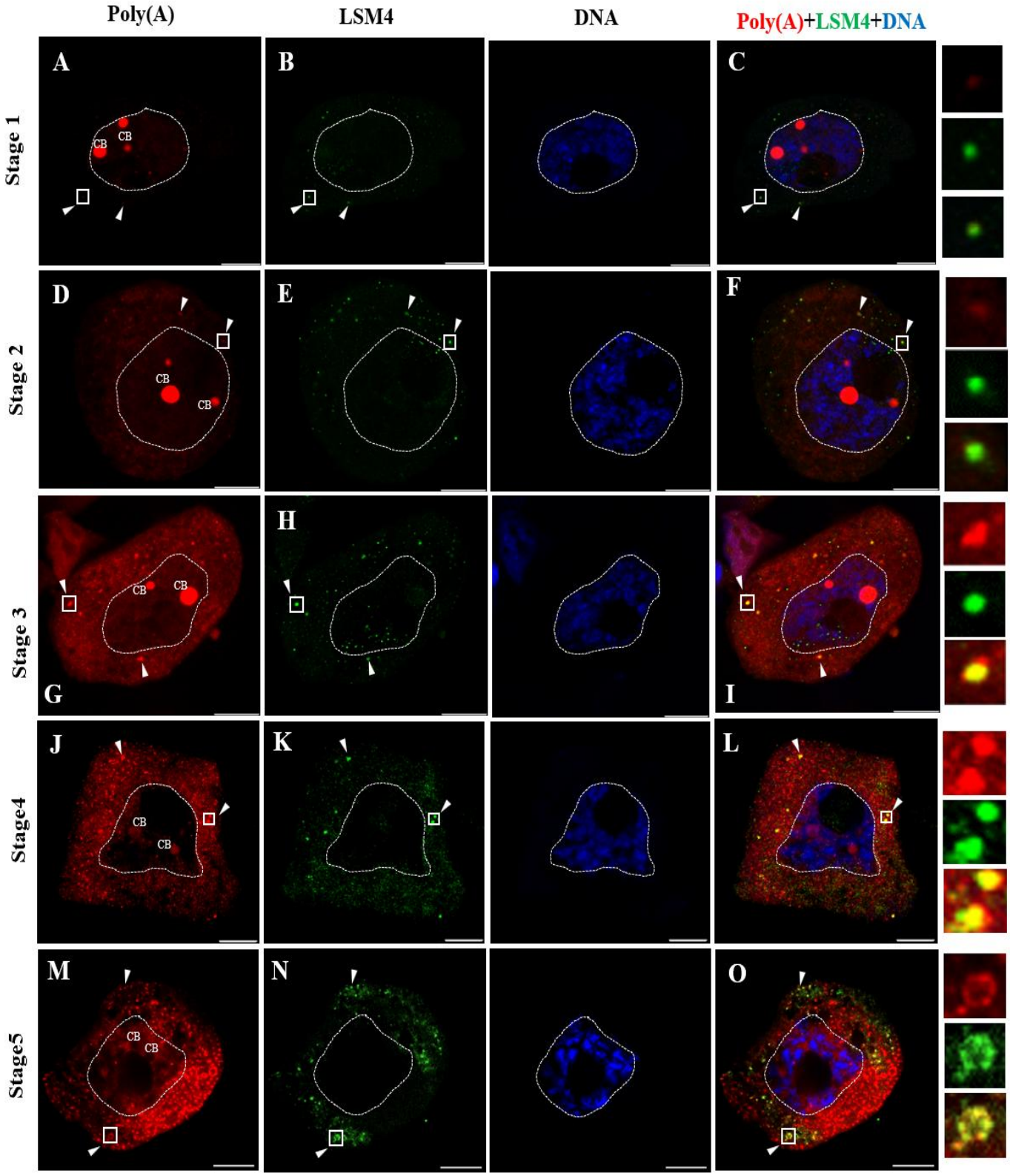

Figure 4-4. Localization of LSM4 proteins and poly(A) RNA in microsporocytes during diplotene. A detailed description is provided in the text. Multiple accumulations of LSM4 proteins colocalized with poly(A) RNA are visible (arrowheads). The right-hand panel represents the magnification of the fragments of the cytoplasm, which are marked with a square, arrowheads pointing to the P-bodies. CB – Cajal body. Scale bar 10 μm.

Figure 4-5. Statistical outcomes of the distribution pattern of LSM4 along with poly(A) RNA transcripts in the cytoplasm and P-bodies. A detailed description is provided in the text. (**A and B**) Fluorescence intensity of poly(A) RNA and LSM4 proteins during the five stages, respectively. (**C and D**) Fluorescence intensity of poly(A) RNA and LSM4 proteins in different types of P-bodies volumes, during the five stages, respectively. (**E**) The mean number of P-bodies per cell in the five stages. (**F**) The mean number of P-bodies per cell based on the P-bodies volume classification. (**G**) The mean volume of each P-body per cell. (**H**) The ratio of the sum volume of each P-body classification to the sum volume of total P-bodies in the five stages. The values are shown as means ± standard errors of the mean (SEMs). Based on Tukey's HSD test, the same letters indicate no significant difference ($p > 0.05$), while different letters indicate significant differences ($p \leq 0.05$).

4.2.3 Colocalization of poly(A) RNA and LSM4

Stage 1: The overall colocalization between poly(A) and LSM4 across the entire cytoplasm and P-bodies is low, averaging around 10% for both (Figures 4-4C, 4-6A and B). The strongest association was observed in 0.1-0.3 μm^3 and 0.3-1.2 μm^3, respectively, while in the absence of larger P-bodies (1.2-6 μm^3 and 6-20 μm^3), the smallest P-bodies show the lowest overlap (Figure 4-6C). The limited overlap implies that P-bodies formed by LSM4 are not yet actively processing poly(A) mRNA. Mander's colocalization of poly(A) RNA with LSM4 in the cytoplasm is about 40%, with 52% inside the P-bodies (Figures 4-6D and F), while LSM4 colocalization with poly(A) RNA is less than 20% (Figures 4-6E and G). At this stage, the colocalization is spread throughout the cytoplasm and within P-bodies. stage 1 likely represents an initial or resting phase with minimal functional engagement between poly(A) RNA and LSM4.

Stage 2: Pearson's colocalization remains low in the entire cytoplasm and P-bodies, increasing slightly to approximately 15% and 13% respectively, across the cytoplasm compared with the stage 1 (Figures 4-4F and 4-6A), with the most colocalization in 0.1-0.3 μm^3, as in the previous stage (Figure 4-6C). The low colocalization indicates that LSM4 proteins are still largely inactive in processing poly(A) mRNA, consistent with stage 1. Mander's analysis shows poly(A) RNA colocalization with LSM4 is decreasing in the cytoplasm to ~20% compared with stage 1, which means the increased cytoplasmic poly (A) RNA in the second stage is not colocalized with the LSM4 proteins in the cytoplasm yet, and results in a reduction of total colocalization (Figures 4-6D and F). LSM4 colocalization with poly(A) RNA is increasing up to ~25% (Figure 4-6E), which is more related to the increase of colocalization in the cytoplasm rather than P-bodies (Figure 4-6G).

Stage 3: Colocalization in this stage rises markedly, reaching nearly 50% across the cytoplasm (Figures 4-4I and 4-6A) and approximately 37% within P-bodies (Figure 4-6B). The strongest overlap was observed in 0.3-1.2 μm^3 and 0.1-0.3 μm^3, respectively. In addition, the colocalization in larger volumes of P-bodies (1.2-6 μm^3 and 6-20 μm^3) was also observed, while it was not in previous stages (Figure 4-6C). This significant increase suggests that poly(A) RNA is now actively concentrated within P-bodies formed by LSM4, where it likely undergoes coordinated processing with LSM4 for deadenylation or co-decapping, marking a clear

departure from the inactivity of earlier stages. Mander's colocalization of poly(A) RNA with LSM4 within the entire cytoplasm is around 40% (Figure 4-6D), with the highest amount (82%) in P-bodies (Figure 4-6F). LSM4 colocalization with poly(A) RNA in the cytoplasm rises to around 70% (Figure 4-6E), the highest across all stages, though around half of this overlap occurs within P-bodies and the other half in the cytoplasm (Figure 4-6G). These indicate that stage 3 is a key phase for the onset of cytoplasmic mRNA processing, with LSM4 potentially facilitating RNA deadenylation and co-decapping.

Stage 4: Colocalization decreases to 35-40% across the cytoplasm (Figures 4-4L and 4-6A) and to approximately 30% within P-bodies (Figure 4-6B). Unlike the previous stage, the highest overlap was observed in 0.1-0.3 μm^3 and 0.3-1.2 μm^3, respectively. The colocalization in 0.1-0.3 μm^3 is slightly lower than the colocalization in the same volume of the previous stage, while colocalization in 0.3-1.2 μm^3 is almost halved compared to the colocalization in the same volume of the previous stage (Figure 4-6C). Mander's analysis reveals almost the same level in poly(A) RNA colocalization with LSM4 as stage 3 (Figure 4-6D), with still the highest amount in P-bodies (Figure 4-6F). LSM4 colocalization with poly(A) RNA is also approximately the same level as stage 3 (Figures 4-6E and G). These results position stage 4 as a continuation of the mRNA processing initiated in stage 3, with LSM4 sustaining a significant, though slightly diminished, role in coordinating poly(A)-tagged mRNA within P-bodies.

Stage 5: Colocalization declines further to 21% across the cytoplasm (Figures 4-4O and 4-6A) and to approximately 20% within P-bodies (Figure 4-6B), while still higher than stage 2. 0.1-0.3 μm^3 volume size retains the highest colocalization, though this is reduced from stages 3 and 4. Unlike stages 3 and 4, there is no colocalization in the 1.2-6 μm^3 volume of P-bodies (Figure 4-6C). Mander's analysis confirms a reduction in poly(A) RNA colocalization with LSM4 (Figure 4-6D); the highest colocalization is in P-bodies rather than the cytoplasm (Figure 4-6F). LSM4 colocalization with poly(A) RNA drops to 40% (Figures 4-6E and F). This stage reflects a winding down of the active processing seen earlier, with LSM4's involvement in poly(A) RNA metabolism decreasing but still present.

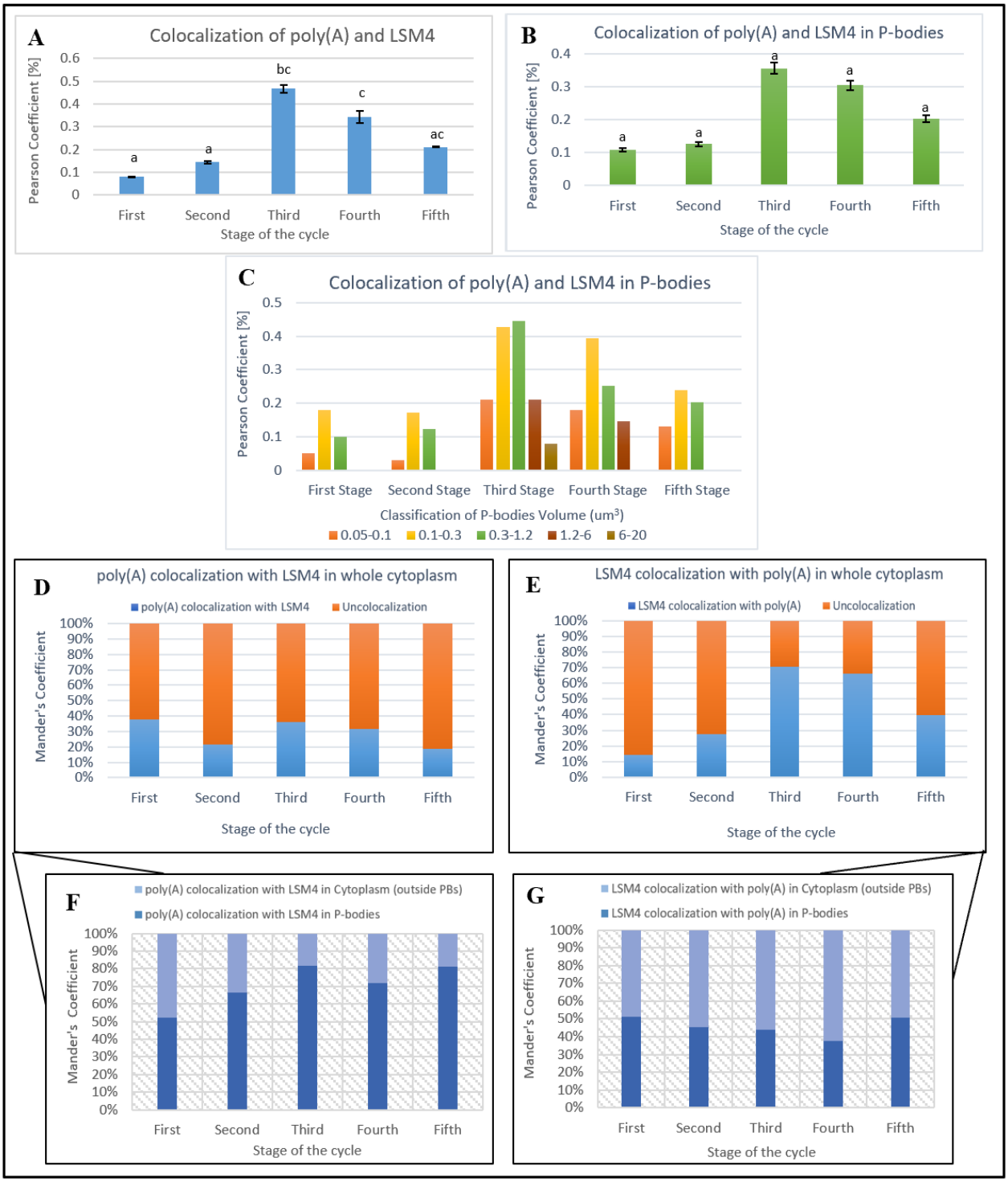

Figure 4-6. Statistical outcomes of the poly(A) RNA and LSM4 colocalization in the cytoplasm and P-bodies. A detailed description is provided in the text. (**A**) Pearson's colocalization coefficient of poly (A) RNA and LSM5 in the whole cytoplasm. (**B**) Pearson's colocalization coefficient of poly (A) RNA and LSM4 in P-bodies. (**C**) Pearson's colocalization coefficient of poly (A) RNA and LSM4 in different types of P-bodies volume sizes. (**D**) Mander's colocalization coefficient of poly (A) RNA with LSM4 in the cytoplasm. (**E**) Mander's colocalization coefficient of LSM4 with poly (A) RNA in the cytoplasm. (**F and G**) Distribution of colocalization between LSM4 and poly (A) RNA in cytoplasm and P-bodies, based on Mander's colocalization coefficient. The values are shown as means ± standard errors of the mean (SEMs). Based on Tukey's HSD test, the same letters indicate no significant difference ($p > 0.05$), while different letters indicate significant differences ($p \leq 0.05$).

4.3 During diplotene prophase I, the DCP2 protein colocalizes with cytoplasmic poly(A) RNA in *Larix Decidua* microsporocytes

The DCP2 protein, as a catalytic enzyme during the decapping process, was selected to be analyzed in the case of its presence during cell development in *Larix decidua* microsporocytes. Observations revealed the occurrence of P-bodies rich in poly(A) RNA and DCP2 protein. Notably, our finding reveals the cytoplasmic co-localization of the poly(A) RNA and DCP2 proteins (Figure 4-7).

4.3.1 Distribution pattern of poly (A) and DCP2 in the Cytoplasm and P-bodies

Stage 1: Results show poly(A) fluorescence intensity following a pattern similar to previous observations (Figures 4-7A and 4-8A). P-bodies contain only a minimal fraction of cytoplasmic poly(A) RNA (Figures 4-8A and 4-8C). The DCP2 protein appears throughout the cytoplasm, with most of that concentrated in P-bodies (Figures 4-7B and 4-8B). Most of these were identified within 0.1-0.3 μm^3 volume (Figure 4-8D).

Stage 2: Nuclear poly(A) RNA levels progressively decline while cytoplasmic concentrations increase (Figures 4-7D and 4-8A). Although poly(A) RNA presence in P-bodies remains minimal compared to later stages, it shows an increase from stage 1 and tends to concentrate in smaller P-bodies (ranging between 0.05-0.1 μm^3 and 0.1-0.3 μm^3) (Figure 4-8C). DCP2 protein levels in the cytoplasm are rising, with more than half detected within P-bodies (Figures 4-7E and 4-8B), suggesting that the increased cytoplasmic poly(A) RNA creates greater demand for DCP2 protein to support decapping activities. Additionally, DCP2 shows its highest concentration in 0.1-0.3 μm^3 volume (Figure 4-8D).

Stage 3: Exhibits a marked increase in cytoplasmic poly(A) RNA (Figures 4-7G, 4-8A), accompanied by more numerous P-bodies, especially those within the 0.1-0.3 μm^3 volume range (Figure 4-8C). While cytoplasmic DCP2 protein levels increase, the concentration within P-bodies remains relatively consistent with previous stages (Figures 4-7H and 4-8B). Unlike earlier stages, the largest P-bodies emerge, though containing minimal DCP2. The highest DCP2 concentrations appear in P-bodies volume 0.1-0.3 μm^3 and 0.3-1.2 μm^3, respectively

(Figure 4-8D). This suggests that despite elevated cytoplasmic poly(A) RNA levels compared to earlier stages, DCP2 activity remains low in both cytoplasm and P-bodies, even as DCP2 quantities increase. It seems to be more required for the next two stages. As the catalytic enzyme of the decapping complex, DCP2 is likely being prepared for subsequent stages. Furthermore, since DCP5 and LSM4 showed high activity in stage 3 and typically function before DCP2 in the pathway, DCP2 activation appears to occur later than these two proteins.

Stage 4: Shows slightly elevated cytoplasmic poly(A) RNA levels compared to stage 3 (Figures 4-7J and 4-8A). Notably, poly(A) RNA localization within P-bodies approximately doubles from the previous stage, with a distinctly different distribution pattern that shifts toward larger P-bodies. Unlike stage 3, the highest concentrations appear in 0.3-1.2 μm^3 volume, followed by 0.1-0.3 μm^3 and 1.2-6 μm^3 volume, respectively (Figure 4-8C). Cytoplasmic DCP2 protein levels continue to increase relative to earlier stages (Figures 4-7K and 4-8B), with more than half now localized to P-bodies (Figure 4-8B). The largest P-bodies remain present at slightly higher levels than in stage 3, with DCP2 predominantly concentrated in the 0.3-1.2 μm^3, 0.1-0.3 μm^3, and 1.2-6 μm^3 volumes, respectively (Figure 4-8D). This stage appears to represent peak DCP2 protein activity compared to all other stages.

Stage 5: Shows a reduction in cytoplasmic poly(A) RNA levels compared to stages 3 and 4, while poly(A) RNA concentration in P-bodies decreases from stage 4 but remains at the same level as stage 3 (Figures 4-7M and 4-8A). The distribution pattern of RNA within P-bodies mirrors that of stage 4, though at somewhat lower levels (Figure 4-8C). DCP2 protein concentrations in both cytoplasm and P-bodies decline relative to stage 4 but remain elevated compared to earlier stages (Figures 4-7N and 4-8B), with over half of cytoplasmic DCP2 still localized to P-bodies (Figure 4-8B). The highest DCP2 concentrations continue to appear in 0.3-1.2 μm^3, 0.1-0.3 μm^3, and 1.2-6 μm^3 volumes, respectively (matching Stage 4's pattern), although the concentration in 1.2-6 μm^3 and 6-20 μm^3 volumes is at the same level of stage 4, the concentration in 0.1-0.3 μm^3 and 0.3-1.2 μm^3 is lower than stage 4 (Figure 4-8D). This suggests DCP2 activity in stage 5 exceeds that of stage 3, while DCP5 and LSM4 activity is lower in stage 5 than in stage 3, further supporting the hypothesis that DCP2 activation occurs later in the sequence.

4.3.2 Alteration in Number and Volume of P-bodies (DCP2)

Stage 1: The mean number of P-body count is less than in the next stages (Figure 4-8E). Most P-bodies in this stage are classified into smaller volumes (0.1-0.3 μm³ and 0.05-0.1 μm³, respectively) (Figure 4-8F), resulting in form smaller mean P-body volume compared to subsequent stages (Figure 4-8G). The 0.1-0.3 μm³ volume represents the largest portion of P-body volume for each classification relative to total P-body volume.

Stage 2: The number of P-bodies shows a slight increase compared to stage 1 (Figure 4-8E). Like the previous stage, the highest counts remain in the smaller volume categories (0.1-0.3 μm³ and 0.05-0.1 μm³, respectively). However, P-bodies in the 0.3-1.2 μm³ range nearly double compared to stage 1 (Figure 4-8F). This move toward larger P-bodies explains the slight increase in mean P-body volume relative to stage 1 (Figures 4-8G and H).

Stage 3: The total number of P-bodies is higher than in the second stage (Figure 4-8E), with the 0.1-0.3 μm³ volume still containing the highest number. While the smallest P-bodies (0.05-0.1 μm³) decrease in number, there is an increase in 0.3-1.2 μm³ and 1.2-6 μm³ compared to both previous stages. Despite this shift, the 0.05-0.1 μm³ volume still outnumbers the 0.3-1.2 μm³ volume (like the previous stages). A few of the largest P-bodies appear in this stage (Figure 4-8F). This gradual increase in larger P-bodies contributes to the increase in mean P-body volume compared to earlier stages (Figures 4-8G and H).

Stage 4: The total P-body count increases compared with stage 3 (Figure 4-8E), with the 0.1-0.3 μm³ volume continuing to show the highest numbers. The smallest P-bodies continue to decrease, while mid-sized (0.3-1.2 μm³) and larger (1.2-6 μm³) P-bodies increase compared to stage 3. Unlike previous stages, the amount of 0.3-1.2 μm³ volume now exceeds that of 0.05-0.1 μm³ volume. This stage also provides a small number of the largest P-bodies (Figure 4-8F). These shifts toward larger volumes result in a substantial increase in average P-body volume compared to stage 3 (Figures 4-8G and H).

Stage 5: The total P-body count remains relatively constant as it was in stage 4 (Figure 4-8E). Like stages 3 and 4, the 0.1-0.3 μm³ volume continues to contain the highest number of P-bodies. The 0.3-1.2 μm³ volume shows growth compared to stage 4. The number of larger P-

bodies (1.2-6 μm³ and 6-20 μm³) is relatively the same as the previous stage (Figure 4-8F). Although the mean P-body volume shows a slight decrease compared to stage 4, it remains higher than in the stages 1, 2, and 3 (Figures 4-8G and H).

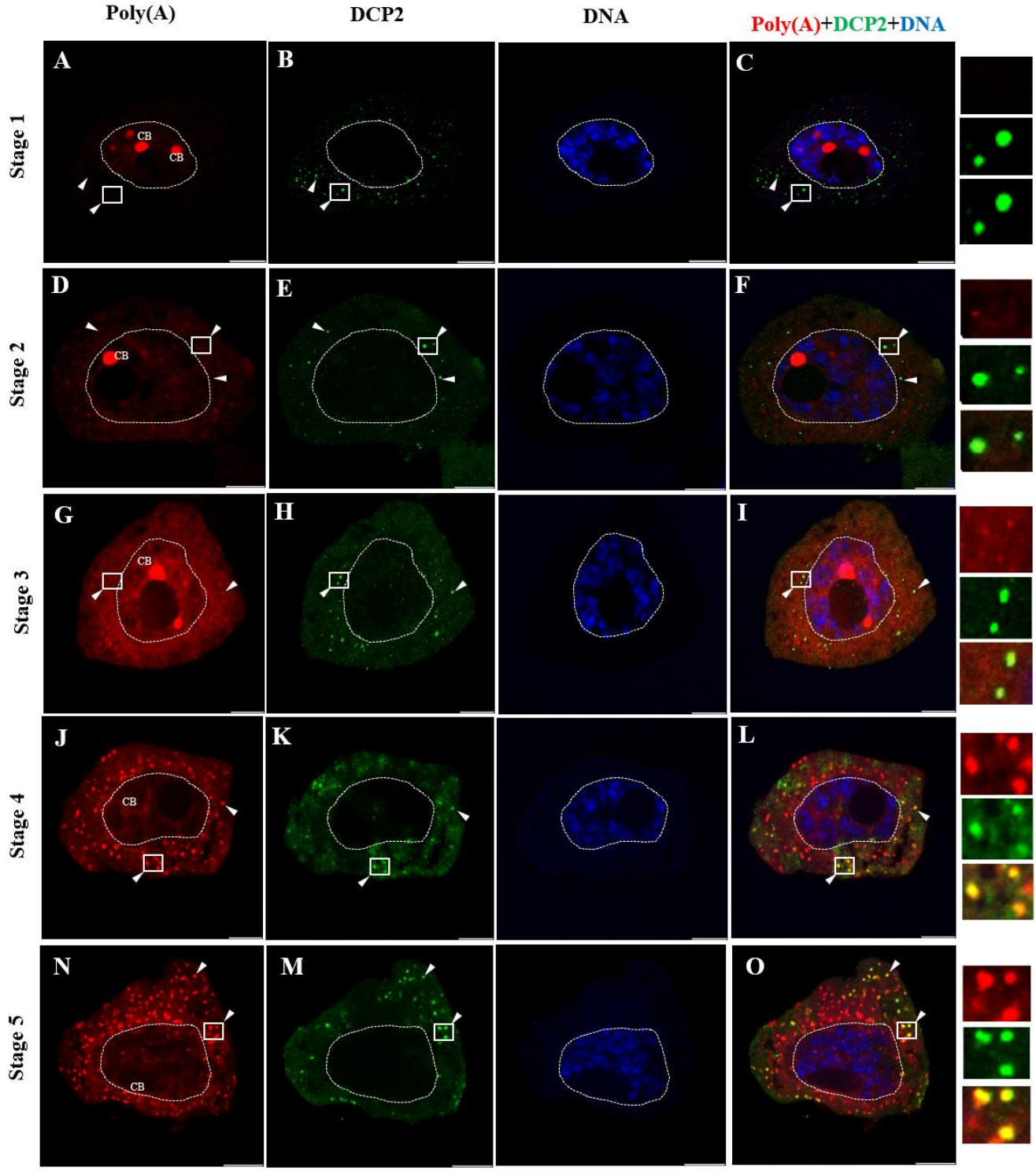

Figure 4-7. Localization of DCP2 proteins and poly(A) RNA in microsporocytes during diplotene. A detailed description is provided in the text. Multiple accumulations of DCP2 proteins colocalized with poly(A) RNA are visible (arrowheads). The right-hand panel represents the magnification of the fragments of the cytoplasm, which are marked with a square, arrowheads pointing to the P-bodies. CB – Cajal body. Scale bar 10 μm.

Figure 4-8. Statistical outcomes of the distribution pattern of DCP2 along with poly(A) RNA transcripts in the cytoplasm and P-bodies. A detailed description is provided in the text. (**A and B**) Fluorescence intensity of poly(A) RNA and DCP2 proteins during the five stages, respectively. (**C and D**) Fluorescence intensity of poly(A) RNA and DCP2 proteins in different types of P-bodies volumes, during the five stages, respectively. (**E**) The mean number of P-bodies per cell in the five stages. (**F**) The mean number of P-bodies per cell based on the P-bodies volume classification. (**G**) The mean volume of each P-body per cell. (**H**) The ratio of the sum volume of each P-body classification to the sum volume of total P-bodies in the five stages. The values are shown as means ± standard errors of the mean (SEMs). Based on Tukey's HSD test, the same letters indicate no significant difference ($p > 0.05$), while different letters indicate significant differences ($p \leq 0.05$).

4.3.3 Colocalization of poly(A) RNA and DCP2

Stage 1: The colocalization between poly(A) and DCP2 throughout the cytoplasm is minimal (less than 5%) compared to the next stages, with P-body colocalization at approximately 15%, which is still low relative to subsequent stages (Figures 4-7C, 4-9A and B). The highest colocalization occurs in the 0.1-0.3 μm^3 and 0.3-1.2 μm^3 volumes, respectively, while the 1.2-6 μm^3 volume shows the least overlap (Figure 4-9C). This limited overlap suggests that DCP2-formed P-bodies are not yet actively engaged in poly(A) mRNA processing. Mander's colocalization analysis shows that about 15% of poly(A) RNA colocalizes with DCP2 in the cytoplasm, less than half of that within P-bodies (Figures 4-9D and F). Similarly, DCP2 colocalization with poly(A) RNA is around 5% (Figures 4-9E and G). During this stage, the colocalization is distributed to both the cytoplasm and P-bodies.

Stage 2: Colocalization in the entire cytoplasm increases compared to the first stage, reaching approximately 30% (Figures 4-7F and 4-9A). P-body colocalization stays relatively unchanged from stage 1 (Figure 4-9B), with the highest levels observed in the 0.3-1.2 μm^3 and 0.05-0.1 μm^3 volume, respectively. The 1.2-6 μm^3 volume shows increased colocalization compared to stage 1 (Figure 4-9C). Mander's analysis reveals a minimal increase in poly(A) RNA colocalization with DCP2 in the entire cytoplasm to ~20% compared to stage 1, indicating that the increased cytoplasmic poly(A) RNA present in stage 2 has not yet substantially colocalized with DCP2 proteins (Figures 4-9D and F). Meanwhile, DCP2 colocalization with poly(A) RNA increases to ~20% (Figure 4-9E), primarily reflecting increased colocalization in the cytoplasm rather than in P-bodies (Figure 4-9G).

Stage 3: Colocalization in this stage is relatively at the same level compared with stage 2 (Figures 4-7I and 4-9A), while it increases to 28% within P-bodies (Figure 4-9B). The highest overlap occurs in the 0.3-1.2 μm^3 and 0.1-0.3 μm^3 volumes, respectively. The 1.2-6 μm^3 volume shows increased colocalization compared to previous stages. Notably, colocalization appears within the largest P-bodies, a feature absent in earlier stages (Figure 4-9C). This progressive increase in P-bodies colocalization stage by stage suggests poly(A) RNA is being prepared to be actively concentrated within P-bodies. Mander's analysis shows poly(A) RNA colocalization with DCP2 throughout the cytoplasm reaches approximately 30% (Figure 4-9D), with the most

occurring within P-bodies (Figure 4-9F). DCP2 colocalization with poly(A) RNA increases to around 43% (Figure 4-9E), though around half of this overlap is found in the P-bodies (Figure 4-9G).

Stage 4: Pearson's colocalization increases dramatically to around 40% across the cytoplasm (Figures 4-7L and 4-9A) and approximately 50% within P-bodies (Figure 4-9B). Colocalization increases across all volume ranges compared to stage 3, with the highest overlap occurring in the 0.3-1.2 μm^3 and 1.2-6 μm^3 volumes, respectively. Colocalization in the largest volume category (6-20 μm^3) nearly doubles compared to the previous stage (Figure 4-9C), indicating a move toward colocalization in larger P-bodies from stage 3 to 4. Mander's analysis confirms a significant increase in poly(A) RNA colocalization with DCP2 to 55% compared to stage 3 (Figure 4-9D), with over half occurring within P-bodies (Figure 4-9F). Similarly, DCP2 colocalization with poly(A) RNA substantially increases to 70% compared to stage 3 (Figures 4-9E and G). This marked increase in colocalization establishes stage 4 as the most active period, where RNA undergoes processing with DCP2 for decapping, indicating that stage 4 for DCP2 activity (like stage 3 for DCP5 and LSM4 activities) represents a critical phase for the cytoplasmic mRNA processing.

Stage 5: Colocalization decreases to 40% across the cytoplasm (Figures 4-7O and 4-9A), though this remains higher than stage 3. The colocalization within P-bodies slightly decreases compared with stage 4 (Figure 4-9B). The 0.3-1.2 μm^3 volume maintains the highest colocalization, despite showing a reduction from stage 4. Colocalization in the largest P-bodies (6-20 μm^3) increases compared to stage 4, while the colocalization in 1.2-6 μm^3 and 0.1-0.3 μm^3 is a bit lower than in stage 4 (Figure 4-9C). Mander's analysis shows the same level of poly(A) RNA colocalization with DCP2 at stage 4 (Figure 4-9D); the highest colocalization occurs in P-bodies rather than the cytoplasm (Figure 4-9F). DCP2 colocalization with poly(A) RNA slightly decreases to 60%, with approximately half observed in P-bodies (Figures 4-9E and F). This stage shows DCP2 activity in stage 5 exceeding that of stage 3, while DCP5 and LSM4 activity are lower in stage 5 than in stage 3, supporting the hypothesis that DCP2 activation occurs later in the sequence.

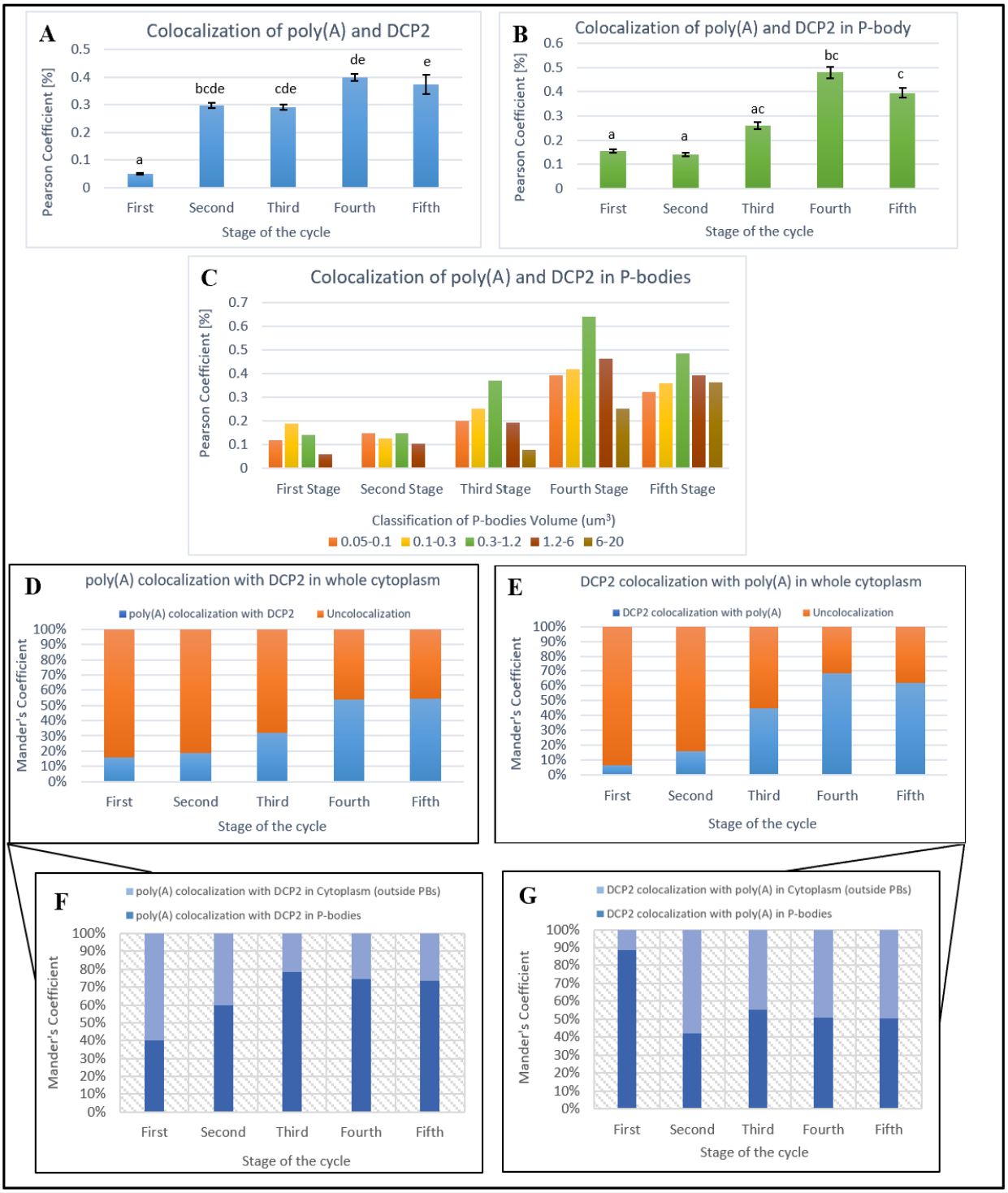

Figure 4-9. Statistical outcomes of the poly(A) RNA and DCP2 colocalization in the cytoplasm and P-bodies. A detailed description is provided in the text. (**A**) Pearson's colocalization coefficient of poly (A) RNA and DCP2 in the whole cytoplasm. (**B**) Pearson's colocalization coefficient of poly (A) RNA and DCP2 in P-bodies. (**C**) Pearson's colocalization coefficient of poly (A) RNA and DCP2 in different types of P-bodies volume sizes. (**D**) Mander's colocalization coefficient of poly (A) RNA with DCP2 in the cytoplasm. (**E**) Mander's colocalization coefficient of DCP2 with poly (A) RNA in the cytoplasm. (**F and G**) Distribution of colocalization between DCP2 and poly (A) RNA in cytoplasm and P-bodies, based on Mander's colocalization coefficient. The values are shown as means ± standard errors of the mean (SEMs). Based on Tukey's HSD test, the same letters indicate no significant difference ($p > 0.05$), while different letters indicate significant differences ($p \leq 0.05$).

4.4 During diplotene prophase I, the EDC4 protein colocalizes with cytoplasmic poly(A) RNA in Larix *decidua* microsporocytes

The EDC4 (VCS) protein, as an enhancer of the decapping complex, was selected to be analyzed in the case of its presence during cell development in *Larix decidua* microsporocytes. Observations revealed the occurrence of P-bodies rich in poly(A) RNA and EDC4 protein. Notably, our finding reveals the cytoplasmic co-localization of the poly(A) RNA and EDC4 proteins (Figure 4-10).

4.4.1 Distribution pattern of poly (A) and EDC4 in the Cytoplasm and P-bodies

Stage 1: The poly(A) fluorescence intensity follows patterns consistent with previous findings and mirrors the DCP2 pattern. Nuclear poly(A) RNA concentrations are significantly elevated compared to cytoplasmic levels (Figures 4-10A and 4-11A). Only a small portion of cytoplasmic poly(A) RNA is found within P-bodies (Figures 4-11A and 4-11C). EDC4 protein is distributed throughout the cytoplasm, with approximately half of it concentrated in P-bodies (Figures 4-10B and 4-11B). Most of these P-bodies were measured within a volume range of 0.1-0.3 μm^3 (Figure 4-11D).

Stage 2: There is a gradual decrease in nuclear poly(A) RNA levels accompanied by increasing cytoplasmic concentrations (Figures 4-10D and 4-11A). While poly(A) RNA presence in P-bodies remains relatively small compared to later stages, it shows an increase from stage 1 and tends to be found predominantly in P-bodies with 0.1-0.3 μm^3 and 0.3-1.2 μm^3 volumes, respectively (Figure 4-11C). Cytoplasmic EDC4 protein levels are increasing, with approximately half of this protein located within P-bodies (Figures 4-10E and 4-11B). This suggests that the rising cytoplasmic poly(A) RNA creates a greater need for EDC4 protein to support the decapping complex. The highest concentration of EDC4 is observed in P-bodies with volumes of 0.1-0.3 μm^3 (Figure 4-11D).

Stage 3: Cytoplasmic poly(A) RNA levels increase dramatically (Figures 4-10G, 4-11A), coupled with an increase within P-bodies, particularly in the 0.1-0.3 μm^3 volume (Figure 4-11C). Both cytoplasmic and P-body EDC4 protein concentrations show increases from previous stages (Figures 4-10H and 4-11B). Unlike earlier stages, the largest P-bodies appear, though

these contain minimal EDC4. The highest EDC4 concentrations are found in P-bodies with volumes of 0.1-0.3 μm³ and 0.3-1.2 μm³, respectively (Figure 4-11D).

Stage 4: Cytoplasmic poly(A) RNA increases modestly compared to stage 3 (Figures 4-10J and 4-11A). Significantly, poly(A) RNA within P-bodies more than doubles from the previous stage, showing a distinctly altered distribution pattern that favors mid-sized and larger P-bodies. Unlike stage 3, the highest concentrations are found in 0.3-1.2 μm³ P-bodies, followed by 0.1-0.3 μm³ and 1.2-6 μm³ volumes, respectively (Figure 4-11C). Cytoplasmic EDC4 protein levels decrease compared to the third stage but are still slightly higher than the second stage (Figures 4-10K and 4-11B), with over half located in P-bodies. The largest P-bodies persist at slightly higher levels than in stage 3, with EDC4 mainly concentrated in P-bodies of 0.3-1.2 μm³, 0.1-0.3 μm³, and 1.2-6 μm³ volumes, respectively (Figure 4-11D).

Stage 5: Exhibits decreased cytoplasmic poly(A) RNA levels compared to stages 3 and 4, while poly(A) RNA concentration in P-bodies shows a reduction from stage 4 but remains higher than stage 3 (Figures 4-10M and 4-11A). The distribution pattern of RNA within P-bodies follows that of stage 4, though at somewhat reduced levels (Figure 4-11C). EDC4 protein concentrations are at the same level in both cytoplasm and P-bodies as it was in stage 4 (Figures 4-10N and 4-11B), with approximately over half of the cytoplasmic EDC4 still found within P-bodies (Figure 4-11B). The highest EDC4 concentrations continue to be observed in P-bodies with 0.3-1.2 μm³, 0.1-0.3 μm³, and 1.2-6 μm³, respectively (Like the pattern in stage 4). In addition, the concentration in larger P-bodies (1.2-6 μm³ and 6-20 μm³) remains approximately at the same level as in stage 4 (Figure 4-11D). The data so far suggest EDC4 activity in stage 5 exceeds that of stage 3, and notably, EDC4 demonstrates patterns remarkably like DCP2.

4.4.2 Alteration in Number and Volume of P-bodies (EDC4)

Stage 1: The total P-body count is lower than in all subsequent stages (Figure 4-11E). P-bodies during this stage are predominantly found in smaller volumes (0.1-0.3 μm³ and 0.05-0.1 μm³, respectively) (Figure 4-11F), resulting in a smaller mean P-body volume compared to later developmental stages (Figure 4-11G and H).

Stage 2: Exhibits a slight increase in total P-body count compared to stage 1 (Figure 4-11E). Like the previous stage, the highest numbers are found in the smaller volume (0.1-0.3 μm^3 and 0.05-0.1 μm^3, respectively). However, P-bodies in the 0.3-1.2 μm^3 and 1.2-6 μm^3 volumes increase compared to stage 1 (Figure 4-11F), which leads to an increase in mean P-body volume relative to the first developmental stage (Figures 4-11G and H).

Stage 3: Shows a slight increase in the total number of P-bodies (Figure 4-11E), with the 0.1-0.3 μm^3 volume maintaining the highest count. The number of smallest P-bodies (0.05-0.1 μm^3) remains relatively consistent with previous stages, while the mid-sized (0.3-1.2 μm^3) and large P-bodies (1.2-6 μm^3) show nearly double the amount compared to stages 1 and 2, which leads to an increase in mean P-body volume (Figures 4-11G and H). Despite this move toward larger P-bodies, the 0.05-0.1 μm^3 volume P-bodies still outnumber those in the 0.3-1.2 μm^3 (like previous stages) (Figure 4-11F).

Stage 4: Exhibits a slightly lower total P-body count than stage 3 (Figure 4-11E). P-bodies with volumes of 0.1-0.3 μm^3 continue to be the most abundant. The smallest P-bodies show ongoing decline, while mid-sized (0.3-1.2 μm^3) increase compared to stage 3. Notably, the number of 0.3-1.2 μm^3 P-bodies surpasses those in the 0.05-0.1 μm^3 range (Unlike stage 3). This stage also features a small population of the largest P-bodies (Figure 4-11F). Ultimately led to a considerable increase in average P-body volume compared to stage 3 (Figures 4-11G and H).

Stage 5: Shows an increase in total P-body count compared to stages 4 and 3 (Figure 4-11E). Like stages 3 and 4, P-bodies with volumes of 0.1-0.3 μm^3 remain the most numerous. P-bodies in the 0.3-1.2 μm^3 volume range show an increase compared to stage 4. The number of larger P-bodies (1.2-6 μm^3 and 6-20 μm^3) remains relatively constant compared to the previous stage (Figure 4-11F). While the mean P-body volume shows a slight decrease compared to stage 4, it continues to be larger than in stages 1, 2, and 3 (Figures 4-11G and H).

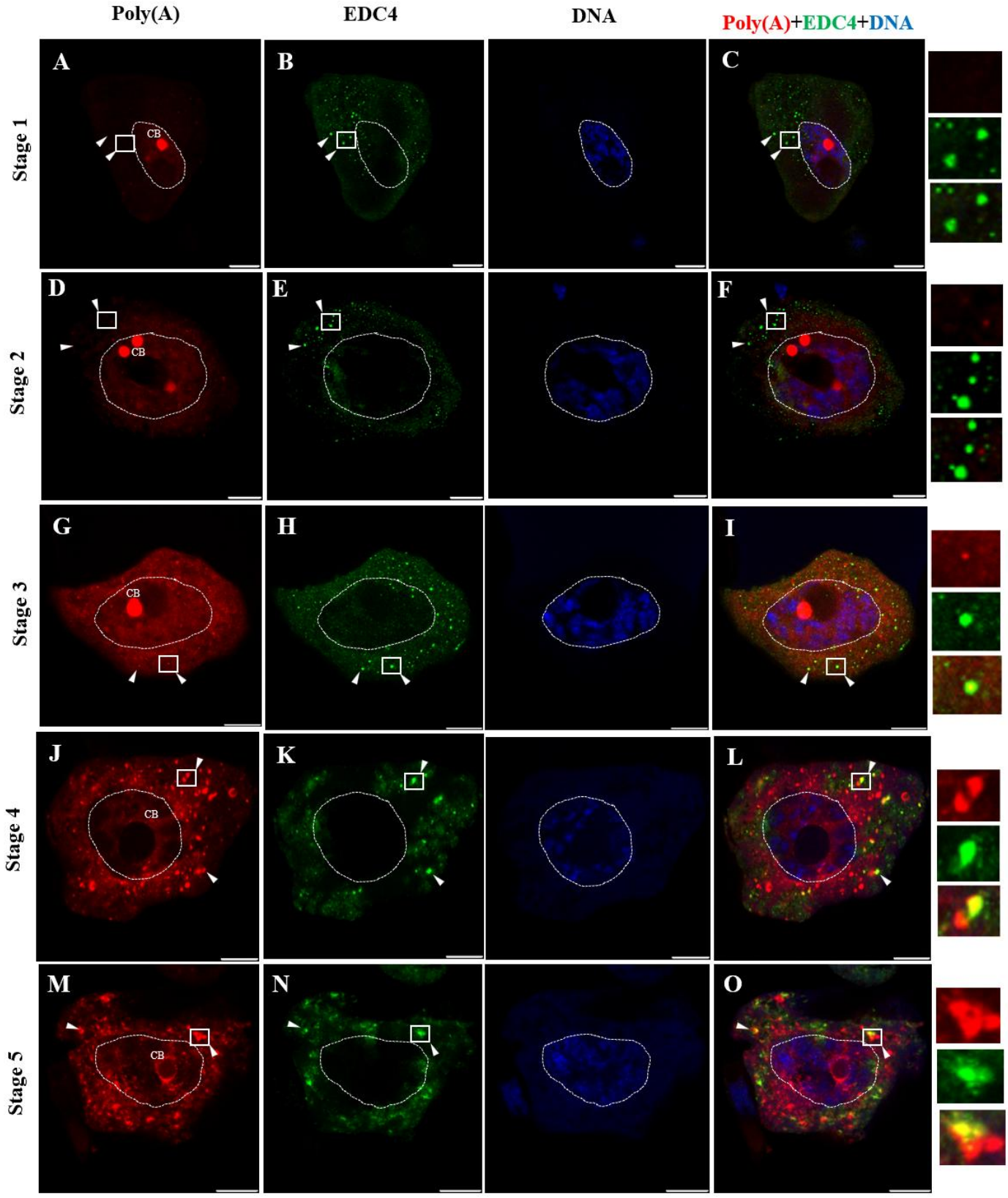

Figure 4-10. Localization of EDC4 proteins and poly(A) RNA in microsporocytes during diplotene. A detailed description is provided in the text. Multiple accumulations of EDC4 proteins colocalized with poly(A) RNA are visible (arrowheads). The right-hand panel represents the magnification of the fragments of the cytoplasm, which are marked with a square, arrowheads pointing to the P-bodies. CB – Cajal body. Scale bar 10 μm.

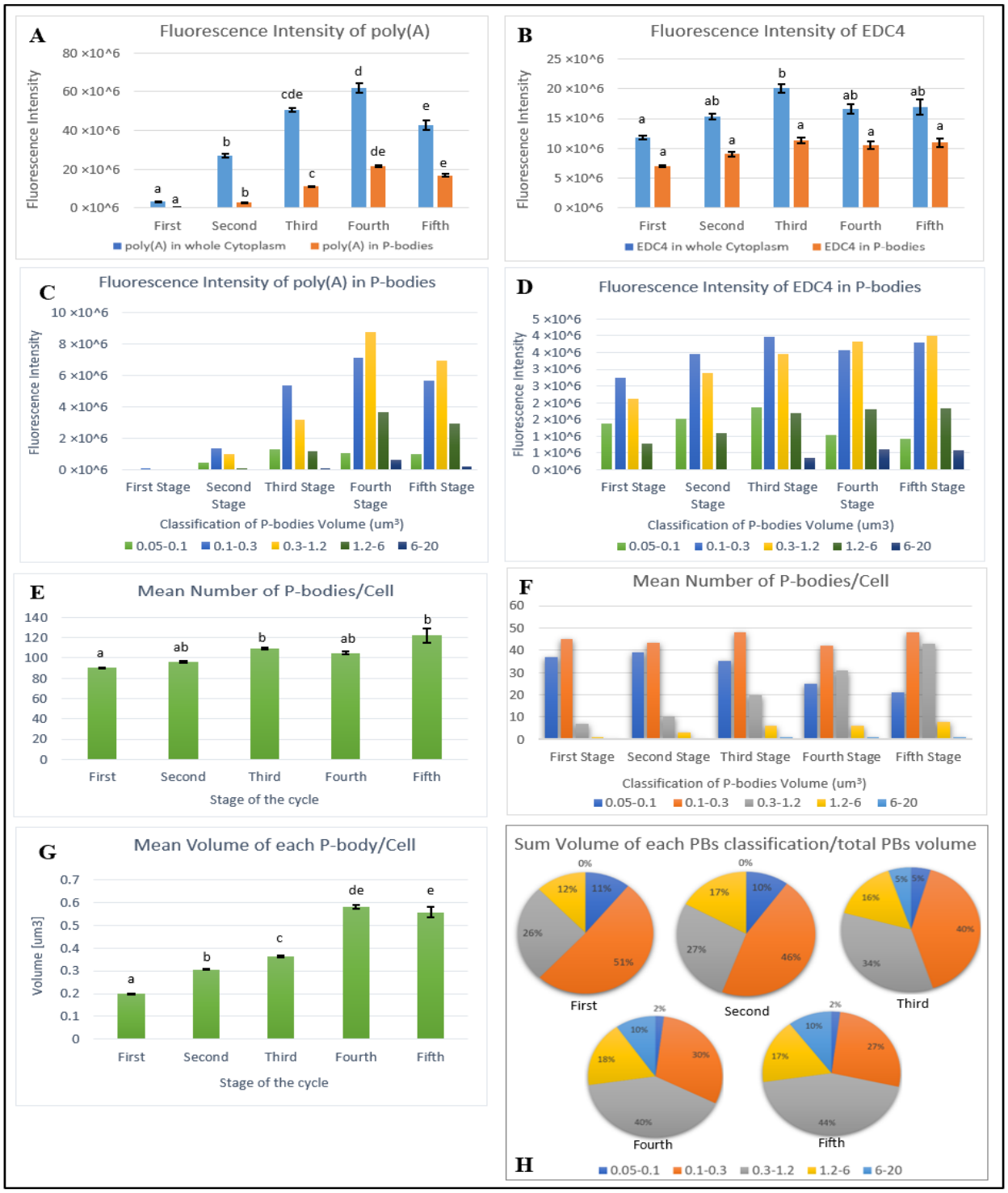

Figure 4-11. Statistical outcomes of the distribution pattern of EDC4 along with poly(A) RNA transcripts in the cytoplasm and P-bodies. A detailed description is provided in the text. (**A and B**) Fluorescence intensity of poly(A) RNA and EDC4 proteins during the five stages, respectively. (**C and D**) Fluorescence intensity of poly(A) RNA and EDC4 proteins in different types of P-bodies volume sizes, during the five stages, respectively. (**E**) The mean number of P-bodies per cell in the five stages. (**F**) The mean number of P-bodies per cell based on the P-bodies volume classification. (**G**) The mean volume of each P-body per cell. (**H**) The ratio of the sum volume of each P-body classification to the sum volume of total P-bodies in the five stages. The values are shown as means ± standard errors of the mean (SEMs). Based on Tukey's HSD test, the same letters indicate no significant difference ($p > 0.05$), while different letters indicate significant differences ($p \leq 0.05$).

4.4.3 Colocalization of poly(A) RNA and EDC4

Stage 1: The colocalization between poly(A) and EDC4 within the cytoplasm is slight, approximately 5%, which is less than observed in the next stages (Figures 4-10C, 4-12A). Within P-bodies, the colocalization reaches about 10%, which remains the least compared to subsequent stages (Figure 4-12B). The most colocalization is seen in specific volume ranges of 0.1-0.3 μm^3 and 0.3-1.2 μm^3, respectively (Figure 4-12C). This restricted association implies that P-bodies formed by EDC4 are not actively participating in poly(A) mRNA processing at this point. According to Mander's colocalization analysis, roughly 15% of poly(A) RNA colocalized with EDC4 in the cytoplasm, of which around 33% within P-bodies (Figures 4-12D and F). In contrast, EDC4 colocalization with poly(A) RNA is approximately 10% (Figures 4-12E and G), with more than half of this interaction occurring within P-bodies.

Stage 2: Cytoplasmic colocalization increases to approximately 30% (Figures 4-10F and 4-12A). The level of P-body colocalization is like stage 1 (Figure 4-12B), with peak levels observed in the 0.3-1.2 μm^3 and 0.1-0.3 μm^3 volume, respectively (Figure 4-12C). Mander's analysis shows unchanged colocalization of poly(A) RNA with EDC4 throughout the cytoplasm compared to stage 1, suggesting that despite increased cytoplasmic poly(A) RNA in stage 2, significant colocalization with EDC4 proteins has not yet occurred, leading to lower overall colocalization (Figures 4-12D and F). Simultaneously, EDC4 colocalization with poly(A) RNA rises to approximately 15% (Figure 4-12E) and shows increased cytoplasmic colocalization rather than P-body colocalization (Figure 4-12G).

Stage 3: Colocalization increases dramatically, reaching 35% throughout the cytoplasm (Figures 4-10I and 4-12A) and about 30% within P-bodies (Figure 4-12B). The strongest overlap is observed in the 0.3-1.2 μm^3 and 0.1-0.3 μm^3 volume ranges, respectively. The 1.2-6 μm^3 volume exhibits enhanced colocalization compared to earlier stages. A key development is the appearance of colocalization within the largest P-bodies, something not seen in previous stages (Figure 4-12C). This sequential increase in colocalization across stages suggests poly(A) RNA is being prepared for the active decapping complex within P-bodies. Mander's analysis indicates that poly(A) RNA colocalization with EDC4 throughout the cytoplasm reaches approximately 40% (Figure 4-12D), with about 57% occurring within P-bodies (Figure 4-12F).

Meanwhile, EDC4 colocalization with poly(A) RNA increases to roughly 50% (Figure 4-12E), with approximately 55% taking place within P-bodies (Figure 4-12G).

Stage 4: Colocalization decreases to 30% compared with stage 3 and reaches the same level as stage 2 throughout the cytoplasm (Figures 4-10L and 4-12A), while about 45% is within P-bodies (around 4 times more than stage 2) (Figure 4-12B). Compared to stage 3, colocalization increases across all volume ranges, with peak overlap in the 0.3-1.2 μm^3 volume. The 1.2-6 μm^3 and 0.1-0.3 μm^3 volumes show similar colocalization levels, and the 1.2-6 μm^3 volume shows approximately triple the colocalization observed in stage 3. Colocalization in the largest volume (6-20 μm^3) increases relative to the previous stage (Figure 4-12C), indicating a progression toward greater colocalization in larger P-bodies from stage 3 to stage 4. Mander's analysis shows an increase in poly(A) RNA colocalization with EDC4, reaching ~45% compared to stage 3 (Figure 4-12D), with most occurring within P-bodies (Figure 4-12F). Similarly, EDC4 colocalization with poly(A) RNA increases significantly to 70% compared to stage 3 (Figures 4-12E and G). This increase in colocalization establishes stage 4 as the most active period among poly(A) RNA and EDC4, suggesting that stage 4 represents a critical phase for cytoplasmic mRNA processing with EDC4 activity, like DCP2.

Stage 5: Colocalization increases to 35% throughout the cytoplasm (As in stage 3) (Figures 4-10O and 4-12A). Colocalization within P-bodies decreases compared to stage 4 but is still higher than in stage 3 (Figure 4-12B). The 0.3-1.2 μm^3 volume continues to show the highest colocalization, despite experiencing a reduction from stage 4. Colocalization in larger P-bodies (1.2-6 μm^3 and 6-20 μm^3) slightly increases compared to stage 4, while colocalization in the 0.1-0.3 μm^3 remains relatively unchanged from stage 4 (Figure 4-12C). Mander's analysis reveals an increasing level of poly(A) RNA colocalization with EDC4 compared to the previous stage, up to 62% (Figure 4-12D), and, like stage 4, the highest colocalization occurs within P-bodies rather than throughout the cytoplasm (Figure 4-12F). EDC4 colocalization with poly(A) RNA shows a slight decrease in level as the previous stage (Figures 4-12E and F). This stage demonstrates that EDC4 activity in stage 5 exceeds that of stage 3, supporting the hypothesis that EDC4, like DCP2 activity, occurs later in the sequence compared to DCP5 and LSM4. This further supports the hypothesis that EDC4 activity is more likely to occur simultaneously with the completion of the decapping complex by DCP2 in order to facilitate the decapping process.

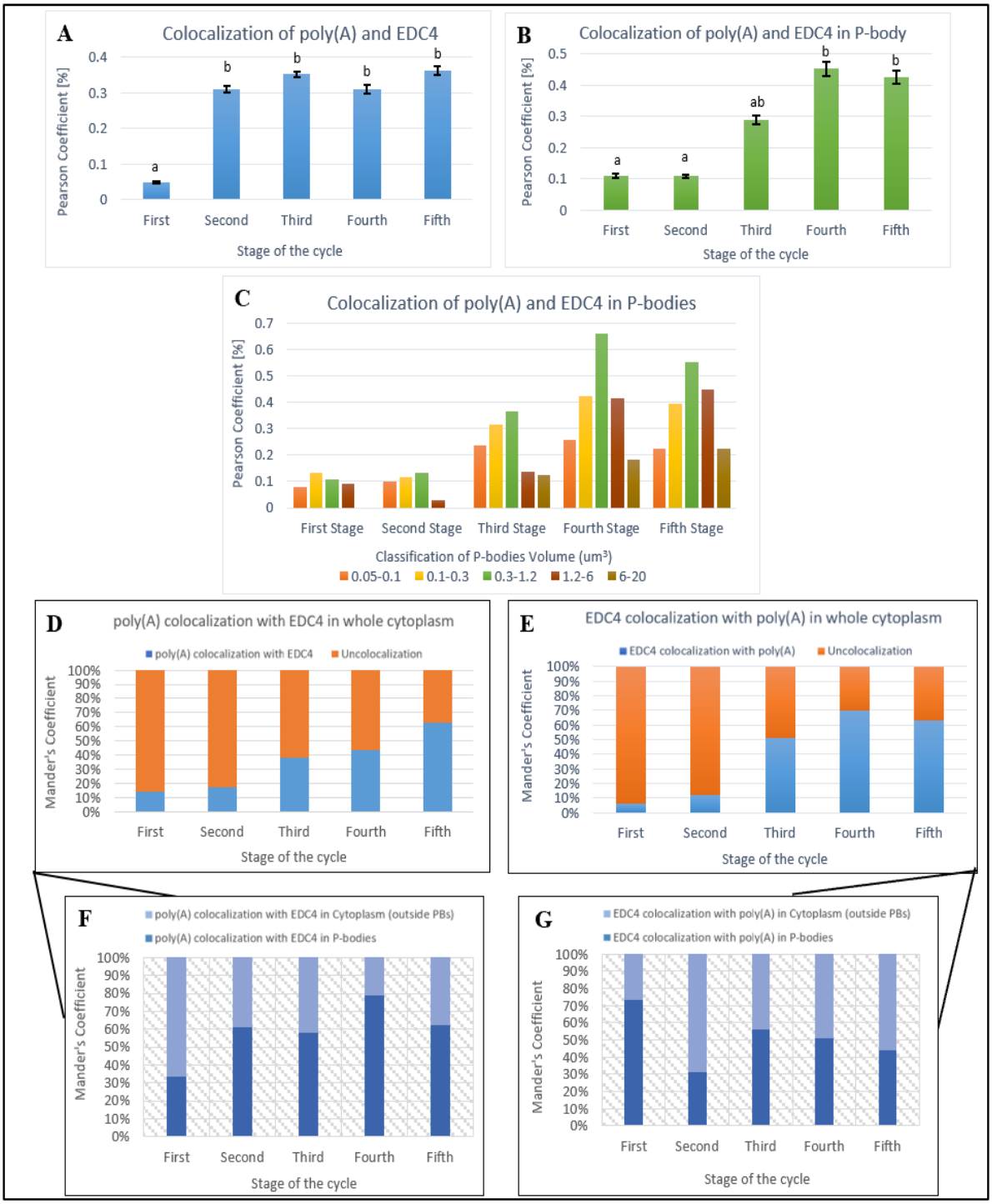

Figure 4-12. Statistical outcomes of the poly(A) RNA and EDC4 colocalization in the cytoplasm and P-bodies. A detailed description is provided in the text. (**A**) Pearson's colocalization coefficient of poly (A) RNA and EDC4 in the whole cytoplasm. (**B**) Pearson's colocalization coefficient of poly (A) RNA and EDC4 in P-bodies. (**C**) Pearson's colocalization coefficient of poly (A) RNA and EDC4 in different types of P-bodies volume sizes. (**D**) Mander's colocalization coefficient of poly (A) RNA with EDC4 in the cytoplasm. (**E**) Mander's colocalization coefficient of EDC4 with poly (A) RNA in the cytoplasm. (**F and G**) Distribution of colocalization between EDC4 and poly (A) RNA in cytoplasm and P-bodies, based on Mander's colocalization coefficient. The values are shown as means ± standard errors of the mean (SEMs). Based on Tukey's HSD test, the same letters indicate no significant difference ($p > 0.05$), while different letters indicate significant differences ($p \leq 0.05$).

4.5 During diplotene prophase I, the XRN4 protein colocalizes with cytoplasmic poly(A) RNA in *Larix decidua* microsporocytes

The XRN4 protein, as a 5'→3' exonucleolytic enzyme, was selected to be analyzed in the case of its presence in P-bodies during cell development in *Larix decidua* microsporocytes. Observations revealed the occurrence of P-bodies rich in poly(A) RNA and XRN4 protein. Notably, our finding reveals the cytoplasmic co-localization of the poly(A) RNA and XRN4 proteins (Figure 4-13).

4.5.1 Distribution pattern of poly (A) and XRN4 in the Cytoplasm and P-bodies

Stage 1: Nuclear poly(A) RNA levels are markedly higher than those in the cytoplasm (Figures 4-13A and 4-14A). Only a small fraction of cytoplasmic poly(A) RNA localizes to P-bodies (Figures 4-14A and C). The XRN4 protein is distributed throughout the cytoplasm, with about half localized within P-bodies (Figures 4-13B and 4-14B). The majority of these P-bodies fall within a volume range of 0.1-0.3 μm^3 (Figure 4-14D).

Stage 2: Nuclear poly(A) RNA levels begin to decline gradually, while cytoplasmic concentrations steadily increase (Figures 4-13D and 4-14A). Although the amount of poly(A) RNA within P-bodies remains relatively low compared to later stages, it rises slightly from stage 1 and is primarily located in P-bodies with volumes of 0.3-1.2 μm^3 and 0.1-0.3 μm^3, respectively (Figure 4-14C). The overall cytoplasmic abundance of XRN4 protein remains similar to that observed in stage 1, but its accumulation within P-bodies increases (Figures 4-13E and 4-14B). This indicates that the elevated cytoplasmic poly(A) RNA levels have not yet influenced the total cytoplasmic concentration of XRN4. The highest levels of XRN4 are detected in P-bodies, ranging from 0.1-0.3 μm^3 in volume (Figure 4-14D).

Stage 3: Cytoplasmic poly(A) RNA levels rise sharply (Figures 4-13G, 4-14A), accompanied by increased accumulation within P-bodies, particularly in 0.1-0.3 μm^3 volume (Figure 4-14C). The overall cytoplasmic concentration of XRN4 protein remains nearly unchanged from previous stages, although its levels within P-bodies show a slight increase (Figures 4-13H and 4-14B). The highest concentrations of XRN4 are observed in P-bodies, ranging from 0.1-0.3 μm^3 and 0.3-1.2 μm^3 in volume, respectively (Figure 4-14D). These findings indicate that,

despite the marked elevation of cytoplasmic poly(A) RNA compared to earlier stages, XRN4 levels remain relatively low in both the cytoplasm and P-bodies.

Stage 4: Cytoplasmic poly(A) RNA levels continue to rise, showing an increase compared to stage 3 (Figures 4-13J and 4-14A). Notably, the amount of poly(A) RNA within P-bodies more than doubles relative to the previous stage. Unlike stage 3, the highest concentrations are now observed in P-bodies with volumes of 0.3-1.2 μm^3 and 0.1-0.3 μm^3, respectively. Additionally, poly(A) RNA levels in large P-bodies (1.2–6 μm^3) are nearly three times higher than in the preceding stage (Figure 4-14C). Cytoplasmic XRN4 protein levels exhibit a substantial increase compared to earlier stages (Figures 4-13K and 4-14B), with a high accumulation within P-bodies. The largest P-bodies (6-20 μm^3) emerge during this stage with low concentration of XRN4, and high XRN4 level is concentrated in P-bodies of 0.3-1.2 μm^3, 0.1-0.3 μm^3, and 1.2-6 μm^3 volumes, respectively (Figure 4-14D). This stage likely represents the peak of XRN4 protein activity across all developmental stages.

Stage 5: Cytoplasmic poly(A) RNA levels decline compared to stage 4, while poly(A) RNA concentrations within P-bodies also decrease but remain higher than those in stage 3 (Figures 4-13M and 4-14A). The distribution pattern of poly(A) RNA within P-bodies differs from that seen in stage 4, with the highest concentrations found in P-bodies measuring 0.3-1.2 μm^3, 1.2-6 μm^3, and 0.1-0.3 μm^3, respectively (Figure 4-14C). XRN4 protein levels decrease in both the cytoplasm and P-bodies compared to stage 4, though they remain elevated relative to stage 3 (Figures 4-13N and 4-14B). Notably, over half of the cytoplasmic XRN4 is localized within P-bodies (Figure 4-14B). The greatest concentrations of XRN4 are observed in P-bodies of 0.3-1.2 μm^3, 1.2-6 μm^3, and 0.1-0.3 μm^3 in volume, respectively. Additionally, XRN4 levels in the largest P-bodies (6-20 μm^3) remain approximately unchanged from stage 4 (Figure 4-14D). These findings suggest that XRN4 activity in stage 5 surpasses that observed in stage 3.

4.5.2 Alteration in Number and Volume of P-bodies (XRN4)

Stage 1: The average number of P-bodies is lower than in the following three stages (Figure 4-14E). During this stage, P-bodies are primarily observed in smaller size ranges, specifically within the 0.1-0.3 μm^3 and 0.05-0.1 μm^3 volumes, respectively (Figure 4-14F). As a result, the

mean P-body volume is smaller compared to that of subsequent developmental stages (Figures 4-14G and H).

Stage 2: Shows an increase in the mean number of P-bodies compared to stage 1 (Figure 4-14E). Similar to the previous stage, the majority are still concentrated in the smaller volume ranges of 0.1-0.3 μm^3 and 0.05-0.1 μm^3. However, there is a noticeable rise in the number of P-bodies within the 0.3-1.2 μm^3 volume range compared to stage 1 (Figure 4-14F), resulting in a slight increase in the average P-body volume relative to the first developmental stage (Figures 4-14G and H).

Stage 3: Displays a slight increase in the average number of P-bodies (Figure 4-14E), with P-bodies in the 0.1-0.3 μm^3 range remaining the most abundant and exceeding counts from earlier stages. The number of the smallest P-bodies (0.05-0.1 μm^3) remains relatively stable compared to previous stages, while mid-sized P-bodies (0.3-1.2 μm^3) nearly double in number relative to stages 1 and 2. This contributes to a slight rise in the average P-body volume (Figures 4-14G and H). Despite the increase in mid-sized P-bodies, the smallest P-bodies (0.05-0.1 μm^3) continue to be more numerous than mid-sized, as observed in earlier stages (Figure 4-14F).

Stage 4: Shows a slightly lower average number of P-bodies compared to stage 3 and is similar to stage 2 (Figure 4-14E). P-bodies within the 0.1-0.3 μm^3 volume range remain the most prevalent. The smallest P-bodies (0.05-0.1 μm^3) continue to decline in number, while mid-sized P-bodies (0.3-1.2 μm^3) increase relative to stage 3. Notably, the number of mid-sized P-bodies now exceeds that of the smallest volume, marking a shift from the pattern observed in stage 3. Additionally, this stage introduces a small number of the largest P-bodies (Figure 4-14F). Collectively, these changes contribute to a noticeable increase in the average P-body volume compared to earlier stages (Figures 4-14G and H).

Stage 5: Demonstrates a reduction in the average number of P-bodies compared to stages 3 and 4, aligning with the count observed in stage 1 (Figure 4-14E). In contrast to earlier stages, P-bodies in the 0.3-1.2 μm^3 volume range are now the most abundant. Meanwhile, the number of small P-bodies (0.05-0.1 μm^3 and 0.1-0.3 μm^3) declines relative to previous stages. The quantity of larger P-bodies (1.2-6 μm^3 and 6-20 μm^3) remains relatively unchanged from stage 4 (Figure

4-14F). These changes contribute to a slight increase in the average P-body volume compared to stage 4 (Figures 4-14G and H).

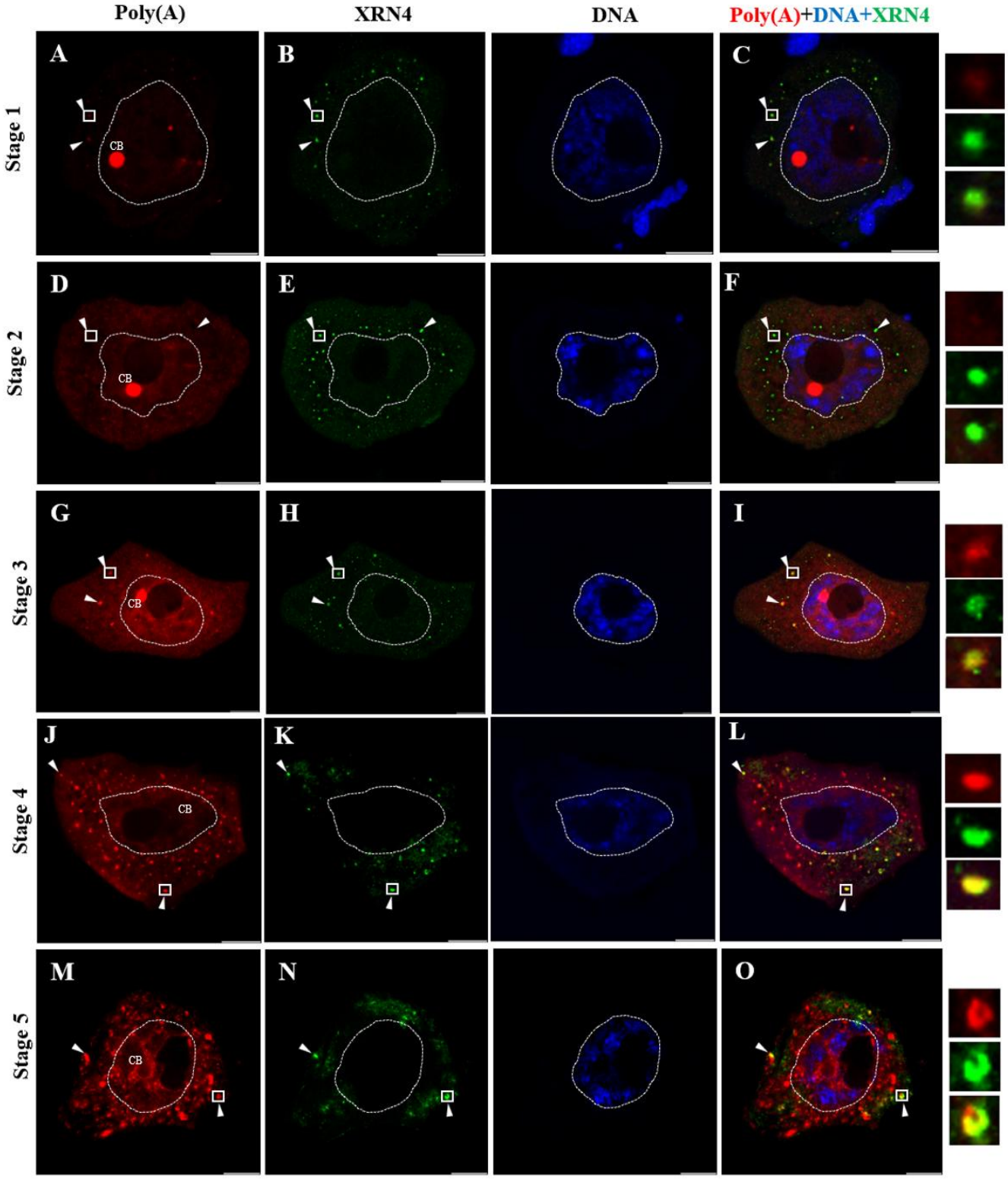

Figure 4-13. Localization of XRN4 proteins and poly(A) RNA in microsporocytes during diplotene. A detailed description is provided in the text. Multiple accumulations of XRN4 proteins colocalized with poly(A) RNA are visible (arrowheads). The right-hand panel represents the magnification of the fragments of the cytoplasm, which are marked with a square, arrowheads pointing to the P-bodies. CB – Cajal body. Scale bar 10 μm.

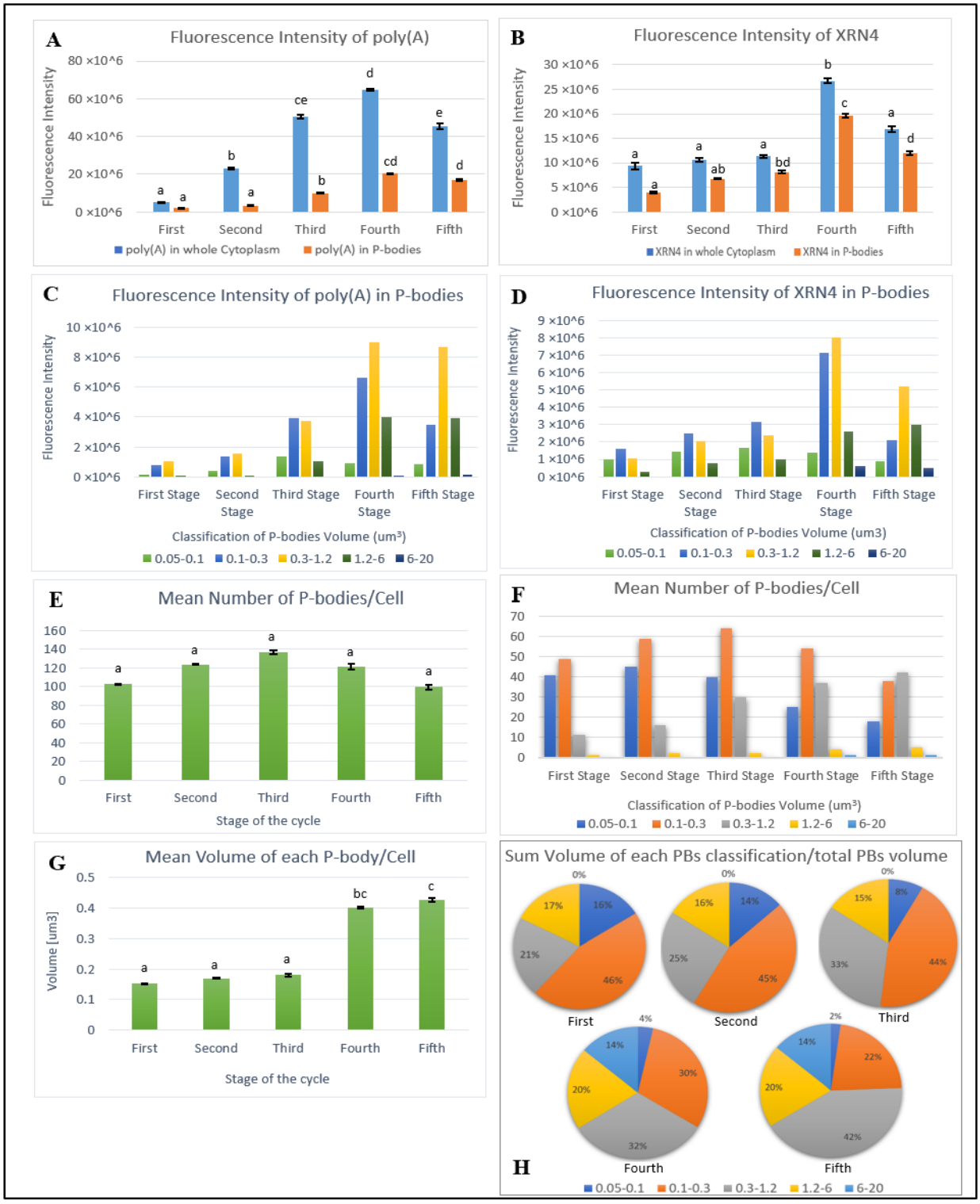

Figure 4-14. Statistical outcomes of the distribution pattern of XRN4 along with poly(A) RNA transcripts in the cytoplasm and P-bodies. A detailed description is provided in the text. (**A and B**) Fluorescence intensity of poly(A) RNA and XRN4 proteins during the five stages, respectively. (**C and D**) Fluorescence intensity of poly(A) RNA and XRN4 proteins in different types of P-bodies volumes, during the five stages, respectively. (**E**) The mean number of P-bodies per cell in the five stages. (**F**) The mean number of P-bodies per cell based on the P-bodies volume classification. (**G**) The mean volume of each P-body per cell. (**H**) The ratio of the sum volume of each P-body classification to the sum volume of total P-bodies in the five stages. The values are shown as means ± standard errors of the mean (SEMs). Based on Tukey's HSD test, the same letters indicate no significant difference ($p > 0.05$), while different letters indicate significant differences ($p \leq 0.05$).

4.5.3 Colocalization of poly(A) RNA and XRN4

Stage 1: The colocalization of poly(A) RNA and XRN4 in the cytoplasm is approximately 35%, making it one of the highest levels observed across all developmental stages (Figures 4-13C, 4-15A). Within P-bodies, the colocalization reaches around 27%, which is greater than that seen in stages 2 and 3 (Figure 4-15B). The strongest colocalization is found in P-bodies with volumes of 0.3-1.2 μm^3 and 0.1-0.3 μm^3, respectively (Figure 4-15C). This high rate of colocalization suggests that, during this stage, XRN4-enriched P-bodies are actively involved in the degradation of poly(A) mRNA. Mander's colocalization analysis further reveals that approximately 60% of poly(A) RNA overlaps with XRN4 in the cytoplasm, primarily within P-bodies (Figures 4-15D and F). Conversely, about 43% of XRN4 colocalizes with poly(A) RNA, with over half of this interaction occurring in the cytoplasm (Figures 4-15E and G).

Stage 2: Colocalization between poly(A) RNA and XRN4 in the cytoplasm decreases to around 20% (Figures 4-13F and 4-15A). Similarly, P-body colocalization drops to 16%, lower than in stage 1 (Figure 4-15B). The highest colocalization levels are still observed in P-bodies with volumes of 0.1-0.3 μm^3 and 0.3-1.2 μm^3 (Figure 4-15C). According to Mander's analysis, colocalization of poly(A) RNA with XRN4 across the cytoplasm falls to about 40%, indicating that the increased cytoplasmic poly(A) RNA in stage 2 is largely unassociated with XRN4 and is more diffusely distributed. This shift results in an overall reduction in total colocalization with XRN4 and a greater proportion of colocalization occurring in the general cytoplasm rather than within P-bodies (Figures 4-15D and F). Meanwhile, XRN4 colocalization with poly(A) RNA rises to approximately 60% (Figure 4-15E), with about half of this colocalization occurring within P-bodies (Figure 4-15G).

Stage 3: Colocalization between poly(A) RNA and XRN4 in the cytoplasm rises to approximately 28%, marking an increase compared to stage 2 (Figures 4-13I and 4-15A), while colocalization within P-bodies reaches around 20% (Figure 4-15B). The highest levels of overlap remain concentrated in P-bodies within the 0.3-1.2 μm^3 and 0.1-0.3 μm^3 volume ranges (Figure 4-15C). Mander's analysis reveals that poly(A) RNA colocalization with XRN4 throughout the cytoplasm increases to about 50% (Figure 4-15D), with roughly 40% of this occurring within P-bodies (Figure 4-15F). In contrast, XRN4 colocalization with poly(A) RNA

remains relatively unchanged compared to stage 2 (Figure 4-15E), although the proportion occurring in P-bodies shows an increase (Figure 4-15G). These findings suggest that as cytoplasmic poly(A) RNA levels gradually rise during stages 2 and 3, colocalization within P-bodies formed by XRN4 correspondingly increases.

Stage 4: Colocalization between poly(A) RNA and XRN4 in the cytoplasm rises to 35%, matching the level observed in stage 1 and exceeding that of stages 2 and 3 (Figures 4-13L and 4-15A). Approximately 40% colocalization occurs within P-bodies, roughly twice the level seen in stages 2 and 3 (Figure 4-15B). Compared to all earlier stages, colocalization increases across all P-body volume ranges, with the highest overlap observed in volumes of 0.3-1.2 μm^3, 1.2-6 μm^3, and 0.1-0.3 μm^3, respectively. Notably, the 1.2-6 μm^3 volume shows nearly four times the colocalization seen in previous stages. Colocalization within the largest P-bodies (6-20 μm^3) also emerges at this stage for the first time (Figure 4-15C), indicating a trend toward greater colocalization in larger P-bodies from stage 3 to 4. Mander's analysis reveals a slight decrease in the overall colocalization of poly(A) RNA with XRN4 in the cytoplasm, down to around 40% compared to stage 3 (Figure 4-15D). However, unlike stage 3, the majority of this colocalization now occurs within P-bodies (Figure 4-15F). Meanwhile, XRN4 colocalization with poly(A) RNA remains relatively consistent with stage 3 (Figures 4-15E and G), although around 65% now occurs within P-bodies, an increase from earlier stages. These findings suggest that stage 4 represents a pivotal phase for cytoplasmic mRNA turnover, where elevated concentrations of both poly(A) RNA and XRN4 protein, coupled with their pronounced colocalization, particularly within P-bodies, highlight active engagement in mRNA degradation.

Stage 5: Colocalization between poly(A) RNA and XRN4 in the cytoplasm declines to 25%, slightly below the level observed in stage 3 (Figures 4-13O and 4-15A). Within P-bodies, colocalization also decreases slightly to 38% compared to stage 4, though it remains nearly twice as high as in stage 3 (Figure 4-15B). The 0.3-1.2 μm^3 volume range continues to exhibit the highest colocalization, despite a reduction from stage 4. In the 1.2-6 μm^3 range, colocalization drops modestly, while the 6-20 μm^3 volume shows an increase relative to stage 4 (Figure 4-15C). According to Mander's analysis, poly(A) RNA colocalization with XRN4 experiences a slight increase compared to stage 4 (Figure 4-15D). As in the previous stage, the majority of this colocalization occurs within P-bodies rather than being dispersed throughout

the cytoplasm (Figure 4-15F). Conversely, XRN4 colocalization with poly(A) RNA shows a slight decline compared to stages 3 and 4 (Figures 4-15E and F). These results suggest a shifting pattern of interaction, where, although overall colocalization is reduced compared to stage 4, P-bodies continue to serve as the primary sites of interaction between XRN4 and poly(A) RNA.

Figure 4-15. Statistical outcomes of the poly(A) RNA and XRN4 colocalization in the cytoplasm and P-bodies. A detailed description is provided in the text. (**A**) Pearson's colocalization coefficient of poly (A) RNA and XRN4 in the whole cytoplasm. (**B**) Pearson's colocalization coefficient of poly (A) RNA and XRN4 in P-bodies. (**C**) Pearson's colocalization coefficient of poly (A) RNA and XRN4 in different types of P-bodies volume sizes. (**D**) Mander's colocalization coefficient of poly (A) RNA with XRN4 in the cytoplasm. (**E**) Mander's colocalization coefficient of XRN4 with poly (A) RNA in the cytoplasm. (**F and G**) Distribution of colocalization between XRN4 and poly (A) RNA in cytoplasm and P-bodies, based on Mander's colocalization coefficient. The values are shown as means ± standard errors of the mean (SEMs). Based on Tukey's HSD test, the same letters indicate no significant difference ($p > 0.05$), while different letters indicate significant differences ($p \leq 0.05$).

4.6 Comparison across all 5 proteins

- Part 1: Intensity, number, and volume of P-bodies (Figures 4-2 DCP5, 4-5 LSM4, 4-8 DCP2, 4-11 EDC4, 4-14 XRN4, panels A–H)

Panel A, poly(A) intensity (cytoplasm vs P-bodies)

Across all proteins, cytoplasmic poly(A) follows the same pattern: low in St. 1, rising in St. 2, peaking in stages 3-4, and declining in stage 5. The share of poly(A) located specifically in P-bodies increases in the later stages 3-4, most clearly for DCP2, EDC4, DCP5, and XRN4, with the highest in stage 4. While for LSM4 highest is in stage 3. (Sup. 1a)

Panel B, Protein intensity (cytoplasm vs P-bodies)

DCP5 peaks in stages 3-4 and falls in stage 5, with most signal in P-bodies throughout. LSM4 also peaks in stages 3-4 and drops in stage 5; about half of its signal is in P-bodies. DCP2 rises to a maximum in stages 4 and decreases slightly in stage 5 (remaining above stages 1-3); its P-body fraction increases over time. EDC4 is high in stages 3-5, peaking in stage 3, with more than half of its signal in P-bodies. XRN4 is low in stages 1-3, shows a pronounced peak in stage 4, and declines in stage 5 (still elevated compared with stages 1-3); the P-body share is especially large in stages 4-5. (Sup. 1b)

Panel C, poly(A) distribution within P-bodies by volume classes

poly(A) RNA is predominantly concentrated in small (0.1-0.3 μm^3) and mid-sized (0.3-1.2 μm^3) P-bodies. However, in stages 4-5, particularly for DCP2, EDC4, and XRN4, a notable shift occurs toward larger P-bodies (1.2-6 μm^3) (Sup. 1c).

Panel D, Protein distribution within P-bodies by volume classes

For DCP5, stage 1 exhibits relatively higher signal intensity in larger P-bodies (1.2-6 μm^3), which shifts toward smaller (0.1-0.3 μm^3) and medium-sized (0.3-1.2 μm^3) classes during stages

2-4, followed by a partial return to larger volumes at stage 5. LSM4 is mainly localized in small to mid-sized P-bodies, with larger structures appearing transiently at stage 3 and disappearing by stage 5. DCP2 and EDC4 display a gradual transition from small to an increased presence in mid-sized and large P-bodies (1.2-6 μm^3) during stages 4-5. For XRN4, stages 1-3 are dominated by small and mid-sized P-bodies, whereas stages 4-5 show a stronger representation of the larger class (1.2-6 μm^3) (Sup. 1d).

Panel E, Mean number of P-bodies per cell

DCP5 and LSM4 exhibit a peak in P-body number around stages 3-4, followed by a decline. DCP2 and EDC4 show a steady increase, reaching a peak or plateau during stages 4-5. XRN4 peaks at stages 3-4, then drops (Sup. 1e).

Panel F, Mean number of P-bodies per cell by volume class

Confirms Panel E: early stages are dominated by small P-bodies. During stages 3-4, both small and mid-sized P-body counts increase markedly. In stages 4-5, DCP2, EDC4, and XRN4 maintain relatively higher numbers of larger P-bodies, reflecting a developmental shift toward larger structures (Sup. 1f).

Panel G, Mean volume of each P-body per cell

DCP5 shows the largest mean volume at stage 1, reaching its minimum at stage 3, followed by a rebound in stages 4-5 to levels comparable to stage 2. LSM4 exhibits the opposite pattern, with the smallest mean volume at stage 1, a peak at stage 3, and a subsequent decline in stages 4-5 to approximately stage 2 levels. DCP2 and EDC4 both increase steadily, peaking at stage 4, with stage 5 values slightly lower but still above those of stages 1-3. XRN4 demonstrates a clear, continuous increase from stages 1 to 4, often peaking at stage 4, and remains elevated at stage 5 (Sup. 1g).

Panel H, Volumetric contribution of P-body classes relative to total P-body volume

P-bodies with mid-volumes of 0.3-1.2 μm^3 often predominate (Figure 5-3B). In stages 4-5, particularly for DCP2, EDC4, and XRN4, there is a marked increase in the volumetric contribution of larger P-bodies (1.2-6 μm^3), indicating a shift toward the formation of more voluminous structures (Sup. 1h).

Part 1 collectively indicates:

Distinct temporal and spatial patterns are observed among the individual decapping and decay proteins, reflecting differences in both timing and P-body organization (size and number). DCP5 and LSM4 exhibit earlier dynamics, with peaks in signal intensity and P-body number at stages 3-4, whereas DCP2, EDC4, and XRN4 peak later, at stages 4-5. Size dynamics also vary: P-bodies associated with DCP5 are largest at the beginning of the cycle, LSM4 reaches its maximum mid-cycle (stage 3), and DCP2, EDC4, and XRN4 show their largest P-bodies during the later stages (4-5). The overall rise in mean P-body number and volume during stages 3-5 correlates with elevated cytoplasmic poly(A) levels, indicating that the decapping machinery modulates P-body abundance and size in response to substrate availability. These findings support a model of sequential recruitment and activation of decay components, accompanied by dynamic remodeling of P-bodies throughout the microsporocyte developmental cycle. The observed timing aligns with the pattern of early peaks for DCP5 and LSM4 (stages 3-4) and later peaks for DCP2, EDC4, and XRN4 (stages 4-5).

- Part 2: Colocalization (Figures 4-3 DCP5, 4-6 LSM4, 4-9 DCP2, 4-12 EDC4, 4-15 XRN4, panels A–G)

Panel A, Pearson colocalization (whole cytoplasm)

DCP5 and LSM4: low in stages 1-2, peak in stage 3, maintained slightly lower in stage 4, and decline in stage 5. DCP2 and EDC4: very low in stage 1, rise in stages 2-3, peak in stage 4 for DCP2 and stage 5 for EDC4. XRN4: relatively high in stage 1 (likely because of processing of "leftover" transcripts from previous cycle), drop in stage 2, rise again to a Stage 4 peak, moderate decline in stage 5 (Sup. 2a).

Panel B, Pearson colocalization (P-bodies)

Trends mirror Panel A, DCP5, and LSM4: low in stages 1-2, peak in stage 3, maintained slightly lower in stage 4, and decline in stage 5. DCP2 and EDC4: very low in stage 1-2, rise in stages 3-5, peak in stage 4 for both. XRN4: relatively high in stage 1, drop in stages 2-3, rise again to a stage 4 peak, moderate decline in stage 5 (Sup. 2b).

Panel C, Pearson colocalization in P-bodies by volume classes

Mid-sized P-bodies (0.3-1.2 μm^3) dominate colocalization for most proteins and stages. In stages 4-5, there is a shift toward larger P-bodies (1.2-6 and 6-20 μm^3), particularly for DCP2, EDC4, and XRN4 (Figure 5-3A).

Panel D, Manders colocalization (fraction of poly(A) colocalizing with the protein)

The most important issue in these panels is to consider the intensity of poly(A) RNA. For instance, panel D related to the LSM4 in the first and third stages shows approximately the same percentage, while the poly (A) intensity in stage 1 is 5 times less than stage 3, which means the colocalization in stage 3 is much higher than in stage 1 (It is more clearly shown in Figure 5-1, colored hatched). So based on this explanation, poly(A)/DCP5 and poly(A)/LSM4 colocalization are highest in stages 3-4, while poly(A)/DCP2 and poly(A)/EDC4 colocalization reach maxima in stages 4-5, and poly(A)/XRN4 colocalization shows higher levels in stages 3-5. Of course, the poly(A)/XRN4 colocalization is relatively high in stage 1 compared with the next stages (likely because of processing of "leftover" transcripts from the previous cycle).

Panel E, Manders colocalization (fraction of the protein colocalizing with poly(A))

This panel reflects the degree of protein engagement, and it also depends on the intensity of each protein in the stages. DCP5/poly(A) and LSM4/poly(A) show the highest colocalization in stages 3-4. DCP2/poly(A), EDC4/poly(A), and XRN4/poly(A) show the highest colocalization in stage 4-5 (Sup. 2e).

Panels F, Manders colocalization (fraction of poly(A) colocalizing with the protein- distribution of colocalization between P-bodies and cytoplasm-outside P-bodies)

At each protein's peak, most poly(A)/proteins Manders-defined colocalization occurs within P-bodies rather than diffusely in the cytoplasm (Sup. 2f). A relative exception is XRN4 in stage 3, where more overlap remains cytoplasmic (with lower P-body levels). By stages 4-5, XRN4 clearly becomes P-body-centric (Figure 5-1, gray hatched).

Panels G, Manders colocalization (fraction of the protein colocalizing with poly(A)- distribution of colocalization between P-bodies and cytoplasm-outside P-bodies)

Panel G illustrates the distribution of protein engagement with poly(A) within and outside of P-bodies, which also correlates with protein intensity across stages. For instance, panel G related to the DCP5 in the first stage shows the highest colocalization in P-bodies rather than outside the P-bodies, and the lowest in stage 4. Since the DCP5 intensity in stage 1 is ~5 times less than in stage 4, it means the DCP5 intensity signal engagement in P-bodies in stage 4 is even higher than in stage 1. Therefore, because of the distribution of DCP5 signal intensity, accompanied by enhanced poly(A) toward the cytoplasm in later stages, the Mander's coefficient shows the following patterns: For DCP5/poly(A), DCP2/poly(A), and EDC4/poly(A), the strongest association occurs at stage 1 within P-bodies, followed by a gradual decline in later stages. In contrast, colocalization outside P-bodies increases over time. LSM4/poly(A) follows a similar trend but with a milder decrease within P-bodies. XRN4/poly(A), however, displays an opposite pattern, showing progressively higher colocalization with poly(A) inside P-bodies at later stages (Sup. 2g).

Part 2 collectively indicates:

Colocalization data confirm a phase shift in poly(A)-protein interactions: DCP5/LSM4 peak earlier stages 3, whereas DCP2/EDC4/XRN4 peak later stages 4-5. P-bodies are the main hubs of these interactions, especially at peak activity. Mander's coefficients imply that at peak phases significant fractions of both the poly(A) pool and individual protein pools engage within P-bodies. High XRN4 colocalization in stage 1 may reflect processing of residual mRNAs from the previous cycle. Overall, colocalization strongly supports a dynamic, sequential model of mRNA degradation in P-bodies during larch microsporocyte development.

4.7 Triple localization of decapping proteins (DCP5, DCP2, EDC4 and LSM4) and degradation protein (XRN4) with poly(A) RNA

The next step in this work focused on the individual P-bodies and their role in cytoplasmic poly(A) RNA degradation and asked whether the decapping and degradation proteins colocalized within the P-bodies. For this purpose, according to the obtained results from double labeling of DCP5, LSM4, DCP2, EDC4 and XRN4 with poly(A) RNA, triple labeling of

DCP5/DCP2/poly(A), DCP2/EDC4/Poly(A), DCP5/LSM4/poly(A) and DCP5/XRN4/poly(A) were performed to assess the colocalization of these proteins within P-bodies. Several images were captured from the different stages, and interestingly, the colocalization of the mentioned proteins was observed within the P-bodies during these stages. It should be mentioned that the DCP5 protein was considered as a main protein for triple colocalization with other proteins because:

1- Unlike the other eukaryotes, the DCP5 protein is the unique decapping protein and P-body marker in Plants.

2- Based on the results mentioned in double labeling, and also some previous studies (71,73). The DCP5 activity is functionally earlier than other proteins during the decapping process.

4.7.1 DCP5 colocalizes with DCP2 (decapping catalytic subunit) within P-bodies, during diplotene prophase I of *Larix decidua* microsporocytes

The results below (Figure 4-16) show the colocalization of DCP5 with DCP2 as the two main decapping proteins within the P-bodies in the cytoplasm. The first 3 stages are given as a representative. Interestingly, the poly(A) RNA localization is also observed inside the P-bodies, which refer to the co-processing of RNAs and the decapping protein's function.

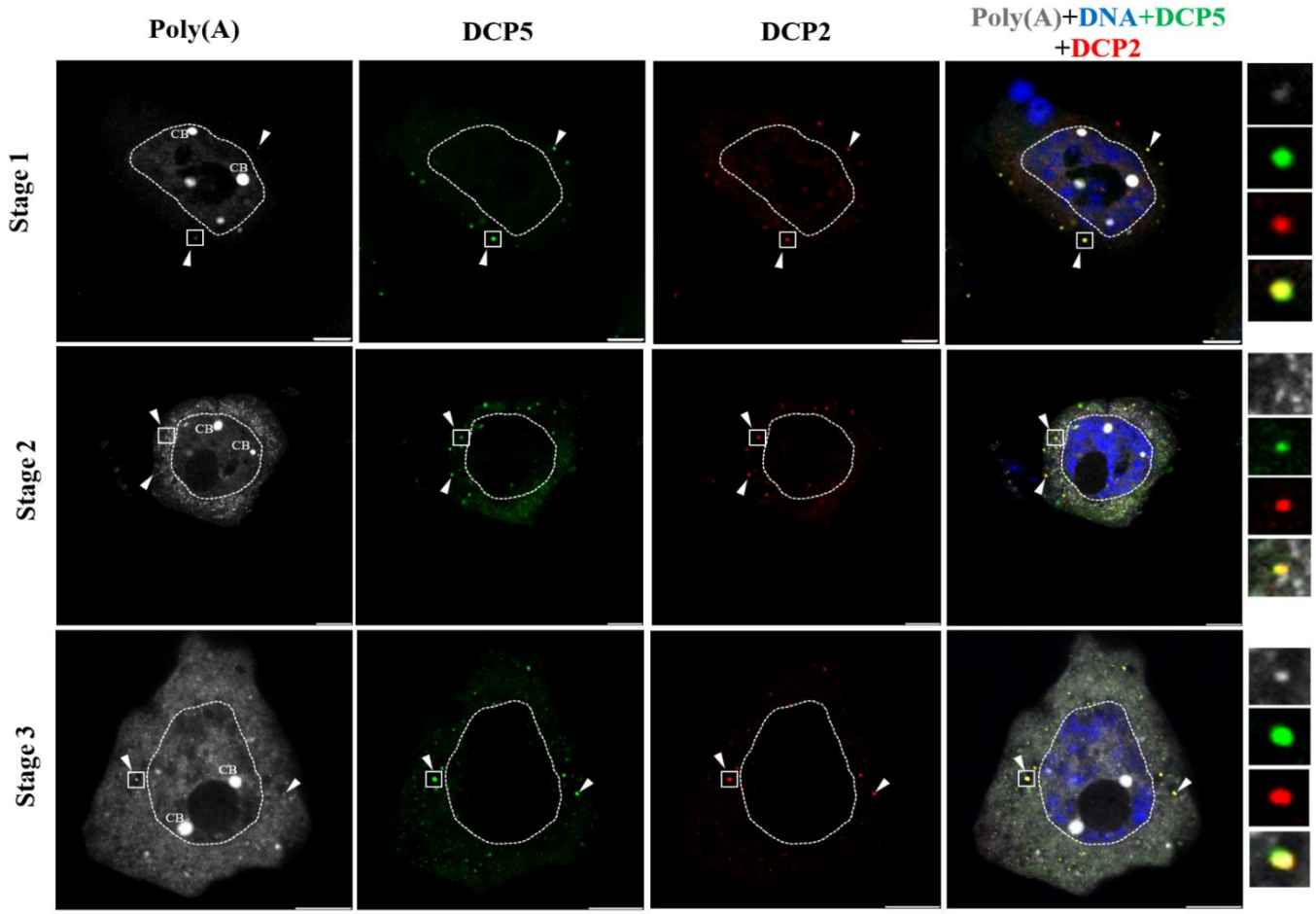

Figure 4-16. Co-localization of DCP5/DCP2/poly(A) in microsporocytes during diplotene. Multiple accumulations of DCP5 proteins colocalized with DCP2 proteins are visible (arrowheads). The right-hand panel represents the magnification of the fragments of the cytoplasm, which are marked with a square, arrowheads pointing to the P-bodies. CB – Cajal body. Scale bar 10 μm.

4.7.2 DCP2 colocalizes with EDC4 (decapping enhancer) within P-bodies, during diplotene prophase I of *Larix Decidua* microsporocytes

According to the result mentioned in double labeling of DCP2/poly(A) and EDC4/poly(A), which indicated that the distribution of both proteins during the 5 stages follows a similar pattern (Parts 4.3 and 4.4), and since EDC4 enhances the catalytic activity of DCP2 during cell development (94,95), therefore, the triple localization between DCP2/EDC4/poly(A) RNA was done to survey in case of the colocalization of both proteins within the P-bodies. Notably, the outcomes confirmed the colocalization of DCP2 and EDC4. The first 3 stages are given as a representative in Figure 4-17.

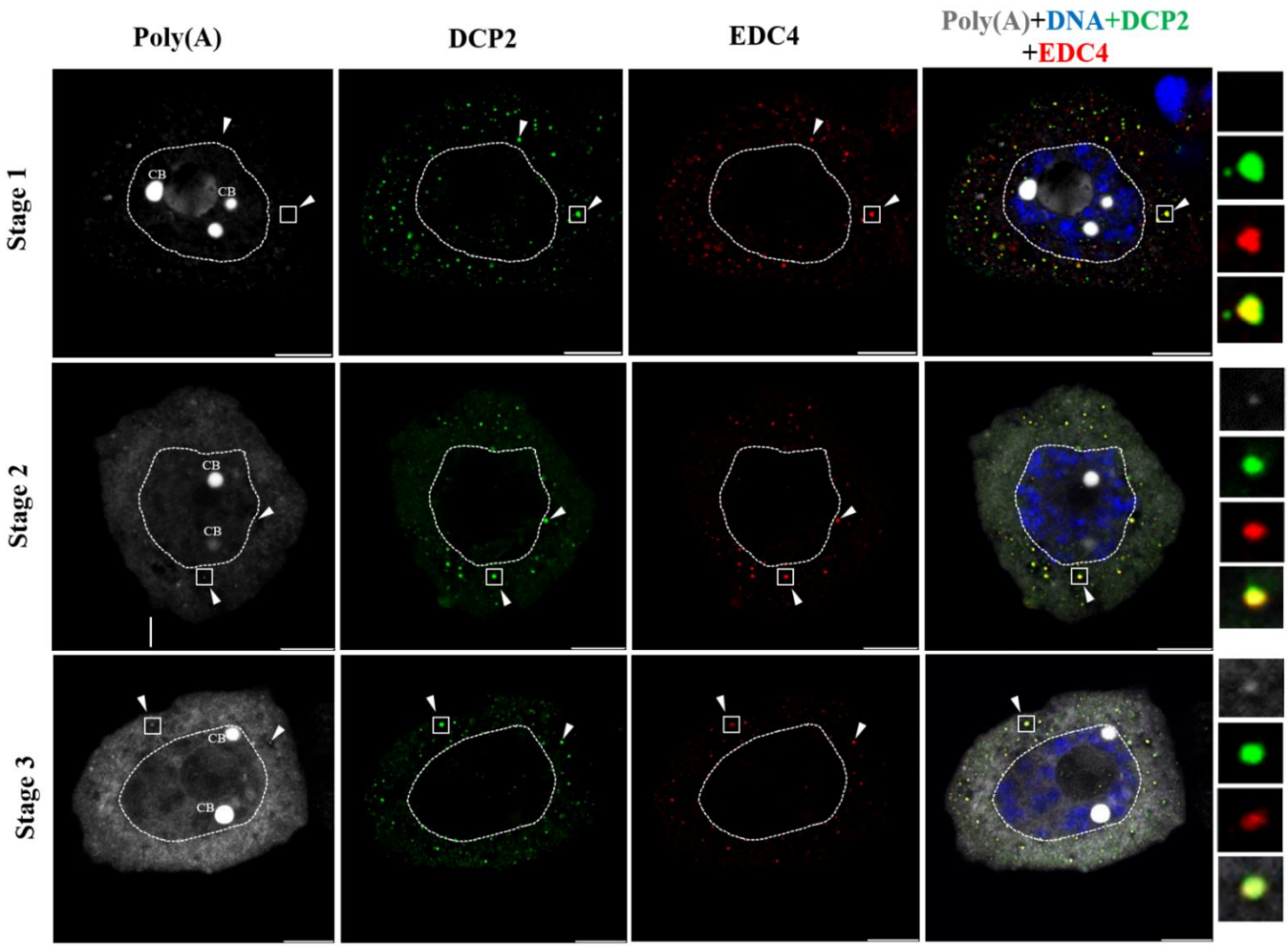

Figure 4-17. Co-localization of DCP2/EDC4/poly(A) in microsporocytes during diplotene. Multiple accumulations of DCP2 proteins colocalized with EDC4 proteins are visible (arrowheads). The right-hand panel represents the magnification of the fragments of the cytoplasm, which are marked with a square, arrowheads pointing to the P-bodies. CB – Cajal body. Scale bar 10 μm.

4.7.3 DCP5 colocalizes with LSM4 (deadenylation factor) in some, but not all, P-bodies during diplotene prophase I of *Larix decidua* microsporocytes

The triple labeling of DCP5/LSM4/poly(A) was proposed for analysis, as both proteins enhance DCP2 recruitment for decapping within P-bodies (73,98,122). The findings reveal that DCP5 and LSM4 colocalize in some P-bodies, but not all, suggesting that while LSM4 contributes to deadenylation, it does not always fully colocalize with the decapping factor in all P-bodies during cell development. This implies that LSM4 is probably not consistently necessary for decapping in P-bodies, or its role in P-bodies is transient, with LSM4 being released from P-bodies once its function is complete. In addition, in this investigation, all 5 stages were evaluated to check the P-bodies containing DCP5/LSM4 during cell development (Figure 4-18).

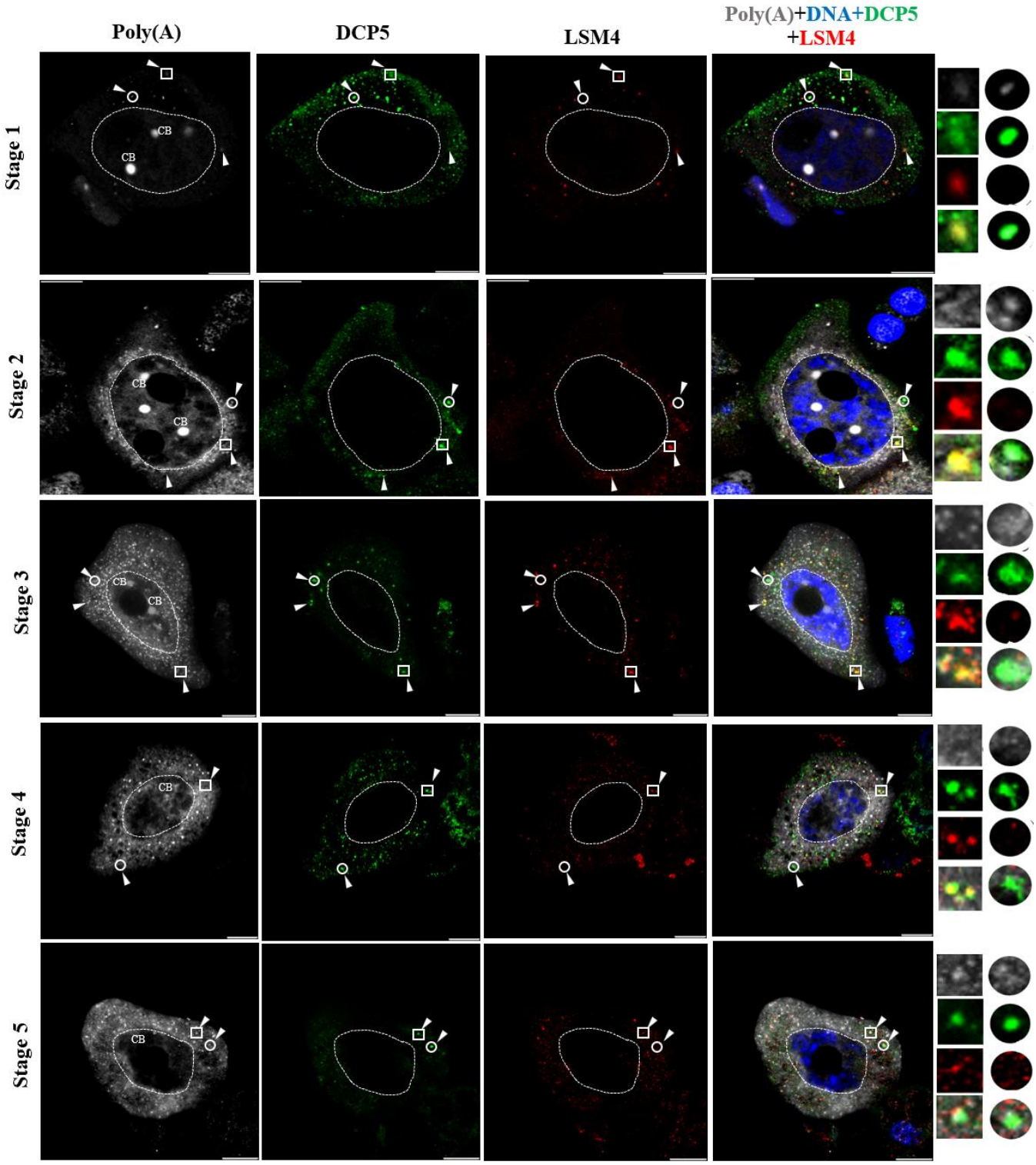

Figure 4-18. Co-localization of DCP5/LSM4/poly(A) in microsporocytes during diplotene. Multiple accumulations of DCP5 proteins colocalized with LSM4 proteins are visible (arrowheads). Arrowheads point to the P-bodies. The right-hand panel represents the magnification of the fragments of the cytoplasm. The square one refers to the P-bodies that include the DCP5/LSM4, while the circle one refers to the P-bodies depleted of LSM4. CB – Cajal body. Scale bar 10 μm.

4.7.4 DCP5 colocalizes with XRN4 (as a 5'→3' exonucleolytic factor) within P-bodies

The triple localization of DCP5/XRN4/poly(A) was performed, as DCP5 and XRN4 proteins, which participate in the initial (decapping) and final (exonucleolytic degradation) steps of 5'→3' RNA degradation, respectively. The results demonstrated that DCP5 and XRN4 colocalize within P-bodies. Figure 4.19 indicates to first 3 stages as representative for DCP5/XRN4/poly(A) colocalization.

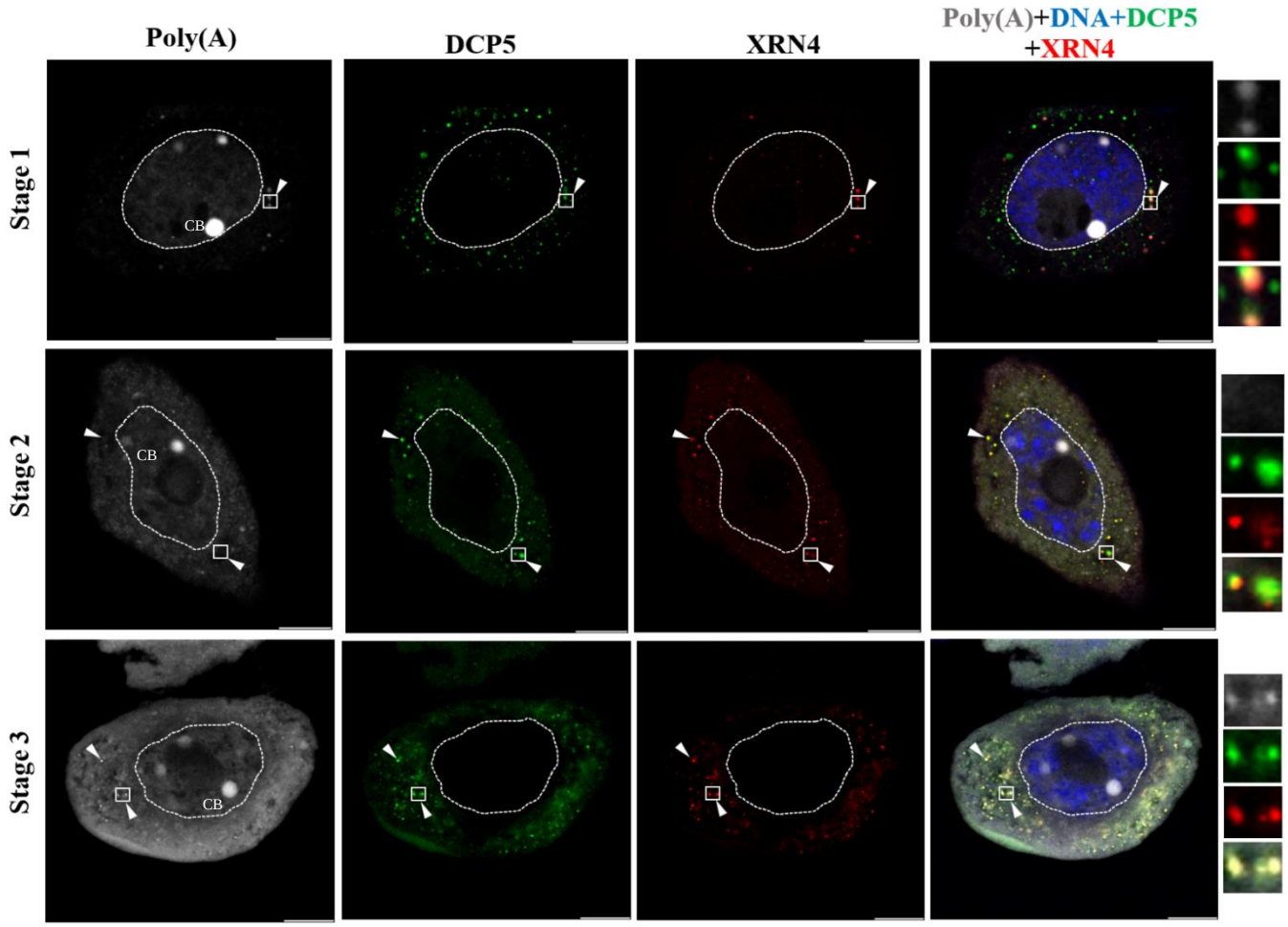

Figure 4-19. Co-localization of DCP5/XRN4/poly(A) in microsporocytes during diplotene. Multiple accumulations of DCP5 proteins colocalized with XRN4 proteins are visible (arrowheads). The right-hand panel represents the magnification of the fragments of the cytoplasm, which are marked with a square, arrowheads pointing to the P-bodies. CB – Cajal body. Scale bar 10 μm.

4.8 Negative evidence for Stress granules (SGs)

To verify whether the studied P-bodies show the overlap with stress granules during cellular development, analysis of the distribution of a protein involved in stress granule assembly was performed, in colocalization with decapping proteins. The PAB2 was used as a stress granule marker (70,197–199). No accumulations of the stress granule marker were noted in P-bodies, suggesting the distinction of examined P-bodies and Stress Granules for the investigated samples at all stages of meiosis in *Larix decidua* (Figure 4-20).

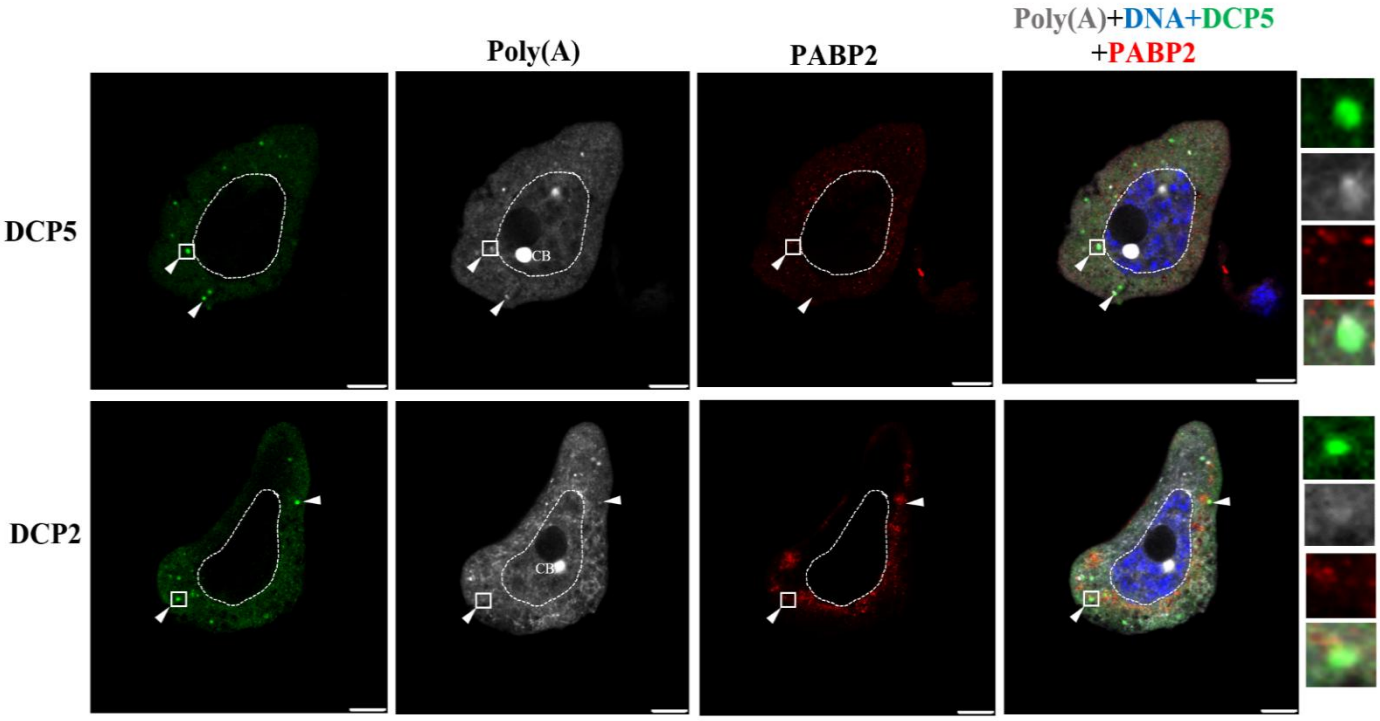

Figure 4-20. Shows no colocalization of DCP5/DCP2 with stress granule marker. No colocalization of PABP2 proteins with DCP5 and DCP2 proteins is visible (arrowheads). The right-hand panel represents the magnification of the fragments of the cytoplasm, which are marked with a square, arrowheads pointing to the P-bodies. CB – Cajal body. Scale bar 10 μm.

4.9 Microscopic analysis confirmed the localized decapping proteins within isolated P-bodies (Cytoplasmic Fractionation)

In order to further investigate P-bodies in the cytoplasm, the cytoplasmic fractionation solution was double-labeled with DCP5/DCP2 and DCP5/XRN4 as representative proteins and visually checked to ensure the isolation of P-bodies (Figure 4-21). The results show that these proteins are colocalized within the isolated P-bodies.

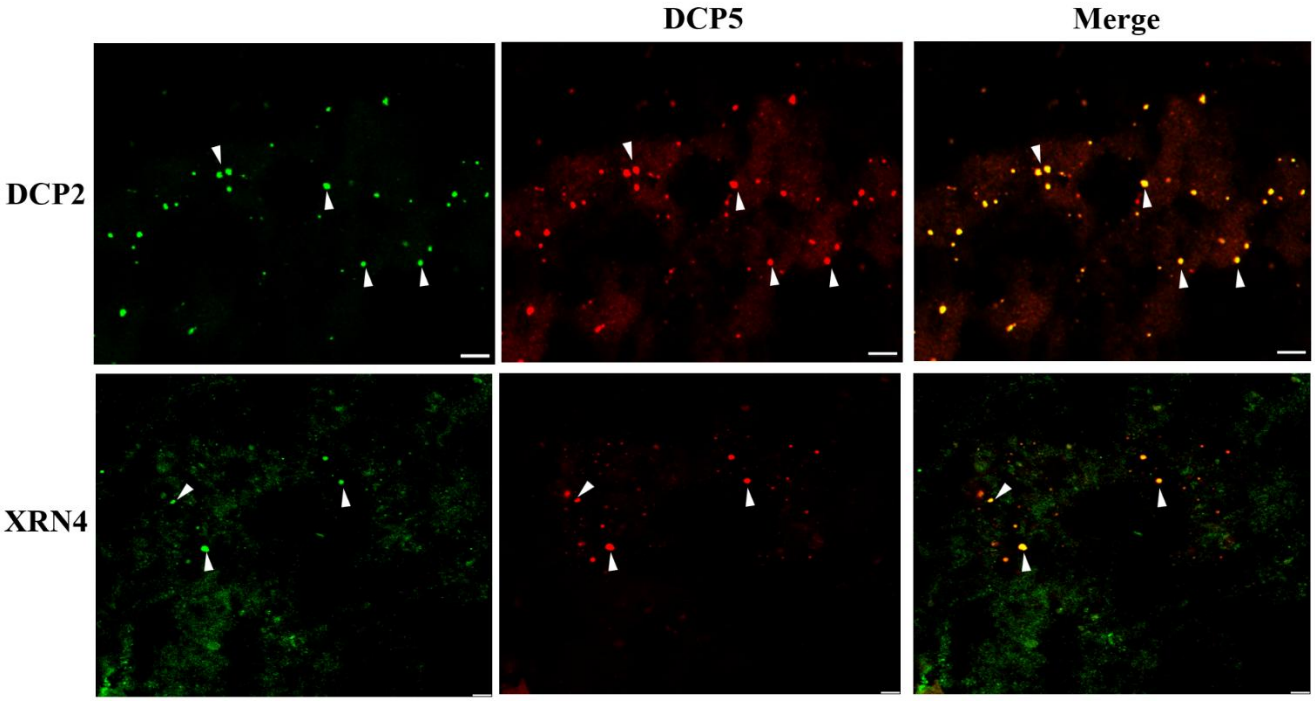

Figure 4-21. Shows the P-bodies from cytoplasmic fractionation. Multiple accumulations of DCP5/DCP2 and DCP5/XRN4 proteins colocalization are visible within the different volume sizes of P-bodies (arrowheads). Scale bar 5 μm.

4.10 Co-Immunoprecipitation analysis confirms the interaction of DCP5/DCP2/EDC4 proteins

The Western blot analysis was performed on the total proteins to confirm the presence and specificity of DCP5, DCP2, EDC4, LSM4, and XRN4 antibodies. This step was critical to validate their localization, as previously observed via confocal microscopy, and to ensure the reliability of subsequent interaction studies. (Figure 4-22) (Sup. 3 and 4, refer to the whole blot and experiment repetition of WB). Since we have already observed the colocalization of DCP5/DCP2, DCP5/LSM4, and DCP5/XRN4, therefore, to determine whether these proteins interact directly, co-immunoprecipitation was carried out using an anti-DCP5 antibody on the protein isolated in cytoplasmic fractionation (P-bodies). The co-immunoprecipitation assay revealed that DCP5 protein successfully precipitated with DCP2 and EDC4, providing evidence of a direct physical interaction between the DCP5/DCP2 and DCP5/EDC4 proteins in the P-bodies (Figure 4-22). These findings align well with the confocal microscopy data, where the colocalization of DCP5/DCP2 and DCP2/EDC4 was visually observed, and co-immunoprecipitation results demonstrate that DCP5 interacts with both DCP2 and EDC4, suggesting that all three proteins could be part of the same complex or compartment, further supporting the hypothesis of their functional relationship within P-bodies.

On the other hand, despite the DCP5/LSM4 and DCP5/XRN4 colocalization observed via confocal microscopy, co-immunoprecipitation experiments revealed no direct physical interaction between DCP5/LSM4 and DCP5/XRN4. This lack of interaction more likely indicates that their presence in the P-bodies does not involve direct binding (It has also been reported in 4.7.3 part related to DCP5/LSM4). P-bodies serve as hubs for RNA metabolism, where proteins like DCP5, LSM4, and XRN4 may transiently associate to perform coordinated functions during cell development without forming stable protein-protein complexes. The colocalization of DCP5 with LSM4 and XRN4 likely reflects their spatial proximity within P-bodies rather than direct physical contact (Which is also confirmed by the "string-db.org", Figure 5-2). It is plausible that these proteins are part of larger, multiprotein assemblies or that their interactions are mediated indirectly through RNA molecules or other P-body components. This model aligns with the observed variability in LSM4 colocalization and the stage-specific patterns of DCP5 and XRN4, highlighting the flexibility, complexity, and heterogeneity of RNA degradation machinery within P-bodies during cell development.

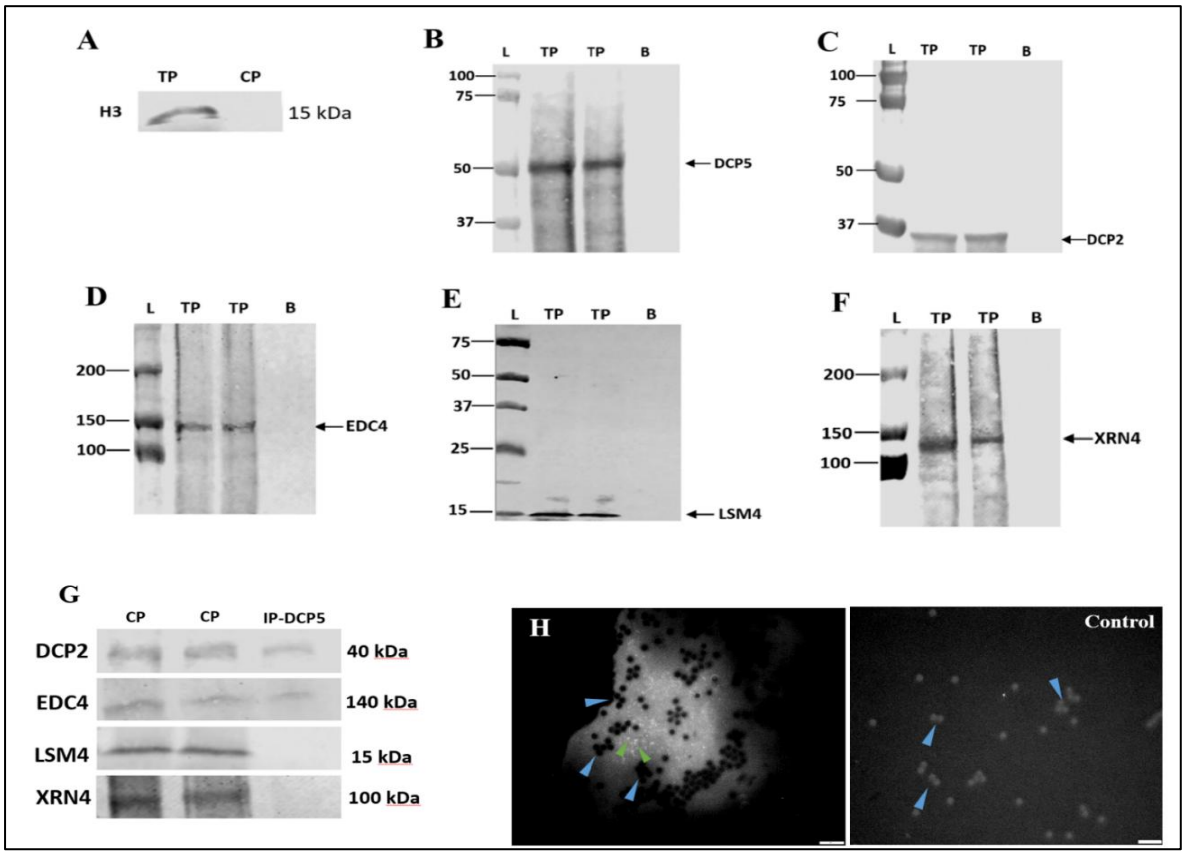

Figure 4-22. Immunoblots related to the Western blot and Co-immunoprecipitation. A) Validation of the cytoplasmic fractionation for the co-immunoprecipitation method (CP-CoIP). Cropped Blot of identification of histone H3 in the total protein by Western blot, and no detection signal in the cytoplasmic fraction for co-immunoprecipitation. **B)** Identification of DCP5 protein. **C)** Identification of DCP2 protein. **D)** Identification of EDC4 (VCS) protein. **E)** Identification of LSM4 protein. **F)** Identification of XRN4 protein. **TP**; Total protein. **L**; Ladder kDa. **B**; Blank. **G)** Cropped blot related to the co-immunoprecipitation of DCP5 with DCP2, EDC4, LSM4, and XRN4. (Whole Blot in Sup. 3) **CP**; refer to the Cytoplasmic fractionation protein. **IP-DCP5;** refer to the sample after immunoprecipitation using DCP5 antibody. **H)** Microscopic confirmation to ensure the presence of P-bodies and beads in the immunoprecipitation (Another example in Sup. 5). **Blue arrow**: refer to the Dynabeads. **Green arrow**: refer to the RNA enrichment-P-bodies. Control also shows no RNA enrichment-P-bodies (Scale bar 10 μm).

4.11 RNA analysis shows the different kinds of transcripts precipitated with decapping proteins

The total isolated RNA was analysed by the bioanalyzer. The analysis confirmed the typical electrophoretic distribution for total RNA, with two intense bands corresponding to 18S and 28S rRNA in the appropriate proportion (RNA integrity index (RIN) = 9.30; Figure 4-23 marked Input). The mRNA isolated from total RNA was also analyzed by bioanalyzer, and in the lane corresponding to mRNA, a non-homogeneous pool of RNA of different lengths was observed, ranging from 25 to 4000 nt (Figure 4-24 marked mRNA). In the lane corresponding to RNA after immunoprecipitation, which was marked by LSM4-RIP, DCP5-RIP, DCP2-RIP, and EDC4-RIP, the non-homogeneous pool of RNA of different lengths was also observed, ranging from 25 to 4000 nt (Figure 4-23). No signal was recorded in the control sample related to the RIP with no antibodies. After qualitative and quantitative analysis, the obtained RNA was used as a template for the synthesis of double-stranded cDNA libraries for sequencing with a commercially available kit, NEBNext® Ultra™ II Directional RNA Library Prep Kit for Illumina®.

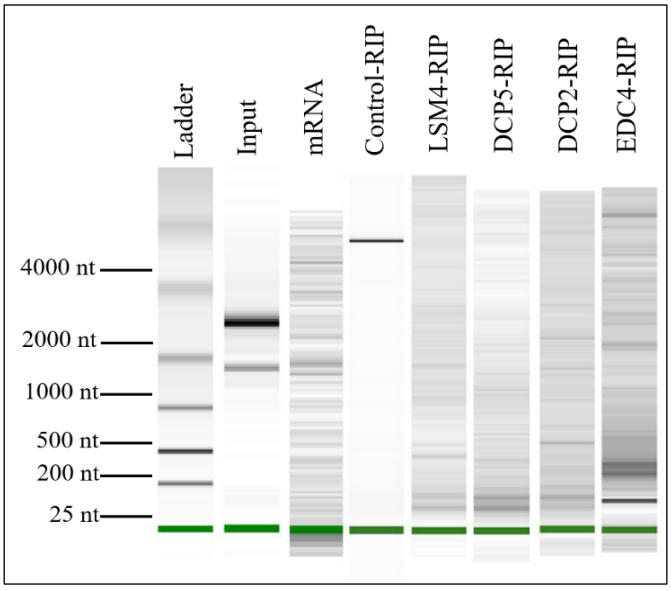

Figure 4-23. Qualitative analysis of RNA. Input refers to the total isolated RNA. **mRNA** refers to polyadenylated (poly(A)) mRNA isolated from total RNA. **Control-IP** refers to control of RIP reaction without antibodies**. LSM4-RIP, DCP5-RIP, DCP2-RIP, and EDC4-RIP;** refer to the RIP reaction with each antibody of interest.

4.11.1 Clustering and comparative analysis of differentially enriched transcripts in RIP-Seq data

Three Biological replicates within each condition (Control, DCP2, DCP5, EDC4, and LSM4) clustered closely together, demonstrating high reproducibility and consistency among replicates (Figure 4-24A). Control samples formed a distinct cluster, whereas IP samples were clearly separated, indicating distinct transcript enrichment profiles associated with each decapping component. The heatmap also revealed partial overlap among certain IP conditions, suggesting that some RNA targets may be bound by multiple proteins within the decapping machinery. Principal Component Analysis (PCA) of rlog-transformed expression counts supported these clustering results (Figure 4-24B). The first two principal components explained 31% and 17% of the total variance, respectively. Replicates from each antibody were tightly grouped, while a clear separation between control and IP samples was observed along PC1. This pattern highlights the robustness of the data and confirms that biological variability among IP conditions reflects true differences in RNA association profiles rather than technical noise. To further investigate shared and condition-specific transcript enrichment, a Venn diagram was generated using genes with adjusted p-values < 0.05 identified by DESeq2 (Figure 4-24C). Each IP condition (DCP2, DCP5, EDC4, and LSM4) exhibited a distinct set of significantly enriched transcripts, with varying degrees of overlap. Overall, these results demonstrate both shared and specific RNA–protein interaction patterns among the analysed decapping complex components.

It is worth noting that XRN4 was not included in the RIP-seq experiments due to its intrinsic role as a 5′→3′ exonuclease. XRN4 catalyzes the degradation of decapped RNAs, leading to the accumulation of highly fragmented and short-lived RNA molecules (127,200,201). As a result, the RNA species bound to XRN4 are often unstable and may be lost during the immunoprecipitation or library preparation steps, making them unsuitable for reliable sequencing.

In addition, XRN4 participates not only in the canonical decapping-dependent RNA decay pathway but also in several decapping-independent degradation routes, including co-translational decay, nonsense-mediated decay (NMD), and miRNA-mediated decay (202–204). Therefore, the RNA population associated with XRN4 could reflect a mixture of transcripts

unrelated to the DCP2, DCP5, EDC4, and LSM4 complex. This would complicate the interpretation of RIP-seq data and obscure the specific interactions related to decapping–mediated mRNA turnover. For these reasons, we restricted the RIP-seq experiments to DCP2, DCP5, EDC4, and LSM4, whose RNA associations are more stable and specifically linked to the early decapping steps. This approach ensured greater reproducibility and biological relevance of the sequencing results.

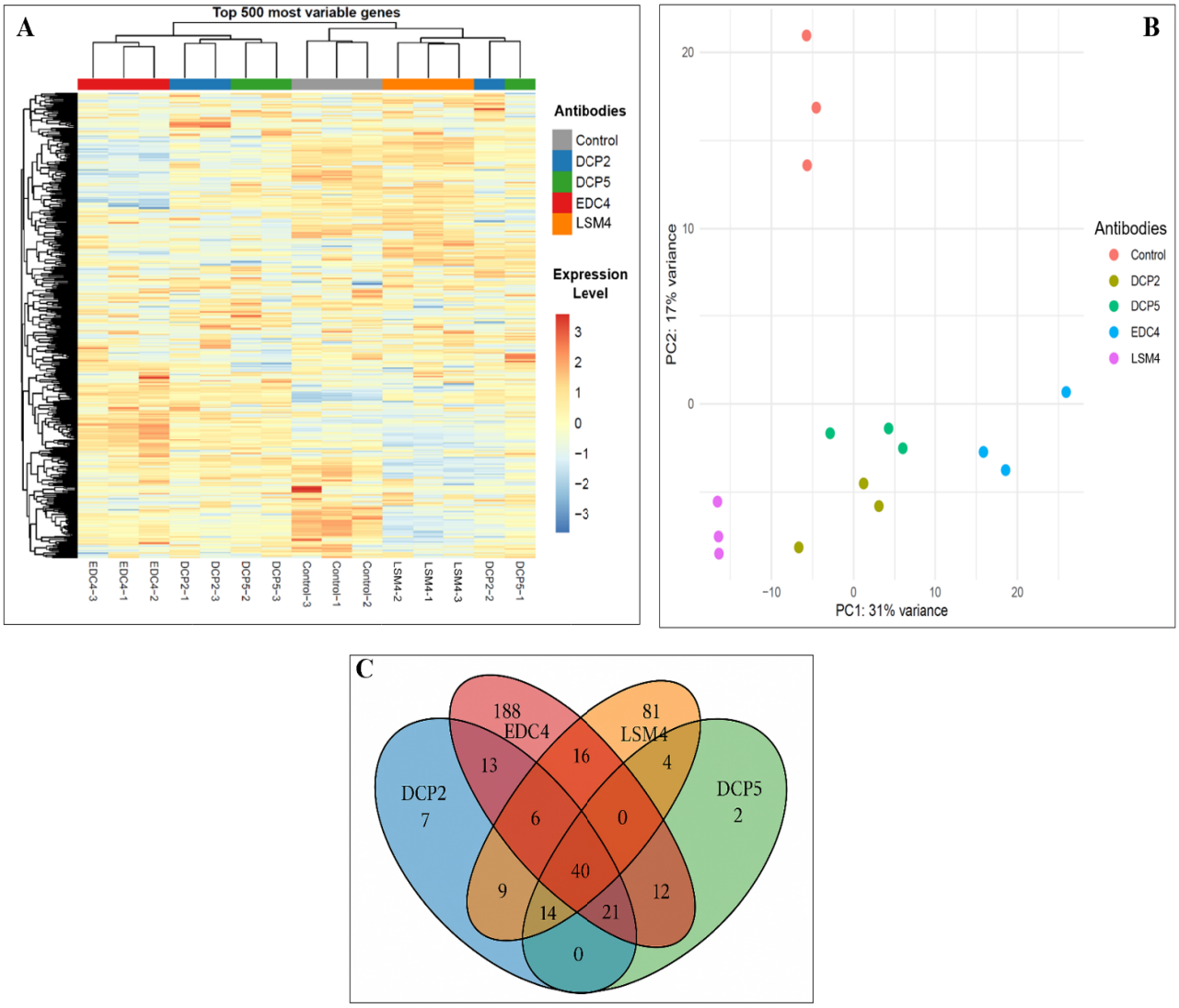

Figure 4-24. **RIP-seq analysis**. **A)** Heatmap showing the top 500 most variable transcripts across all samples after rlog transformation (DESeq2). Rows represent transcripts and columns represent biological replicates of each condition (Control, DCP2, DCP5, EDC4, and LSM4). Color intensity corresponds to relative expression levels. Hierarchical clustering indicates strong grouping of replicates and clear separation between control and IP samples. **B)** PCA plot based on rlog-transformed expression counts. Each point represents one biological replicate from Control or IP antibodies (DCP2, DCP5, EDC4, and LSM4). PC1 and PC2 explain 31% and 17% of the total variance, respectively, showing tight clustering of replicates and clear separation between experimental groups. **C)** Venn diagram showing the overlap of significantly enriched transcripts (P-Value < 0.05) among IP samples (DCP2, DCP5, EDC4, and LSM4). Overlapping regions indicate transcripts significantly enriched in more than one IP condition, while unique regions represent condition-specific enrichment.

4.11.2 Annotation and identification of transcripts associated with decapping proteins

As a result of RIP-Seq analysis, a total of 413 transcript sequences were obtained that specifically co-precipitated with the DCP2, DCP5, EDC4, and LSM4 proteins, either individually or as co-partners among the decapping proteins (Table 4-1).

Table 4-1. 413 numbers of sequences identified in Venn diagram and 216 number of annotated potential mRNAs

Proteins	Number of sequences	Number of Annotated
EDC4	188	122
LSM4	81	34
DCP2	7	6
DCP5	2	2
EDC4 & LSM4	16	10
DCP2 & EDC4	13	6
DCP5 & EDC4	12	7
DCP2 & LSM4	9	3
DCP5 & LSM4	4	2
DCP2 & DCP5 & EDC4	21	9
DCP2 & DCP5 & LSM4	14	2
DCP2 & EDC4 & LSM4	6	2
DCP2 & DCP5 & EDC4 & LSM4	40	11

216 transcripts were identified as potential mRNAs that interact with DCP2, DCP5, EDC4, and LSM4 (Others were not assigned any similar proteins against the reference genome). GO enrichment and functional analysis revealed that the common targets of DCP2, DCP5, EDC4, and LSM4 include mRNA-encoding proteins localized to several cell components (Table 4-2) and involved in a variety of molecular functions (Table 4-3).

Table 4-2. The Cellular compartments related to the annotated transcripts.

Cellular Component	Number of GO
Membrane	93
Mitochondria	89
Chloroplast	42
Cytoplasm	12
Nucleus	12
Ribosome	12
Endoplasmic reticulum	6
Extracellular region	6
Small ribosomal subunit	5
Cytoskeleton	3
Cell wall	2
P-body	1

Table 4-3. The Molecular function of annotated transcripts.

Molecular Function	Number of GO
Dehydrogenase activity	36
Ion binding	25
ATP binding	18
RNA binding	15
Quinone binding	15
Structural molecule activity	14
NAD Binding	12
ATPase activity	9
Reductase activity	9
Oxidase activity	8
Ligase activity	6
Endopeptidase activity	6
Nucleic acid binding	6
DNA binding	5
Endonuclease activity	5
DNA polymerase activity	5
Transporter activity	4
Heme binding	4
Translation elongation factor activity	4
Protein binding	4
GTPase activity	3
GTP binding	3
ATP hydrolysis activity	3
Hydrolase activity	3
Transcription coactivator	2
Chromatin binding	2
Protein heterodimerization activity	2
Transcription initiation factor activity	2

Chlorophyll binding	2
Triphosphatase activity	1
Lipid binding	1
RNA polymerase activity	1
Protein dimerization activity	1

5. Discussion

5.1 Temporal and spatial convergence suggests that decapping-dependent degradation drives the decline of poly(A) RNA levels in *Larix decidua* microsporocytes during diplotene

The regulation of mRNA stability and degradation is pivotal in modulating gene expression during developmental processes in plants. This study explores the roles of decapping and degradation proteins, associated with cytoplasmic bodies called P-bodies, and regulating poly(A) RNA levels during the diplotene stage of prophase I in *Larix decidua* microsporocytes. So far, cytoplasmic structures in which Sm proteins and mRNA would accumulate simultaneously have been reported in *Larix decidua* microsporocytes. These are plant cells of the male germ line, which in the studied period (prophase I meiosis diplotene) undergo a series of strictly controlled chromatin reorganization processes (181), aimed at preparing the cell for division and the formation of the male gametophyte (pollen). However, no study has investigated the interaction of DCP5, DCP2, EDC4, LSM4, and XRN4 proteins during plant cell development within P-bodies, P-bodies' dynamics, and their association with mRNAs. On the other hand, the decapping and cytoplasmic degradation processes in *Larix decidua* are still unknown. Our findings provide novel insights into the spatial and temporal dynamics of these processes during plant cell development, addressing the hypotheses outlined in the doctoral thesis. Regarding the performed research on *Larix decidua* microsporocytes, during diplotene, which lasts about five months in this species, few bursts of de novo transcription trigger a cycle including five stages of increased levels of poly-adenylated RNA (poly(A) RNA) in the cell (181), in which a single cycle lasts 10-11 days, with the first stage (stage 1) lasting the longest (8-9 days), and 2-5 stages are much shorter and only last several hours each (Figure 2-1) (184). As outcomes from the former studies, the nuclear poly(A) RNA is being distributed and additionally accumulated in several spherical assemblies that refer to Cajal bodies (CBs) in the nucleus. On the other hand, cytoplasmic poly(A) RNA is mainly spread in the cytoplasm’s surroundings and occasionally appears in small clusters, and a significant decrease in poly(A) RNA levels was reported at the final stage of poly(A) transcript distribution in the cytoplasm (181). In this investigation, we have evaluated the role of DCP5 and DCP2 proteins as decapping factors (73,94), EDC4 and LSM4 proteins as decapping co-factors (94,205), and

XRN4 as a 5'→3' degradation factor (127), regarding the cytoplasmic distribution pattern of poly(A) RNA and dynamics of P-bodies during the diplotene phase to analyze whether the mentioned reduction of cytoplasmic poly(A) RNA in the last stage of the poly(A) RNA cycle is caused by the decapping system. In the literature to date, the decapping system and localization of P-bodies in the cytoplasm have been demonstrated in animal cells (206,207) and mammalian spermatocytes (208,209). In plant cells under environmental changes like stress, several studies have reported the association of DCP5 (73,95,114,210), DCP2 (70,99,201,211,212), EDC4 (95,99,103,213,214), LSM4 (98), and XRN4 (70,201) with RNA transcripts to perform the decapping process and analyze the P-bodies formed by these proteins. While just a few studies focused on plant cell development and unstressed conditions and reported the role of some of these proteins in regulating RNA transcripts within P-bodies and the cytoplasm to conduct the decapping process (73,88,94,103,215). Therefore, in this doctoral thesis, in addition to confirming that the decreases of the cytoplasmic transcripts at the last stage of poly(A) RNA cycle could be related to the decapping-dependent mRNA decay process, we also confirmed the presence of P-bodies and their dynamics during plant cell development, which no study already reported in plant cells.

5.2 Cytoplasmic poly(A) RNA transcripts colocalize with the decapping protein complex and degradation protein to undergo decapping and decay processing

The study reveals a highly dynamic and developmentally regulated relationship between cytoplasmic mRNA pools (marked by poly(A) RNA) and the decapping factors (DCP5 and DCP2), decapping co-factors (EDC4 and LSM4), and the degradation protein (XRN4) during 5 stages of the poly(A) RNA cycle in diplotene prophase I of *Larix decidua* microsporocytes. This dynamic is intricately linked to P-body formation, suggesting a tightly controlled program for mRNA decapping and degradation essential for microsporocyte development. The data strongly support distinct phases of mRNA processing activity:

5.2.1 DCP5 distribution pattern and interaction with poly(A) RNA

Decapping of mRNA is quite vital, primarily for maintaining the homeostasis of functional mRNA. It is suggested that at least three steps are involved in the P-body function and decapping. First, mRNAs are translationally arrested and sequestered from the polysomes.

Second, sequestered mRNAs initiate the formation of mRNPs with P-body protein constituents, and subsequently, mRNPs are assembled into P-bodies. Third, mRNAs are decapped and then degraded (Figure 1-9). Based on this model, DCP5 may arrest mRNA translation first and then recruit DCP2 to assemble the mRNPs into P-bodies. P-body formation mediated by DCP5 is required for efficient decapping in vivo, although DCP5 has no direct effect on DCP2 decapping activity in vitro (71,73,215,216). Additionally, DCP5 and DCP1 accumulate during seed maturation, but decrease upon germination, while DCP2 is induced post-germination, suggesting a dynamic assembly of P-bodies for the mRNA decapping process during this transition. This dynamic change ensures that mRNAs are appropriately managed to support germination and early growth. This adaptability and phenotypic consequences are less commonly discussed but highlight P-bodies' versatility in plant physiology. Moreover, DCP5 mutants show abnormal leaves and vascular defects, indicating that as a P-bodies component regulates mRNAs critical for leaf morphology and vascular system development (73). Regarding this matter, the DCP5, as a unique protein of P-bodies and pre-decapping in plants, was subjected to colocalization with cytoplasmic poly(A) RNA during the 5 stages of the poly(A) RNA cycle. In the earliest stages 1 and 2 (Low Activity/Preparation), poly(A) RNA remains largely nuclear, with only trace amounts in the cytoplasm and negligible overlap with DCP5. This reflects a preparatory phase in which mRNA decapping is minimal. With the onset of stage 3 (Peak Processing), cytoplasmic poly(A) RNA levels rise sharply and colocalize extensively with DCP5 in mid-sized P-bodies (0.3-1.2 μm^3), indicating accelerated decapping activity. In stage 4 (Sustained Processing), this high degree of colocalization is maintained, albeit at a slightly reduced level, while P-body size distribution remains centered on the mid-sized range. By stage 5 (Resolution/Transition), mirror a winding-down of peak decapping activity and a shift in how the cell handles the remaining mRNA, cytoplasmic poly(A) levels decline, yet colocalization shifts toward larger P-bodies (1.2-6 μm^3 and 6-20 μm^3), even exceeding stage 1 values for those size classes. In short, stage 5 is not simply “another processing burst” but probably rather the clean-up and hand-off phase that both resolves the remaining workload and reconfigures the machinery for the cell’s next act. This pattern can be explained by two factors. First, although nuclear export of new transcripts diminishes compared with stages 3 and 4, the remaining influx still requires processing, sustaining decapping within P-bodies. Second, as overall DCP5 diffusion wanes, the protein becomes increasingly

sequestered in these larger granules. The continued entry of mRNAs, together with residual unprocessed RNA, drives the recruitment and local concentration of DCP5, promoting aggregation into larger P-bodies. Collectively, these observations suggest that, as the poly(A) cycle progresses, the cell reorganizes its decapping machinery, consolidating DCP5 into fewer but larger foci, to maintain efficient mRNA turnover even under conditions of reduced substrate and enzyme availability.

In total, stages 3 and 4 emerge as the most critical phases, exhibiting the highest P-body numbers and colocalization levels, indicative of peak mRNA processing activity. Stage 3, in particular, stands out as a pivotal point, likely preparing the cell for subsequent developmental changes through enhanced decapping. The observed reduction in poly(A) RNA levels by stage 5 aligns with prior reports (181) and suggests that DCP5, as a decapping factor, could partially contribute to this decline. While other decay pathways (e.g., deadenylation, 3'→5' degradation by exosome) or reduced transcription could contribute, the direct colocalization of the decapping factor DCP5 with poly(A) RNA within the cytoplasm and P-bodies, peaking just before the decline and persisting during it, points towards decapping-mediated degradation being one of the mechanisms resulting in mRNA reduction. The stage 5 reduction likely represents the culmination of degradation initiated primarily in stages 3 and 4. The high colocalization in stage 3 illustrated ~50% of cytoplasmic poly(A) RNA signal intensities associated with DCP5, and ~75% occurs within P-bodies (Figure 4-3D and F), suggesting that a significant fraction, potentially over half of cytoplasmic poly(A) RNA, may be processed by DCP5 during peak stages.

5.2.2 DCP2 distribution pattern and interaction with poly(A) RNA

The decapping process is accomplished by the recruitment of a protein complex formed by the DCP2 catalytic subunit and its cofactors (122). DCP2 forms the conserved core of the decapping complex. The enzyme DCP2 catalyzes the removal of the mRNA cap, producing m^7GDP and an mRNA molecule with a monophosphate at its 5′ end. This decapping step is considered irreversible and marks the mRNA for degradation by the 5′→3′ exonuclease XRN. DCP2 features an N-terminal Nudix/MutT domain, commonly associated with pyrophosphatases, which plays an essential role in its decapping activity (217). Most investigations of DCP2 have

been done under stress conditions. In *Arabidopsis*, when cells are exposed to a temperature of 40°C, DCP1 and DCP2 cluster together to form PB-like granules in the cytoplasm. Once the heat treatment is discontinued, the P-bodies gradually break down, and their components disperse evenly throughout the cytoplasm (218). Heat shock or oxidative insults promote DCP2-mediated decapping by increasing substrate delivery to P-bodies, and alter P-body dynamics (larger, more numerous granules), coupling environmental cues directly to mRNA turnover and enabling rapid reprogramming of gene expression in response to changing conditions (70). On the other hand, mutants DCP2 exhibit seedling lethality and vascular defects, underscoring the decapping and P-bodies' role in the early development of the plant (88). Analyses of RNA decay in DCP2 mutants found that some mRNAs showed no decay, suggesting obligate decay via decapping by DCP2 and 5'→3' exoribonuclease activity during early seedling development, and other mRNAs are degraded from 3'→5' via exosome, but how specific mRNA substrates are targeted to a particular mRNA decay pathway is largely unknown (215). In this investigation, after evaluating the DCP5 protein as a trigger of the decapping process, we also subsequently analyzed the distribution of DCP2 protein in the poly(A) RNA cycle. In stages 1 and 2, DCP2 is diffusely distributed in the cytoplasm and most of that within P-bodies, with minimal colocalization with poly(A) RNA, indicating low association of cytoplasmic poly(A) RNA with DCP2. Stage 3 marks a shift, with increased cytoplasmic poly(A) RNA levels and more DCP2 accumulation in small (0.1-0.3 µm3) and mid-sized (0.3-1.2 µm3) P-bodies, respectively, though colocalization remains moderate. The peak occurs in stage 4, where the highest colocalization was observed across the cytoplasm and within P-bodies (Figure 4-9A and B), particularly in mid-sized (0.3-1.2 µm3) and large (1.2-6 µm3) volumes (Figure 4-9C). This suggests DCP2 actively associates with poly(A) RNA, a role sustained but diminished in stage 5, where colocalization decreases but remains elevated compared to earlier stages.

Based on the results, stage 4 with the highest colocalization and more involvement of P-bodies, and then stage 5 with diminished colocalization relative to stage 4 but higher than the other stages in terms of association of poly(A) and DCP2 and also involvement of P-bodies, emerge as the most critical for DCP2-mediated decapping, aligning with its function as a catalytic enzyme activated downstream of DCP5 (71,73). The reduction in poly(A) RNA likely results

from DCP2 activity, with colocalization data suggesting up to 55% of cytoplasmic transcripts signal intensities are associated with DCP2 (Figure 4-9D) and around 70% occur within P-bodies (Figure 4-9F).

5.2.3 LSM4 distribution pattern and interaction with poly(A) RNA

The decapping complex has a low intrinsic enzymatic activity and requires several accessory proteins, such as the LSM 1-7 heptameric complex and EDC4 (VCS) (122). The LSM1-7 heptameric complex mainly functions in the cytoplasm, where it aids in mRNA degradation. It is responsible for recognizing the deadenylated mRNAs and binding to the 3' ends of oligoadenylated mRNAs that are targeted for decay. By recognizing and binding oligoadenylated 3′ ends of mRNAs targeted for decay, LSM1-7 plays a pivotal role in decapping (98,121). Loss-of-function mutations affecting any of these subunits result in stabilization of mRNAs in vivo by impairing mRNA decay via the 5'→3' pathway without affecting deadenylation (219). Among these 7 proteins of the heptameric complex, LSM1 is the most studied yet in the decapping process and P-bodies assembly, and what makes it specific for decapping and analysis because of its absence in the LSM2-8 heptameric complex, which acts as a splicing complex. LSM1 may shuttle between P-bodies and stress granules depending on physiological or environmental conditions (220). LSM1 participates in the assembly of P-bodies by influencing the localization of VCS and DCP2 (72). In addition to LSM1, the *Arabidopsis* LSM3 and LSM4 localize to cytoplasmic foci in root tips of stably transformed plants (98). In human cells, knockdown of LSM1 and LSM4 leads to a reduction of P-bodies (221). LSM4 activity in the decapping process and P-bodies assembly has been well-known in yeast. So far, studies have revealed that the Q/N rich sequence of the LSM4 C-terminus makes the LSM4 a key member of the LSM1-7 complex during P-bodies assembly and the decapping process (124,222). However, in most eukaryotes, this C-terminal region consists of RGG domains instead of Q/N-rich sequences. The RGG domain of LSM4 enhances P-body accumulation in human cells (124), while the plant LSM4 also consists of the RGG domain (Uniport ID: F4K4E3). A study in *Arabidopsis* demonstrated that under heat stress, LSM3 and LSM4 proteins localize to P-bodies in root cells (98). The literature primarily discussed LSM4 and other LSM proteins in the context of stress responses rather than under basal conditions in *Arabidopsis* or other plants. Therefore, in addition to two decapping proteins (DCP5 and DCP2),

LSM4 was assessed as a decapping cofactor protein in this investigation, as well. In stages 1 and 2 of the poly(A) RNA cycle, despite the LSM4 distribution throughout the cytoplasm, and around half localizes to P-bodies, showing minimal colocalization with poly(A) RNA. This suggests low mRNA processing activity early on, like the DCP5 and DCP2 patterns. By stage 3, a marked shift occurs along with high cytoplasmic poly(A) RNA levels, and a peak of colocalization with LSM4 in P-bodies, particularly in mid-sized (0.3-1.2 µm3) and small volume (0.1-0.3 µm3), respectively (Figure 4-6C). This indicates that LSM4 actively engages with poly(A) RNA, likely assisting in decapping. Stage 4 sustains this interaction, albeit at a slightly reduced level, while stage 5 experiences a decline in both poly(A) RNA levels and colocalization, marking the end of active processing related to the LSM4.

Ultimately, stages 3 and 4 emerge as the most critical, with stage 3 being pivotal due to the surge in P-body activity and colocalization. Based on the ~40% of cytoplasmic poly(A) RNA signal intensities associated with LSM4, which ~82% occurs within P-bodies (Figure 4-6D and F), LSM4, as a cofactor, reinforces of low intrinsic activity of decapping proteins (122) may target a portion of cytoplasmic poly(A) RNA along with the decapping protein.

5.2.4 EDC4 distribution pattern and interaction with poly(A) RNA

In *Homo sapiens, Drosophila melanogaster,* and *Arabidopsis thaliana,* EDC4 is required for P-bodies' integrity and promotes a physical bridge between decapping enzyme and its co-activator DCP2 and DCP1, respectively (223). EDC4 is known as VCS (VARICOSE) in plants and HEDLS/Ge-1 in metazoans, enhances DCP2 activity as a scaffold protein of the decapping complex (70). EDC4 functions as a developmental brake on DCAP2–mediated decapping in P-bodies in embryonic development of *C. elegans*, recruits a ubiquitin ligase module to coordinate mRNA and protein turnover (224). A plant study found that interactions between DCP2 and DCP1 depended on the presence of VCS. These studies raised the possibility that the developmental defects in VCS mutants might arise due to defects in the assembly of the mRNA decapping complex (215). Co-localization of EDC4 and DCP5 in P-bodies of *Arabidopsis* during stress conditions has already confirmed that EDC4 during critical conditions is localized within plant P-bodies (210). While no study has reported its localization in P-bodies during basal plant cell development. The current study examined the localization of EDC4 as a scaffold

protein of the decapping complex with mRNA during the poly(A) RNA cycle. In stages 1 and 2, EDC4 is diffusely distributed in the cytoplasm and most within P-bodies with minimal colocalization with poly(A) RNAs. As development progresses, in stage 3, despite the highest amount of EDC4 in the cytoplasm and P-bodies, the colocalization of cytoplasmic poly(A) RNA and EDC4 is still lower than next two stages (Figure 4-12D), suggests despite higher cytoplasmic poly(A) RNA levels compared to earlier stages, EDC4 association with poly(A) RNA remains low in both the cytoplasm and P-bodies, even as EDC4 quantities increase (Resembles DCP2, while shows in opposition to DCP5 and LSM4). EDC4, like DCP2, is likely being prepared to be more activated for the next 2 stages. The peak occurs in stages 4 and 5, where the EDC4 is more accumulated within mid-sized (0.3-1.2 um3), large (1.2-6 um3), and small (0.1-0.3 um3) P-bodies, and the highest accumulation of cytoplasmic poly(A) RNA is observed within P-bodies (Figure 4-12F). In addition, the association of cytoplasmic poly(A) RNA with EDC4 is at the highest level. It remains unclear whether EDC4 associates with the decapping complex within P-bodies after the complex has already been fully assembled by DCP2 or concurrently during its assembly; however, localization indicates that EDC4 seems to act downstream of DCP5 and LSM4 within P-bodies.

Eventually, stages 4 and 5 appear to be the most critical for EDC4 activity, marked by the highest colocalization and P-body activity, indicating peak decapping processing. This stage likely sets the stage for significant mRNA processing, influencing subsequent cellular events. The reported reduction of poly(A) RNA in the final stage more likely aligns with EDC4's role in decapping processing. Given its heightened activity in stage 4, it is plausible that EDC4 drives this reduction by initiating decapping-dependent degradation that manifests fully in stage 5. The substantial colocalization in stages 4 and 5 suggests a significant portion, potentially 45-62% of cytoplasmic poly(A) RNA signal intensities, is associated with EDC4 (Figure 4-12D), of which around 62-80% are within P-bodies (Figure 4-12F). This is an inference based on spatial overlap.

5.2.5 XRN4 distribution pattern and interaction with poly(A) RNA

XRN4 (5'→3' exoribonuclease) operates as a key component of the mRNA decay pathway downstream of the decapping process initiated by decapping proteins. After decapping is

completed, XRN4 takes over and degrades the mRNA, effectively lowering the pool of available transcripts. Removal of the cap structure produces RNAs with 5′ monophosphates, which are the preferred substrates of the 5′→3′ exoribonucleases (125). A study on *Arabidopsis* immunity showed that DCP5 interaction with DCP1 likely helps keep XRN4 in close proximity to decapped substrates. This scaffolding ensures that once DCP2 has removed the cap, XRN4 is right at hand to process the exposed 5′ end (113). XRN4-*Arabidopsis* has been reported to co-localize with DCP1 in P-bodies and is likely to directly or indirectly regulate some miRNAs within P-bodies (225). XRN4-*Arabidopsis* mutants maintain P-bodies but show altered mRNA decay kinetics, emphasizing how P-bodies selectively maintain mRNA stability under particular conditions, and indicate XRN4 is not essential for P-body assembly (215). XRN4 and LARP1 localize to P-bodies during heat stress, cooperating with DCP1 and DCP2 to expedite the turnover of heat-sensitive mRNAs (201). Blocking 5′→3′ mRNA degradation by XRN4 mutants showed the P-bodies enlargement due to inhibited mRNP efflux (70). In this investigation, in addition to investigating decapping proteins and cofactors of the decapping process, XRN4 localization as the 5′→3′ exoribonuclease protein was analyzed with the mRNA during the poly(A) RNA cycle. Stage 1, despite the lowest distribution of XRN4 and poly(A) RNA in the cytoplasm, exhibits a high colocalization in the cytoplasm, especially within mid-sized P-bodies, compared to reported proteins, which show markedly lower activity at this stage. Indicates that the XRN4 is active within the P-bodies and highlights XRN4's distinct function in initiating transcript turnover, setting it apart from other decapping-related proteins analyzed. This likely suggests that XRN4 is associated with residual cytoplasmic poly(A) RNA from the previous cycle, transcripts that have already undergone decapping and remain in the cytoplasm for further degradation. It is worth noting that, although the colocalization is high in this stage but it is not comparable with the colocalization in the next stages, as they have different intensities of cytoplasmic poly (A) RNA. Stage 2, with a still low amount of poly(A) RNA and XRN4 and minimal colocalization in the cytoplasm and P-bodies relative to the next stages, shows the low association of XRN4 with cytoplasmic poly(A) RNA. As development progresses, in stage 3, despite the high amount of cytoplasmic poly(A) RNA, the amount of XRN4 is still at the same level as the previous stages, with slight increases in colocalization. Stage 4 marks a peak, with both XRN4 and poly(A) RNA levels surging, high colocalization in the cytoplasm and in P-bodies (Figure 4-15A and B), especially in mid-sized (0.3-1.2 μm^3) and

large P-bodies (1.2-6 μm^3) (Figure 4-15C). In stage 5, cytoplasmic poly(A) RNA and XRN4 protein concentration decrease, with colocalization dropping in the cytoplasm but remaining high in P-bodies.

After all, stage 4 are the most significant stage and suggesting peak mRNA turnover according to the highest level of poly(A) RNA and XRN4 in the cytoplasm and P-bodies (Figures 4-14A and B), and highest colocalization with around 40% of cytoplasmic poly(A) RNA associated with XRN4 (Figure 4-15D), of which around 80% are within P-bodies (Figure 4-15F). Stages 5 and 3 are the next in line and can both be regarded as particularly significant. Both stages exhibit high colocalization, with approximately 50% of cytoplasmic poly(A) RNA associated with XRN4 (Figure 4-15D). This is even higher than in stage 4, despite stage 4 having the highest overall levels of poly(A) RNA and XRN4. As a result, the absolute amount of poly(A) RNA associated with XRN4 in stage 4 still exceeds that in stages 3 and 5, despite its lower colocalization percentage. Stages 3 and 5 also display similar levels of cytoplasmic poly(A) RNA (Figure 4-14A). However, due to the higher levels of XRN4 in the cytoplasm and P-bodies during stage 5 compared to stage 3, colocalization in stage 3 primarily occurs in the cytoplasm rather than focused within the P-bodies, whereas in stage 5, it predominantly takes place in the P-bodies (Figures 4-15C and F). The colocalization implies XRN4 targets a portion of poly(A) RNA, so the reduction of poly(A) RNA in the last stage may appear to be partially driven by XRN4 activity from stages 3 to 5.

Collectively, these findings indicate the phase shift between decapping and co-decapping factors, which suggest the order of events: DCP5/LSM4 (organization/pre-decapping; stage 3) → DCP2/EDC4 (catalysis; stage 4) → XRN4 (completion of 5′→3′ decay; stages 4/5). This yields a logical sequence: initial arrest/redirecting of mRNA → full engagement of the decapping complex→exonucleolytic degradation.

5.3 Most important stages considered as a trigger of poly(A) RNA reduction

To determine the most important stages among 5 stages for triggering poly(A) RNA reduction, across all proteins studied (DCP5, LSM4, DCP2, EDC4, and XRN4), we integrated the contributions of poly(A) RNA colocalized with all proteins (Figure 5-1): Stage 3 shows critical for DCP5 and LSM4 (initiation of decapping). It likely serves as the starting point for mRNA

processing, with high colocalization and P-body activity preparing the cell for degradation. Stage 4 is highlighted by all five proteins (DCP5, DCP2, LSM4, EDC4, XRN4) as a peak phase of degradation activity. It features the highest colocalization levels for DCP2, EDC4, and XRN4, and significant involvement for DCP5 and LSM4, indicating it is the central stage for active mRNA breakdown. Stage 5 seems to be more important for DCP2, EDC4, and XRN4 (as the colocalization of these proteins with poly(A) RNA is still high, while the colocalization of DCP5 and LSM4 with poly(A) RNA is low), where the reduction in poly(A) RNA becomes evident. However, this stage primarily reflects the outcome of degradation initiated earlier. Therefore, the reduction observed in stage 5 is the culmination of earlier stages' efforts, suggesting that stages 3 and 4 are the primary triggers. Among them, stage 4 stands out due to its universal significance across all proteins, making it the peak of the degradation process, while stage 3 is critical for its initiating role. Thus, stages 3 and 4 are collectively the most important for driving poly(A) RNA reduction.

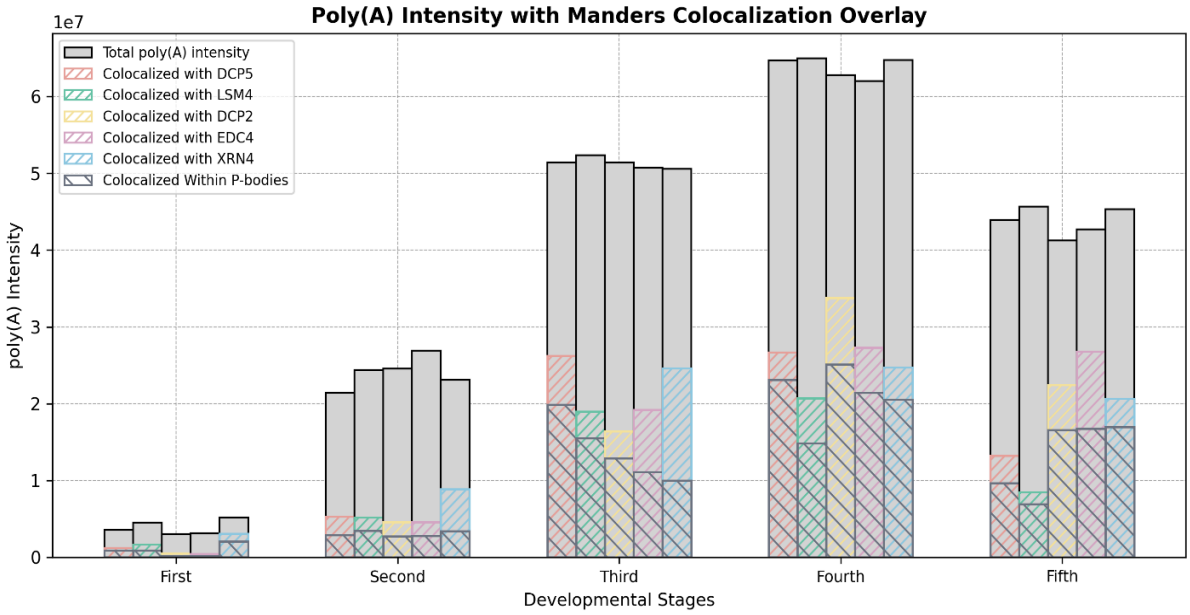

Figure 5-1. Mander's colocalization of poly (A) with all Proteins. Bar chart showing total poly(A) signal intensity (gray bars) and the amount of poly(A) colocalized with five proteins (colored hatched overlays: DCP5, LSM4, DCP2, EDC4, and XRN4), and the fraction of colocalization within P-bodies (gray hatch) across five developmental stages. The colored hatched portions represent the Mander's colocalization coefficient in whole cytoplasm (converted to the amount of poly(A) intensity) overlaid proportionally on the amount of total poly(A) intensity. The gray hatched portions represent the Mander's colocalization coefficient within P-bodies across whole cytoplasmic colocalization. Each color corresponds to a specific protein, as indicated in the legend.

5.4 Multi-Protein Interactions and Functional Complexes in P-bodies

P-bodies as critical hubs for mRNA decapping and degradation, orchestrating the activities of multiple proteins to regulate transcript stability during the diplotene stage of *Larix decidua* microsporocyte development. Recent studies indicated that the plant P-bodies function in both translational repression and mRNA decapping by the colocalization of DCP5, EDC4, DCP2, and XRN4 proteins (70,73,94,215). The triple localization, coupled with co-immunoprecipitation assays in this study, provides novel insights into the spatial and functional relationships among decapping proteins (DCP5, LSM4, EDC4, DCP2) and the degradation protein XRN4 within P-bodies of *Larix decidua* microsporocyte, shedding light on their coordinated roles in mRNA decay. The colocalization of DCP5 and DCP2 within P-bodies underscores their collaborative role in initiating mRNA decapping (Figure 4-16). DCP5's co-presence with DCP2 suggests the formation of a functional decapping complex. This is corroborated by co-immunoprecipitation data confirming a direct physical interaction between DCP5 and DCP2. The additional colocalization of poly(A) RNA within these P-bodies indicates that these structures are the sites of mRNA processing, consistent with their role in post-transcriptional regulation. This finding aligns with previous studies in *Arabidopsis*, where DCP5 works as an upstream factor of DCP2 activity (71), highlighting a conserved mechanism in plants distinct from other eukaryotes. Similarly, the triple labeling of DCP2, EDC4, and poly(A) RNA reveals a tight spatial association within P-bodies (Figure 4-17). EDC4, known to enhance DCP2's catalytic activity as an upstream factor (71), and interacts with DCP5 by co-localizing in P-bodies (95), likely stabilizes or activates the decapping complex, as evidenced by their direct interaction in co-immunoprecipitation assays (Figure 4-22G). This synergy is critical during stages of high decapping demand, as seen in the sustained poly(A) RNA processing observed in five stages. These results suggest that DCP5, DCP2, and EDC4 form a core decapping module within P-bodies (Figure 5-2B), optimizing the removal of the 5' cap from mRNA transcripts.

5.4.1 Partial Colocalization and Functional Nuances

Despite LSM1-LSM7 proteins co-localizing and co-immunoprecipitating with DCP1 and different mRNAs in P-bodies of yeast (226), and *Arabidopsis* (98). Studies also showed that the

Arabidopsis LSM1-7 complex co-immunoprecipitates with PAT1 (as a protein localized in P-bodies) and co-localizes with DCP2 and EDC4 in P-bodies (98,227), suggesting that, together with DCP1 and DCP5, it participates in the *Arabidopsis* decapping machinery (118). However, we reported that the colocalization of DCP5 with LSM4 is less consistent, occurring in some but not all P-bodies across the five stages of poly(A) RNA cycle (Figure 4-18). Moreover, the lack of direct interaction between DCP5 and LSM4 in co-immunoprecipitation assays further supports this interpretation (Figures 4-22G and 5-2). The lack of overlap in some P-bodies suggests that LSM4's role in P-bodies may be transient or due to the heterogeneity of P-bodies components (228,229), potentially linked to its function. Rather than forming a stable complex, their co-presence in P-bodies may reflect RNA-mediated or indirect interactions, possibly facilitating the transition from deadenylation to decapping. As it is also confirmed by previous studies, that alternative multivalent protein–protein interactions could drive P-body assembly in the absence of LSM4. These results suggest that the network of multivalent protein–protein and protein–RNA interactions (with the exception of a few essential factors) is more important than individual components or interactions for P-body assembly. This is consistent with a major role for multivalent interactions in LLPS (230). This variability aligns with LSM4's role in enhancing decapping recruitment, suggesting a sequential rather than simultaneous function within P-bodies.

5.4.2 Integration with Degradation Pathways

The colocalization of DCP5 with XRN4, within P-bodies (Figure 4-19), demonstrates that both decapping and degradation steps of mRNA turnover can occur in close proximity. This spatial arrangement likely enhances efficiency by allowing decapped mRNAs to be rapidly degraded by XRN4 (125). However, the absence of direct interaction within P-bodies between DCP5 and XRN4 in co-immunoprecipitation experiments likely indicates that their association is not through stable binding but rather through shared localization within P-bodies (Figure 5-2), possibly mediated by mRNA substrates or other components, or indicates that the removal of the cap structure produces RNAs with 5' monophosphates, which are the preferred substrates of the 5'→3' exoribonucleases which refer the activity of XRN4 is downstream of the role of the decapping complex (125). This organization supports a model where P-bodies act as dynamic assemblies, coordinating sequential decay processes during microsporocyte development.

This assessment confirmed that the proteins of the P-bodies can be categorized into conserved proteins and dynamic proteins, which align with the previous data in *Arabidopsis* (110). DCP2, DCP5, VCS, and XRN4 are considered the conserved proteins, while LSM4 shows dynamic behavior.

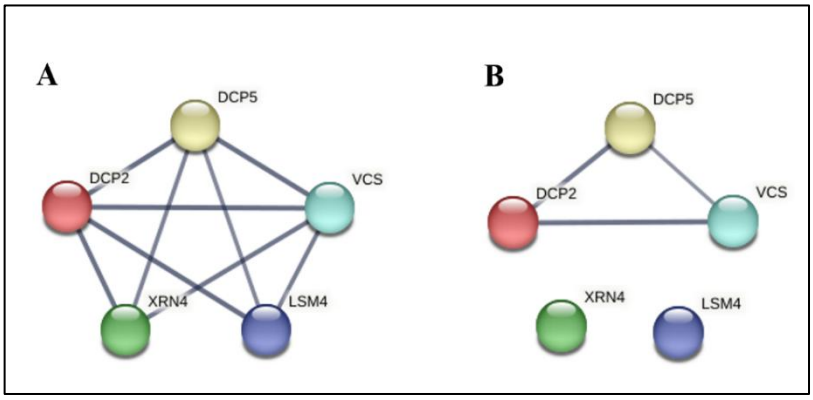

Figure 5-2. Schematic illustration of interaction of DCP5, DCP2, EDC4 (VCS), LSM4 and XRN4 proteins. This visualized network comes from the (https://string-db.org/), multiple protein identifiers. **A)** The edges indicate functional protein associations with a confidence of 0.70. **B)** The edges indicate that the proteins are part of a physical complex with a confidence of 0.70.

5.5 Active P-body volumes and dynamics

To analyze the volume sizes and number of P bodies in *Larix decidua* microsporocytes and how they were affected by different levels of the poly(A) RNA in a cycle, I examined how their number and size change across all protein and mRNA distributions. In *Larix decidua* microsporocytes, P-bodies serve as auxiliary structures for mRNA regulation, with their assembly facilitated by the proteins DCP5, LSM4, DCP2, EDC4, and XRN4. So far, studies have primarily focused on the structural size of P-bodies under environmental stress conditions (231), with little attention given to their dynamics during developmental processes. Therefore, due to the absence of standardized P-body size data in plants during basal conditions and developmental process, this study established five volume categories to classify them: smallest (0.05-0.1 µm3), small (0.1-0.3 µm3), mid-sized (0.3-1.2 µm3), large (1.2-6 µm3), and largest (6-20 µm3). The dynamics of P-body number, volume size, and colocalization with poly(A) RNA varied across developmental stages, reflecting the evolving requirements of mRNA processing during microsporocyte development. Across all investigated proteins, mid-sized P-

bodies, ranging from 0.3-1.2 μm3, showed the most involvement among other P-bodies sizes with the highest colocalization with poly(A) RNA (Figure 5-3A), and highest portion in total volume of P-bodies (Figure 5-3B), especially in 3, 4, and 5 stages, highlighting their pivotal role in mRNA turnover. This recurring prominence indicates that mid-sized P-bodies are particularly well-suited for efficient transcript regulation, especially during periods of active cellular development, making them a focal point of this analysis. As development progressed through stages 2 to 5, distinct patterns emerged in P-body dynamics. From stages 2 to 4, the number of P-bodies increased steadily, reaching a peak in stages 3 and 4. During these stages, small P-bodies (0.1-0.3 μm3) and mid-sized P-bodies (0.3-1.2 μm3) were the most prevalent, likely supporting rapid mRNA processing once high levels of mRNA around the cytoplasm to meet the demands of active growth. By stage 5, a noticeable shift occurred toward large P-bodies (1.2-6 μm3), suggesting a transition to bulk mRNA degradation as developmental processes began to stabilize. These observations reveal a clear progression in P-body assembly and function throughout microsporocyte development in *Larix decidua*. During stages 3 and 4, small and mid-sized P-bodies supported mRNA turnover. In contrast, the predominance of larger P-bodies in stage 5 points to a role in bulk mRNA degradation, likely clearing transcripts as development concludes. The consistent significance of mid-sized P-bodies across all stages underscores their critical contribution to mRNA regulation, offering valuable insights into the molecular mechanisms governing the decapping-dependent degradation process during the *Larix decidua* developmental process.

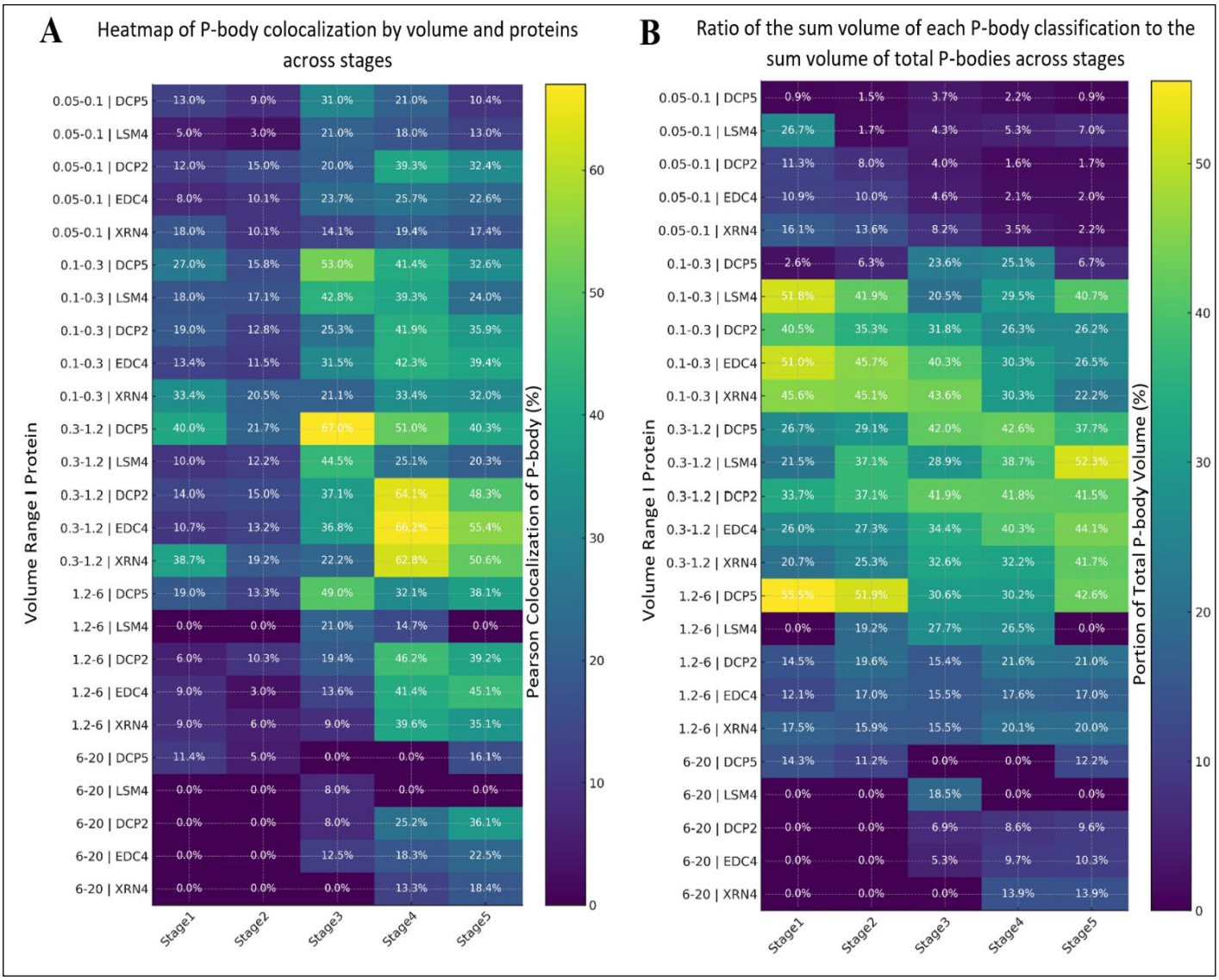

Figure 5-3. Heatmap of P-body Pearson Colocalization (A), Proportional Volume Contribution of P-body Classifications (B), Across Proteins, Volumes, and Stages. **(A)** This heatmap visualizes the percentage of Pearson colocalization within P-bodies for five proteins (DCP5, LSM4, DCP2, EDC4, XRN4) across five volume ranges (0.05-0.1, 0.1-0.3, 0.3-1.2, 1.2-6, 6-20 μm³) and five developmental stages (Stages 1-5). Each cell shows the colocalization percentage. This representation highlights which volume–protein combinations exhibit maximal P-body colocalization at each stage. **(B)** This heatmap displays the ratio of the summed volume of each P-body classification to the total P-body volume for five proteins (DCP5, LSM4, DCP2, EDC4, XRN4) across five volume ranges (0.05-0.1, 0.1-0.3, 0.3-1.2, 1.2-6, 6-20 μm³) and five developmental stages (Stages 1-5). Each cell represents the proportion (%) of total P-body volume contributed by that protein–volume category at a given stage. This visualization highlights shifts in the relative volumetric contribution of distinct P-body populations during development. (color-coded from low [dark purple] to high [yellow]) with the exact value overlaid. Volumes are grouped on the y-axis (in ascending order from smallest to largest), and stages progress from left to right on the x-axis.

5.6 RIP-seq analysis reveals shared and specific RNA targets of decapping-related proteins

The RIP-seq analysis of DCP2, DCP5, EDC4, and LSM4 provides molecular evidence that complements and extends the microscopy and co-immunoprecipitation results obtained in this study. While the confocal and Co-IP data demonstrated the physical and spatial association of these proteins within P-bodies, the RIP-seq results now reveal the functional overlap and specificity of their RNA targets, giving deeper insight into how these proteins cooperate or act independently in RNA metabolism during microsporogenesis in *Larix decidua*.

Specific RNA associations

Each of the four analyzed proteins bound to a distinct set of RNA molecules, consistent with their known or proposed roles in the mRNA decapping pathway. After annotating the RIP-seq data, 6 transcript sequences of 7 precipitated transcripts with DCP2, 2 of 2 precipitated transcripts with DCP5, 122 of 188 precipitated transcripts with EDC4, and 34 of 81 precipitated transcripts with LSM4, were well annotated by the reference genome of *Larix Decidua*. DCP2 and DCP5 displayed a relatively small set of RNA targets, probably consistent with their role as the catalytic decapping enzyme and supporting their regulatory function, rather than a broad RNA-binding capacity. EDC4 had the largest RNA-binding profile, which aligns with its known role as an enhancer of decapping activity and a component that may bridge multiple protein–RNA complexes as a scaffolding protein during decapping. LSM4 is associated with a relatively wide range of transcripts, which is consistent with its participation in multiple RNA processing and decapping steps in the cytoplasm, possibly extending beyond P-body–localized events.

Shared RNA targets indicate functional cooperation

The presence of numerous shared RNA sequences among the precipitated transcripts highlights that these proteins are components of coordinated RNA decay networks and enrichment mechanisms rather than as isolated units. The combination of DCP2/ EDC4 (13 shared RNAs) and DCP5/ EDC4 (12 shared RNAs) reinforces the strong physical and functional link between these decapping factors, as already supported by co-localization and co-immunoprecipitation data. EDC4/ LSM4 (16 shared RNAs) and the triple combinations (e.g., DCP2/DCP5/EDC4 with 21 shared RNAs) suggest that decapping components may assemble in dynamic complexes

that engage the same RNA molecules at different stages of degradation. The detection of 40 common RNAs bound by all four proteins (DCP2, DCP5, EDC4, and LSM4) provides compelling evidence for a core set of mRNA substrates that are collectively processed by the decapping proteins.

5.6.1 Functional annotation of RIP-seq targets reveals the molecular context of P-body–associated RNAs

The GO-based classification of RNA sequences associated with DCP2, DCP5, EDC4, and LSM4 provides valuable insight into the molecular and subcellular context of the transcripts targeted by these decapping-related proteins. The identified transcripts are distributed across several functional categories, reflecting the diverse physiological processes regulated by decapping and associated RNA decay. A large proportion of the annotated transcripts are related to membrane (93), mitochondrial (89), and chloroplast (42) components, indicating that many of the target RNAs encode proteins localized in or associated with the energy-producing organelles. The most represented molecular functions among the annotated targets include dehydrogenase activity (36), ion binding (25), and ATP/RNA binding (18/15), followed by DNA binding and nuclease activity. This profile suggests that decapping–associated RNAs encompass a wide variety of enzymatic and regulatory transcripts, many of which are involved in energy metabolism, redox regulation, and nucleic acid processing. The presence of RNAs related to translation elongation factor, transcription initiation factor activity, and ribosomal protein functions highlights the role of decapping complexes in controlling mRNAs that govern translation efficiency and mRNA turnover.

6. Conclusion

These findings extend our understanding of the decapping-dependent mRNA decay, clarifying when and where P-bodies assemble and operate during plant development. They reveal a coordinated network of protein interactions that govern mRNA regulation across the five-stage poly(A) RNA cycle in *Larix decidua* microsporocytes during diplotene. This study shows that P-bodies form and are dynamically regulated as part of a developmental programme, recruiting decapping and degradation factors in a reproducible temporal order that aligns with the poly(A) RNA cycle and culminates in a late-cycle decline of cytoplasmic poly(A) RNA. Stage-specific patterns of colocalization between cytoplasmic poly(A) RNA and decapping/degradation proteins provide temporal insights into the control of mRNA decay.

Key Points:

P-bodies are active during normal development. Visible P-bodies assemble in *Larix decidua* microsporocytes during diplotene and display regulated dynamics across the poly(A) cycle, demonstrating that P-body assembly is not restricted to stress responses but is integral to developmental mRNA regulation.

mRNA turnover is stage-programmed. The five-stage poly(A) RNA cycle (stages 1-5) is coupled to discrete cytoplasmic decapping/decay activities, with the global poly(A) decline toward the end of the cycle. stages 3-5 are particularly critical for cytoplasmic processing.

Sequential recruitment of proteins defines a timeline. Protein engagement follows a reproducible order across cells: organizational/pre-decapping factors (DCP5, LSM4) rise earlier (stage 3), the catalytic decapping core (DCP2, EDC4/VCS) engages at stage 4, and the 5′→3′ exonuclease XRN4 participates at stages 4/5, together defining a mechanistic timeline for cytoplasmic mRNA decay.

P-bodies act as principal reaction hubs. Quantitative colocalization indicates that most poly(A)-protein overlap occurs within P-bodies at peak stages, identifying these foci as principal sites where decapping and downstream processing are concentrated.

P-body size classes are functionally relevant. Mid-sized P-bodies (0.3-1.2 μm^3) dominate across stages as the main "workhorse" population; larger P-bodies (1.2-6 μm^3) increase when the catalytic decapping core and XRN4 engage (stages 4/5), consistent with higher throughput processing.

DCP5/DCP2/EDC4 form a candidate core decapping module. Co-immunoprecipitation from P-body/cytoplasmic fractions and triple-label imaging support stable interactions among DCP5, DCP2, and EDC4, while LSM4 and XRN4 show more transient or stage-dependent associations, suggesting a core module supported by parallel or dynamic partners.

Distinct protein dynamics imply different operational roles. DCP5 shows an early/larger profile with fragmentation at an intermediate stage and partial re-consolidation later; LSM4 peaks mid-cycle and behaves transiently; DCP2/EDC4 and XRN4 peak late, together indicating organizational, catalytic, and cleanup roles respectively across the cycle.

Stage 4 is the control point; stage 5 is resolution. Activity (protein recruitment and P-body involvement) centers on stage 4, likely suggesting active decapping and degradation, while stage 5 reflects the resolution/cleanup of decay initiated earlier.

P-bodies are not stress granules in this context. The examined foci do not overlap with the stress-granule marker (PAB2), supporting their identity as P-bodies operating in a developmental programme.

Supply-responsive remodeling links machinery to substrate load. Changes in P-body number, total/volume class distribution, and increased poly(A) enrichment in P-bodies at stages 3-4 indicate that P-body assembly adapts to cytoplasmic poly(A) abundance.

RIP-seq identifies shared and specific RNA targets. RIP-seq captured both shared and protein-specific sets of transcripts (including a core set bound by all four proteins), GO terms implicate mitochondrial, chloroplast, and membrane-associated transcripts and functions linked to metabolism and translation, providing candidates for future functional tests.

Causality is suggested but not overstated. Spatiotemporal overlap (colocalization, recruitment timing, co-IP and RIP-seq) strongly supports a contribution of decapping-mediated 5′→3′ decay to the late-cycle poly(A) decline, without excluding other mechanisms (e.g.,

deadenylation → exosome, transcriptional downregulation). The thesis, therefore, frames a clear experimental agenda for genetic and functional tests.

7. Perspectives

The present study provides new insights into the spatial organization and molecular composition of P-bodies and decapping complexes in *Larix decidua* microsporocytes. Several avenues can now deepen our understanding of the post-transcriptional regulation mediated by decapping and degradation:

1. Targeted RNA visualisation. Building on RIP-seq targets, design specific fluorescent RNA probes for these transcripts. Use confocal microscopy to map their spatial distribution and assess colocalization with the identified P-body proteins, providing direct visual evidence for the physical association between defined mRNAs and P-body components.

2. Pathway integration. Examine potential interactions between the decapping/degradation proteins studied here (DCP5, DCP2, EDC4, LSM4, XRN4) and other RNA-decay pathways, such as nonsense-mediated decay (NMD; e.g., SMG7, UPF1) and no-go/non-stop decay (NGD/NSD; e.g., Pelota1). Defining overlap and crosstalk may establish P-bodies as integrated hubs where multiple RNA-decay routes converge.

3. Development–stress crosstalk. Given the relationship between stress responses and RNA-granule dynamics, test how environmental or physiological stress reshapes the localization and behaviour of these P-body proteins, and probe their interplay with stress granules. This will clarify how P-bodies participate in stress-induced post-transcriptional regulation in plant cells.

4. Live-cell dynamics in additional models. Investigate the dynamic behaviour of P-bodies and the transient role of LSM4 using live-cell imaging in other plant systems. Real-time tracking of P-body formation and dissolution will inform on the kinetics and reversibility of these condensates under diverse developmental conditions.

8. Literature

1. Laham-Karam N, Pinto GP, Poso A, Kokkonen P. Transcription and translation inhibitors in cancer treatment. Front Chem. 2020;8:276.
2. Cramer P. Organization and regulation of gene transcription. Nature. 2019;573(7772):45–54.
3. Plaschka C, Lariviere L, Wenzeck L, Seizl M, Hemann M, Tegunov D, et al. Architecture of the RNA polymerase II–Mediator core initiation complex. Nature. 2015;518(7539):376–80.
4. Proudfoot NJ. Transcriptional termination in mammals: Stopping the RNA polymerase II juggernaut. Science (1979). 2016;352(6291):aad9926.
5. Pereira B, Billaud M, Almeida R. RNA-binding proteins in cancer: old players and new actors. Trends Cancer. 2017;3(7):506–28.
6. Singh G, Pratt G, Yeo GW, Moore MJ. The clothes make the mRNA: past and present trends in mRNP fashion. Annu Rev Biochem. 2015;84(1):325–54.
7. Corbett AH. Post-transcriptional regulation of gene expression and human disease. Curr Opin Cell Biol. 2018;52:96–104.
8. Buxbaum AR, Haimovich G, Singer RH. In the right place at the right time: visualizing and understanding mRNA localization. Nat Rev Mol Cell Biol. 2015;16(2):95–109.
9. Puria R, Rohilla S, Kaur S. Translation—Process and control. In: Emerging Concepts in Ribosome Structure, Biogenesis, and Function. Elsevier; 2021. p. 183–211.
10. Merrick WC, Pavitt GD. Protein synthesis initiation in eukaryotic cells. Cold Spring Harb Perspect Biol. 2018;10(12):a033092.
11. Singh PK, Singh P, Singh RP, Singh RL. From gene to genomics: tools for improvement of animals. In: Advances in Animal Genomics. Elsevier; 2021. p. 13–32.
12. He RZ, Luo DX, Mo YY. Emerging roles of lncRNAs in the post-transcriptional regulation in cancer. Genes Dis. 2019;6(1):6–15.
13. Hocine S, Singer RH, Grünwald D. RNA processing and export. Cold Spring Harb Perspect Biol. 2010;2(12):a000752.
14. Ramanathan A, Robb GB, Chan SH. mRNA capping: biological functions and applications. Nucleic Acids Res. 2016;44(16):7511–26.
15. Martinez-Rucobo FW, Kohler R, van de Waterbeemd M, Heck AJR, Hemann M, Herzog F, et al. Molecular basis of transcription-coupled pre-mRNA capping. Mol Cell. 2015;58(6):1079–89.
16. Lee Y, Rio DC. Mechanisms and regulation of alternative pre-mRNA splicing. Annu Rev Biochem. 2015;84(1):291–323.

17. Poverennaya I V, Roytberg MA. Spliceosomal introns: features, functions, and evolution. Biochemistry (Moscow). 2020;85:725–34.

18. Shi Y. Mechanistic insights into precursor messenger RNA splicing by the spliceosome. Nat Rev Mol Cell Biol. 2017;18(11):655–70.

19. Will CL, Lührmann R. Spliceosome structure and function. Cold Spring Harb Perspect Biol. 2011;3(7):a003707.

20. Meyer K, Koester T, Staiger D. Pre-mRNA splicing in plants: in vivo functions of RNA-binding proteins implicated in the splicing process. Biomolecules. 2015;5(3):1717–40.

21. Elkon R, Ugalde AP, Agami R. Alternative cleavage and polyadenylation: extent, regulation and function. Nat Rev Genet. 2013;14(7):496–506.

22. Tian B, Manley JL. Alternative polyadenylation of mRNA precursors. Nat Rev Mol Cell Biol. 2017;18(1):18–30.

23. Tian B, Graber JH. Signals for pre-mRNA cleavage and polyadenylation. Wiley Interdiscip Rev RNA. 2012;3(3):385–96.

24. Misra A, Green MR. From polyadenylation to splicing: Dual role for mRNA 3'end formation factors. RNA Biol. 2016;13(3):259–64.

25. Weill L, Belloc E, Bava FA, Méndez R. Translational control by changes in poly (A) tail length: recycling mRNAs. Nat Struct Mol Biol. 2012;19(6):577–85.

26. Wente SR, Rout MP. The nuclear pore complex and nuclear transport. Cold Spring Harb Perspect Biol. 2010;2(10):a000562.

27. Köhler A, Hurt E. Exporting RNA from the nucleus to the cytoplasm. Nat Rev Mol Cell Biol. 2007;8(10):761–73.

28. Terry LJ, Wente SR. Flexible gates: dynamic topologies and functions for FG nucleoporins in nucleocytoplasmic transport. Eukaryot Cell. 2009;8(12):1814–27.

29. Singh G, Pratt G, Yeo GW, Moore MJ. The clothes make the mRNA: past and present trends in mRNP fashion. Annu Rev Biochem. 2015;84(1):325–54.

30. Sen R, Barman P, Kaja A, Ferdoush J, Lahudkar S, Roy A, et al. Distinct functions of the cap-binding complex in stimulation of nuclear mRNA export. Mol Cell Biol. 2019;

31. Khan GA, Deforges J, Reis RS, Hsieh YF, Montpetit J, Antosz W, et al. The transcription and export complex THO/TREX contributes to transcription termination in plants. PLoS Genet. 2020;16(4):e1008732.

32. Merkle T. Nucleo-cytoplasmic transport of proteins and RNA in plants. Plant Cell Rep. 2011;30:153–76.

33. Ehrnsberger HF, Grasser M, Grasser KD. Nucleocytosolic mRNA transport in plants: export factors and their influence on growth and development. J Exp Bot. 2019;70(15):3757–63.

34. Carmody SR, Wente SR. mRNA nuclear export at a glance. J Cell Sci. 2009;122(12):1933–7.

35. Heath CG, Viphakone N, Wilson SA. The role of TREX in gene expression and disease. Biochemical Journal. 2016;473(19):2911–35.

36. Katahira J. mRNA export and the TREX complex. Biochimica et Biophysica Acta (BBA)-Gene Regulatory Mechanisms. 2012;1819(6):507–13.

37. Wickramasinghe VO, Laskey RA. Control of mammalian gene expression by selective mRNA export. Nat Rev Mol Cell Biol. 2015;16(7):431–42.

38. Walsh MJ, Hautbergue GM, Wilson SA. Structure and function of mRNA export adaptors. Portland Press Ltd.; 2010.

39. Zhao Q, Leung S, Corbett AH, Meier I. Identification and characterization of the Arabidopsis orthologs of nuclear transport factor 2, the nuclear import factor of ran. Plant Physiol. 2006;140(3):869–78.

40. Ehrnsberger HF, Grasser M, Grasser KD. Nucleocytosolic mRNA transport in plants: export factors and their influence on growth and development. J Exp Bot. 2019;70(15):3757–63.

41. Sonenberg N, Hinnebusch AG. Regulation of translation initiation in eukaryotes: mechanisms and biological targets. Cell. 2009;136(4):731–45.

42. Dever TE, Green R. The elongation, termination, and recycling phases of translation in eukaryotes. Cold Spring Harb Perspect Biol. 2012;4(7):a013706.

43. Hinnebusch AG. The scanning mechanism of eukaryotic translation initiation. Annu Rev Biochem. 2014;83(1):779–812.

44. Dever TE, Dinman JD, Green R. Translation elongation and recoding in eukaryotes. Cold Spring Harb Perspect Biol. 2018;10(8):a032649.

45. Blanchet S, Ranjan N. Translation phases in eukaryotes. Ribosome Biogenesis: Methods and Protocols. 2022;217–28.

46. Rodnina M V. The ribosome in action: Tuning of translational efficiency and protein folding. Protein Science. 2016;25(8):1390–406.

47. Salas-Marco J, Bedwell DM. GTP hydrolysis by eRF3 facilitates stop codon decoding during eukaryotic translation termination. Mol Cell Biol. 2004;

48. Gomes E, Shorter J. The molecular language of membraneless organelles. Journal of Biological Chemistry. 2019;294(18):7115–27.

49. Alberti S. The wisdom of crowds: regulating cell function through condensed states of living matter. J Cell Sci. 2017;130(17):2789–96.

50. Brangwynne CP, Tompa P, Pappu R V. Polymer physics of intracellular phase transitions. Nat Phys. 2015;11(11):899–904.

51. Fung HYJ, Birol M, Rhoades E. IDPs in macromolecular complexes: the roles of multivalent interactions in diverse assemblies. Curr Opin Struct Biol. 2018;49:36–43.

52. Hyman AA, Weber CA, Jülicher F. Liquid-liquid phase separation in biology. Annu Rev Cell Dev Biol. 2014;30(1):39–58.

53. Elbaum-Garfinkle S, Brangwynne CP. Liquids, fibers, and gels: the many phases of neurodegeneration. Dev Cell. 2015;35(5):531–2.

54. Mitchell SF, Parker R. Principles and properties of eukaryotic mRNPs. Mol Cell. 2014;54(4):547–58.

55. Shin Y, Brangwynne CP. Liquid phase condensation in cell physiology and disease. Science (1979). 2017;357(6357):eaaf4382.

56. Ivanov P, Kedersha N, Anderson P. Stress granules and processing bodies in translational control. Cold Spring Harb Perspect Biol 11: a032813. 2019.

57. Kearly A, Nelson ADL, Skirycz A, Chodasiewicz M. Composition and function of stress granules and P-bodies in plants. In: Seminars in cell & developmental biology. Elsevier; 2024. p. 167–75.

58. Anderson P, Kedersha N, Ivanov P. Stress granules, P-bodies and cancer. Biochimica et Biophysica Acta (BBA)-Gene Regulatory Mechanisms. 2015;1849(7):861–70.

59. Riggs CL, Kedersha N, Ivanov P, Anderson P. Mammalian stress granules and P bodies at a glance. J Cell Sci. 2020;133(16):jcs242487.

60. Hubstenberger A, Courel M, Bénard M, Souquere S, Ernoult-Lange M, Chouaib R, et al. P-body purification reveals the condensation of repressed mRNA regulons. Mol Cell. 2017;68(1):144–57.

61. Campos-Melo D, Hawley ZCE, Droppelmann CA, Strong MJ. The integral role of RNA in stress granule formation and function. Front Cell Dev Biol. 2021;9:621779.

62. Teixeira D, Sheth U, Valencia-Sanchez MA, Brengues M, Parker R. Processing bodies require RNA for assembly and contain nontranslating mRNAs. Rna. 2005;11(4):371–82.

63. Balagopal V, Parker R. Polysomes, P bodies and stress granules: states and fates of eukaryotic mRNAs. Curr Opin Cell Biol. 2009;21(3):403–8.

64. Nissan T, Parker R. Analyzing P-bodies in Saccharomyces cerevisiae. Methods Enzymol. 2008;448:507–20.

65. Strome S, Wood WB. Immunofluorescence visualization of germ-line-specific cytoplasmic granules in embryos, larvae, and adults of Caenorhabditis elegans. Proceedings of the National Academy of Sciences. 1982;79(5):1558–62.

66. Eddy EM. Fine structural observations on the form and distribution of nuage in germ cells of the rat. Anat Rec. 1974;178(4):731–57.

67. Sheth U, Parker R. Decapping and decay of messenger RNA occur in cytoplasmic processing bodies. Science (1979). 2003;300(5620):805–8.

68. Teixeira D, Sheth U, Valencia-Sanchez MA, Brengues M, Parker R. Processing bodies require RNA for assembly and contain nontranslating mRNAs. Rna. 2005;11(4):371–82.

69. Liu J, Valencia-Sanchez MA, Hannon GJ, Parker R. MicroRNA-dependent localization of targeted mRNAs to mammalian P-bodies. Nat Cell Biol. 2005;7(7):719–23.

70. Weber C, Nover L, Fauth M. Plant stress granules and mRNA processing bodies are distinct from heat stress granules. The Plant Journal. 2008;56(4):517–30.

71. Xu J, Chua NH. Processing bodies and plant development. Curr Opin Plant Biol. 2011;14(1):88–93.

72. Maldonado-Bonilla LD. Composition and function of P bodies in Arabidopsis thaliana. Front Plant Sci. 2014;5:201.

73. Xu J, Chua NH. Arabidopsis decapping 5 is required for mRNA decapping, P-body formation, and translational repression during postembryonic development. Plant Cell. 2009;21(10):3270–9.

74. Xiong L, Gong Z, Rock CD, Subramanian S, Guo Y, Xu W, et al. Modulation of abscisic acid signal transduction and biosynthesis by an Sm-like protein in Arabidopsis. Dev Cell. 2001;1(6):771–81.

75. Zeitelhofer M, Karra D, Macchi P, Tolino M, Thomas S, Schwarz M, et al. Dynamic interaction between P-bodies and transport ribonucleoprotein particles in dendrites of mature hippocampal neurons. Journal of Neuroscience. 2008;28(30):7555–62.

76. Zeitelhofer M, Macchi P, Dahm R. Perplexing bodies: The putative roles of P-bodies in neurons. RNA Biol. 2008;5(4):244–8.

77. Eulalio A, Behm-Ansmant I, Izaurralde E. P bodies: at the crossroads of post-transcriptional pathways. Nat Rev Mol Cell Biol. 2007;8(1):9–22.

78. Jang GJ, Yang JY, Hsieh HL, Wu SH. Processing bodies control the selective translation for optimal development of Arabidopsis young seedlings. Proceedings of the National Academy of Sciences. 2019;116(13):6451–6.

79. Chantarachot T, Bailey-Serres J. Polysomes, stress granules, and processing bodies: a dynamic triumvirate controlling cytoplasmic mRNA fate and function. Plant Physiol. 2018;176(1):254–69.

80. Covarrubias AA, Reyes JL. Post-transcriptional gene regulation of salinity and drought responses by plant microRNAs. Plant Cell Environ. 2010;33(4):481–9.

81. Blake LA, Watkins L, Liu Y, Inoue T, Wu B. A rapid inducible RNA decay system reveals fast mRNA decay in P-bodies. Nat Commun. 2024;15(1):2720.

82. Forbes Beadle L, Love JC, Shapovalova Y, Artemev A, Rattray M, Ashe HL. Combined modelling of mRNA decay dynamics and single-molecule imaging in the Drosophila embryo uncovers a role for P-bodies in 5′ to 3′ degradation. PLoS Biol. 2023;21(1):e3001956.

83. Liu TT, Yang Q, Li M, Zhong B, Ran Y, Liu LL, et al. LSm14A plays a critical role in antiviral immune responses by regulating MITA level in a cell-specific manner. The Journal of Immunology. 2016;196(12):5101–11.

84. Parker R, Sheth U. P bodies and the control of mRNA translation and degradation. Mol Cell. 2007;25(5):635–46.

85. Floris M, Mahgoub H, Lanet E, Robaglia C, Menand B. Post-transcriptional regulation of gene expression in plants during abiotic stress. Int J Mol Sci. 2009;10(7):3168–85.

86. Nsengimana B, Khan FA, Ngowi EE, Zhou X, Jin Y, Jia Y, et al. Processing body (P-body) and its mediators in cancer. Mol Cell Biochem. 2022;477(4):1217–38.

87. Behm-Ansmant I, Rehwinkel J, Doerks T, Stark A, Bork P, Izaurralde E. mRNA degradation by miRNAs and GW182 requires both CCR4: NOT deadenylase and DCP1: DCP2 decapping complexes. Genes Dev. 2006;20(14):1885–98.

88. Iwasaki S, Takeda A, Motose H, Watanabe Y. Characterization of Arabidopsis decapping proteins AtDCP1 and AtDCP2, which are essential for post-embryonic development. FEBS Lett. 2007;581(13):2455–9.

89. Kim MH, Sonoda Y, Sasaki K, Kaminaka H, Imai R. Interactome analysis reveals versatile functions of Arabidopsis COLD SHOCK DOMAIN PROTEIN 3 in RNA processing within the nucleus and cytoplasm. Cell Stress Chaperones. 2013;18(4):517–25.

90. Thran M, Link K, Sonnewald U. The Arabidopsis DCP2 gene is required for proper mRNA turnover and prevents transgene silencing in Arabidopsis. The Plant Journal. 2012;72(3):368–77.

91. Wurm JP, Sprangers R. Dcp2: an mRNA decapping enzyme that adopts many different shapes and forms. Curr Opin Struct Biol. 2019;59:115–23.

92. Panigrahi GK, Satapathy KB. Arabidopsis DCP5, a decapping complex protein interacts with ubiquitin-5 in the processing bodies. 2020;

93. Chantarachot T, Bailey-Serres J. Polysomes, stress granules, and processing bodies: a dynamic triumvirate controlling cytoplasmic mRNA fate and function. Plant Physiol. 2018;176(1):254–69.

94. Xu J, Yang JY, Niu QW, Chua NH. Arabidopsis DCP2, DCP1, and VARICOSE form a decapping complex required for postembryonic development. Plant Cell. 2006;18(12):3386–98.

95. Panigrahi GK, Sahoo A, Satapathy KB. The processing body component varicose plays a multiplayer role towards stress management in Arabidopsis. Plant Physiology Reports. 2024;29(1):186–92.

96. Jang GJ, Jang JC, Wu SH. Dynamics and functions of stress granules and processing bodies in plants. Plants. 2020;9(9):1122.

97. Liu Y, Gao W, Wu S, Lu L, Chen Y, Guo J, et al. AtXRN4 affects the turnover of chosen miRNA* s in Arabidopsis. Plants. 2020;9(3):362.

98. Perea-Resa C, Hernández-Verdeja T, López-Cobollo R, Castellano M del M, Salinas J. LSM proteins provide accurate splicing and decay of selected transcripts to ensure normal Arabidopsis development. Plant Cell. 2012;24(12):4930–47.

99. Perea-Resa C, Carrasco-López C, Catalá R, Turečková V, Novak O, Zhang W, et al. The LSM1-7 complex differentially regulates Arabidopsis tolerance to abiotic stress conditions by promoting selective mRNA decapping. Plant Cell. 2016;28(2):505–20.

100. Roux ME, Rasmussen MW, Palma K, Lolle S, Regué ÀM, Bethke G, et al. The mRNA decay factor PAT 1 functions in a pathway including MAP kinase 4 and immune receptor SUMM 2. EMBO J. 2015;34(5):593–608.

101. Zuo Z, Roux ME, Dagdas YF, Rodriguez E, Petersen M. PAT m RNA decapping factors are required for proper development in Arabidopsis. FEBS Lett. 2024;598(9):1008–21.

102. Li Q, Liu N, Liu Q, Zheng X, Lu L, Gao W, et al. DEAD-box helicases modulate dicing body formation in Arabidopsis. Sci Adv. 2021;7(18):eabc6266.

103. Bhullar DS, Sheahan MB, Rose RJ. RNA processing body (P-body) dynamics in mesophyll protoplasts re-initiating cell division. Protoplasma. 2017;254:1627–37.

104. Zhang ZJ, Gao Q, Fang XD, Ding ZH, Gao DM, Xu WY, et al. CCR4, a RNA decay factor, is hijacked by a plant cytorhabdovirus phosphoprotein to facilitate virus replication. Elife. 2020;9:e53753.

105. Chou WL, Chung YL, Fang JC, Lu CA. Novel interaction between CCR4 and CAF1 in rice CCR4–NOT deadenylase complex. Plant Mol Biol. 2017;93:79–96.

106. Chou WL, Chung YL, Fang JC, Lu CA. Novel interaction between CCR4 and CAF1 in rice CCR4–NOT deadenylase complex. Plant Mol Biol. 2017;93:79–96.

107. Chantarachot T, Bailey-Serres J. Polysomes, stress granules, and processing bodies: a dynamic triumvirate controlling cytoplasmic mRNA fate and function. Plant Physiol. 2018;176(1):254–69.

108. Panigrahi GK, Satapathy KB. Formation of Arabidopsis poly (A)-specific ribonuclease associated processing bodies in response to pathogenic infection. 2020;

109. Blagojevic A, Baldrich P, Schiaffini M, Lechner E, Baumberger N, Hammann P, et al. Heat stress promotes Arabidopsis AGO1 phase separation and association with stress granule components. iScience. 2024;27(3).

110. Huang Z, Xu Z, Liu X, Chen G, Hu C, Chen M, et al. Exploring the Role of the Processing Body in Plant Abiotic Stress Response. Curr Issues Mol Biol. 2024;46(9):9844–55.

111. Chicois C, Scheer H, Garcia S, Zuber H, Mutterer J, Chicher J, et al. The UPF1 interactome reveals interaction networks between RNA degradation and translation repression factors in Arabidopsis. The Plant Journal. 2018;96(1):119–32.

112. Cairo A, Vargova A, Shukla N, Capitao C, Mikulkova P, Valuchova S, et al. Meiotic exit in Arabidopsis is driven by P-body–mediated inhibition of translation. Science (1979). 2022;377(6606):629–34.

113. Yu X, Li B, Jang GJ, Jiang S, Jiang D, Jang JC, et al. Orchestration of processing body dynamics and mRNA decay in Arabidopsis immunity. Cell Rep. 2019;28(8):2194–205.

114. Wang W, Wang C, Wang Y, Ma J, Wang T, Tao Z, et al. The P-body component DECAPPING5 and the floral repressor SISTER OF FCA regulate FLOWERING LOCUS C transcription in Arabidopsis. Plant Cell. 2023;35(9):3303–24.

115. Wang Z, Yang Q, Zhang D, Lu Y, Wang Y, Pan Y, et al. A cytoplasmic osmosensing mechanism mediated by molecular crowding–sensitive DCP5. Science (1979). 2024;386(6721):eadk9067.

116. Tharun S. Roles of eukaryotic Lsm proteins in the regulation of mRNA function. Int Rev Cell Mol Biol. 2008;272:149–89.

117. Tharun S, He W, Mayes AE, Lennertz P, Beggs JD, Parker R. Yeast Sm-like proteins function in mRNA decapping and decay. Nature. 2000;404(6777):515–8.

118. Catalá R, Carrasco-López C, Perea-Resa C, Hernández-Verdeja T, Salinas J. Emerging roles of LSM complexes in posttranscriptional regulation of plant response to abiotic stress. Front Plant Sci. 2019;10:167.

119. Zhou L, Hang J, Zhou Y, Wan R, Lu G, Yin P, et al. Crystal structures of the Lsm complex bound to the 3′ end sequence of U6 small nuclear RNA. Nature. 2014;506(7486):116–20.

120. Chowdhury A, Mukhopadhyay J, Tharun S. The decapping activator Lsm1p-7p–Pat1p complex has the intrinsic ability to distinguish between oligoadenylated and polyadenylated RNAs. Rna. 2007;13(7):998–1016.

121. Chowdhury A, Mukhopadhyay J, Tharun S. The decapping activator Lsm1p-7p–Pat1p complex has the intrinsic ability to distinguish between oligoadenylated and polyadenylated RNAs. Rna. 2007;13(7):998–1016.

122. Charenton C, Taverniti V, Gaudon-Plesse C, Back R, Seraphin B, Graille M. Structure of the active form of Dcp1–Dcp2 decapping enzyme bound to m7GDP and its Edc3 activator. Nat Struct Mol Biol. 2016;23(11):982–6.

123. Kruszka K, Kufel J. Arabidopsis thaliana LSM proteins function in mRNA splicing and degradation. Acta Biochim Pol. 2006;53(Supplement 1).

124. Arribas-Layton M, Dennis J, Bennett EJ, Damgaard CK, Lykke-Andersen J. The C-terminal RGG domain of human Lsm4 promotes processing body formation stimulated by arginine dimethylation. Mol Cell Biol. 2016;36(17):2226–35.

125. Rymarquis LA, Souret FF, Green PJ. Evidence that XRN4, an Arabidopsis homolog of exoribonuclease XRN1, preferentially impacts transcripts with certain sequences or in particular functional categories. Rna. 2011;17(3):501–11.

126. Song W, Li Y, Niu Y, Wu Y, Bao Y, Yu X. Global characterization of XRN 5′-3′ exoribonucleases and their responses to environmental stresses in plants. Diversity (Basel). 2021;13(12):612.

127. Carpentier MC, Deragon JM, Jean V, Be SHV, Bousquet-Antonelli C, Merret R. Monitoring of XRN4 targets reveals the importance of cotranslational decay during Arabidopsis development. Plant Physiol. 2020;184(3):1251–62.

128. Nagarajan VK, Jones CI, Newbury SF, Green PJ. XRN 5′→ 3′ exoribonucleases: structure, mechanisms and functions. Biochimica et Biophysica Acta (BBA)-Gene Regulatory Mechanisms. 2013;1829(6–7):590–603.

129. Geisler S, Coller J. XRN1: a major 5′ to 3′ exoribonuclease in eukaryotic cells. Enzymes. 2012;31:97–114.

130. Balagopal V, Parker R. Polysomes, P bodies and stress granules: states and fates of eukaryotic mRNAs. Curr Opin Cell Biol. 2009;21(3):403–8.

131. Xu J, Chua N. Dehydration stress activates Arabidopsis MPK6 to signal DCP1 phosphorylation. EMBO J. 2012;31(8):1975–84.

132. Kedersha N, Stoecklin G, Ayodele M, Yacono P, Lykke-Andersen J, Fritzler MJ, et al. Stress granules and processing bodies are dynamically linked sites of mRNP remodeling. J Cell Biol. 2005;169(6):871–84.

133. Zeke A, Schad E, Horvath T, Abukhairan R, Szabo B, Tantos A. Deep structural insights into RNA-binding disordered protein regions. Wiley Interdiscip Rev RNA. 2022;13(5):e1714.

134. Jonas S, Izaurralde E. The role of disordered protein regions in the assembly of decapping complexes and RNP granules. Genes Dev. 2013;27(24):2628–41.

135. Maciej VD, Mateva N, Schwarz J, Dittmers T, Mallick M, Urlaub H, et al. Intrinsically disordered regions of tristetraprolin and DCP2 directly interact to mediate decay of ARE-mRNA. Nucleic Acids Res. 2022;50(18):10665–79.

136. Huang Z, Xu Z, Liu X, Chen G, Hu C, Chen M, et al. Exploring the Role of the Processing Body in Plant Abiotic Stress Response. Curr Issues Mol Biol. 2024;46(9):9844–55.

137. Van Der Lee R, Buljan M, Lang B, Weatheritt RJ, Daughdrill GW, Dunker AK, et al. Classification of intrinsically disordered regions and proteins. Chem Rev. 2014;114(13):6589–631.

138. Foressi NN, Cruz Rodríguez L, Wilke N, Celej MS. Cation-Driven Modulation of Tau Condensates: Insights into Liquid–Liquid Phase Separation and Rheological Properties. Biomacromolecules. 2025;

139. Nott TJ, Petsalaki E, Farber P, Jervis D, Fussner E, Plochowietz A, et al. Phase transition of a disordered nuage protein generates environmentally responsive membraneless organelles. Mol Cell. 2015;57(5):936–47.

140. Molliex A, Temirov J, Lee J, Coughlin M, Kanagaraj AP, Kim HJ, et al. Phase separation by low complexity domains promotes stress granule assembly and drives pathological fibrillization. Cell. 2015;163(1):123–33.

141. Lin Y, Protter DSW, Rosen MK, Parker R. Formation and maturation of phase-separated liquid droplets by RNA-binding proteins. Mol Cell. 2015;60(2):208–19.

142. Elbaum-Garfinkle S, Kim Y, Szczepaniak K, Chen CCH, Eckmann CR, Myong S, et al. The disordered P granule protein LAF-1 drives phase separation into droplets with tunable viscosity and dynamics. Proceedings of the National Academy of Sciences. 2015;112(23):7189–94.

143. Lin Y, Protter DSW, Rosen MK, Parker R. Formation and maturation of phase-separated liquid droplets by RNA-binding proteins. Mol Cell. 2015;60(2):208–19.

144. Burke KA, Janke AM, Rhine CL, Fawzi NL. Residue-by-residue view of in vitro FUS granules that bind the C-terminal domain of RNA polymerase II. Mol Cell. 2015;60(2):231–41.

145. Feric M, Vaidya N, Harmon TS, Mitrea DM, Zhu L, Richardson TM, et al. Coexisting liquid phases underlie nucleolar subcompartments. Cell. 2016;165(7):1686–97.

146. Buchan JR. Stress granule and P-body clearance: Seeking coherence in acts of disappearance. In: Seminars in Cell & Developmental Biology. Elsevier; 2024. p. 10–26.

147. Franks TM, Lykke-Andersen J. The control of mRNA decapping and P-body formation. Mol Cell. 2008;32(5):605–15.

148. Kulkarni M, Ozgur S, Stoecklin G. On track with P-bodies. Biochem Soc Trans. 2010;38(1):242–51.

149. Wang C, Schmich F, Srivatsa S, Weidner J, Beerenwinkel N, Spang A. Context-dependent deposition and regulation of mRNAs in P-bodies. Elife. 2018;7:e29815.

150. Riyazuddin R, Verma R, Singh K, Nisha N, Keisham M, Bhati KK, et al. Ethylene: a master regulator of salinity stress tolerance in plants. Biomolecules. 2020;10(6):959.

151. Li W, Ma M, Feng Y, Li H, Wang Y, Ma Y, et al. EIN2-directed translational regulation of ethylene signaling in Arabidopsis. Cell. 2015;163(3):670–83.

152. Merchante C, Brumos J, Yun J, Hu Q, Spencer KR, Enríquez P, et al. Gene-specific translation regulation mediated by the hormone-signaling molecule EIN2. Cell. 2015;163(3):684–97.

153. Wang C, Schmich F, Srivatsa S, Weidner J, Beerenwinkel N, Spang A. Context-dependent deposition and regulation of mRNAs in P-bodies. Elife. 2018;7:e29815.

154. Hubstenberger A, Courel M, Bénard M, Souquere S, Ernoult-Lange M, Chouaib R, et al. P-body purification reveals the condensation of repressed mRNA regulons. Mol Cell. 2017;68(1):144–57.

155. Youn JY, Dunham WH, Hong SJ, Knight JDR, Bashkurov M, Chen GI, et al. High-density proximity mapping reveals the subcellular organization of mRNA-associated granules and bodies. Mol Cell. 2018;69(3):517–32.

156. Zhou Y, Ćorović M, Hoch-Kraft P, Meiser N, Mesitov M, Körtel N, et al. m6A sites in the coding region trigger translation-dependent mRNA decay. Mol Cell. 2024;84(23):4576–93.

157. Murakami S, Olarerin-George AO, Liu JF, Zaccara S, Hawley B, Jaffrey SR. m6A alters ribosome dynamics to initiate mRNA degradation. Cell. 2025;

158. Cai Z, Tang Q, Song P, Tian E, Yang J, Jia G. The m6A reader ECT8 is an abiotic stress sensor that accelerates mRNA decay in Arabidopsis. Plant Cell. 2024;36(8):2908–26.

159. Chantarachot T, Sorenson RS, Hummel M, Ke H, Kettenburg AT, Chen D, et al. DHH1/DDX6-like RNA helicases maintain ephemeral half-lives of stress-response mRNAs. Nat Plants. 2020;6(6):675–85.

160. Coller J, Parker R. Eukaryotic mRNA decapping. Annu Rev Biochem. 2004;73(1):861–90.

161. Buchan JR, Muhlrad D, Parker R. P bodies promote stress granule assembly in Saccharomyces cerevisiae. J Cell Biol. 2008;183(3):441–55.

162. Reineke LC, Lloyd RE. Diversion of stress granules and P-bodies during viral infection. Virology. 2013;436(2):255–67.

163. van Leeuwen W, Rabouille C. Cellular stress leads to the formation of membraneless stress assemblies in eukaryotic cells. Traffic. 2019;20(9):623–38.

164. Riggs CL, Kedersha N, Ivanov P, Anderson P. Mammalian stress granules and P bodies at a glance. J Cell Sci. 2020;133(16):jcs242487.

165. Bhattacharyya SN, Habermacher R, Martine U, Closs EI, Filipowicz W. Stress-induced reversal of microRNA repression and mRNA P-body localization in human cells. In: Cold Spring Harbor symposia on quantitative biology. Cold Spring Harbor Laboratory Press; 2006. p. 513–21.

166. Bashkirov VI, Scherthan H, Solinger JA, Buerstedde JM, Heyer WD. A mouse cytoplasmic exoribonuclease (mXRN1p) with preference for G4 tetraplex substrates. J Cell Biol. 1997;136(4):761–73.

167. Ingelfinger D, Arndt-Jovin DJ, Lührmann R, Achsel T. The human LSm1-7 proteins colocalize with the mRNA-degrading enzymes Dcp1/2 and Xrn1 in distinct cytoplasmic foci. Rna. 2002;8(12):1489–501.

168. Sheth U, Parker R. Decapping and decay of messenger RNA occur in cytoplasmic processing bodies. Science (1979). 2003;300(5620):805–8.

169. Borbolis F, Ranti D, Papadopoulou MD, Dimopoulou S, Malatras A, Michalopoulos I, et al. Selective destabilization of transcripts by mRNA decapping regulates oocyte maturation and innate immunity gene expression during ageing in C. elegans. Biology (Basel). 2023;12(2):171.

170. Coller J, Parker R. Eukaryotic mRNA decapping. Annu Rev Biochem. 2004;73(1):861–90.

171. Roy R, Rajyaguru PI. Stress granules and p-bodies: An insight into mRNA translational control and decay. 2018;

172. Chen CA, Shyu A. Mechanisms of deadenylation-dependent decay. Wiley Interdiscip Rev RNA. 2011;2(2):167–83.

173. Zhang X, Guo H. mRNA decay in plants: both quantity and quality matter. Curr Opin Plant Biol. 2017;35:138–44.

174. Tharun S, Parker R. Targeting an mRNA for decapping: displacement of translation factors and association of the Lsm1p–7p complex on deadenylated yeast mRNAs. Mol Cell. 2001;8(5):1075–83.

175. Sharif H, Conti E. Architecture of the Lsm1-7-Pat1 complex: a conserved assembly in eukaryotic mRNA turnover. Cell Rep. 2013;5(2):283–91.

176. Zheng D, Ezzeddine N, Chen CYA, Zhu W, He X, Shyu AB. Deadenylation is prerequisite for P-body formation and mRNA decay in mammalian cells. J Cell Biol. 2008;182(1):89–101.

177. Pederson T. The nucleus introduced. Cold Spring Harb Perspect Biol. 2011;3(5):a000521.

178. Taliansky ME, Love AJ, Kołowerzo-Lubnau A, Smoliński DJ. Cajal bodies: evolutionarily conserved nuclear biomolecular condensates with properties unique to plants. Plant Cell. 2023;35(9):3214–35.

179. Kołowerzo A, Smoliński DJ, Bednarska E. Poly (A) RNA a new component of Cajal bodies. Protoplasma. 2009;236:13–9.

180. Rudzka M, Wróblewska-Ankiewicz P, Majewska K, Hyjek-Składanowska M, Gołębiewski M, Sikora M, et al. Functional nuclear retention of pre-mRNA involving Cajal bodies during meiotic prophase in European larch (Larix decidua). Plant Cell. 2022;34(6):2404–23.

181. Kołowerzo-Lubnau A, Niedojadło J, Świdziński M, Bednarska-Kozakiewicz E, Smoliński DJ. Transcriptional activity in diplotene larch microsporocytes, with emphasis on the diffuse stage. PLoS One. 2015;10(2):e0117337.

182. Smoliński DJ, Wróbel B, Noble A, Zienkiewicz A, Górska-Brylass A. Periodic expression of Sm proteins parallels formation of nuclear Cajal bodies and cytoplasmic snRNP-rich bodies. Histochem Cell Biol. 2011;136:527–41.

183. Hyjek-Składanowska M, Bajczyk M, Gołębiewski M, Nuc P, Kołowerzo-Lubnau A, Jarmołowski A, et al. Core spliceosomal Sm proteins as constituents of cytoplasmic mRNPs in plants. The Plant Journal. 2020;103(3):1155–73.

184. Majewska K, Wróblewska-Ankiewicz P, Rudzka M, Hyjek-Składanowska M, Gołębiewski M, Smoliński DJ, et al. Different patterns of mRNA nuclear retention during meiotic prophase in larch microsporocytes. Int J Mol Sci. 2021;22(16):8501.

185. Rudzka M, Wróblewska-Ankiewicz P, Majewska K, Hyjek-Składanowska M, Gołębiewski M, Sikora M, et al. Functional nuclear retention of pre-mRNA involving Cajal bodies during meiotic prophase in European larch (Larix decidua). Plant Cell. 2022;34(6):2404–23.

186. Smoliński DJ, Niedojadło J, Noble A, Górska-Brylass A. Additional nucleoli and NOR activity during meiotic prophase I in larch (Larix decidua Mill.). Protoplasma. 2007;232:109–20.

187. Ansorg A, Bornkessel K, Witte OW, Urbach A. Immunohistochemistry and multiple labeling with antibodies from the same host species to study adult hippocampal neurogenesis. J Vis Exp. 2015;(98):52551.

188. Schneider CA, Rasband WS, Eliceiri KW. NIH Image to ImageJ: 25 years of image analysis. Nat Methods. 2012;9(7):671–5.

189. Dey PM. The plant, the cell and its molecular components. Plant biochemistry. 1997;1–47.

190. Oliva M, Butenko Y, Hsieh TF, Hakim O, Katz A, Smorodinsky NI, et al. FIE, a nuclear PRC2 protein, forms cytoplasmic complexes in Arabidopsis thaliana. J Exp Bot. 2016;erw373.

191. Nabakooza G, Wagner DD, Momin N, Marine RL, Weldon WC, Oberste MS. Sequence-matching adapter trimmers generate consistent quality and assembly metrics for Illumina sequencing of RNA viruses. BMC Res Notes. 2024;17(1):308.

192. Langmead B, Salzberg SL. Fast gapped-read alignment with Bowtie 2. Nat Methods. 2012;9(4):357–9.

193. Grabherr MG, Haas BJ, Yassour M, Levin JZ, Thompson DA, Amit I, et al. Full-length transcriptome assembly from RNA-Seq data without a reference genome. Nat Biotechnol. 2011;29(7):644–52.

194. Bryant DM, Johnson K, DiTommaso T, Tickle T, Couger MB, Payzin-Dogru D, et al. A tissue-mapped axolotl de novo transcriptome enables identification of limb regeneration factors. Cell Rep. 2017;18(3):762–76.

195. Ahmad S, Jose da Costa Gonzales L, Bowler-Barnett EH, Rice DL, Kim M, Wijerathne S, et al. The UniProt website API: facilitating programmatic access to protein knowledge. Nucleic Acids Res. 2025;gkaf394.

196. Li B, Dewey CN. RSEM: accurate transcript quantification from RNA-Seq data with or without a reference genome. BMC Bioinformatics. 2011;12(1):323.

197. Ivanov P, Kedersha N, Anderson P. Stress granules and processing bodies in translational control. Cold Spring Harb Perspect Biol. 2019;11(5):a032813.

198. Kubiak DJ, Szczesniak MW, Ostrowska K, Bielewicz D, Bhat SS, Niedojadlo K, et al. Impact of m6A Modification and Transcript Quantity on mRNA Composition in Plant Stress Granules. J Exp Bot. 2025;eraf046.

199. Newbury SF, Mühlemann O, Stoecklin G. Turnover in the Alps: an mRNA perspective: Workshop on Mechanisms and Regulation of mRNA Turnover. EMBO Rep. 2006;7(2):143–8.

200. Nagarajan VK, Kukulich PM, von Hagel B, Green PJ. RNA degradomes reveal substrates and importance for dark and nitrogen stress responses of Arabidopsis XRN4. Nucleic Acids Res. 2019;47(17):9216–30.

201. Merret R, Descombin J, Juan Y ting, Favory JJ, Carpentier MC, Chaparro C, et al. XRN4 and LARP1 are required for a heat-triggered mRNA decay pathway involved in plant acclimation and survival during thermal stress. Cell Rep. 2013;5(5):1279–93.

202. Han W, Hou B, Lee W, Chan T, Lin T, Chen H. Arabidopsis mRNA decay landscape shaped by XRN 5'-3' exoribonucleases. The Plant Journal. 2023;114(4):895–913.

203. Yu X, Willmann MR, Anderson SJ, Gregory BD. Genome-wide mapping of uncapped and cleaved transcripts reveals a role for the nuclear mRNA cap-binding complex in cotranslational RNA decay in Arabidopsis. Plant Cell. 2016;28(10):2385–97.

204. Carpentier MC, Receveur AE, Boubegtitene A, Cadoudal A, Bousquet-Antonelli C, Merret R. Genome-wide analysis of mRNA decay in Arabidopsis shoot and root reveals the importance of co-translational mRNA decay in the general mRNA turnover. Nucleic Acids Res. 2024;52(13):7910–24.

205. Franks TM, Lykke-Andersen J. The control of mRNA decapping and P-body formation. Mol Cell. 2008;32(5):605–15.

206. Borbolis F, Syntichaki P. Biological implications of decapping: beyond bulk mRNA decay. FEBS J. 2022;289(6):1457–75.

207. Cassani M, Seydoux G. Specialized germline P-bodies are required to specify germ cell fate in Caenorhabditis elegans embryos. Development. 2022;149(21):dev200920.

208. Li RM, Zhang MN, Tang QY, Song MG. Global deletion of the RNA decapping enzyme Dcp2 postnatally in male mice results in infertility. Biochem Biophys Res Commun. 2020;526(2):512–8.

209. Swetloff A, Conne B, Huarte J, Pitetti JL, Nef S, Vassalli JD. Dcp1-bodies in mouse oocytes. Mol Biol Cell. 2009;20(23):4951–61.

210. Hoffmann G, Mahboubi A, Bente H, Garcia D, Hanson J, Hafrén A. Arabidopsis RNA processing body components LSM1 and DCP5 aid in the evasion of translational repression during Cauliflower mosaic virus infection. Plant Cell. 2022;34(8):3128–47.

211. Gutierrez-Beltran E, Moschou PN, Smertenko AP, Bozhkov P V. Tudor staphylococcal nuclease links formation of stress granules and processing bodies with mRNA catabolism in Arabidopsis. Plant Cell. 2015;27(3):926–43.

212. Jan A, Maruyama K, Todaka D, Kidokoro S, Abo M, Yoshimura E, et al. OsTZF1, a CCCH-tandem zinc finger protein, confers delayed senescence and stress tolerance in rice by regulating stress-related genes. Plant Physiol. 2013;161(3):1202–16.

213. Soma F, Mogami J, Yoshida T, Abekura M, Takahashi F, Kidokoro S, et al. ABA-unresponsive SnRK2 protein kinases regulate mRNA decay under osmotic stress in plants. Nat Plants. 2017;3(1):1–8.

214. Soma F, Takahashi F, Suzuki T, Shinozaki K, Yamaguchi-Shinozaki K. Plant Raf-like kinases regulate the mRNA population upstream of ABA-unresponsive SnRK2 kinases under drought stress. Nat Commun. 2020;11(1):1373.

215. Goeres DC, Van Norman JM, Zhang W, Fauver NA, Spencer M Lou, Sieburth LE. Components of the Arabidopsis mRNA decapping complex are required for early seedling development. Plant Cell. 2007;19(5):1549–64.

216. Franks TM, Lykke-Andersen J. The control of mRNA decapping and P-body formation. Mol Cell. 2008;32(5):605–15.

217. Franks TM, Lykke-Andersen J. The control of mRNA decapping and P-body formation. Mol Cell. 2008;32(5):605–15.

218. Motomura K, Le QTN, Hamada T, Kutsuna N, Mano S, Nishimura M, et al. Diffuse decapping enzyme DCP2 accumulates in DCP1 foci under heat stress in Arabidopsis thaliana. Plant Cell Physiol. 2015;56(1):107–15.

219. Tharun S. Lsm1-7-Pat1 complex: A link between 3'and 5'-ends in mRNA decay? RNA Biol. 2009;6(3):228–32.

220. Cornes E, Porta-De-La-Riva M, Aristizábal-Corrales D, Brokate-Llanos AM, García-Rodríguez FJ, Ertl I, et al. Cytoplasmic LSM-1 protein regulates stress responses through the insulin/IGF-1 signaling pathway in Caenorhabditis elegans. Rna. 2015;21(9):1544–53.

221. Novotný I, Podolská K, Blažíková M, Valášek LS, Svoboda P, Staněk D. Nuclear LSm8 affects number of cytoplasmic processing bodies via controlling cellular distribution of Like-Sm proteins. Mol Biol Cell. 2012;23(19):3776–85.

222. Reijns MAM, Alexander RD, Spiller MP, Beggs JD. A role for Q/N-rich aggregation-prone regions in P-body localization. J Cell Sci. 2008;121(15):2463–72.

223. Gudkova D, Panasyuk G, Nemazanyy I, Zhyvoloup A, Monteil P, Filonenko V, et al. EDC4 interacts with and regulates the dephospho-CoA kinase activity of CoA synthase. FEBS Lett. 2012;586(20):3590–5.

224. Vidya E, Jami-Alahmadi Y, Mayank AK, Rizwan J, Xu JMS, Cheng T, et al. EDC-3 and EDC-4 regulate embryonic mRNA clearance and biomolecular condensate specialization. Cell Rep. 2024;43(10).

225. Liu Y, Gao W, Wu S, Lu L, Chen Y, Guo J, et al. AtXRN4 affects the turnover of chosen miRNA* s in Arabidopsis. Plants. 2020;9(3):362.

226. Tharun S, He W, Mayes AE, Lennertz P, Beggs JD, Parker R. Yeast Sm-like proteins function in mRNA decapping and decay. Nature. 2000;404(6777):515–8.

227. Golisz A, Sikorski PJ, Kruszka K, Kufel J. Arabidopsis thaliana LSM proteins function in mRNA splicing and degradation. Nucleic Acids Res. 2013;41(12):6232–49.

228. Sankaranarayanan M, Emenecker RJ, Wilby EL, Jahnel M, Trussina IREA, Wayland M, et al. Adaptable P body physical states differentially regulate bicoid mRNA storage during early Drosophila development. Dev Cell. 2021;56(20):2886–901.

229. Fujimura K, Katahira J, Kano F, Yoneda Y, Murata M. Selective localization of PCBP2 to cytoplasmic processing bodies. Biochimica et Biophysica Acta (BBA)-Molecular Cell Research. 2009;1793(5):878–87.

230. Luo Y, Na Z, Slavoff SA. P-bodies: composition, properties, and functions. Biochemistry. 2018;57(17):2424–31.

231. Hamada T, Yako M, Minegishi M, Sato M, Kamei Y, Yanagawa Y, et al. Stress granule formation is induced by a threshold temperature rather than a temperature difference in Arabidopsis. J Cell Sci. 2018;131(16):jcs216051.

232. Krummel DAP, Nagai K, Oubridge C. Structure of spliceosomal ribonucleoproteins. F1000 Biol Rep. 2010;2:39.

9. Supplementary

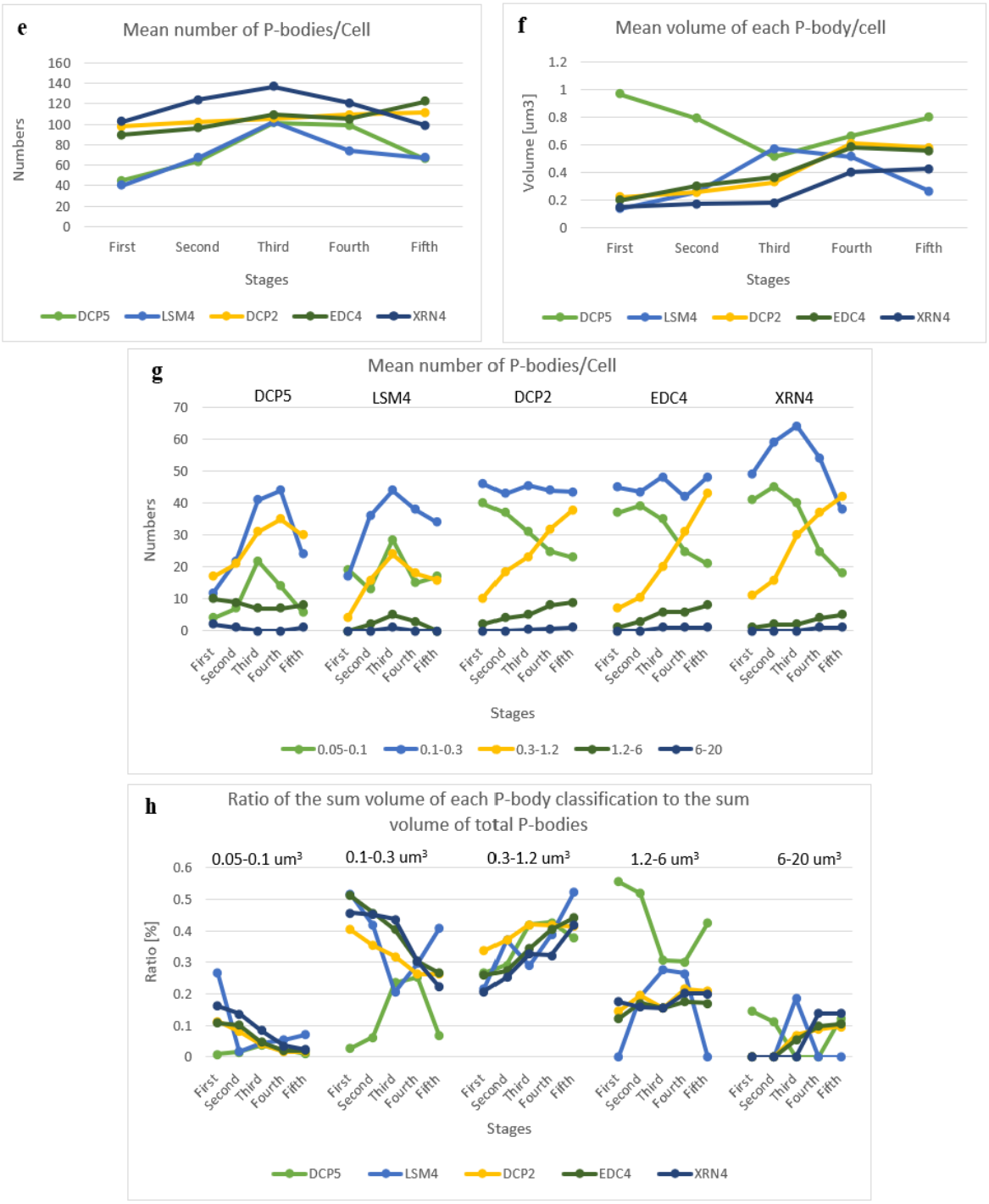

Sup. 1. Merged graph from figures 4-2, 4-5, 4-8, 4-11, 4-14.

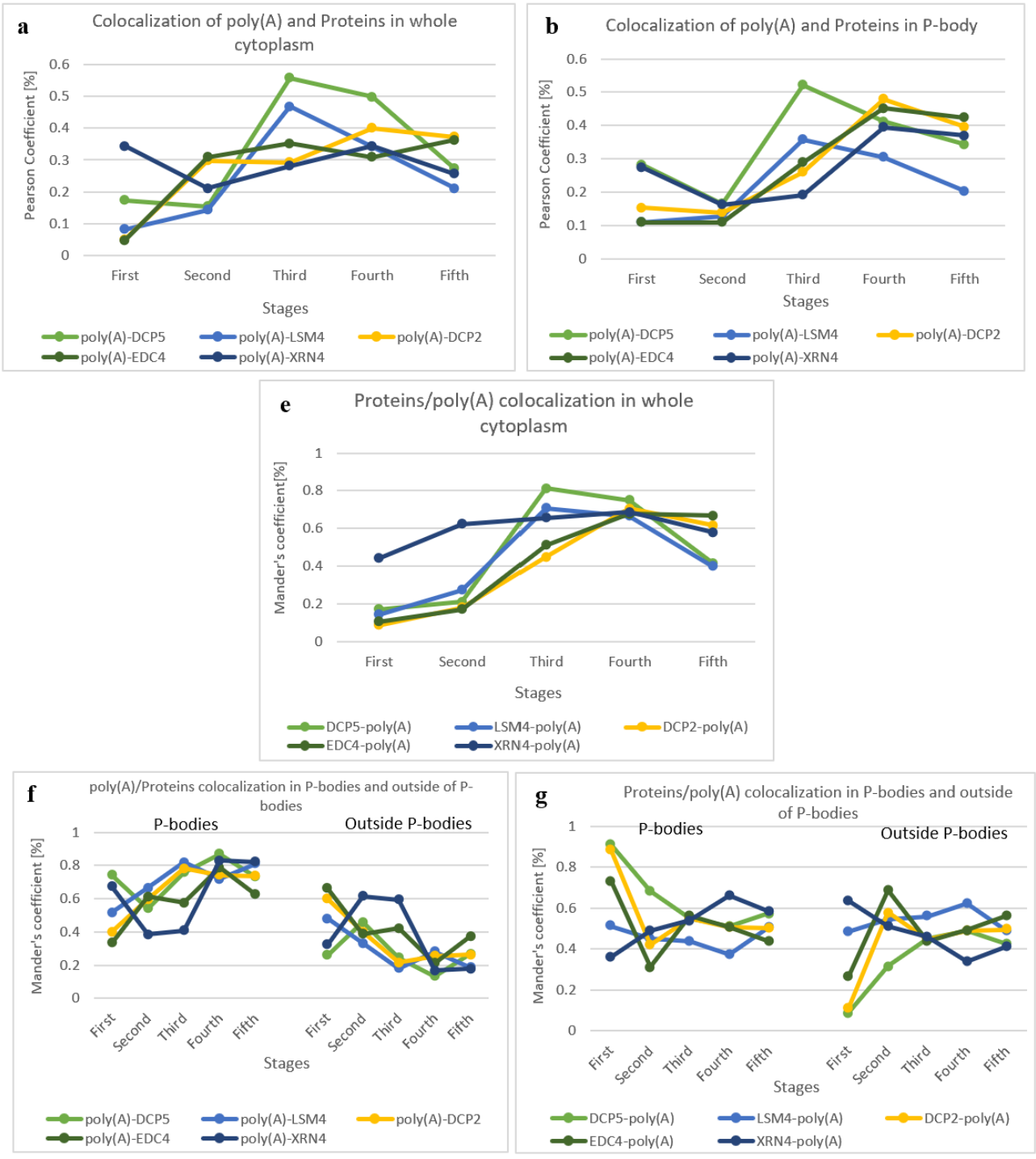

Sup. 2. Merged graph from figures 4-3, 4-6, 4-9, 4-12, 4-15.

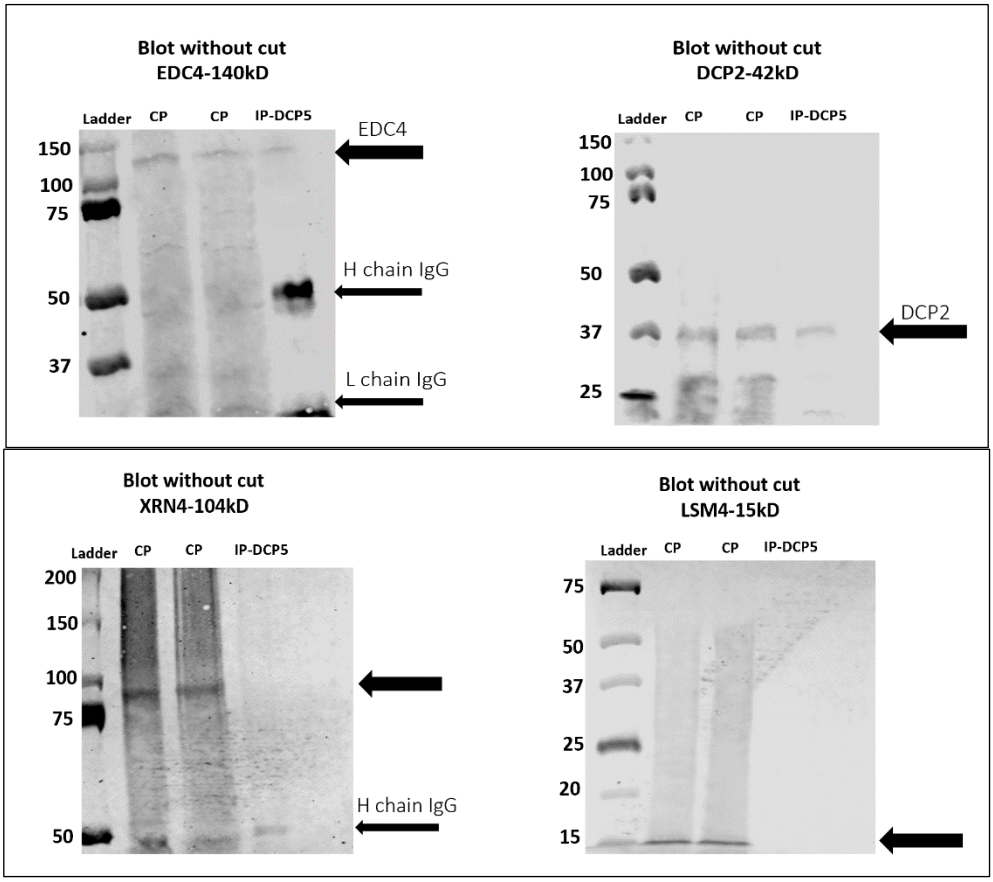

Sup. 3. Whole Blot of IP confirmation

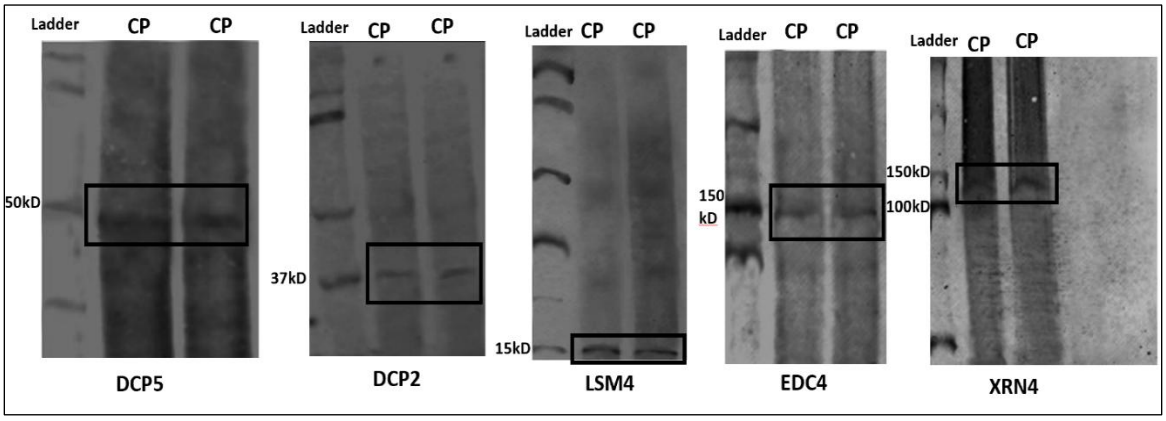

Sup. 4. Whole Blot of western blot repetition

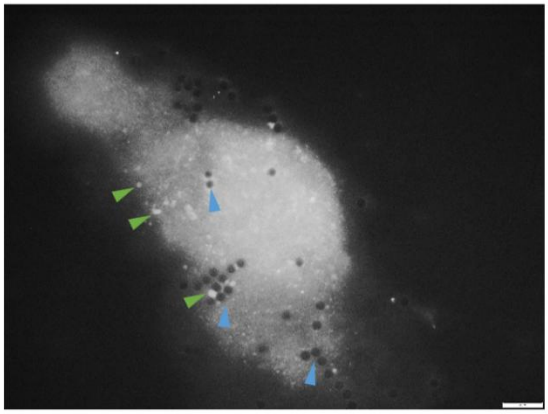

Sup. 5. Another example of dynabead-P-bodies. Blue arrow: refer to the Dynabeads. Green arrow: refer to the RNA enrichment-P-bodies (Scale bar 10 μm).